CHARLES LEE POWELL STRUCTURAL RESEARCH LABORATORIES

CALTRANS SRMD TEST FACILITY

Report No.
SRMD–2006/05-rev3

Performance of Lead-Rubber and Sliding Bearings under Different Axial Load and Velocity Conditions.

Gianmario Benzoni – Chiara Casarotti

Report submitted to California Department of Transportation under contract No 59A0437

May 2008

Department of Structural Engineering
University of California, San Diego
La Jolla, California 92093-0085

Charles Lee Powell Structural Research Laboratories
Caltrans SRMD Test Facility

Report No. SRMD -2006/05-rev3

Performance of Lead-Rubber and Sliding Bearings under Different Axial Load and Velocity Conditions.

By
Gianmario Benzoni
University of California San Diego
And
Chiara Casarotti
University of Pavia, Italy.

Report submitted to California Department of Transportation under contract No 59A0437

Department of Structural Engineering
University of California San Diego
La Jolla, California 92093-0085

May 2008

TABLE OF CONTENTS

LIST OF FIGURES

LIST OF TABLES

ACKNOWLEDGMENTS

The research described in this report was funded by the California Department of Transportation (Caltrans) under contract No. 59A0437. The authors gratefully acknowledge the support of Mr. D. Lee, program manager, for the invaluable contribution to this project.

Conclusions and recommendations in this report are those of the authors and should not be construed to imply endorsement by Caltrans.

ABSTRACT

A series of tests on full scale devices for bridge application were completed. Two types of isolators were considered: lead-rubber bearings and sliding bearings. The main performance characteristics of these devices were already acquired through extensive testing campaigns designed for their specific applications. A more systematic analysis of their performance was considered necessary to enrich the knowledge of the device behavior under different loading conditions. Specifically the focus of this project was to address the effects of the applied axial load, the varying levels of velocity and the repetition of cycles on the performance characteristics.

The response variations were analyzed, for a low, medium and high level of applied vertical load, defined based on the design load of the bearing. A large spectrum of testing velocities was applied, ranging from very slow tests (0.254 mm/s) to high speed tests (1270 mm/s).

Peak shear force, yield force, stiffness, energy dissipated per cycle, friction coefficient and damping was estimated and compared among the different loading conditions. A specific numerical model, for lead-rubber bearings, able to take into account the effects of strain rate and repetition of cycles, is proposed.

The effects of bi-directional motions and of unequal distribution of vertical loads between bearings installed in parallel were also investigated.

INTRODUCTION

In March 2000, The California Department of Transportation initiated an unprecedented experimental program of full scale testing of Seismic Response Modification Devices (SRMD) part of the Toll Bridge Program. The program, that included the construction of the Caltrans SRMD Testing Facility at UCSD, initiate a truly new era in the field of seismic isolation and energy dissipation. The development of this technology, in fact was progressing to a stage of maturity that desperately needed experimental verification of the extensive industrial and academic work completed in the previous three decades. The use of reduced scale testing was the major restraint to confirm numerical theories of material performance under conditions difficult or impossible to scale, to validate performance of assembled devices and to transfer research results to higher performance devices. New isolators/dissipators never fully tested under realistic loading conditions as well as conventional devices, extended in dimensions and performance to fit bridge requirements, were tested. Specifically the Caltrans SRMD Testing Facility completed, in three years of operation, the full series of tests for devices to be used on bridges as: Benicia-Martinez, Richmond San Rafael, Coronado, San Francisco- Oakland Bay and many others in the United States and around the World (Benzoni et al. 2000), (Benzoni et al. 2001), (Benzoni, Innamorato 2003). Many aspects of isolation device performance were researched, during the testing programs at the SRMD facility at UCSD. Fundamental performance characteristics were evaluated, and even commonly used devices were tested under first-time conditions. For instance, full scale sliding bearings, up to 3.6 m in diameter, were tested under design and ultimate vertical load (peak load= 54,000 kN), in a range of full displacement and with peak velocity up to 1.8 m/s. Elastomeric devices were tested under design vertical loads at different velocities for a range of shear strains up to 450%.

The testing protocol, for the above mentioned devices, was developed by Caltrans based on the specific rationale of the bridge projects (Mellon, 1997). Even though the content of the database allows the assessment of the main performance characteristics of the devices, some aspect was not fully investigated in the performed tests. In particular the applied axial load was for most of the tests maintained at the constant level indicated as design load. Extreme tests with particularly high loads were also completed but mainly with the purpose of validation of the macroscopic integrity

of the device. The combination of applied action also was oriented to the estimate of performance parameters considered critical for the projects. The lack of a systematic investigation of the bearing performance across a range of realistic vertical loads and testing velocities was the main focus of the present research project. Even though the results obtained cannot be considered representative of all the possible scenarios of conditions experienced by the isolators in their service life, they indicate a range of critical parameters that should be carefully investigated by the designers. The knowledge of the performance characteristics, more sensitive to the above mentioned actions, is in fact critical for two aspects. First of all it should guide a comprehensive program of prototype and production testing for future applications and second, it represents a reference datum to be integrated in the design of effective maintenance and health monitoring approaches.

CHAPTER 1 - LEAD-RUBBER BEARINGS

OBSERVATION FROM PREVIOUS TESTS ON LEAD_RUBBER BEARINGS.

Four different lead-core elastomeric bearings were tested as part of different projects for Caltrans bridge applications. The main bearing characteristics are reported in Table 1. The testing protocols, for the devices were established based on the specific application cases. For this reason, results cannot always be presented in a uniform format. An attempt to extract general information from all set of tests and compare them among different devices was however pursued.

As presented in Table 1, the tested devices are quite different in diameter (1054 mm – 1409 mm), height (489 mm - 773 mm) and lead-core diameter (279 mm – 381). Unit 3 is designed with a different configuration of lead components. Instead of a single cylinder three different cores are placed in a concentric configuration.

All bearings were tested at the Caltrans SRMD testing Facility at University of California San Diego. The SRMD testing facility consists of a 6 DOFs shake table specifically designed for full scale testing of isolators and energy dissipators. The displacement range of the table in longitudinal direction is +/- 1.22 m with a maximum horizontal capacity of 9,000 kN and a vertical load up to 53,400 kN can be applied. The peak velocity of the table longitudinal motion is 1.8 m/s.

The bearings, installed on the SRMD shaking table were connected to an overhead reaction frame. The table, lifted from the at-rest position, applies the required vertical load and maintains the load through the test via a force control algorithm. Figure 1 shows a typical bearing installation in the testing rig. The horizontal motion is instead applied in a displacement control mode, with the shape of the cycle (constant velocity, sinusoidal or other) required by the test specifications. Forces are obtained from the four load cells mounted on each horizontal actuator of the SRMD rig and from pressure transducers. A data correction procedure was applied in order to remove force components due to inertia and machine friction. More information about the testing rig and the data reduction procedure can be found in (Benzoni et al. 1998).

Bearing Characteristics	**1 Coronado**	**2 RSR type A**	**3 RSR type B**	**4 RSR type C**
Diameter of rubber (mm)	1054.1	1257.3	1409.7	1155.7
Cover (mm)	19.0	19.0	19.0	19.0
Lead-core diameter (mm)	279.4	381.0	292.1 3 places	368.3
Overall isolator height (mm)	489.2	773.1	673.1	542.9
Top/Bottom plate diameter (mm)	1117 x 1117	1422 x 1371	1600 x 1473	1117 x 1117
Top/Bottom plate thickness (mm)	44.4	50.8	50.8	44.4
Internal top/bottom plate thickness (mm)	44.4	38.1	38.1	44.4

Table 1 Geometry data

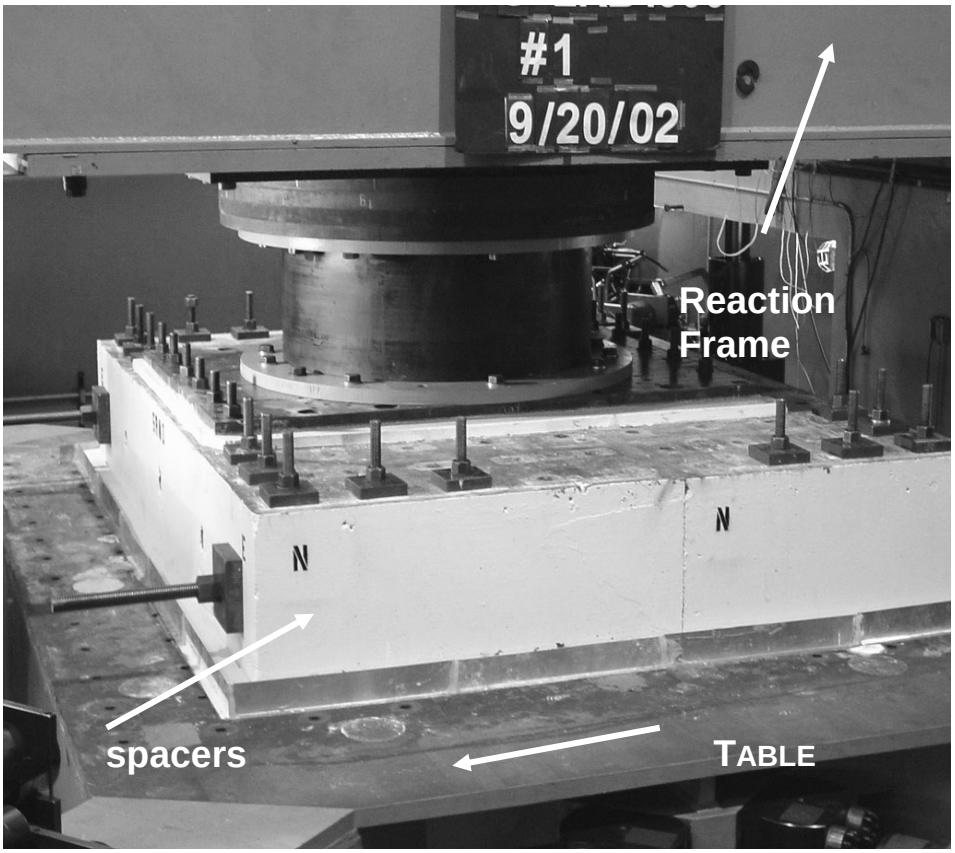

Figure 1 Typical bearing installation

Bearing 1											
Test	**1**	**2**	**3**	**4**	**5**	**6**	**7**	**8**	**9**	**10**	**11**
Speed (m/s) Freq. (Hz)	1.51 0.5	0.37 0.5	0.75 0.5	1.13 0.5	1.51 0.5	1.51 0.41	1.51 0.5	1.51 0.5	1.51 0.5	1.51 0.5	
# cycles	3	3	3	3	3	5	5	5	5	3	
Shear strain (%)	158	40	79	119	158	190	158	158	158	158	
Compression Load (kN)	2482	2482	2482	2482	2482	2482	2482	2482	2482	2482	

Bearing 2											
Speed (m/s) Freq. (Hz)	0.005 0.001	0.472 0.45	0.942 0.45	1.414 0.45	1.52 0.36	1.52 0.36	1.52 0.36	1.52 0.36	1.52 0.36	1.52 0.30	1.52 0.30
# cycles	4	4	4	4	3	3	3	3	3	3	3
Shear strain (%)	165	41	83	124	165	165	165	165	165	198	198
Compression Load (kN)	3403	3403	3403	3403	3403	3403	3403	3403	3403	4884	2402

Bearing 3											
Speed (m/s) Freq. (Hz)	0.005 0.001	0.327 0.45	0.652 0.45	0.980 0.45	1.31 0.45	1.31 0.45	1.31 0.45	1.31 0.45	1.31 0.45	1.52 0.44	1.52 0.44
# cycles	4	4	4	4	4	4	4	4	4	3	3
Shear strain (%)	137	34	69	103	137	137	137	137	137	165	165
Compression Load (kN)	6806	6806	6806	6806	6806	6806	6806	6806	6806	9764	2958

Bearing 4											
Speed (m/s) Freq. (Hz)	0.005 0.002	0.269 0.48	0.538 0.48	0.810 0.48	1.079 0.48	1.079 0.48	1.079 0.48	1.079 0.48	1.079 0.48	1.295 0.48	1.295 0.48
# cycles	4	4	4	4	4	4	4	4	4	3	3
Shear strain (%)	113	28	57	85	113	113	113	113	113	136	136
Compression Load (kN)	3403	3403	3403	3403	3403	3403	3403	3403	3403	4884	2402

All tests repeated in 90 deg. direction

Table 2 Test Protocol of Lead-Rubber Bearings for Different Caltrans Projects

The results presented here refer to the prototype devices, tested under a wide range of shear strain and velocity. Testing conditions are reported in Table 2. All the bearings were tested under a complete protocol in one direction of motion and re-tested under identical conditions in a perpendicular direction. Time between all the tests was allowed to restore ambient temperature for the device. Temperature was measured only at the surface of the bearings, due to the lack of internally located sensors. For each test a sinusoidal motion was required, symmetric in amplitude with respect to the zero position of the bearing. Particular attention was dedicated to minimize the level of acceleration at the start and end of the test. For high speed tests, half a loop, at reduced amplitude, was added before and after the desired displacement time history in order to achieve the peak velocity for first and last loop without significant acceleration component. The results associated with the entrance and exit loops were neglected in the following analyses. For this reason, the definition of loop number, used in this report is intended for discussion purposes only.

Bearing Performance Characteristics

Characteristic Strength Q_d

The characteristic strength was calculated as:

$$Q_d = \left[\frac{Q_1^{''} d_{\max}/2 - Q_1^{'} d_{\min}/2}{(d_{\max} - d_{\min})/2} - \frac{Q_2^{'} d_{\max}/2 - Q_2^{''} d_{\min}/2}{(d_{\max} - d_{\min})/2} \right] / 2 \qquad (1)$$

where $Q_1^{'}$, $Q_1^{''}$, $Q_2^{'}$ and $Q_2^{''}$ are the shear forces at 50% of the peak horizontal displacements, as indicated in Figure 2. Displacements $d_{\max}$ and $d_{\min}$ represent the peak shear displacements. Based on Eq. 1, Q_d is obtained as average of the two zero-displacement-force intercepts per cycle of the dotted line (see Figure 2) connecting the experimental points at half the peak shear displacements.

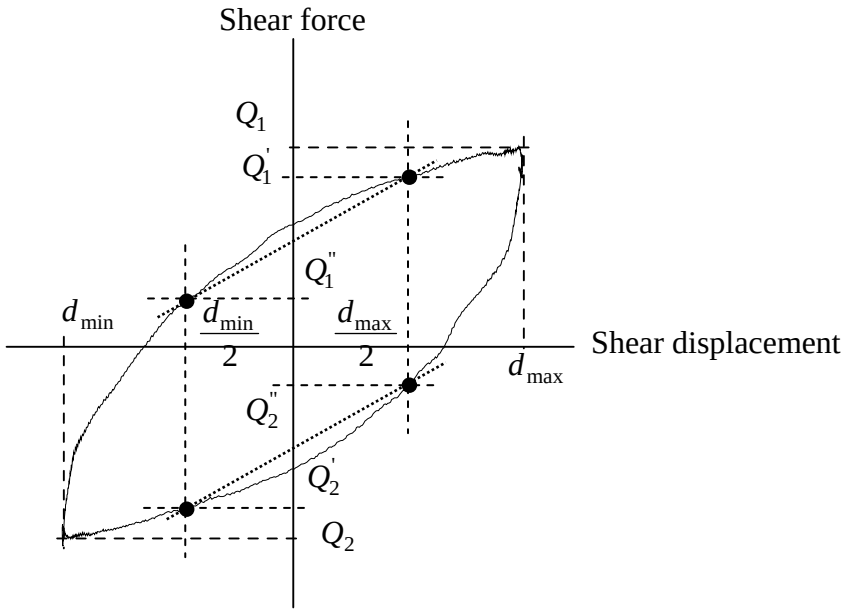

Figure 2- Force-displacement definitions for lead rubber bearings

By definition and due to the sinusoidal shape of the motion, Q_d represents the shear force experienced by the bearing at peak velocity. Each value of Q_d was preliminary normalized with respect to the shear force, at zero displacement, of the corresponding slow speed test. When groups of tests were completed (e.g. repetition of tests in orthogonal direction etc.), results from high speed tests were normalized with the Q_d values from low speed tests of the same group. For bearing 2, 3 and 4, the slow tests were performed at 0.005 m/s. Bearing 1 was instead tested at a minimum velocity of 0.37 m/s, considered here too high to provide an effective influence of the testing velocity. For this reason the results from bearing 1 were not included in Figure 3 that shows the normalized characteristic strength (Q_{dn}), for different cycles and testing velocity

An increase of Q_d with testing speed is visible in Figure 3, with a peak of about 1.45 at 1.52 m/s for the first loop. The ratio reduces for the subsequent cycles and the effect of velocity reaches its peak at progressively lower speed. For the 4th cycle a maximum increase of shear force of about 10% of the experimental force at low velocity is achieved. Scatter around the polynomial (2nd order) trend-line is higher for the third and fourth cycle.

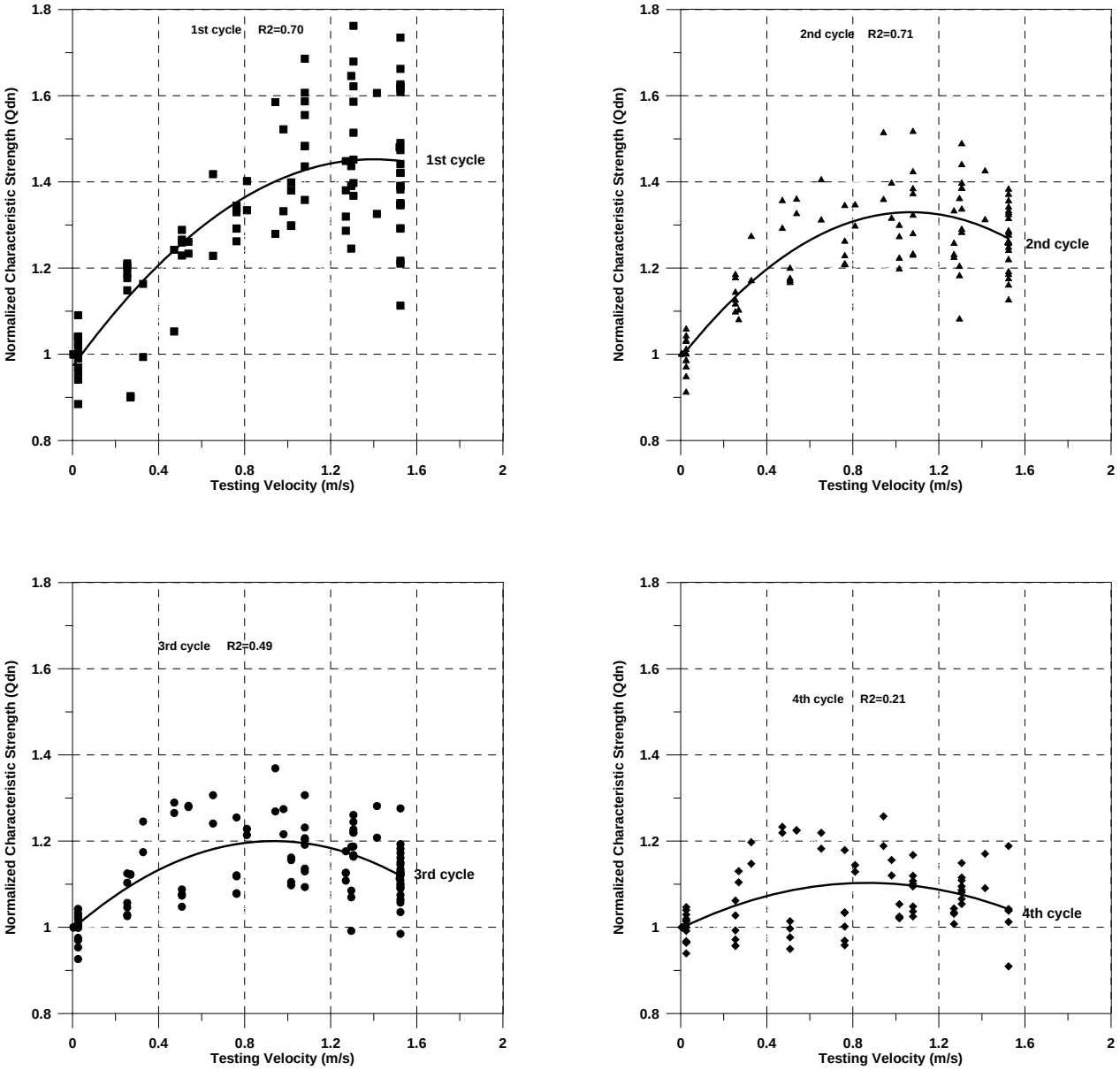

Figure 3 – Normalized Characteristic Strength Function of Peak Velocity

To compare the results from different tests, the ratio between characteristic strength for the ith cycle, Q_{di} and the force for the third cycle, Q_{d3}, is presented in Figure 4. The choice of the third cycle, as a reference, is arbitrary but has the advantage of providing results far away for the start and the end of the test. For all the bearings the trend indicates a major reduction in yield force from the first to the second cycle for high speed tests. The subsequent reduction from the second cycle to the third one and from the third one to the fourth one is almost constant. The scatter of the results appears also to be less pronounced for high speed than low speed tests. The average values

of the ratio Q_{di}/Q_{d3} for cyle 1, 2 and 4 and high velocity tests are 1.46, 1.16 and 0.89, compared with the values 1.24, 1.05 and 0.97 of the low speed tests. Test repetitions (2^{nd} set or 90 degrees tests) do not involve a significant variation in characteristic strength.

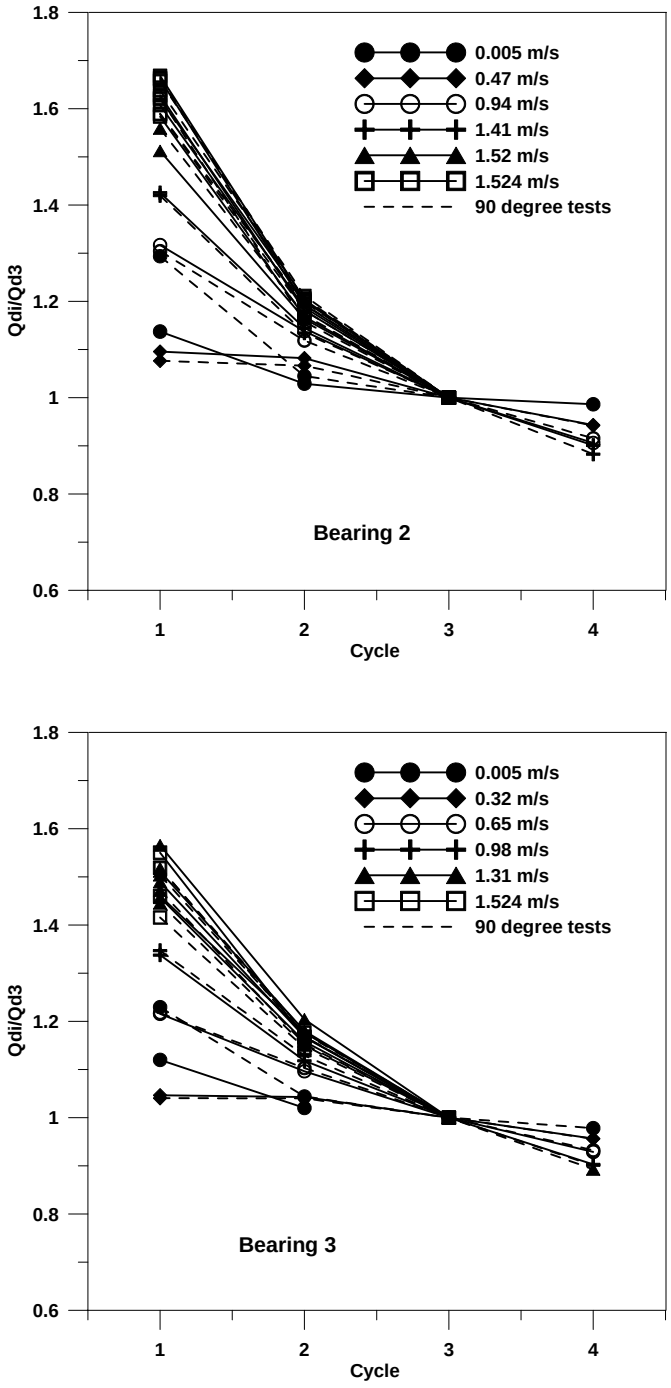

Figure 4 Ratio of Characteristic strength for Each Cycle to the Force of the Third Cycle

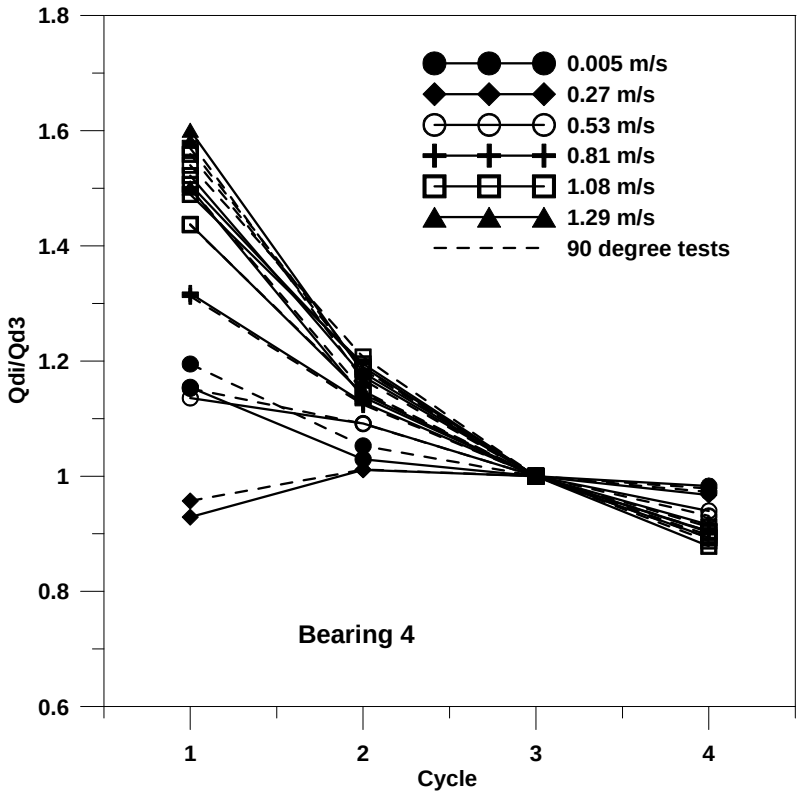

Figure 4 (cont.) Ratio of Characteristic strength for Each Cycle to the Force of the Third Cycle

Effective and post-yield stiffness.

Effective stiffness was calculated, for each cycle of loading, as indicated in the AASHTO Guide Specifications [AASHTO, 2000]:

$$K_{eff} = \frac{F_p - F_n}{\Delta_p - \Delta_n} \tag{2}$$

where Δ_p and Δ_n are the maximum positive and negative shear displacements, respectively, and F_p and F_n are the values of shear force at maximum and minimum displacement, respectively.

The post-yield stiffness K_d was calculated by the equation:

$$K_d = \left[\frac{Q_1^{'} - Q_1^{''}}{(d_{\max} - d_{\min})/2} + \frac{Q_2^{''} - Q_2^{'}}{(d_{\max} - d_{\min})/2} \right] / 2 \tag{3}$$

where $Q_1^{'}$, $Q_1^{''}$, $Q_2^{'}$, $Q_2^{''}$, $d_{\max}$ and $d_{\min}$ are indicated in Fig. 2.

Figure 5 presents the effective and post-yield stiffness results, for bearing 2,3 and 4. For bearing 1, as indicated above, the results for low speed testing are not available. The reported results are relative to devices tested at the same shear strain for the two extreme velocity values. Comparison between slow and fast testing indicates a general increase of effective stiffness with testing speed particularly evident for the first cycle. For the first test, the un-scragged properties of the bearing can justify the higher values of stiffness associated to the initial phase of testing. The apparent recovery of the elastomer characteristics, for the first slow test, after the high speed sequence (90 degree test), appears consistent with observations by other authors (Thompson et al,m 2000) (Constantinou et al., 1999). The sequence of high speed tests could, in fact, have generated internal increase of temperature, associated to more rapid and complete recovery.

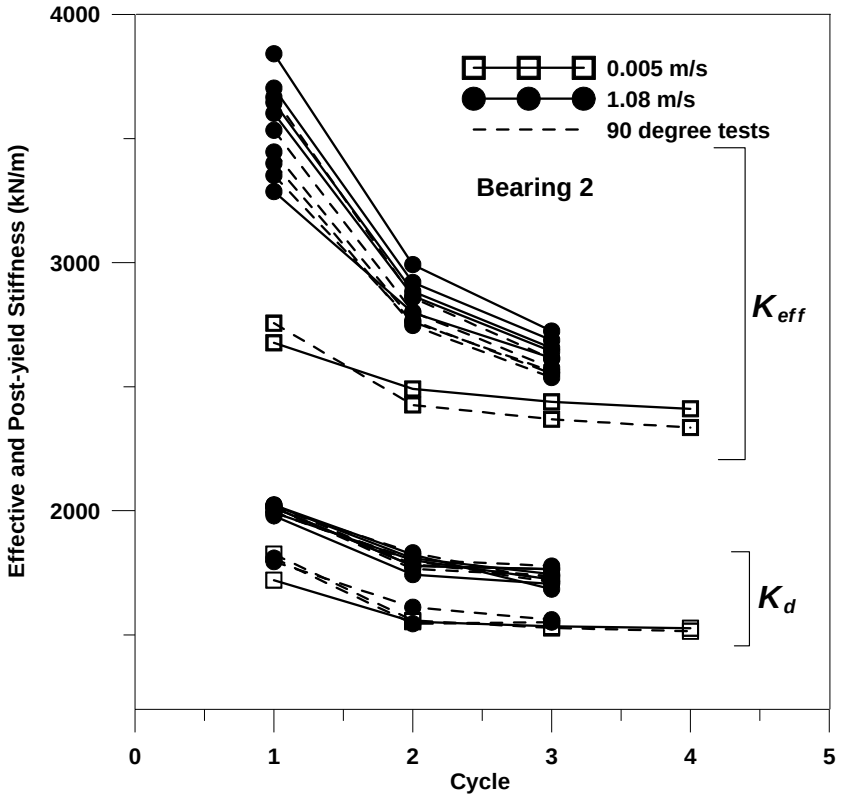

Figure 5 Effective and Post-yield Stiffness for Bearing 2

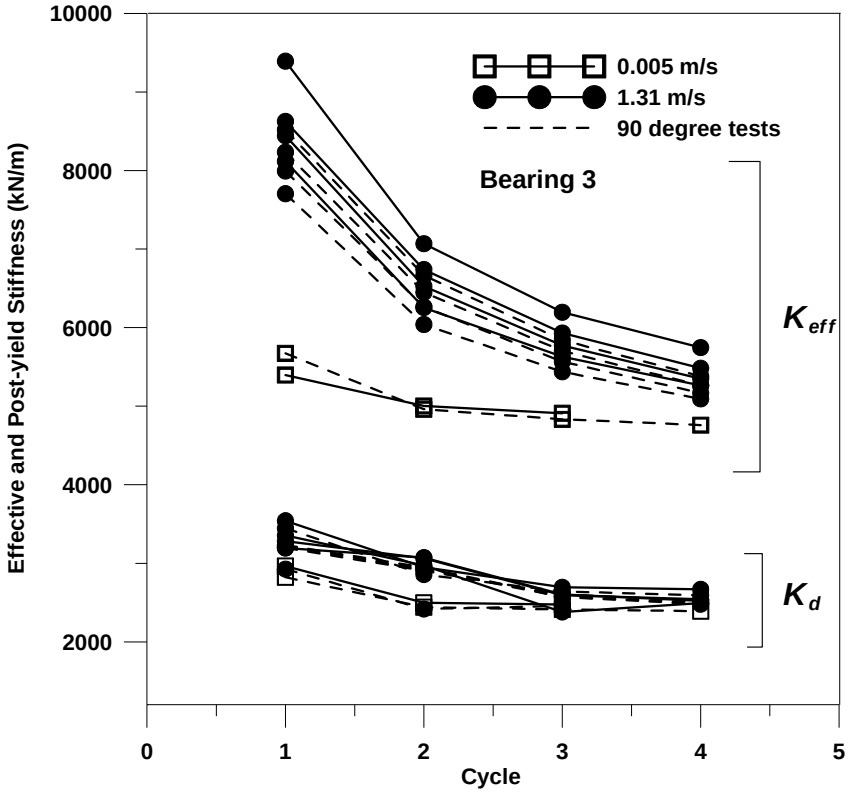

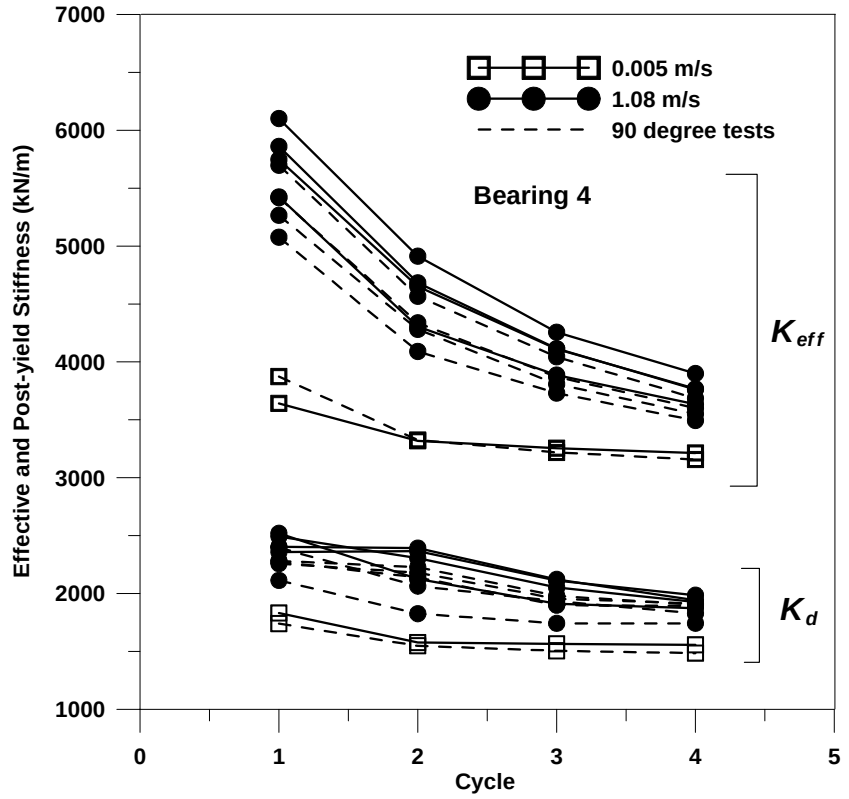

Figure 5 (cont.) Effective and Post-yield Stiffness for Bearing 3 and 4.

The results for tests at high velocity show a larger scatter than for low speed tests, at least for the first two cycle. The K_{eff} values for cycle 3 and 4 are more uniform despite the significant differences in bearing design. Average values indicate, for bearing 2, an increase of effective stiffness from low to high speed tests equal to 30%, 15% and 0.9% at cycle 1, 2 and 3, respectively. Bearing 3 and 4 show an higher increase equal to 50%, 32%, 20% and 13% for cycles 1 to 4, respectively.

The post-yield stiffness values (K_d) indicate a less significant variation with testing speed. The maximum variation in post-yield stiffness is associated with bearing 4 showing an increase of K_d equal to 37.7%, 51%, 36% and 29% for cycle 1, 2, 3 and 4, respectively. The stiffness reduction between cycles does not appear to be substantial.

Damping

The comparison of test results, in terms of damping ratios is reported in Figure 6. For each bearing, data at constant shear strain and at both low and high testing velocity were used.

The damping ratios were calculated as:

$$\varsigma_{eq} = \frac{1}{2\pi}\frac{EDC}{K_{eff}\Delta^2} \qquad (4)$$

were EDC represents the hysteresis loop area and Δ is the average between the positive and negative peak displacements.

Only the data for bearing 2, 3 and 4 allow for the comparison between damping characteristics at the boundary values of test velocities, for motions at constant shear strain. For Bearing 2, the maximum increment of damping ratios, from low to high speed tests, are 17% 11% and 3.8% for first, second and third cycle, respectively. The variations were obtained as an average between the results of tests in two orthogonal direction of motion (0 deg. and 90 deg). For bearing 3 increments with velocity are reduced to 7%, 4.5% and 1.3% from first to third cycle. Bearing 4 instead indicates an increase in equivalent damping only associated to the first three cycles, in the order of 12%, 5% and 3%, respectively.

It must be noted that bearing 2, 3 and 4 represent devices with very large diameter lead cores. Further research should be developed to associate variations of damping ratios (together with other performance characteristics) with the lead-core dimensions.

Based on the limited results presented here, it appears that the increments in damping ratios with velocity are particularly significant for the devices with larger lead core.

Bearing 1 shows a significant reduction of the ratio ς_{eq} from cycle 1 to 5, equal to approximately 34%.

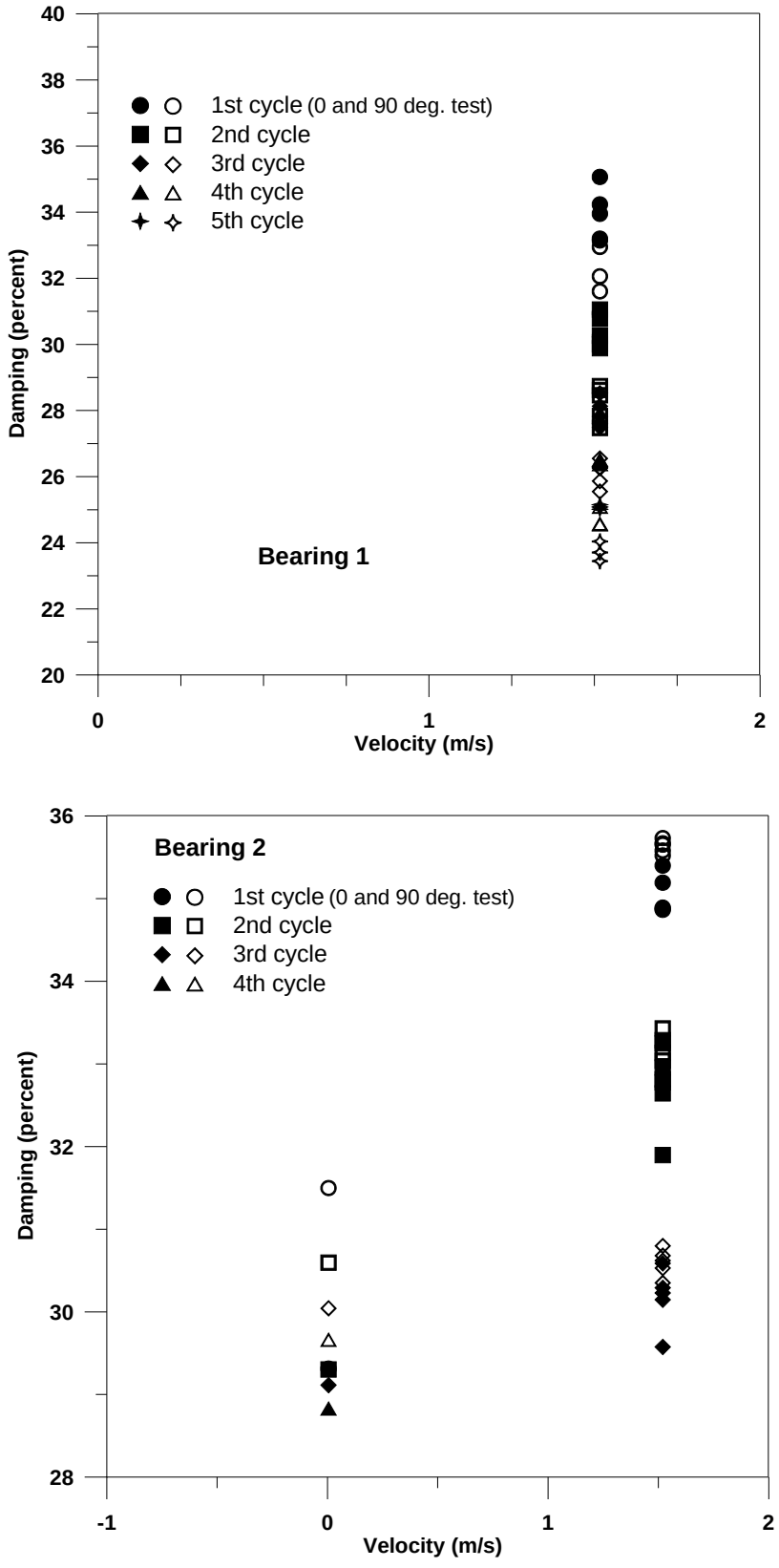

Figure 6 Damping Ratio versus Testing Velocity (Bearing 1 and 2)

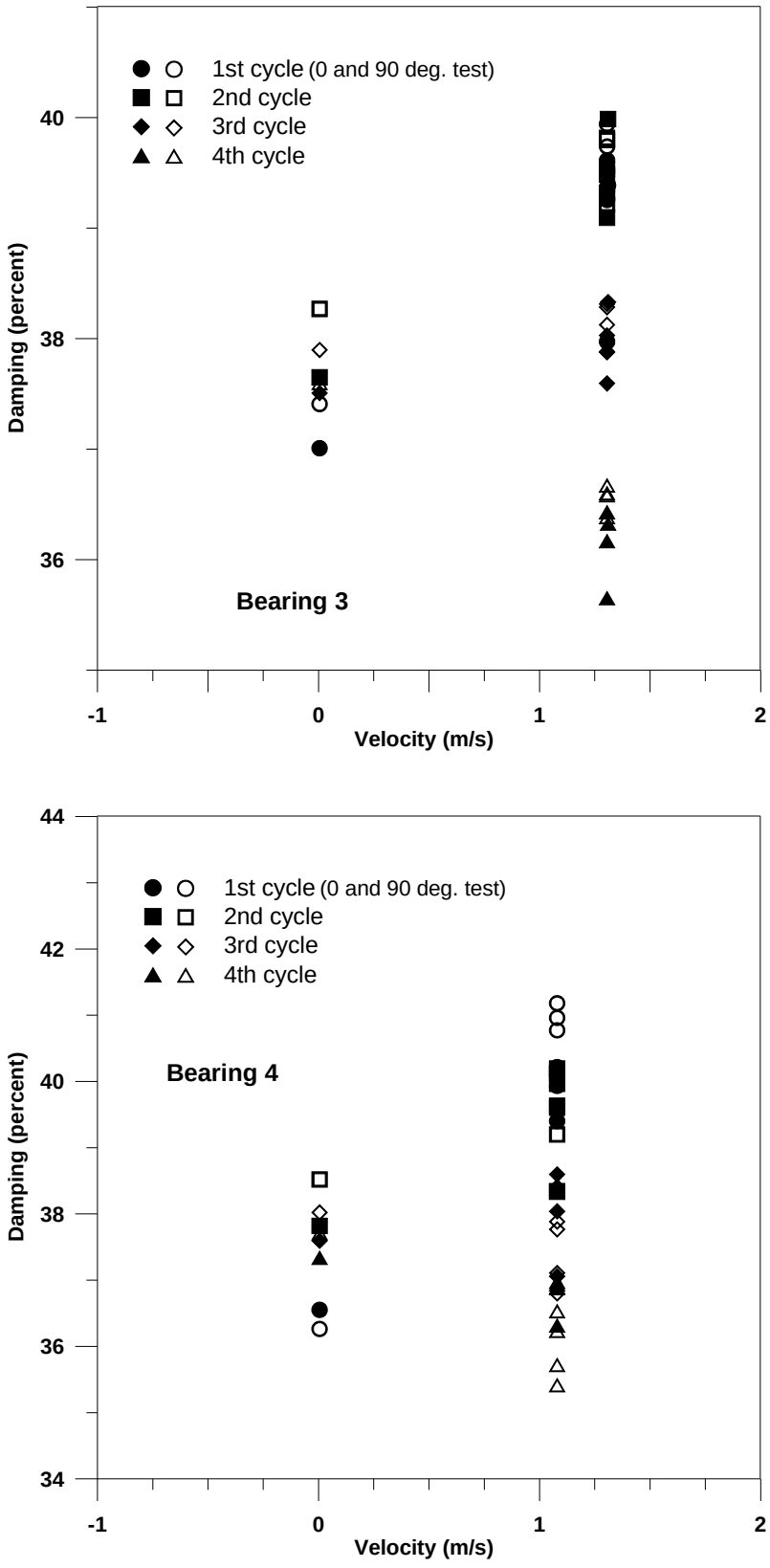

Figure 6 (cont.) Damping Ratio versus Testing Velocity (Bearing 3 and 4)

NEW TESTS

As visible from Table 2, the existing database was lacking a systematic investigation of the effects of the vertical load and testing velocity. Results are difficult to compare due, for instance, to the different ranges of shear strain applied and the largely different bearing characteristics. In order to evaluate specifically the effects of vertical load, test velocity and repetition of cycles on the bearing performance, a single bearing, identical in characteristics to the one included in Table 1 as Bearings 1, was tested under a specifically designed testing protocol.

The bearing was tested at the Caltrans Seismic Response Modification Device (SRMD) Testing Facility at the University of California San Diego campus. For this specific tests the specimen was installed and connected to the table surface and to the overhead vertical reaction frame as described above for previous tests and shown in Figure 1.

Details of the experimental program are reported in Table 3. In order to obtain results for the three required cycles not corrupted by the effects of the table acceleration at the beginning and end of the tests, an entrance and exit half loop was introduced. The amplitude of these starting and ending ramps was equal to the maximum test amplitude and the required peak velocity was achieved at the point of zero horizontal displacement. Figure 7 shows a typical displacement time history commanded to the table. It is visible the entrance and exit portion of the displacement time history (dashed line) that results in a total travel of four full cycles at peak amplitude. A sinusoidal waveform was utilized for all the tests. The definition of loop number is based on the exclusion of the entrance and exit ramps.

The selection of the vertical load range and of the test frequency was motivated by the focus of this project to study the effects of the applied vertical load and the test peak velocity (strain rate). For this reason, the peak displacement applied was maintained constant for all the tests at a value equivalent to 100% shear strain. The vertical load ranges between 2224 kN and 5783 kN for all the test velocity sets. The design vertical load for this specific bearing and for its specific bridge application was 2480 kN. A lower limit for the vertical load (1335 kN) was also included in test cb10. The results of this test and of test cb16, however, are not included in the present study due to difficulties experienced in maintaining a constant vertical load during very high speed tests. It must be noted, in fact, that the amplitude of the applied vertical load for these tests (1335 kN and 2224 kN) is very low compared with the full capacity of the testing machine (53400 kN).

Test name	Vertical load	Displ.	Shear Strain	Freq.	Peak Velocity	No. cycles	Waveform
	(kN)	(mm)	%	(Hz)	(mm/s)		
cb1	2224	304.8	100	0	0.762	3	sine
cb2	4004	304.8	100	0	0.762	3	sine
cb3	5783	304.8	100	0	0.762	3	sine
cb4	2224	304.8	100	0.186	355.6	3	sine
cb5	4004	304.8	100	0.186	355.6	3	sine
cb6	5783	304.8	100	0.186	355.6	3	sine
cb7	2224	304.8	100	0.371	711.2	3	sine
cb8	4004	304.8	100	0.371	711.2	3	sine
cb9	5783	304.8	100	0.371	711.2	3	sine
cb10	1335	304.8	100	0.5	957.58	3	sine
cb11	2224	304.8	100	0.5	957.58	3	sine
cb12	3114	304.8	100	0.5	957.58	3	sine
cb13	4004	304.8	100	0.5	957.58	3	sine
cb14	4893	304.8	100	0.5	957.58	3	sine
cb15	5783	304.8	100	0.5	957.58	3	sine
cb16	2224	304.8	100	0.663	1270	3	sine
cb17	4004	304.8	100	0.663	1270	3	sine
cb18	5783	304.8	100	0.663	1270	3	sine
cb19	3114	304.8	100	0.5	957.58	6	3 cycles at 76.2 mm 3 cycles at 304.8 mm
cb20	3114	304.8	100	0.5	957.58	6	2 cycles at 76.2 mm, 2 cycles at 152.4 mm 2 cycles at 304.8 mm

Note: test cb8 was repeated as test cb8b

Table 3. Testing Summary (New Tests)

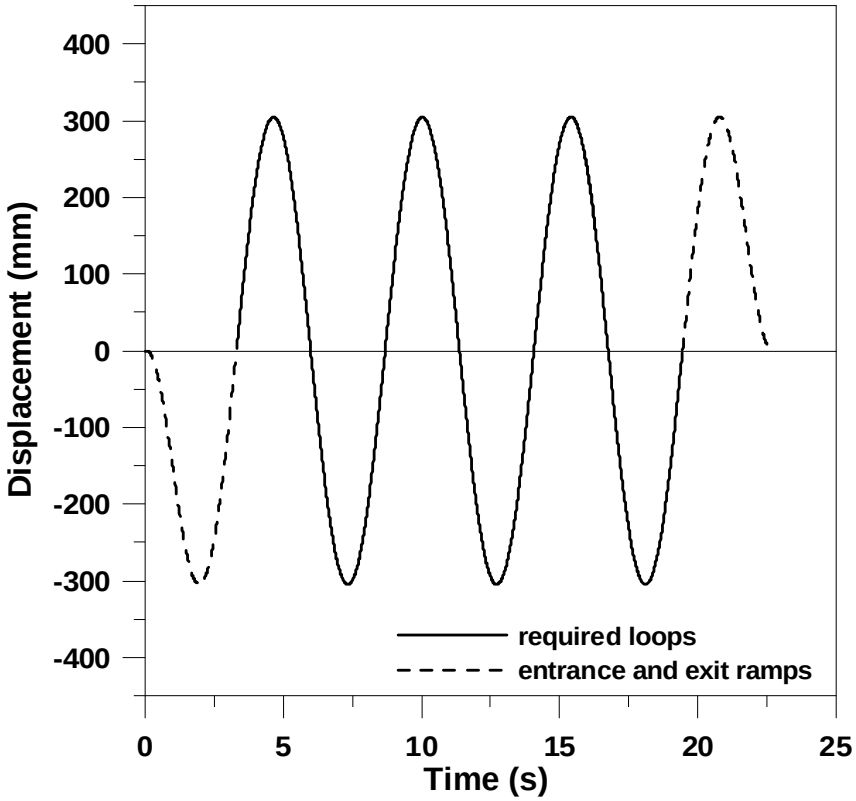

Figure 7. Typical test displacement time history

When this situation is coupled with a motion of the table at very high speed, difficulties can be experienced in maintaining a constant value of applied vertical load.

Tests cb1, cb2 and cb3 represent the low velocity tests and were used as a reference to study the effects of the higher strain rates. Test cb19 and cb20 were designed to investigate the response variation of the device for a gradual increase of the displacement amplitude. For test cb19 the peak displacement cycles are anticipated by three cycles at 25% shear strain and for test cb20 the maximum amplitude is obtained after cycling at 25% and 50% shear strain. Tests were conducted with an interval of 30 min between subsequent runs in order to re-condition the bearing to a common level of initial temperature.

Peak Shear Force

The absolute maximum positive and negative shear force for each test and for the three loops are reported in Figure 8 (a, b, c and d) versus the test peak velocity and the applied vertical load.

Figure 8(d) shows the average of positive and negative peak force values for each loop. Despite the scatter of results, at a given vertical load, due to the effect of the test velocity, it is visible the limited effect of the vertical load on this response parameter, over the vertical load range. This is also confirmed by Figure 8(a), 8(b) and 8(c) when compared to each other. Figure 8(d) shows the results of two additional tests at the intermediate vertical load of 3114kN (cb12) and 4893 kN (cb14).

The peak force associated with the very slow tests (cb1, cb2, cb3) are in a range of approximately 707 kN to 766 kN (Figure A-1), with a maximum reduction between first and third cycle equal to 5%. The effect of the vertical load appears to contribute, for these tests, only for a maximum reduction of 5%, at the first cycle. For tests at higher velocities, the different load levels generate a maximum variation of the peak force values equal to 4% for the first cycle at the velocity of 711.2 mm/s (Figure A-3). From Figure 8 it is visible how the test velocity has more effects on the shear force results than the amplitude of the applied vertical load. As it is shown from Figure 8a, 8b and 8c, the peak force for the first cycles appear to be more sensitive to the strain rate effect, with a maximum increment at peak velocity of 1270 mm/s, with respect to the slow tests, of 70.6%, 73.8% and 64.5% for vertical loads equal to 2224 kN, 4004 kN and 5783 kN, respectively (Figure A-6). For the second and third cycle the previous variations reduce to a consistent average of 45% and 30%, respectively (Figure A-7 and A-8). The performance appears very symmetric between positive and negative forces, except for the first cycle, where the positive results (i.e. the very first peak shear force) exceed the forces in the reversed direction of motion.

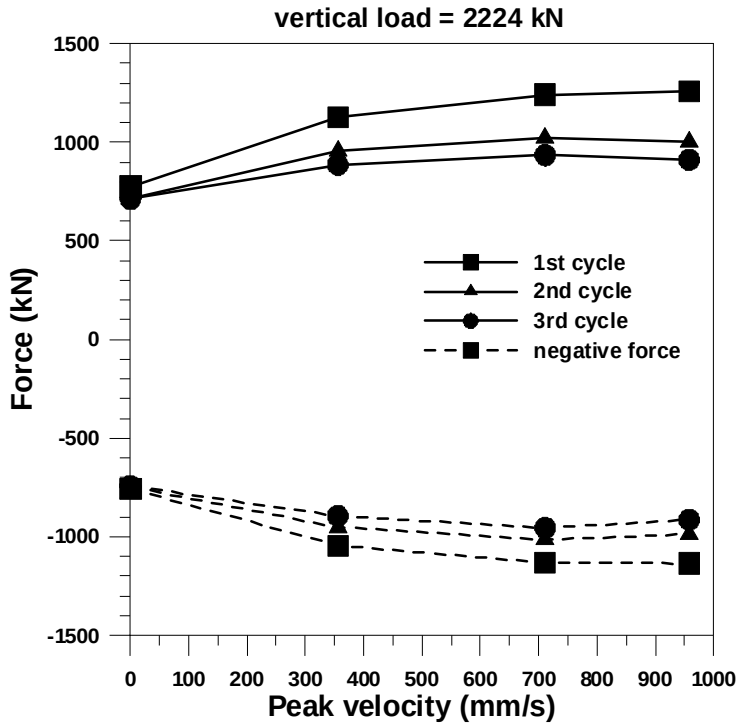

(a)

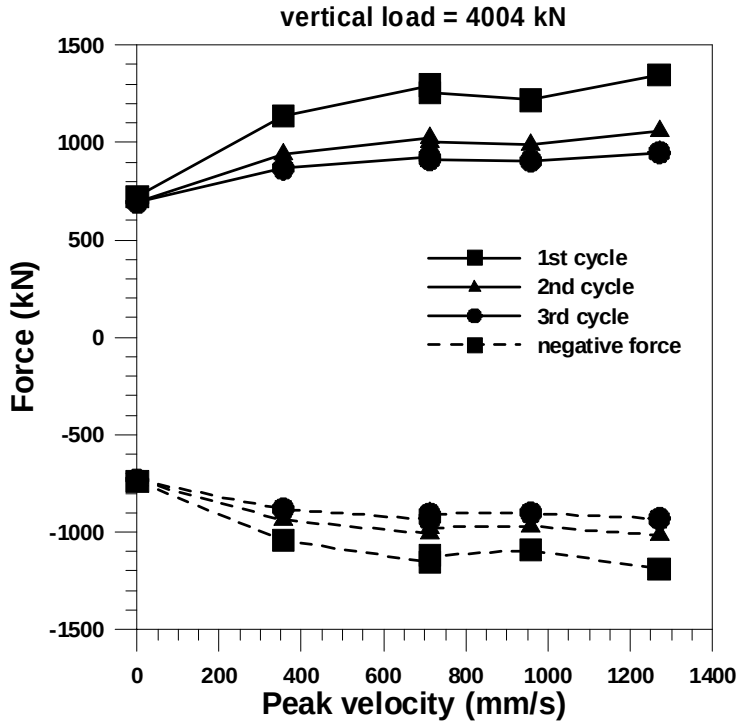

(b)

Figure 8. Peak Shear Forces At Different Testing Speed And Vertical Loads

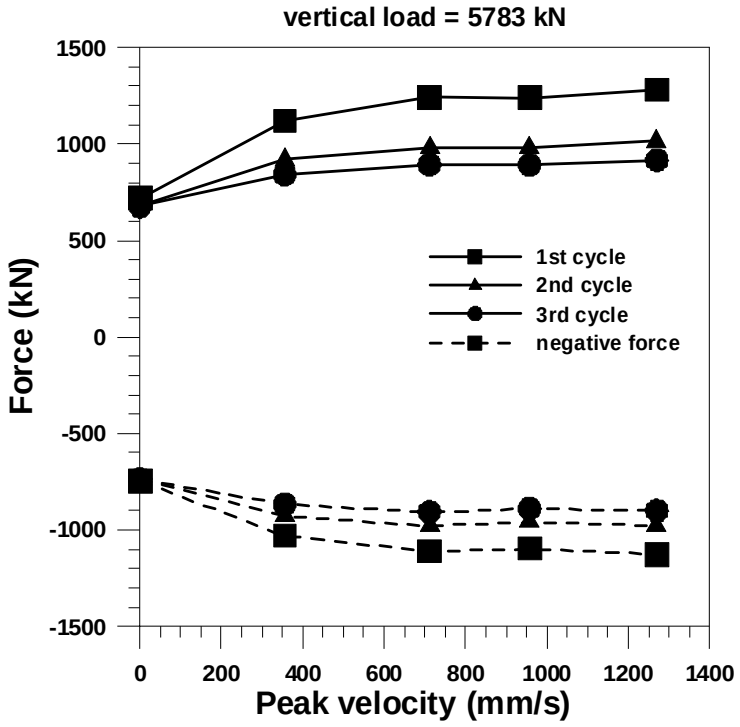

(c)

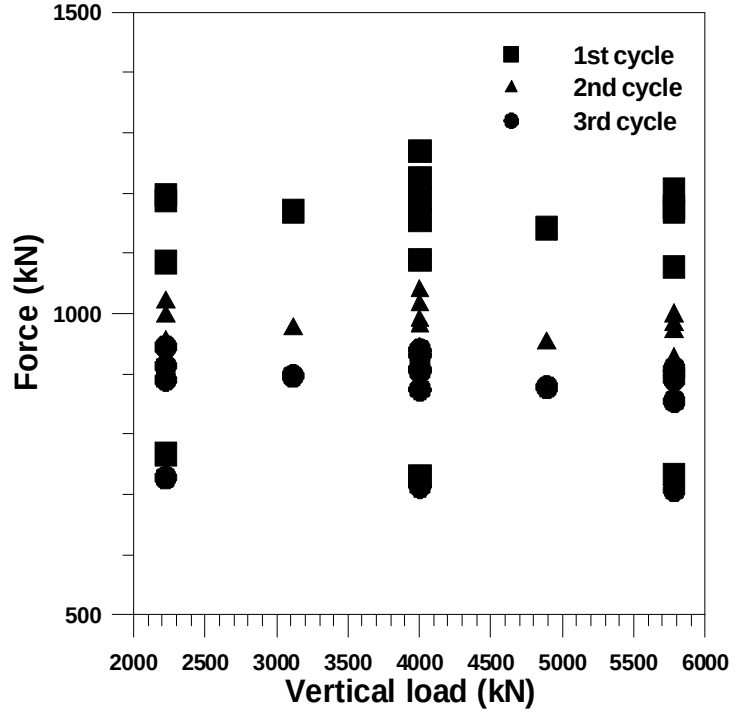

(d)

Figure 8 (cont.) Peak Shear Forces At Different Testing Speed And Vertical Loads

Characteristic strength Q_d

The characteristic strength was calculated as indicated in Eq. 1 and Figure 2.

The calculated values of Q_d are reported in Table 4. Two sets of forces are reported in the same table. The first set (Q_d loop1, loop2, loop3) consists of the characteristic strengths calculated using Equation 1, for each of the three loading cycles. These values will be referred as "calculated" in what follows. The other set (Q_d ex loop1, loop2 loop3), called "experimental", contains the average between positive and negative forces, experimentally recorded at zero displacement. Their variation, in percent, with respect to the forces obtained through Eq. 1 is reported in parenthesis. The disagreement can appear significant with a maximum value of 25%. However, it must be noted that the experimental results often reflect a local response associated with the oscillations in the applied vertical load. For this reason the "calculated" values appear more appropriate for the study of this response parameter and will be used in what follows.

The trend of the effect of the amplitude of the vertical load on the average characteristic strengths (see Figure 9(d)) appears very similar to what observed in terms of maximum force (Figure 8(d)).The maximum change in characteristic strength, at a given speed and for different vertical loads, is equal to 7.6% (occurring at velocity of 711 mm/s). The force values corresponding to the tests at 0.76 mm/s are visualized as the lowest symbols in Figure 9(d), in the range of Q_d =350 to 400 kN. For these low velocity tests, a negligible variation due to repeated cycles is also visible. In general terms, the larger scatter between Q_d values among different velocities is associated with the result of the first cycle. At constant vertical load, Figure 9(a), 9(b) and 9(c) indicate a more significant effect of the strain rate than noticed in terms of peak shear force.

For the first cycle the increasing test velocity is associated to a maximum Q_d increase of 76%, 103% and 89% at the three different vertical load levels, respectively. The variation is reduced for the second cycle to an average increment of 67% and of 46% for the third loop. The peak of characteristic strength is reached at different test velocities, for different vertical loads. It is noticeable the negligible difference between results for slow speed tests.

Test	Vert. load	Peak Vel.	Qd loop 1	Qd loop 2	Qd loop 3	Qd ex. loop 1	Qd ex. loop 2	Qd ex. loop 3
	(kN)	(mm/s)	(kN)	(kN)	(kN)	(kN)	(kN)	(kN)
cb1	2224	0.762	395.09	369.48	369.17	374.31 (-5.5)	355.97 (-3.8)	350.38 (-5.3)
cb4	2224	355.6	637.26	548.28	490.76	710.39	635.62	494.74
						(+11.4)	(+15.9)	(+0.8)
cb7	2224	711.2	694.12	581.72	511.69	772.39	678.72	523.52
						(+11.2)	(+16.6)	(+2.3)
cb11	2224	957.6	664.27	532.3	466.65	734.42	661.51	526.31
						(+10.5)	(+24.2)	(+12.8)
cb12	3114	957.6	654.89	525.9	459.16	715.98	645.45	518.7
						(+9.3)	(+22.7)	(+12.9)
cb2	4004	0.762	377.48	368.79	368.34	386.88	356.23	352.88
						(+2.5)	(-3.5)	(-4.3)
cb5	4004	355.6	659.73	548.45	485.66	724.11	631.26	488.05
						(+9.7)	(+15.1)	(+0.5)
cb8	4004	711.2	747.07	599.86	517.91	812.93	712.36	532.98
						(+8.8)	(+18.7)	(+2.9)
cb8b	4004	711.2	723.01	580.99	499.92	781.67	689.82	517.93
						(+8.1)	(+18.7)	(+3.6)
cb13	4004	957.6	666.38	538.98	471.25	733.44	656.5	523
						(+10.0)	(+21.8)	(+10.9)
cb17	4004	1270	769.44	633.05	554.59	810.69	716.68	509.07
						(+5.3)	(+13.2)	(-8.9)
cb14	4893	957.6	659.65	524.47	458.61	729.48	645.98	511.24
						(+10.6)	(+23.1)	(+11.4)
cb3	5783	0.762	395.29	378.17	376.99	415.81	369.63	365.4
						(+5.2)	(-2.3)	(-3.2)
cb6	5783	355.6	670.4	547.86	482.14	721.2	627.9	483.24
						(+7.5)	(+14.6)	(+0.2)
cb9	5783	711.2	743.53	593.55	509.95	805.39	700.39	525.81
						(+8.3)	(+18.0)	(+3.11)
cb15	5783	957.6	689.77	545.16	476.18	755.25	667.54	532.91
						(+9.5)	(+22.4)	(+11.9)
cb18	5783	1270	746.81	610.28	538.59	795.19	684.44	489.03
						(+6.5)	(+12.1)	(-10.1)

Table 4. Numerical and Experimental Characteristic strength

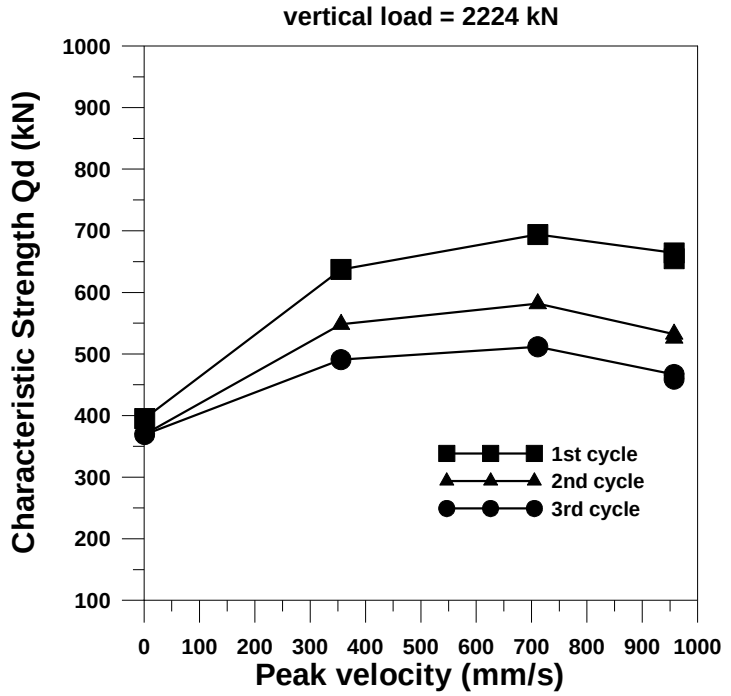

(a)

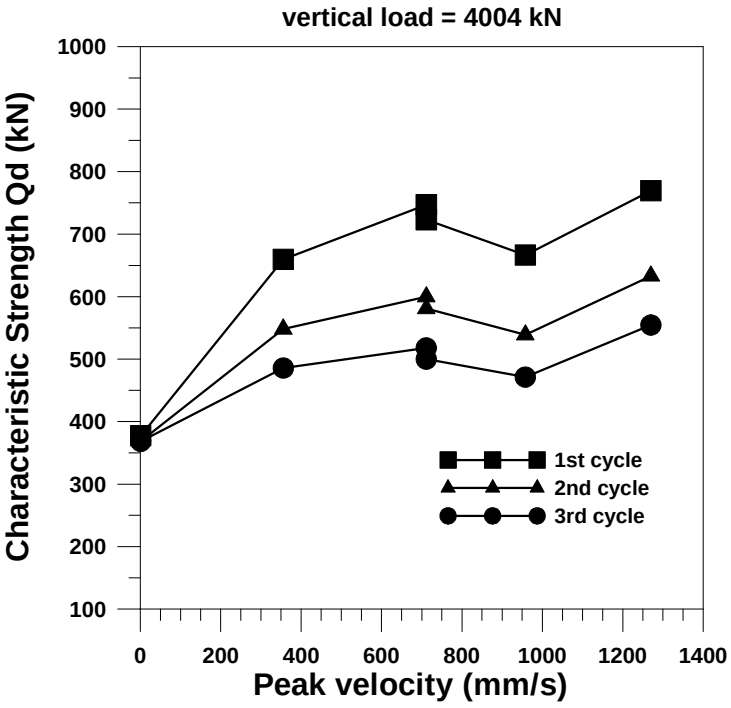

(b)

Figure 9. Characteristic strength for Different Vertical Load and Test Velocity

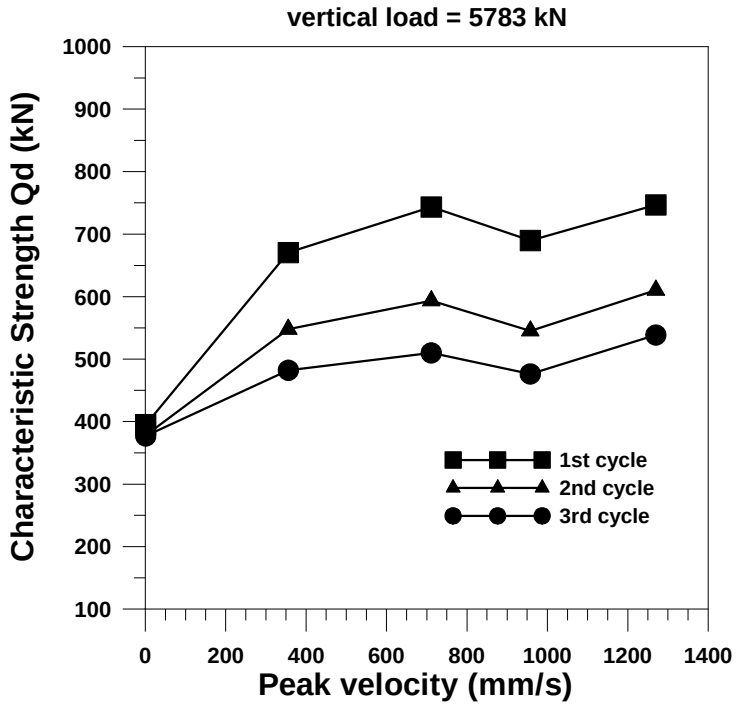

(c)

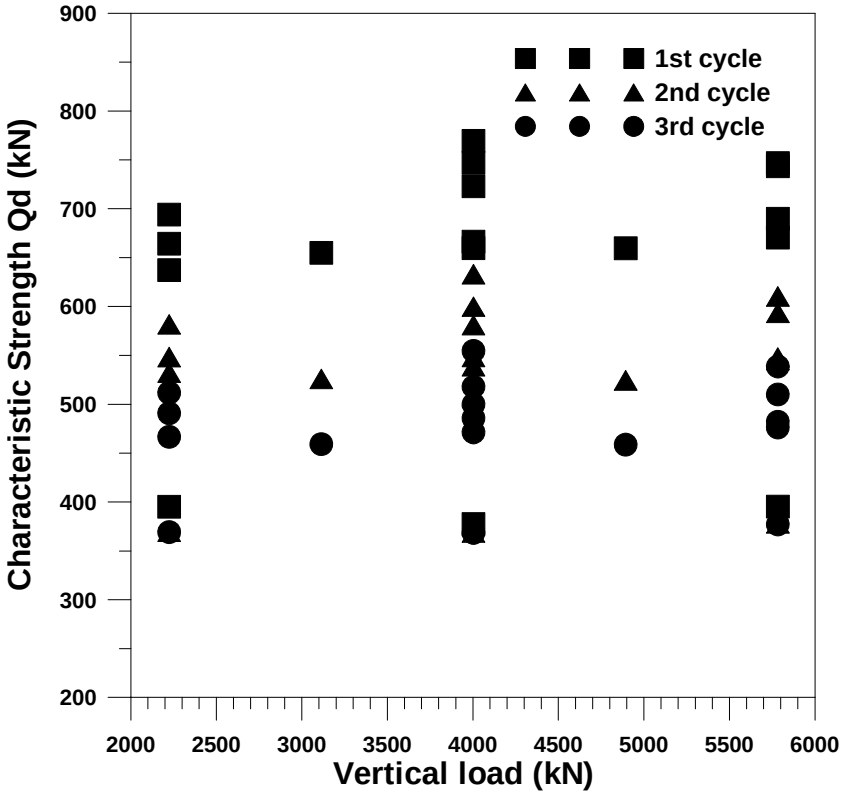

(d)

Figure 9 (cont.) Characteristic strength for Different Vertical Load and Test Velocity

In order to establish a parameter for a new numerical model that takes into account the variation of the characteristic strength between cycles, the results were normalized to the data obtained from the second loop. The approach to refer to a reference cycle allows to compare the results to a sort of "average" performance of the device, isolated from peculiar test conditions introduced at the beginning and the end of the test. The selection is however simply operational, and does not affect the content of the findings. Figure 10(a) and (b) report the Q_d results after normalization to the characteristic strength of the second cycle (Q_{d2}) for different vertical loads and velocities. For bearing performance under high strain rate, an average reduction of 25% and 15% appears to be reasonable for the transition from first to second cycle and from second to third cycle, respectively.

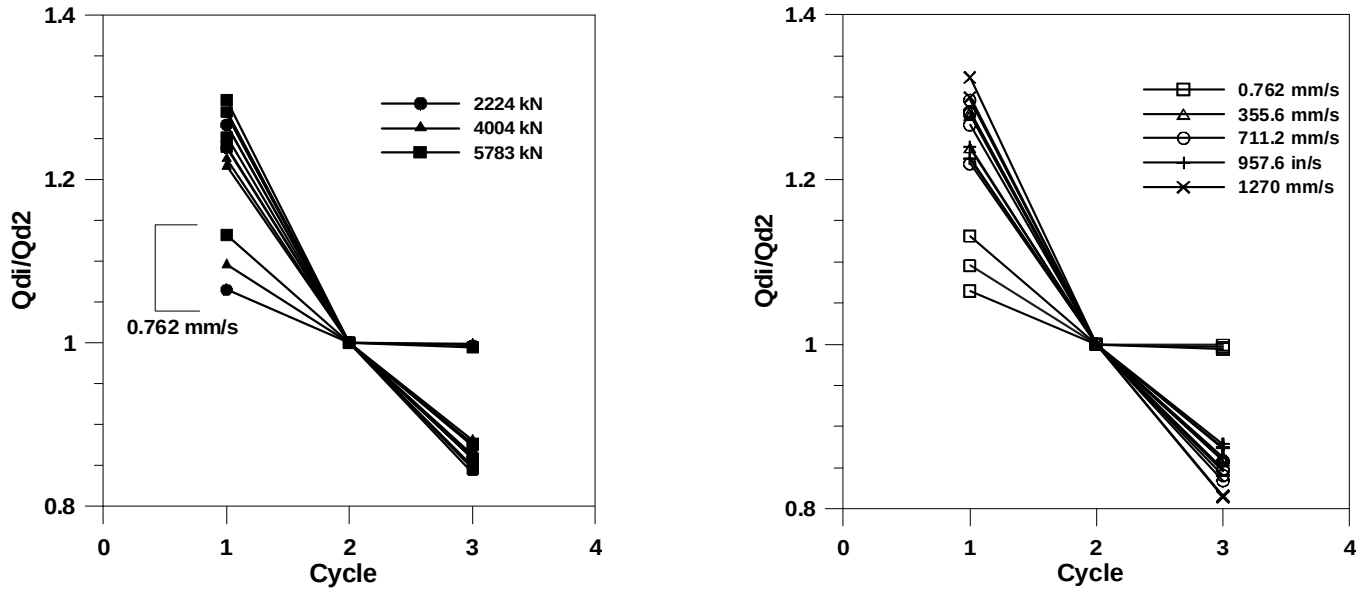

Figure 10. Ratio of Characteristic strength of Each Cycle to the Force of the Second Cycle

Effective (K_{eff}) and Post-Yield Stiffness (K_d)

The effective stiffness and post-yield stiffness were calculated based on Eq. 2 and Eq. 3, respectively.

Figure 11 shows the values of K_{eff} for the set of completed tests plotted versus the peak test velocity. The solid and dashed lines, relative to the different cycles, indicate a negligible difference between responses under different vertical loads. Comparison between slow and fast motions indicates instead a general increase of effective stiffness with speed, particularly evident for the first cycle. The peak increment of the effective stiffness due to the test velocity confirms the constant trend across the range of vertical loads and was calculated as 52%, 34% and 22% for the first, second and third cycle, respectively.

The normalization of the effective stiffness to the value of the second sinusoidal loop, plotted in Figure 12(a) and (b), indicates a wider scatter of results for the first cycle, for both load and velocity variation. The spread of results appears instead limited for the third cycle. The average value of the normalized effective stiffness for the first and third cycle is 1.2 and 0.95, respectively, for tests at high speed. The reduction of K_{eff} for slow speed tests appears to take place only between first and second cycle, with a decrease of about 5%.

The post-yield stiffness results (K_d) are plotted in Figure 13 and indicate a slightly higher effect of the applied vertical load compared to what obtained in terms of effective stiffness. It is visible a uniform reduction with cycling loading and a consistent peak value achieved at a maximum test velocity of 958 mm/s. For all the cycles and the test velocity values, the increase of vertical load is associated with a reduction of post-yield stiffness. Table 5 reports the maximum variation, in percentage, at different velocity levels. The effect of the test velocity is quite significant for the first cycle with an average increase of 60% for higher strain rate with respect to the slow tests. For successive loops the increase of K_d at high test speed follows a trend consistent with what observed for the first cycle of motion and reaches an average of about 50% and 40% for the second and third cycle, respectively. Figure 14(a) and 14(b) present the normalized values of K_d, with respect to the result of the second cycle, for the considered range of vertical loads and test velocities. For the high speed tests the average ratio of the K_d's in each cycle to the K_d value of the second cycle is 1.15 and 0.93 for the first and third cycle, respectively.

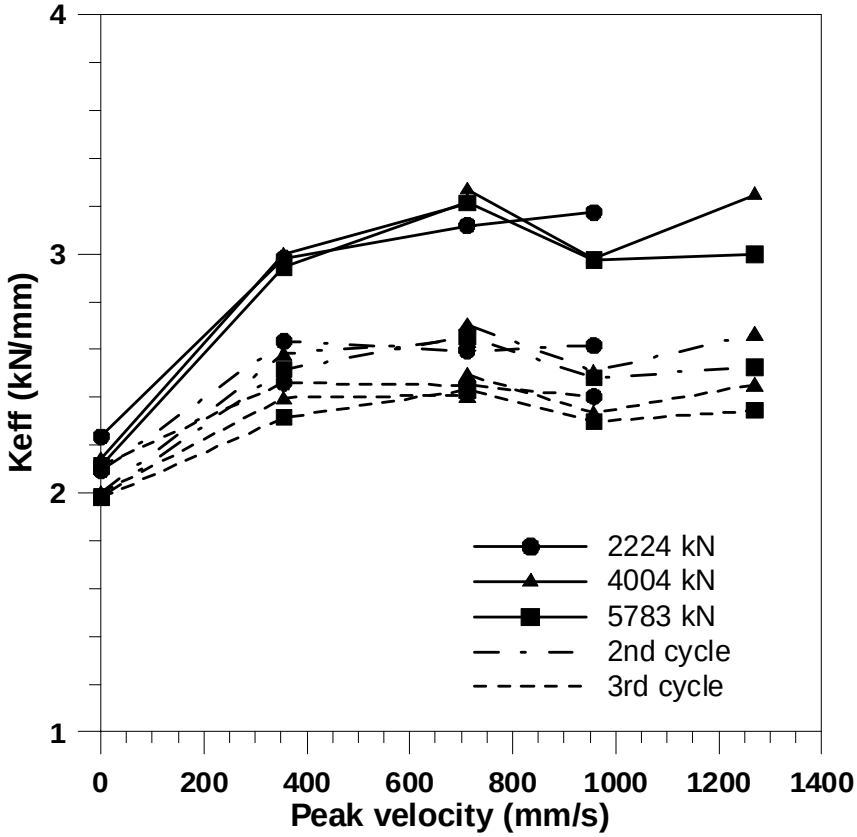

Figure 11. Effective Stiffness vs Testing Speed and Vertical Loads

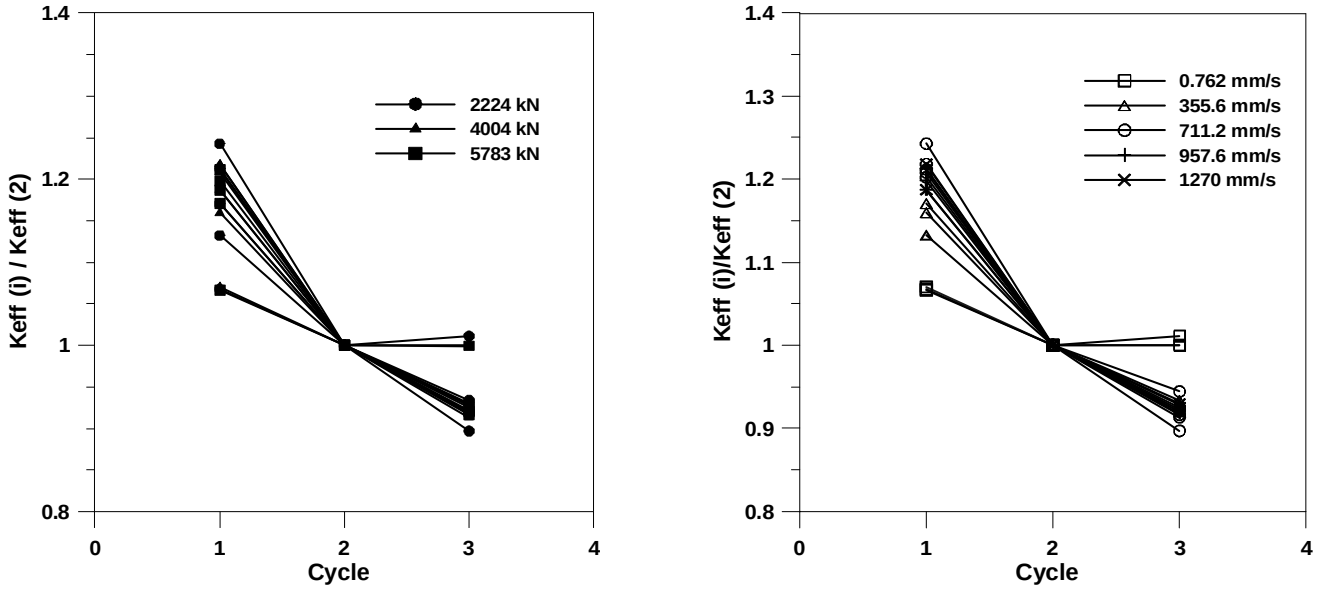

(a) (b)

Figure 12. Normalized Effective Stiffness Function of Vertical Load and Test Velocity

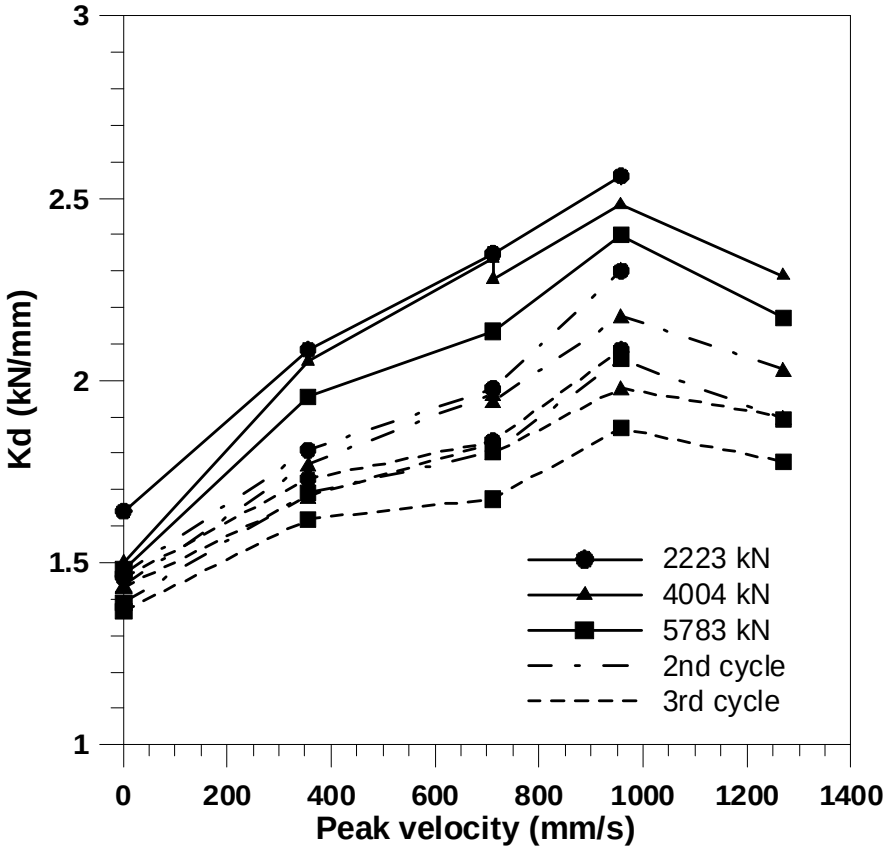

Figure 13. Post-Yield Stiffness vs Testing Speed at different Vertical Loads

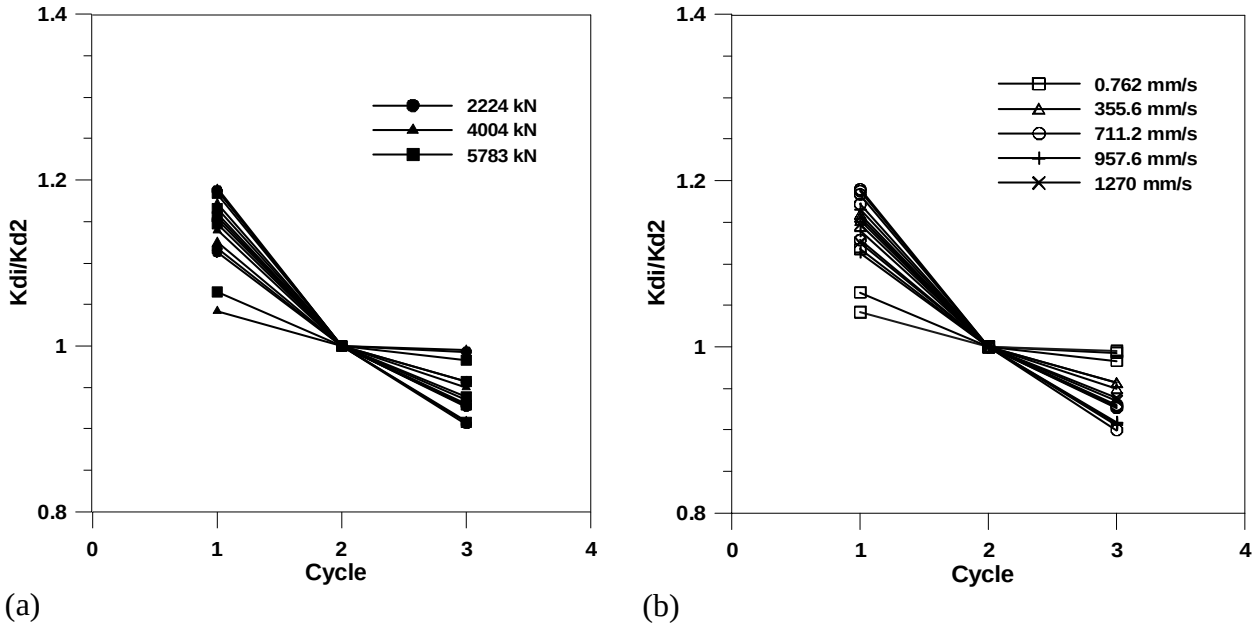

Figure 14. Normalized Post-Yield Stiffness

Cycle	v = 0.762 mm/s	v = 355.6 mm/s	v = 711.2 mm/s	v = 957.6 mm/s	v = 1270 mm/s
1	-9.7	-6.2	-12.0	-6.6	-4.8
2	-4.8	-6.1	-15.8	-10.8	-6.9
3	-6.8	-6.5	-13.4	-10.5	-6.8

Table 5. Maximum reduction (%) of K_d due to increasing vertical load, for different test velocities and cycles

Damping

The comparison of test results at constant shear strain and low and high testing velocity is reported in Figure 15, in terms of damping ratio .

The damping ratios were calculated consistently with Eq. 4.

The effects of the vertical load on the damping ratio results appears limited with maximum variation equal to 5-10% for the first cycle, 5-12% for the second cycle and 5-13% for the third cycle. The higher influence was noticed for the tests at very slow velocity.

More visible effects are observed due to the variation of peak velocity. For the first cycle a constant increase of damping ratio, equal to 29%, is associated with high velocity tests when compared with slow tests, as a clear consequence of the increase of the shear forces with the velocity. This increase is experienced for all the values of vertical load. The increment reduces to an average of about 19% and 14% for the second and third cycle, respectively. For the second and third cycle, the increase in damping ratio, due to velocity effects, decreases with increasing vertical loads.

The normalized plots of Figure 16 clearly show the scatter of results particularly in terms of variation of the damping ratio from the first cycle to the second cycle.

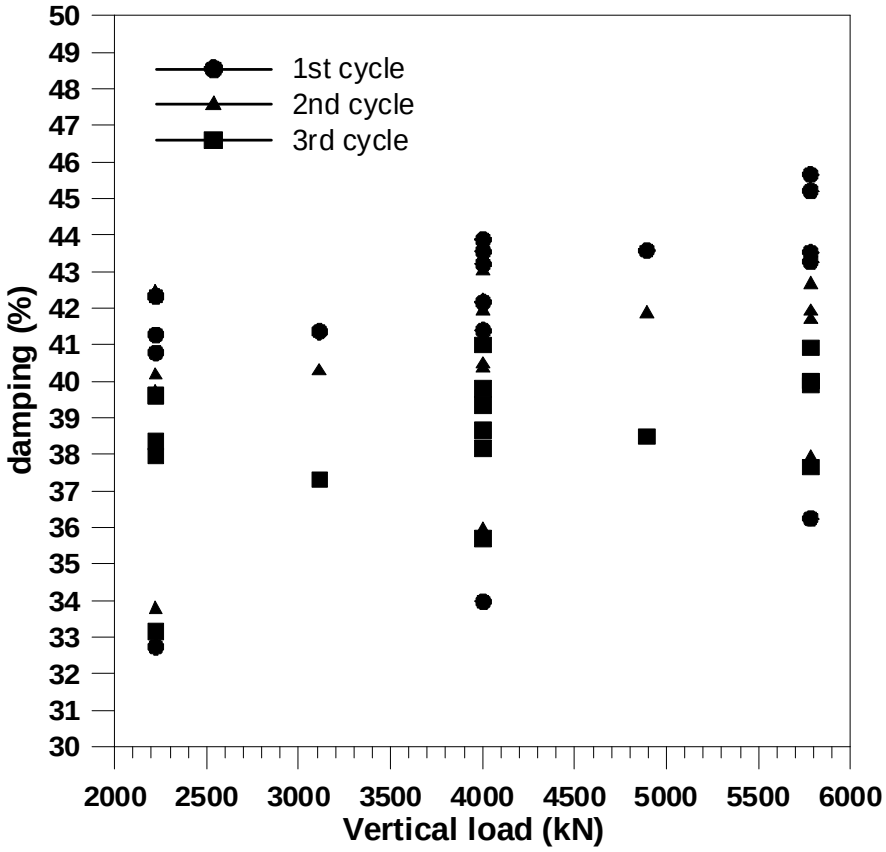

Figure 15. Damping ratio vs Vertical load

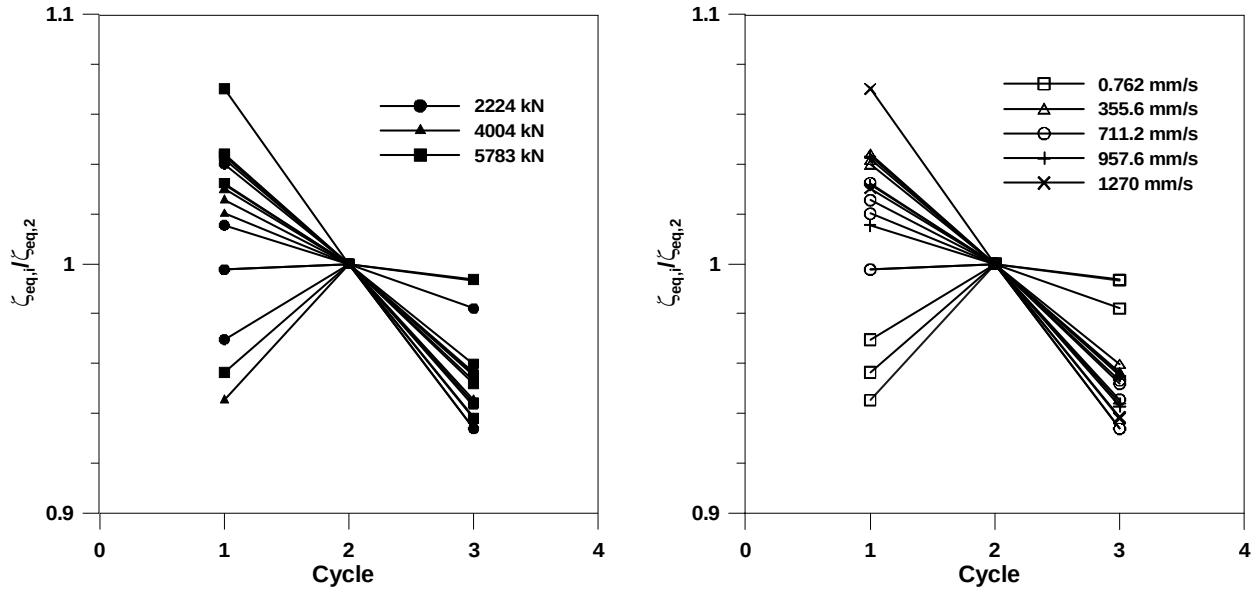

(a) (b)

Figure 16. Normalized Damping Ratio

Gradual Increase of Displacement Amplitude

Tests cb19 and cb20 were completed in order to evaluate the effects of preliminary low amplitude cycles on the peak response parameters of the full amplitude loops. The result of these two tests were compared with the results of test cb12 that was completed at the same amplitude, vertical load and speed. Data indicate a non-uniform effect of the preliminary low amplitude cycles. A maximum increment of peak force, with respect to the results of test cb12, was found in the order of 19% and 28% for tests cb19 and cb20, respectively. Results from tests cb12, cb19 and cb20 are compared, in terms of peak force, characteristic strength and post-yield stiffness in Figure A-41, Figure A-42 and Figure A-43, respectively.

Due to the limited and scattered nature of these data, any clear trend cannot be withdrawn, and no effect of gradual increase of displacement amplitude has been implemented in the proposed model.

PROPOSED MODEL

An existing analytical hysteresis model, developed by Kikuchi and Aiken (Kikuchi and Aiken, 1997) was analyzed and adapted to the experimental response of the tested bearing. The original approach was proposed for four types of elastomeric seismic isolation bearings, including lead-rubber isolators. The empirical model was prompted by a lack of availability of an analytical modeling tool that can capture the non-linearities and stiffnening behavior observed from experimental data and dependent on shear strains.

I order to facilitate the recognition of differences and developments, the notation and format of the original model was maintained. For this reason the parameters Q_d and $Q_{\max}$ are referred as F_u and F_m, respectively.

Kikuchi's model proposes the total shear force F as sum of two contributes F_1 and F_2, where:

$$F_1 = \frac{1}{2}(1-u)F_m\left[x + \text{sgn}(X)|x|^n\right] \tag{5}$$

and

$$F_2 = \pm uF_m\left(1 - 2e^{-a(1\pm x)} + b(1\pm x)\,e^{-c(1\pm x)}\right) \tag{6}$$

where X is the shear displacement and the positive and negative sign applies for $\dot{X} > 0$ and $\dot{X} < 0$, respectively. In the previous equations x is the normalized shear displacement (x=displacement/peak displacement), the parameter n specifies the stiffening effect and F_m is the peak shear force. The ratio of the shear force at zero displacement F_u, to F_m is indicated as u and the two parameters a and b are calculated numerically from the following equations:

$$\frac{1-e^{-2a}}{a} = 1 - \frac{\pi\zeta_{eq}}{2u} \tag{7}$$

$$b = c^2\left(\frac{\pi\zeta_{eq}}{u} - \left[2 + \frac{2}{a}\left(e^{-2a} - 1\right)\right]\right) \tag{8}$$

where ζ_{eq} is the equivalent viscous damping ratio and the parameter c is a predetermined constant, suggested equal to 4.0 for lead-rubber bearings.

A first attempt to use the existing model to reproduce the experimental database was performed with an initial parametric study on the set of the suggested parameters. All the above parameters a, b and c where individually considered in terms of their effects on the shape of the hysteresis loop, for the specific bearing under study. The level of shear strain (100%), intentionally maintained constant for these series of tests, did not allow the validation of the capacity of the original model to reproduce the non-linear behavior observed at high shear strain rate. However, a mono-dimensional minimization of the error, introduced by each parameter, was performed and the optimum set of variables did not provide an adequate reproduction of the recorded hysteretic response. This suggested a strong dependency of the existing approach on the peculiar characteristics of the devices originally employed for the model validation.

Numerical difficulties were also detected in the application of the original model. The force F_2, for instance, as given in the Eq. (6), appears to be not properly defined. In fact, when Eq. (7) is substituted in Eq. (8) the parameters b turns to be identically equal to zero. The suggested equations of the original model also indicated a discontinuity of the numerical response at maximum and minimum peak displacement, approaching with positive and negative velocity, and did not include any effect due to strain rate. For the above mentioned reasons a modified model is proposed.

A particular effort was dedicated to design the model as dependent only on the mechanical and geometric characteristics of the device, without any assumption about response characteristics. However, a set of derived quantities, commonly defined in literature, were used. Specifically:

Rubber Stiffness: $$K_{rubber} = \frac{G_{rubber} A_{rubber}}{t} \quad (9)$$

Lead Stiffness: $$K_{lead} = \frac{G_{lead} A_{lead}}{t} \quad (10)$$

Shear force at zero displ. (Characteristic strength): $$Q_d = \tau_{lead} A_{lead} \quad (11)$$

Peak Shear force : $$Q_{\max} = Q_d + K_{rubber}\Delta = F_{\max} \quad (12)$$

Equivalent viscous damping ratio: $$\zeta_{eq} = \frac{2}{\pi} Q_d \left(\frac{1}{Q_{\max}} + \frac{Q_d}{Q_m K_{lead} \Delta} \right) \quad (13)$$

where A represents the cross sectional area, t the total height of the rubber and Δ the peak displacement. For τ_{lead} and G_{lead} the values of 10.5 Mpa and 130 Mpa were assumed,

respectively. It must be noted that Eq. (13) is a pure manipulation of Eq. (4), for the case of an elasto-plastic cycle with hardening.

The first component of the total shear force F_1 was maintained unchanged from the original model. It was re-organized as a function of the characteristic strength Q_d:

$$F_1 = \frac{1}{2}(1/u - 1)Q_d\left[x + \mathrm{sgn}(X)|x|^n\right] \tag{14}$$

The influence of the parameter n and of the ratio u is clearly recognizable: varying u, the effective stiffness of the cycle varies linearly and increasing n the force-displacement curve becomes nth parabolic, allowing the description of the non linear behavior.

It must be noted that the force F_1, at zero displacement, is equal to zero, and at maximum displacement is equal to the force increment from Q_d to $Q_{\max}$:

$$\lim_{x\to\pm1} F_1 = \pm(Q_{\max} - Q_d) \tag{15}$$

This implies specific conditions on the second force component F_2, i.e.:

$$\lim_{x\to0} F_2 = sign(\dot{X})Q_d \tag{16}$$

$$\lim_{x\to\pm1} F_2 = \pm Q_d \tag{17}$$

and Eq. (16) and (17), are only satisfied if c=a+ln2 and b=4. For this reason, the second component F_2 of the total shear force is proposed in the following modified equation:

$$F_2 = sign(\dot{X})F_u\left(1 - 2e^{-a\left(1+sign(\dot{X})x\right)} + 4(1 + sign(\dot{X})x)e^{-(a+\ln 2)\left(1+sign(\dot{X})x\right)}\right) \tag{18}$$

where the only remaining parameter a could be obtained from Eq. (7), which imposes that the analytical and experimental hysteresis loop areas are equal.

The component F_2 is thus forced to be equal to the values of $\pm Q_d$, at zero and maximum displacements. This component of shear force can, of course, exceed the characteristic strength value along the range of displacements.

The format of Eq. (18) solves also the discontinuity at the maximum and minimum displacement, present in the original model, and obtained by approaching the maximum displacement with positive and negative velocity.

It must be noted that both the components F_1 and F_2 are presented, in the new model, as direct function of the characteristic strength Q_d. The overall shear force can thus be expressed as:

$$F = F_1 + F_2 = Q_d f(x) \quad (19)$$

This characteristic allows a more direct implementation of the variations due to the phenomena discussed in this report, specifically the effects of the strain rate and of cycling. In fact, the force Q_d, that represents the force developed by the bearing at the peak of the motion velocity, is the response parameter that appears to be more significantly affected by the previous mentioned effects. Moreover, while the variation of the other response quantities has been presented as a function of the maximum cycle velocity, the variation of the characteristic strength can be considered a function of the instantaneous velocity, being Q_d the only parameter obtained when instantaneous and maximum cycle velocities coincide.

The analyses of the experimental results of the response modifications due to different level of vertical loads generally indicated a very limited effect on the bearing response. For this reason the structure of the model was not modified in order to take into account the contribution of the vertical load. As indicated before, the effects of cycling are instead evident, particularly for high velocity motions. The presented graphs of the normalized characteristic strength (Q_d) show an average reduction of the component Q_d equal to 18% from first to second cycle and 28% from first to third cycle. The reduction factor, due to cycling, was implemented in the model as:

$$Q_{d,c2} = 0.82\, Q_{d,c1} \quad (20)$$

$$Q_{d,c3} = 0.72\, Q_{d,c1} \quad (1)$$

where $Q_{d,ci}$ is the characteristic strength for the ith cycle. For cycles subsequent to the third one, a constant reduction of 28%, with respect to the first loop, was assumed.

The effects of the velocity are introduced through two possible function of the strain rate $\dot{\gamma}(t)$, obtained from a regression on the experimental database:

$$Q_d(t) = \frac{\overline{Q}_d}{2}(1 + \dot{\gamma}(t)^{0.14}) \quad (22)$$

$$0.8\overline{Q}_d \le Q_d(t)$$

and

$$Q_d(t) = 0.75\overline{Q}_d\left(1 + \frac{\arctan(2\dot{\gamma}(t))}{\pi}\right) \qquad (23)$$

$$0.8\overline{Q}_d \le Q_d(t) \le 1.125\overline{Q}_d$$

where $\overline{Q}_d$ is the characteristic strength as defined in Eq. (11). Both equations, in case of very low strain rates (less than 8%) were forcedly limited to the value of 0.8 $\overline{Q}_d$.

The structure of Eq. (22) is consistent with relationships suggested in literature (Skinner et Al., 1993), but it has no upper bound and approaches the zero strain rate with a steep trend. An alternative equation (Eq. (23)) has been derived to avoid numerical instabilities if the velocity should reach very high values, being mathematically bounded. In general terms, however, the two equations provide a very similar representation of the phenomenon.

The phases of development of the proposed model are briefly illustrated in Figure 17. Figure 17(a) shows the comparison between an experimental and analytical curve. The numerical response is based on the Kichuchi-Aiken model, simply modified to solve the continuity issues of the shear force definition. The effects of the strain rate are implemented in Figure 17(b), with a visible improvement in the agreement between the two curves, in the regions of low velocity (reversal of motion). The effects of this modification are only demonstrated in Figure 17(b) for the velocity variations along the same cycle. However, the proposed model proved to be able to incorporate this capability for different motions, at different velocity content, as generally experienced by a bearing during a seismic event. Finally Figure 17(c) indicates the capacity of the proposed model to reproduce the effects of cycling by the degradation of the shear force at zero displacement.

In order to validate the proposed model against the available database of test results, the numerical response was compared with the entire set of experimental results described above. Eq. (23) was selected to take into account the effect of strain rate. An example of the analytical and experimental results for the lead-rubber bearing response are presented in Figure 18(a) and 18(b) for low and high speed tests, respectively.

A good agreement between the experimental (dashed line) and analytical (solid line) response was obtained, not only in terms of peak shear force but also in terms of degradation between cycles and effect of test velocity. It must be noted that the experimental cycles, for the test at high velocity (cb18), present some oscillation due to instantaneous variations of the applied vertical load, during the test at very high speed.

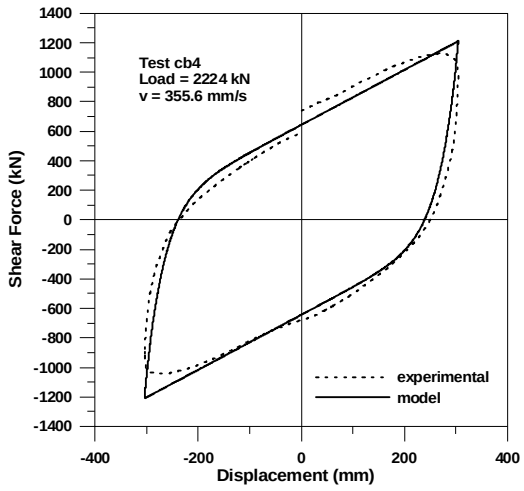

(a)

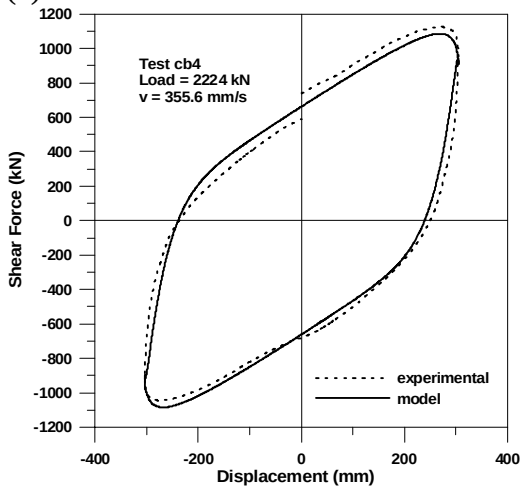

(b)

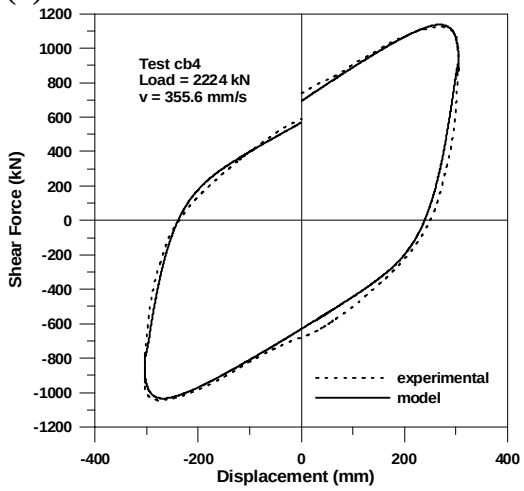

(c)

Figure 17. Development Steps Of The Proposed Model

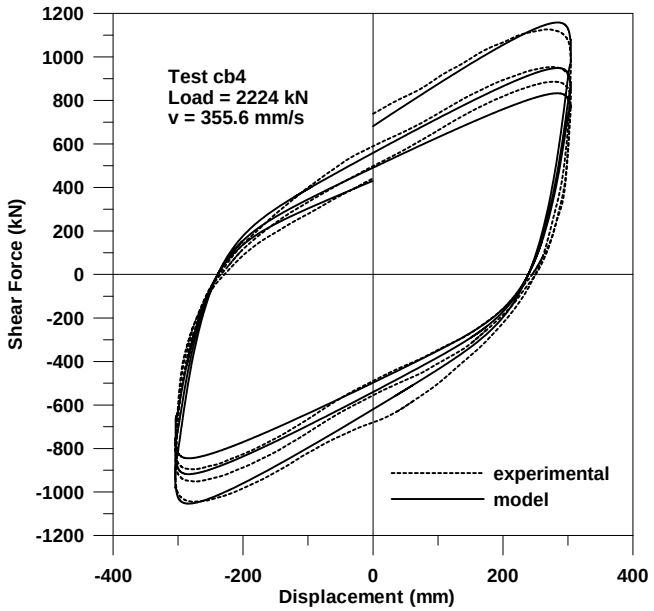

(a)

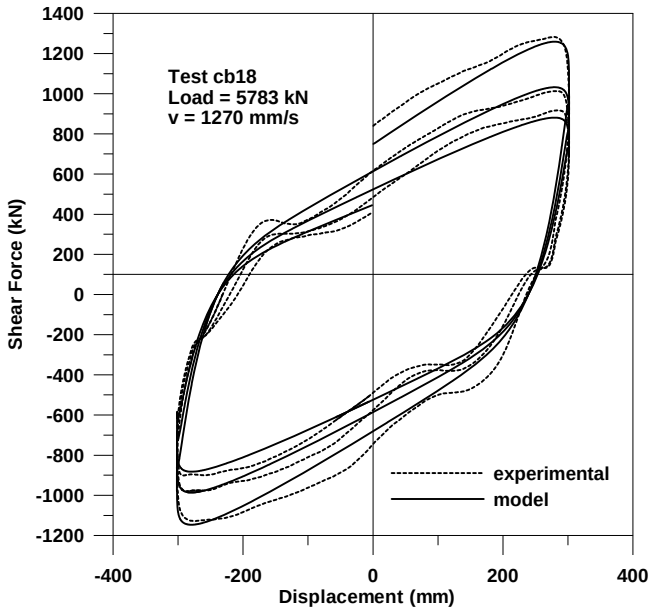

(b)

Figure 18. Experimental And Numerical Results For Test At Low (a) And High Velocity (b)

CHAPTER 2 - SLIDING BEARINGS

OBSERVATION FROM PREVIOUS TESTS ON SLIDING BEARINGS.

A set of data is available in the SRMD database from previously completed tests on sliding bearings, tested as part of the Toll Bridge program.

The bearings were tested under a specified protocol (Caltrans, 1999)) that did not include many variations of vertical loads and testing velocity. This incompleteness together with some specific observation motivated the scope of this phase of the present research project. Some significant result, from available tests, is presented to anticipate particular aspects further developed as part of this analytical and experimental program.

Effects on friction coefficients.

Figure 19 shows the friction coefficients obtained, for the first cycle, under the limited range of vertical loads required by the above mentioned testing protocol.

The scatter of results does not indicate a consistent trend and it is clear that the majority of tests were completed under the same vertical load of about 13,500 kN. All the compared tests were completed at the same peak velocity of 102 mm/s. As mentioned above, the effects generated by different vertical loads could not be systematically investigated. Even though results are available for nominal and extreme load conditions, results appear difficult to combine and compare. Several tests, in fact, even though tested under different vertical loads, were completed also at different ranges of peak velocity.

An attempt was made to evaluate, for the existing tests, the effects of the peak test velocity on the friction coefficients. The friction coefficient μ was normalized, for these tests, to the maximum friction coefficient (μ_{max}) obtained for the same device during all the tests at the same applied vertical load, in order to allow a comparison independent on other testing characteristics. It must be noted that the maximum value of friction (μ_{max}) is obtained from the data at velocities up to 102 mm/s. This condition justifies values of the ratio μ/μ_{max} greater than one for high speed tests. Figure 20 and Figure 21 show a significant influence of the peak velocity of the applied motion on the friction coefficients, clearly a crucial parameter of the device performance. Figure 20 indicates a regular increase of the normalized friction coefficient up to a certain value of peak velocity (~ 100 mm/s). For motions at higher speed the behavior is quite scattered and certainly not enough documented due to lack of data points. An enlargement (Figure 21) of the same graph,

limited to 200 mm/s, confirms the rapid increase of μ/μ_{max} for velocities up to 75 mm/s and a tendency to reach a plateau for faster motions.

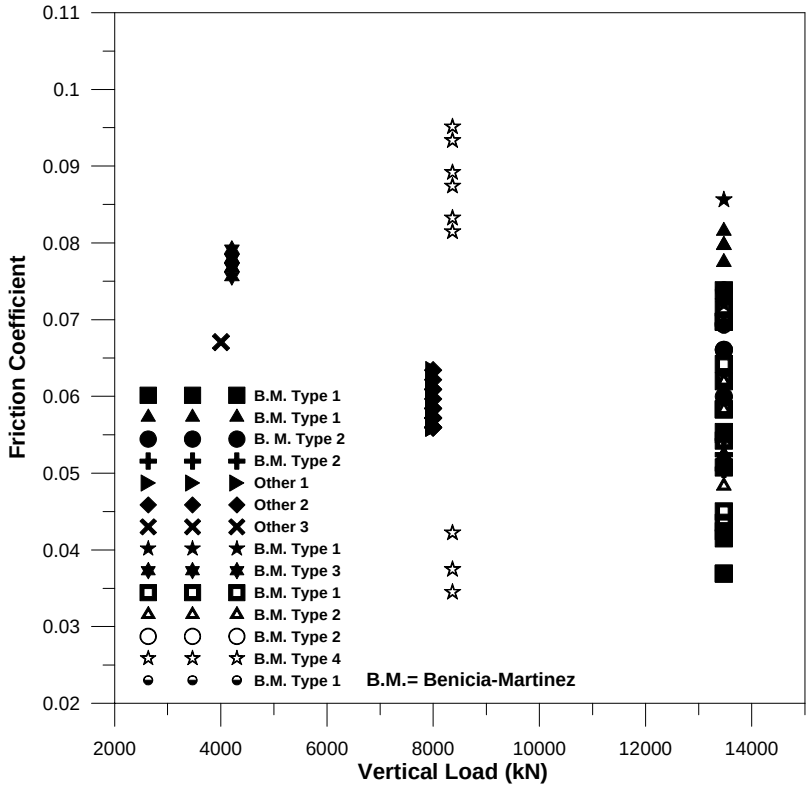

Figure 19 – SRMD database- Friction Coefficients versus Applied Vertical Load

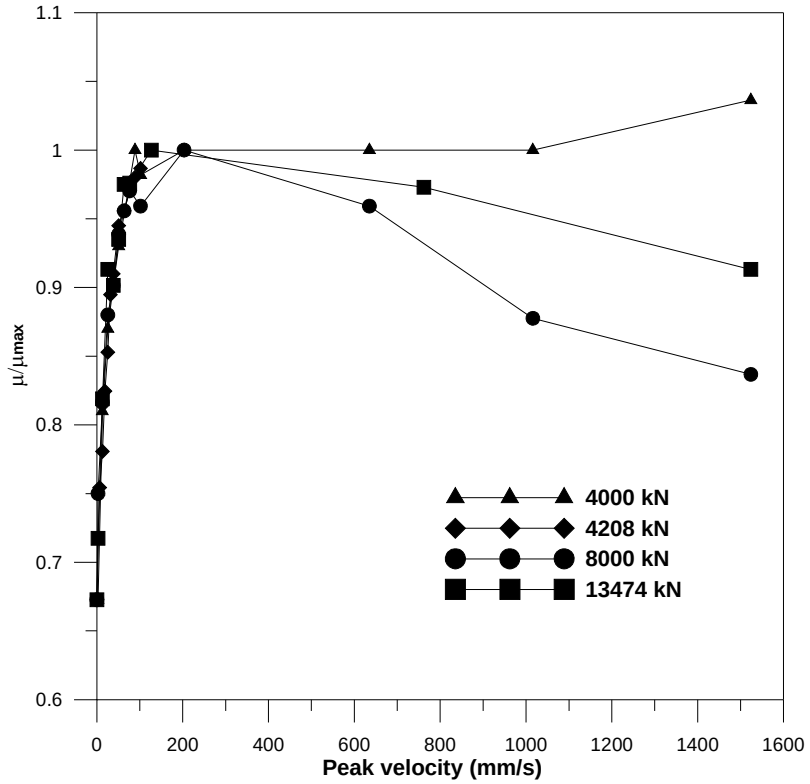

Figure 20 – SRMD database- Effects of peak velocity on friction coefficients.

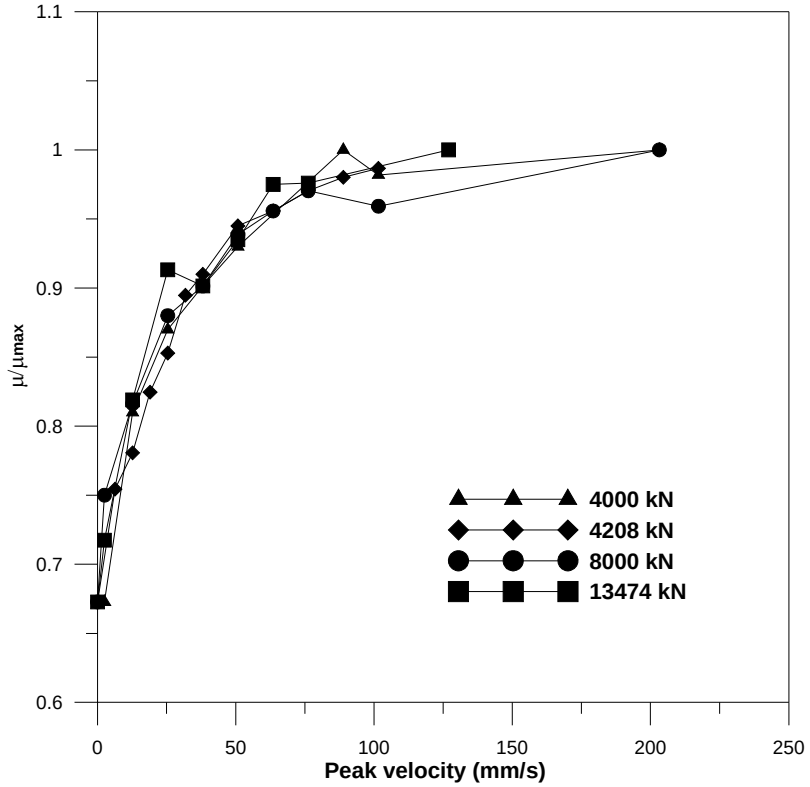

Figure 21 – SRMD database- Effects of peak velocity (up to 200 mm/s) on friction coefficients.

Effects on Restoring Stiffness (K_{ra})

A series of results are presented in Figure 22 in terms of variation of the restoring stiffness k_{ra} with respect to the theoretical value K_{th} calculated as:

$$K_{th} = \frac{Vload}{R} \tag{24}$$

were *Vload* is the applied vertical load and R the radius of curvature of the concave plate.

The experimental restoring stiffness was calculated from the best-fit straight line of the experimental data between +/- 75% of the peak displacement. The slope of the two interpolating lines, one for the upper and one for the lower portion of each cycle, was averaged to obtain the value k_{ra}. Figure 22 includes the variation of k_{ra} from the results of different bearings, tested under different conditions.

A maximum increment of 15% is observed for a relative low vertical load. A general increase of measured restoring stiffness, with respect to the theoretical value, is observed for the lower range of applied vertical loads. For higher loads the variation is quite scattered, including cases of reduction (up to 16%) predominantly associated to the higher values of applied load.

The theoretical equation for the estimate of the restoring stiffness appears quite unreliable as will be discussed in what follows.

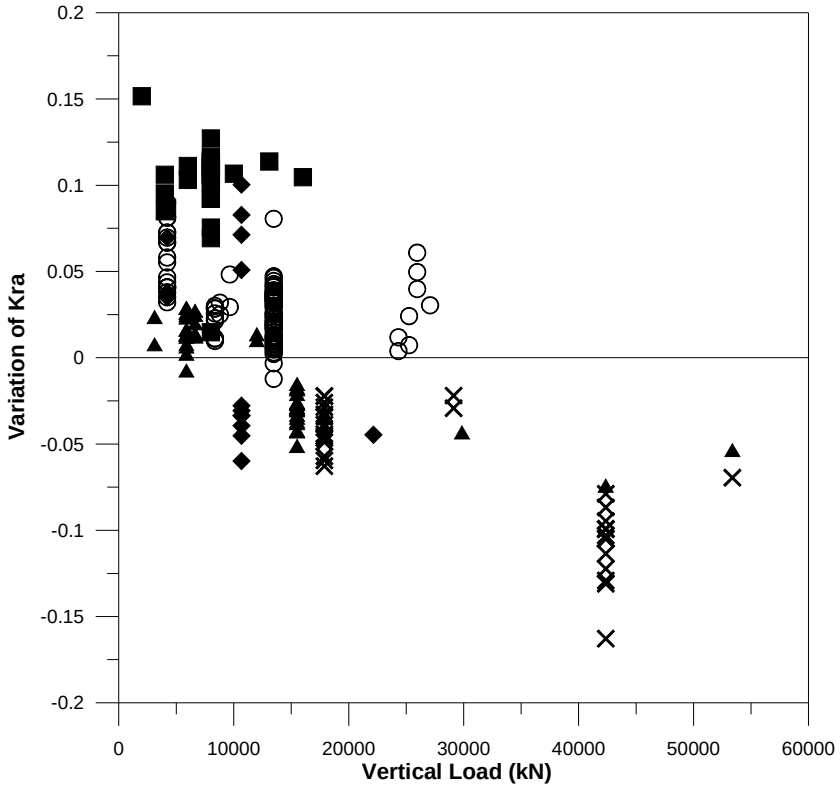

Figure 22 – SRMD database- Restoring stiffness variation with respect to theoretical value, as function of vertical load.

NEW TESTS:

A set of sliding bearings, with concave surface, were tested as part of this research project in April and August 2006. The bearings were preliminary submitted to a series of tests based on protocols developed for specific projects and, at manufacturer authorization, further tested in order to investigate the effects of vertical load variation as well as velocity.
The complete results of the tests are not disclosed in order to protect the manufacturer legal property of the product, however, the observations related to the specific objectives of this research project are presented here in general terms. It must be noted that the bearings are very similar, in concept, with the Friction Pendulum bearings installed by Caltrans on the Benicia-Martinez bridge. The diameter of the concave plate of the bearings tested for this research was 1050 mm in diameter. A major difference with respect to the bearings utilized by Caltrans, is the composite friction material used on the slider and on the top plate. For these specific devices the material is an un-lubricated polymer composite liner with 415 MPa compressive yield strength.
The data analysis was organized in order to extract, when possible, general trends that can be associated to the device concept and not specifically to the sliding material utilized.

A matrix of performed tests is presented in Table 6. The tests are divided in three categories: tests at low, medium and high vertical load. Specifically the low, medium and high values of applied load were 3263, 6525 and 13050 kN, respectively. The medium load of 6525 kN represented the design vertical load for the devices. For each set of load a wide range of velocities was selected. The lowest speed of 0.254 mm/s is considered as a reference for the study of the velocity effects. A sinusoidal input, with amplitude equal to 200 mm was used for all the tests and except for the low velocity tests two fully reversed cycles were completed. Table 6 also shows that two tests at low and high vertical load, limited to a displacement of 70 mm, were completed. In some case tests with identical parameters were repeated due to unsatisfactory performance of the testing rig or the need to verify performance characteristics under different conditions (for instance bearing temperature). In this case, tests are labeled with the letter R. Time was allowed between tests in order to avoid over-heating of the sliding surfaces of the isolator.

The installation procedure of the devices on the testing machine is consistent with the standard installation of isolation devices. The devices were set on the platen and leveled over dense foam

rings that seal the tie-down holes on the table and at the same time provide a gap between bottom plate of the bearing and table surface. Hydro-Stone grout was pumped into the gap and cured. After 1 day of curing the tie-down bolts were tightened to the desired pretension force using a calibrated hydraulic wrench. Top adapting plates were bolted to the vertical reaction frame and the articulated slider inserted before re-assembling the device with the use of the table vertical motion. Figure 23 shows the typical bearing installation on the table.

Figure 23 Typical sliding bearing installation

TEST	Vload (kN)	Displ (mm)	Vel. (mm/s)	# cycles	Motion direction
VEL-L-1	3263	70	0.254	1	Long
VEL-L-1-R	3263	70	0.254	1	Long
VEL-L-1-2	3263	200	0.254	1	Long
VEL-L-2	3263	200	1.27	2	Long
VEL-L-3	3263	200	5	2	Long
VEL-L-4	3263	200	10	2	Long
VEL-L-5	3263	200	20	2	Long
VEL-L-6	3263	200	50	2	Long
VEL-L-7	3263	200	100	2	Long
VEL-L-8	3263	200	200	2	Long
VEL-L-9	3263	200	400	2	Long
VEL-L-10	3263	200	800	2	Long
VEL-M-1	6525	200	0.254	1	Long
VEL-M-1-R	6525	200	0.254	1	Long
VEL-M-2	6525	200	1.27	2	Long
VEL-M-3	6525	200	5	2	Long
VEL-M-4	6525	200	10	2	Long
VEL-M-5	6525	200	20	2	Long
VEL-M-6	6525	200	50	2	Long
VEL-M-7	6525	200	100	2	Long
VEL-M-8	6525	200	200	2	Long
VEL-M-8-R	6525	200	200	2	Long
VEL-M-9	6525	200	400	2	Long
VEL-M-10	6525	200	800	2	Long
VEL-H-1	13050	70	0.254	1	Long
VEL-H-1-R	13050	70	0.254	1	Long
VEL-H-1-2	13050	200	0.254	1	Long
VEL-H-2	13050	200	1.27	2	Long
VEL-H-3	13050	200	5	2	Long
VEL-H-4	13050	200	10	2	Long
VEL-H-5	13050	200	20	2	Long
VEL-H-6	13050	200	50	2	Long
VEL-H-7	13050	200	100	2	Long
VEL-H-8	13050	200	200	2	Long
VEL-H-8-R	13050	200	200	2	Long
VEL-H-9	13050	200	400	2	Long
VEL-H-9-R	13050	200	400	2	Long
VEL-H-10	13050	200	800	2	Long

Table 6 – Tests matrix for sliding bearings

Performance characteristics of the tested devices are summarized in Table 7(a), 7(b) and 7(c) for low, medium and high vertical load, respectively

Test	Vload	Displ.	vel	cycle	Fmax	Fmin	F0	Kra	Keff	EDC	FC_{F0}	FCedc	beq
	kN	mm	(mm/s)		(kN)	(kN)	(kN)	(kN-mm)	(kN-mm)	(kN-mm)	(%)	(%)	(%)
vel-L-1	3263	70	0.254	1	354.65	-353.17	259.90	1.09	5.00	73844	7.97	8.09	47.94
vel-L-1-R	3263	70	0.254	1	376.59	-372.96	270.86	1.16	5.15	76660	8.31	8.39	48.30
vel-L-1-2	3263	200	0.254	1	528.45	-567.58	308.31	1.27	2.74	245550	9.46	9.41	35.66
vel-L-2	3263	200	1.27	1	508.58	-517.74	260.12	1.20	2.56	211170	7.98	8.09	32.73
		200		2	521.59	-527.37	267.13	1.22	2.62	215730	8.19	8.27	32.73
vel-L-3	3263	200	5	1	529.32	-549.33	285.45	1.23	2.66	230860	8.76	8.84	34.39
		200		2	534.65	-534.41	284.71	1.22	2.66	231320	8.73	8.86	34.54
vel-L-4	3263	200	10	1	538.53	-536.85	297.46	1.23	2.68	241900	9.12	9.24	35.68
		200		2	534.04	-540.06	292.00	1.21	2.66	238530	8.96	9.12	35.44
vel-L-5	3263	200	20	1	544.15	-541.64	306.94	1.25	2.70	251650	9.41	9.60	36.72
		200		2	527.58	-522.47	285.77	1.19	2.61	239130	8.76	9.12	36.04
vel-L-6	3263	200	50	1	545.93	-525.84	313.13	1.23	2.66	258485	9.60	9.86	38.17
		200		2	500.35	-490.93	264.88	1.18	2.46	222709	8.12	8.49	35.54
vel-L-7	3263	200	100	1	529.98	-510.52	312.77	1.17	2.59	257239	9.59	9.81	39.15
		200		2	472.36	-462.38	239.60	1.17	2.33	209585	7.35	8.00	35.51
vel-L-8	3263	200	200	1	478.15	-459.94	303.02	1.12	2.34	250343	9.29	9.56	42.29
		200		2	435.18	-419.08	243.30	1.14	2.13	204050	7.46	7.79	37.87
vel-L-9	3263	200	400	1	509.86	-476.03	315.46	1.28	2.44	256566	9.68	9.76	41.16
		200		2	455.47	-413.30	258.23	1.32	2.16	214634	7.92	8.19	39.15
vel-L-10	3263	200	800	1	635.97	-548.53	318.55	1.52	2.92	273808	9.77	10.34	36.21
				2	498.14	-468.23	259.66	1.43	2.39	211514	7.96	8.03	34.50

Table 7(a) Results for low level vertical load.

Test	Vload	Displ.	vel	cycle	Fmax	Fmin	F0	Kra	Keff	EDC	FC_{F0}	FCedc	beq
	kN	mm	(mm/s)		(kN)	(kN)	(kN)	(kN-mm)	(kN-mm)	(kN-mm)	(%)	(%)	(%)
vel-m-1	6525	200	0.254	1	891.52	-885.36	373.06	2.50	4.44	303730	5.72	5.82	27.19
vel-m-1-R	6525	200	0.254	1	821.13	-859.06	352.51	2.47	4.20	281430	5.40	5.39	26.65
vel-m-2	6525	200	1.27	1	894.42	-884.14	390.85	2.51	4.45	314050	5.99	6.02	28.10
				2	897.84	-895.13	396.82	2.50	4.48	319470	6.08	6.12	28.35
vel-m-3	6525	200	5	1	928.82	-905.62	424.13	2.53	4.58	344090	6.50	6.58	29.82
				2	921.43	-905.89	417.07	2.50	4.56	338720	6.39	6.48	29.53
vel-m-4	6525	200	10	1	929.88	-901.78	437.27	2.56	4.57	351180	6.70	6.71	30.45
				2	910.37	-891.94	396.80	2.49	4.50	336200	6.08	6.43	29.62
vel-m-5	6525	200	20	1	932.04	-891.73	440.01	2.60	4.54	355090	6.74	6.78	30.87
				2	887.38	-863.95	376.02	2.50	4.36	318960	5.76	6.08	28.83
vel-m-6	6525	200	50	1	920.20	-872.61	430.26	2.66	4.46	350690	6.59	6.68	30.95
				2	829.72	-809.56	332.34	2.53	4.07	276000	5.09	5.25	26.63
vel-m-7	6525	200	100	1	895.59	-851.25	403.76	2.64	4.34	333032	6.19	6.34	30.17
				2	802.82	-774.47	290.40	2.57	3.92	249085	4.45	4.75	25.00
vel-m-8	6525	200	200	1	854.15	-828.31	381.34	2.63	4.18	316897	5.84	6.04	29.81
				2	780.08	-748.08	271.18	2.61	3.80	234572	4.16	4.47	24.31
vel-m-8-R	6525	200	200	1	871.80	-851.70	409.88	2.68	4.28	336373	6.40	6.40	30.86
				2	774.80	-752.13	282.01	2.58	3.79	238563	4.32	4.54	24.72
vel-m-9	6525	200	400	1	802.36	-754.13	376.55	2.73	3.86	312934	5.77	5.95	31.76
				2	694.38	-663.68	258.78	2.69	3.38	224979	3.97	4.29	26.23
vel-m-10	6525	200	800	1	842.86	-761.80	363.67	2.73	3.96	309379	5.58	5.84	30.25
				2	709.11	-676.93	229.49	2.69	3.44	209798	3.52	3.99	23.91

Table 7(b) Results for medium level vertical load.

Test	Vload	Displ.	vel	cycle	Fmax	Fmin	F0	Kra	Keff	EDC	FC_{F0}	FCedc	beq
	kN	mm	(mm/s)		(kN)	(kN)	(kN)	(kN-mm)	(kN-mm)	(kN-mm)	(%)	(%)	(%)
vel-h-1	13050	70	0.254	1	812.66	-829.35	442.86	4.83	11.73	127360	3.39	3.48	35.26
vel-h-1-R	13050	70	0.254	1	835.09	-820.46	479.78	5.12	11.82	136110	3.68	3.72	37.38
vel-h-1-2	13050	200	0.254	1	1441.00	-1569.60	509.80	5.05	7.52	404170	3.91	3.87	21.36
vel-h-2	13050	200	1.27	1	1461.30	-1512.40	456.97	4.95	7.43	367630	3.50	3.52	19.69
				2	1504.70	-1554.20	512.77	4.99	7.65	408350	3.93	3.91	21.25
vel-h-3	13050	200	5	1	1532.60	-1552.30	544.33	5.03	7.70	434340	4.17	4.15	22.37
				2	1570.20	-1586.90	559.66	5.01	7.87	450740	4.29	4.31	22.75
vel-h-4	13050	200	10	1	1584.90	-1590.00	583.32	5.13	7.91	468100	4.47	4.47	23.38
				2	1583.20	-1579.00	553.29	5.07	7.88	451300	4.24	4.31	22.63
vel-h-5	13050	200	20	1	1591.50	-1567.00	567.86	5.22	7.86	463040	4.35	4.41	23.21
				2	1537.70	-1526.60	495.63	5.09	7.62	417890	3.80	3.98	21.58
vel-h-6	13050	200	50	1	1550.10	-1493.70	527.35	5.32	7.56	428406	4.04	4.08	22.27
				2	1421.10	-1435.90	383.65	5.11	7.10	349803	2.94	3.33	19.37
vel-h-7	13050	200	100	1	1512.40	-1500.50	496.28	5.34	7.50	404360	3.80	3.85	21.26
				2	1363.97	-1374.70	350.18	5.15	6.82	300279	2.68	2.86	17.37
vel-h-8	13050	200	200	1	1546.00	-1493.10	473.78	5.42	7.57	388597	3.63	3.71	20.28
				2	1360.41	-1326.9	293.58	5.21	6.70	255364	2.25	2.44	15.09
vel-h-8-R	13050	200	200	1	1495.80	-1385.90	471.22	5.56	7.17	374119	3.61	3.57	20.57
				2	1277.60	-1262.20	214.73	5.12	6.33	211656	1.65	2.02	13.22
vel-h-9	13050	200	400	1	1347.26	-1336.82	436.55	5.45	6.69	352122	3.35	3.36	20.81
				2	1238.48	-1203.51	213.54	5.26	6.09	194977	1.64	1.86	12.69
vel-h-9-R	13050	200	400	1	1394.13	-1345.95	489.55	5.58	6.81	379204	3.75	3.61	21.92
				2	1209.33	-1193.31	199.18	5.18	5.98	184865	1.53	1.76	12.21
vel-h-10	13050	200	800	1	1340.17	-1306.30	421.07	5.59	6.51	345118	3.23	3.25	20.44
				2	1168.34	-1171.67	221.24	5.40	5.78	182118	1.69	1.76	12.25

Table 7(c) Results for high level vertical load.

For Tables 7(a), 7(b) and 7(c) the following symbols and meanings were used:

Vload: Applied vertical load (kN)

Displ: Amplitude of the sinusoidal displacement input (mm)

Vel: Peak velocity of the sinusoidal input (mm/s)

Fmax: Maximum recorded force (kN)

Fmin: Minimum recorded force (kN)

F0: Average force at zero displacement. This value was obtained by calculating the best fit straight lines for the force-displacement response in the range of +/- 0.75 times the maximum displacement. Two lines are obtained, for the top and bottom portion of the response cycle. The two intersection of these lines with the axis at zero displacement are averaged to obtain F0.

Kra: Average of the restoring stiffness associated with the two "best fit" straight lines.

Keff: Effective stiffness calculated as in Eq. (2).

EDC: Energy dissipated per cycle (kN-mm)

FC_{F0}: Friction coefficient (%) obtained from F0 and the applied vertical load (W):

$$FC_{F0} = \frac{F_0}{W} \tag{25}$$

FC_{EDC}: Friction coefficient (%) obtained from the EDC and the average maximum displacement (D_{av}):

$$FC_{EDC} = \frac{EDC}{4WD_{av}} \qquad D_{av} = \frac{D_{\max} - D_{\min}}{2} \tag{26}$$

beq: Equivalent viscous damping, calculated as in Eq. (4).

Peak Restoring Force

The peak restoring force results are plotted in Figure 24 versus the applied vertical load. The force values are obtained as average between the maximum and minimum recorded reactions. It must be noted, as visible in Tables 7(a), 7(b) and 7(c), that the maximum detected difference between positive and negative peak force is equal to 13.7, 9.6 and 8.9% for low, medium and high load tests, respectively. This indicates a more stable response associated with higher vertical load. The higher variation between reversed peaks is also associated to test VEL-L-10 that represent the most difficult situation for testing machine control. It is, in fact, corresponding to a low value of axial load and a high velocity motion. The average value of difference (in percentage) between

positive and negative peak force is however very limited, with variations equal to 3.47%, 3.45% and 2.16% for low, medium and high load, respectively. These observations justify the use of the average between reversed peak forces to study the effects of vertical load and test velocity.

In Figure 24 the average of the results at each different applied load were also connected by a line (solid for the first cycle and dashed for the second one). The trend of both lines clearly indicate a linear variation of the peak restoring force with vertical load amplitude. For the first cycle the ratio between restoring force and applied vertical load, for low, medium and high load is 0.16, 0.13 and 0.11, respectively. Ratios reduce to 0.15, 0.12 and 0.10 for the second cycles. The increase of vertical load appears to introduce an incrementally higher influence of the peak velocity as indicated by the larger scatter of the data symbols at higher vertical load.

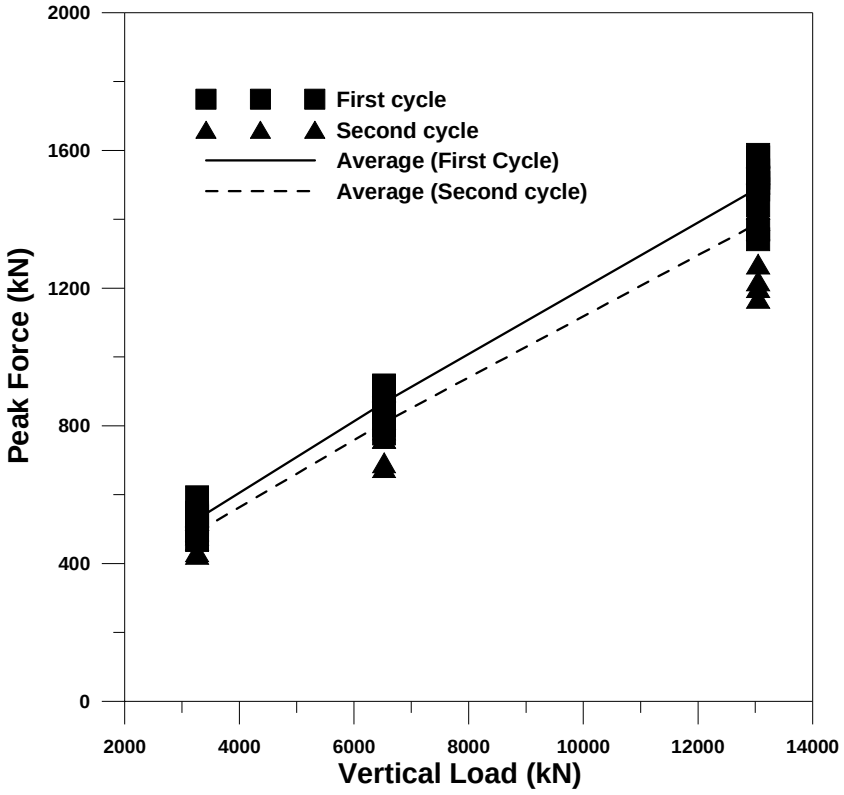

Figure 24 – Average Peak Force versus Applied Vertical Load

Figure 25, Figure 26 and Figure 27 show the average peak force as function of the test speed, for each level of vertical load. The plots on the top indicate the complete range of velocities, while the bottom graphs are limited to a peak motion velocity of 100 mm/s. All cases show a steady increase of the maximum force with velocity up to 20 mm/s. Only the low axial load case indicate an exception for the test at very low speed (VEL-L-1-2, velocity =0.254 mm/s). After the 20 mm/s threshold a reduction of peak force is experienced for a variable range. In fact the trend of force reduction is reversed at 200 mm/s for the low vertical load case (Figure 25). For medium applied load the range is extended to 400 mm/s and further extended for the higher load where forces are still reduced at the peak velocity of 800 mm/s. Assuming as a reference the results of the slow tests (v=0.254 mm/s), the maximum restoring force increment is reported in Table 8, in column 2. It must be noted that for uniformity among the three vertical load cases the peak force increment value of Table 8 at 3263 kN refers to the increase of restoring forces developed up to 20 mm/s and thus does not include the peak at very high velocity.

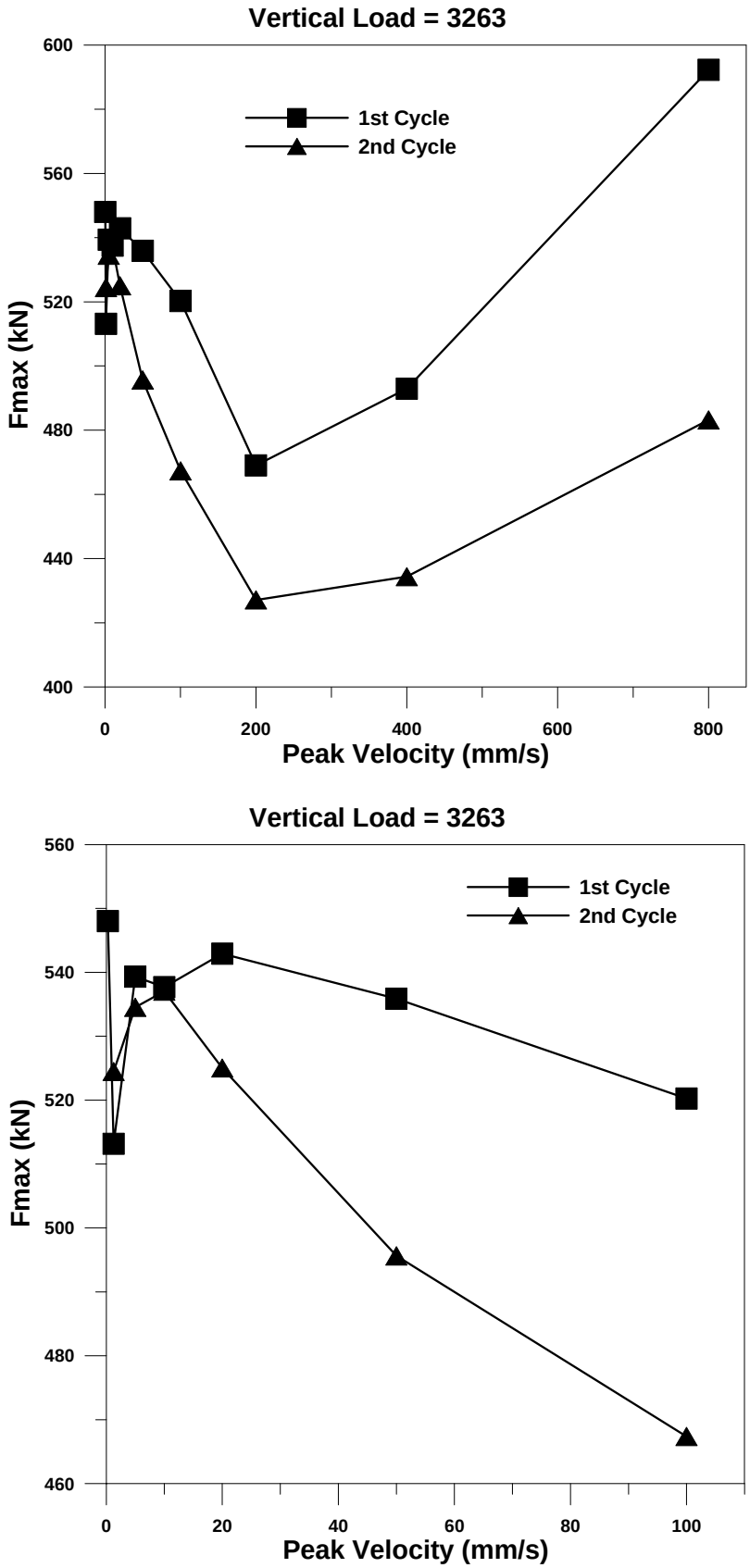

Figure 25 – Peak Restoring Force versus Peak Velocity (Applied Vertical Load = 3263 kN)

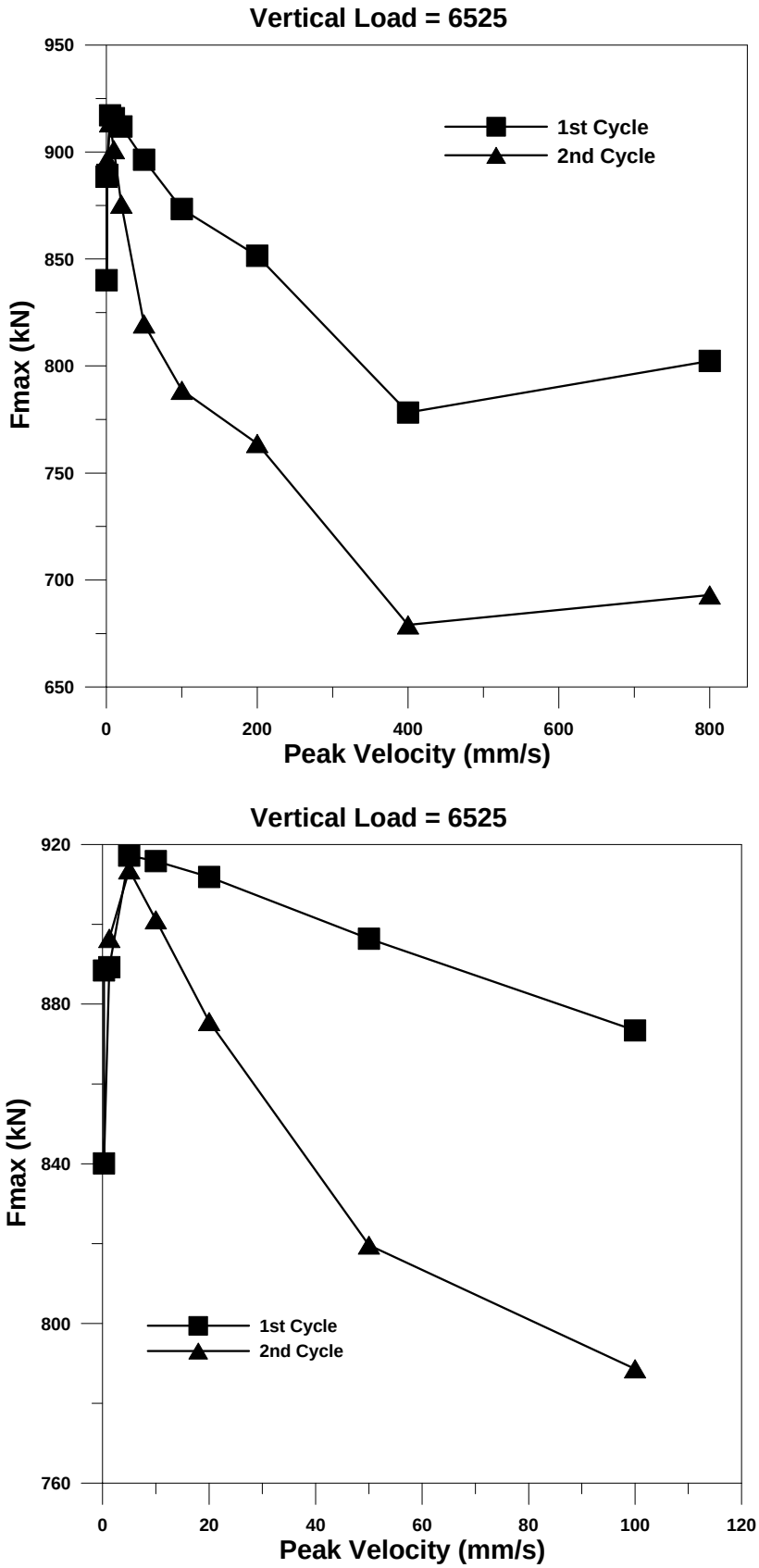

Figure 26 – Peak Restoring Force versus Peak Velocity (Applied Vertical Load = 6525 kN)

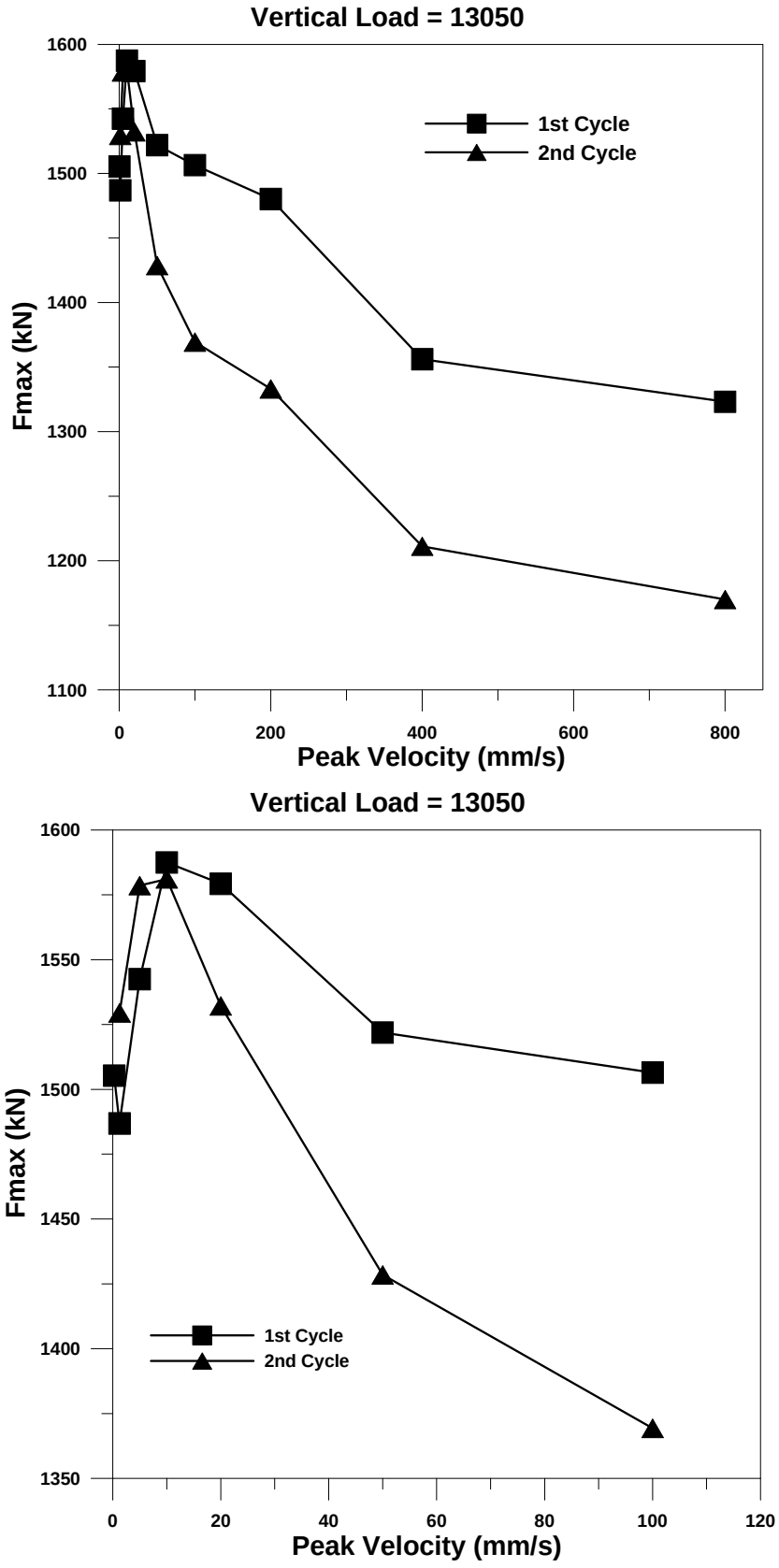

Figure 27 – Peak Restoring Force versus Peak Velocity (Applied Vertical Load = 13050 kN)

The ratio between maximum and minimum restoring force, at constant vertical load and for different test velocities, is also reported in Table 8. As anticipated, an increase of importance of the velocity effects with applied vertical loads is confirmed. The second cycles appear to be more sensitive to the velocity variations.

Vertical Load (kN)	Peak Force increment	Max Force/ Min Force (1^{st} cycle)	Max Force/ Min Force (2^{nd} cycle)
3263	5.8%	1.17	1.25
6525	3.2 %	1.18	1.34
13050	5.4 %	1.20	1.35

Table 8 – Ratio between maximum and minimum force obtained at constant vertical load and different motion velocity.

It can also be noted, from Figures 25, Figure 26 and Figure 27 that the reduction of forces from first to second cycle is negligible in the low velocity range and tends to increase with velocity. The maximum reduction of restoring force, at peak velocity of 800 mm/s, is 18%, 13% and 11% for low, medium and high vertical load, respectively. Similarly to what presented for the lead-core rubber bearing, the variation of peak restoring force, as function of cycling, is presented in Figure 28, where the maximum force was normalized with respect to the value obtained during the second cycle. It is visible the negligible influence of the cycling effects for values of velocities up to about 10 mm/s and the reduction of this effect with increasing vertical load. The thermal effects appear to justify this phenomenon. In fact at high velocity and high vertical loads it is expected that a significant temperature rise develops already during the first cycle.

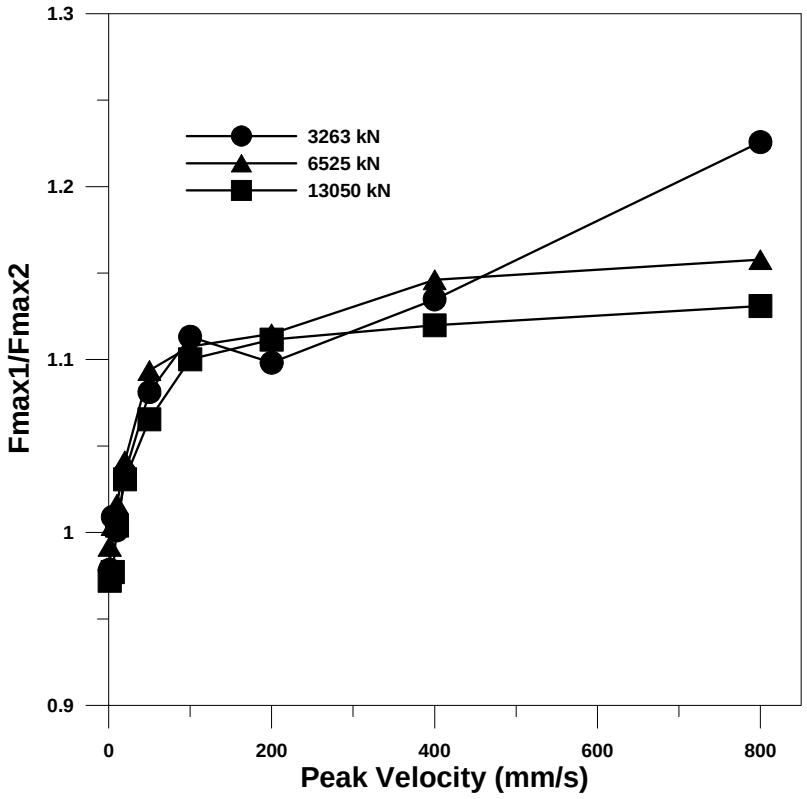

Figure 28 – Peak restoring force normalized to second cycle results.

Energy Dissipated Per Cycle (Edc)

Figure 29, Figure 30 and Figure 31 show an initial increase of EDC with peak velocity in the range from 0.254 mm/s to 80 mm/s.

The initial portion of the curves appear to become steeper with increasing vertical load. The maximum value of energy dissipated per cycle is, in fact, achieved at a motion speed linearly reduced with the amplitude of the applied load. Specifically, for low, medium and high load, the peak EDC of the first cycle is reached at 50 mm/s, 20 mm/s and 10 mm/s, respectively. The maximum increase of the energy value, with respect to the slow test results, is 5.27%, 21.36% and 15.8% for the three vertical load cases. The amount of dissipated energy appears also to reduce significantly above the velocity of 80 mm/s, except for the low vertical load case. The ratio between maximum EDC at low-medium velocity and EDC at 800 mm/s is 0.94, 1.15, and 1.36 from low to high vertical load cases, for the first cycle.

The variation between the EDC of the first and second cycle is presented in Figure 32. It can be noted that for low and medium level of vertical load the maximum variation is achieved at about 100 mm/s. For higher velocity a very slightly increasing ratio is maintained. The trend appears quite different for the case study at 13050 kN of vertical load. In this case the ratio increases with velocity up to 400 mm/s, reaching a peak of 1.9.

The reduction of energy from first to second cycle, at the peak velocity of 800 mm/s, is equal to 23%, 32% and 47% for low, medium and high load, respectively.

For tests repeated at the same peak velocity, results were averaged.

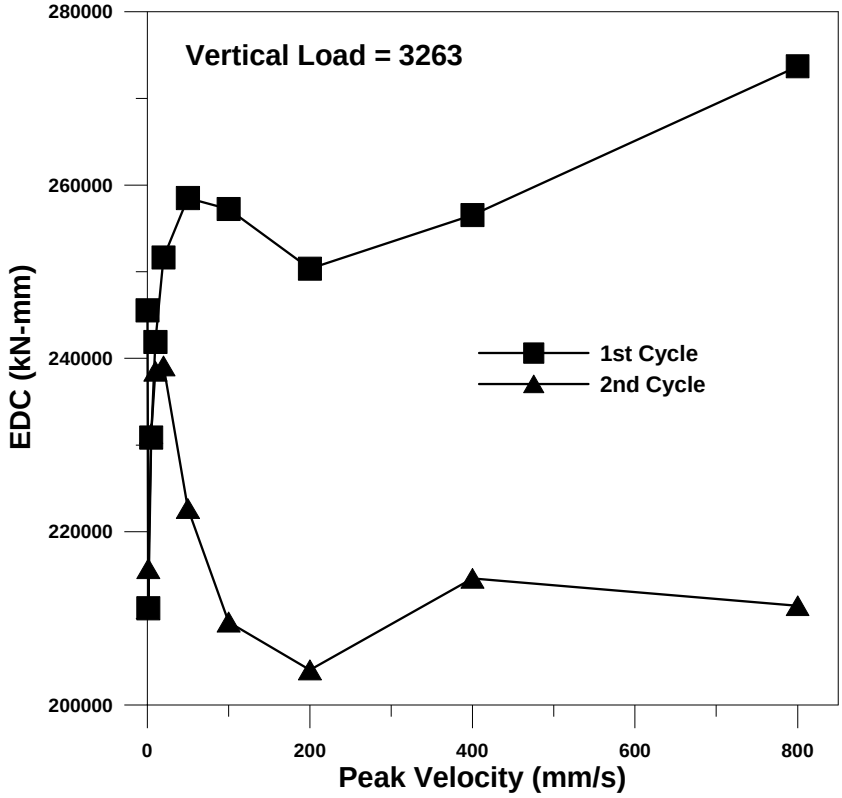

Figure 29 EDC versus peak velocity (Low vertical load)

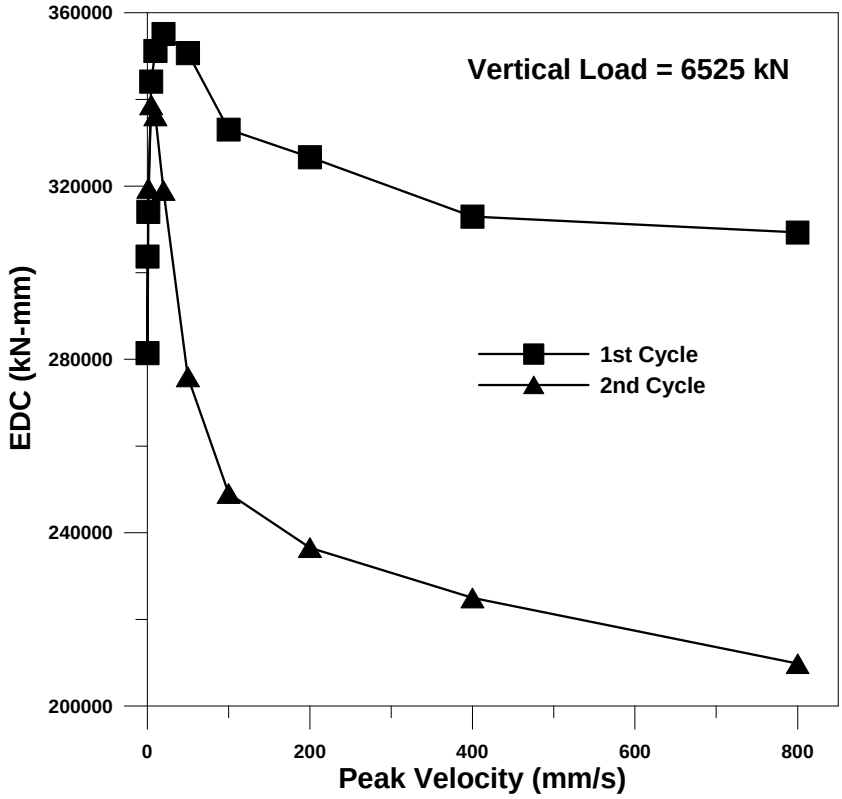

Figure 30 EDC versus peak velocity (Medium vertical load)

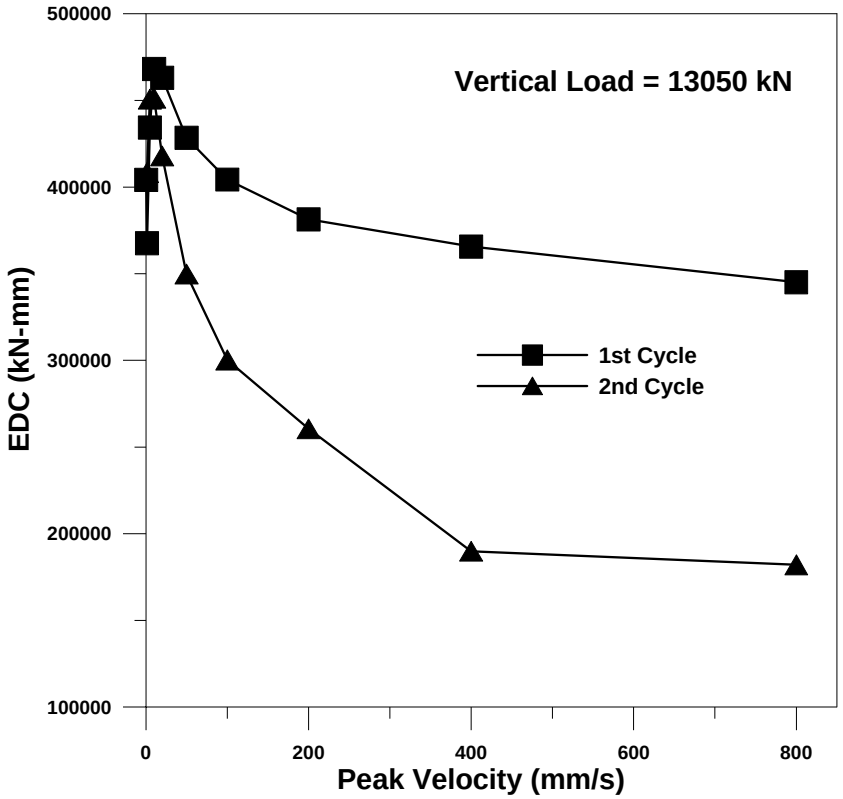

Figure 31 EDC versus peak velocity (High vertical load)

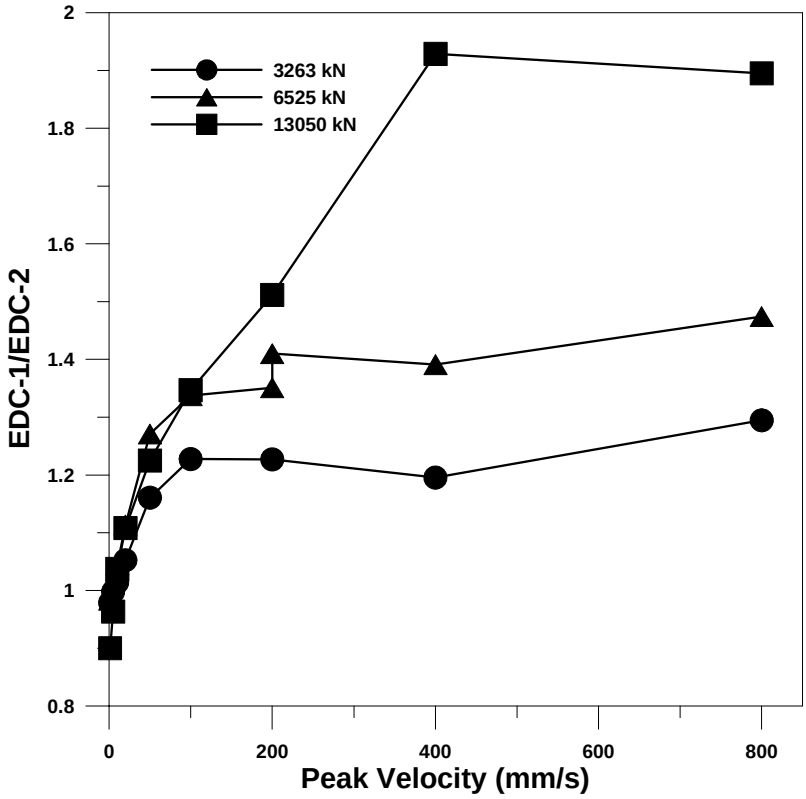

Figure 32 Ratio between EDC of first and second cycle.

Friction Coefficient

The two equations used to estimate the friction coefficient (Eq. 25 for FC_{FO} and Eq. 26 for FC_{EDC}) produced very similar results. The average difference is in the order of 3% between the two approaches, with FC_{FO} resulting, in general, in a smaller coefficient. In what follows the definition of FC_{FO} was used.

Figure 33 shows the friction coefficients, for the first cycle, associated to different vertical loads and velocities.

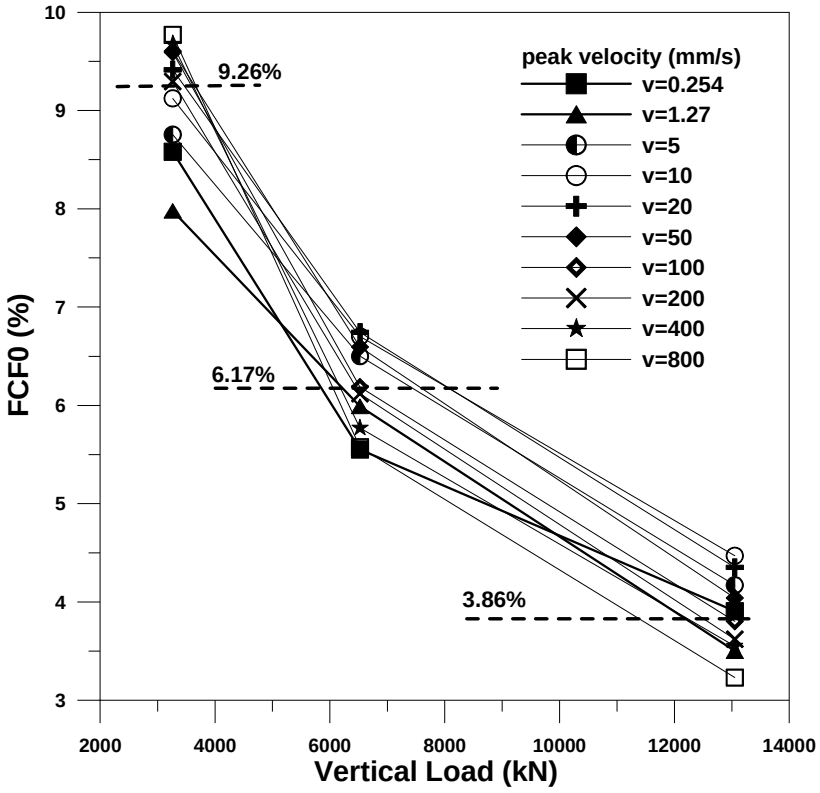

Figure 33 Friction coefficient versus vertical load

At constant vertical load the results for Vload=3263 kN indicate the larger scatter, particularly associated with the test at slow speed (v=0.254 mm/s and v=1.27 mm/s). The average coefficient of friction is 9.26% (indicated in the graph by a dashed line). Each increment of vertical load (increment of 100%) corresponds to a reduction of friction coefficient equal to 33.3% and 37.4%. The graph indicates a variation of FC_{FO}, at constant applied load, equal to 22%, 21% and 28% for low, medium and high load, respectively.

Figure 34, Figure 35 and Figure 36 present the friction coefficient results, for the first and second cycle, at different vertical loads and as a function of the peak velocity. The top plots report the complete range of test velocities. The bottom graphs instead are limited to 100 mm/s. The graphs confirme the importance of the effect due to the test velocity. The increasing range of friction coefficient with velocity, as already observed in terms of peak restoring forces, extends up to 20 mm/s for medium and high vertical loads. For low vertical load (Figure 34) instead, a limited reduction is observed from the very slow test (v=0.254 mm/s) to the test at 1.27 mm/s and at higher test velocities only for the 100 and 200 mm/s cases. The significant reduction from first and second cycle is evident for all cases. For the second cycle the peak friction coefficient is achieved at lower velocities and with a ratio to the first cycle peak of 0.93, 0.94 and 0.95 for low, medium and high vertical load, respectively. The maximum increment of friction coefficient, with respect to the slow speed tests, is very similar for all the vertical load cases and approximately equal to 21%.

Theoretical Model

In order to simplify the comparison between the three vertical load cases and to validate existing numerical models, the results, limited to the first cycle, were normalized to the maximum friction coefficient of each vertical load case. This procedure was first applied to data already part of the SRMD Database, obtained from different bearings tested under different protocols. Figure 37 shows the friction coefficient results (normalized) from previous tests.

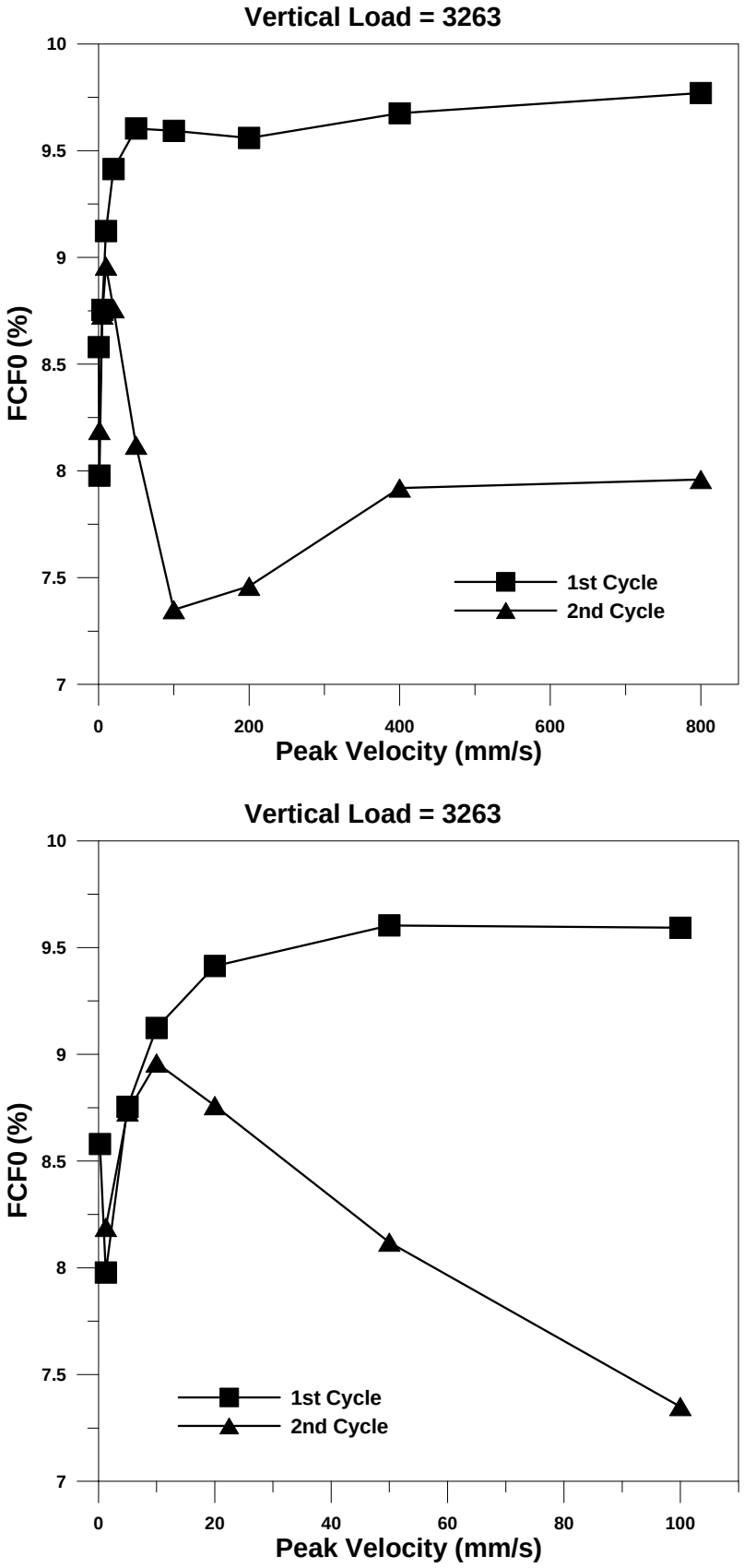

Figure 34 Friction coefficients for low vertical load.

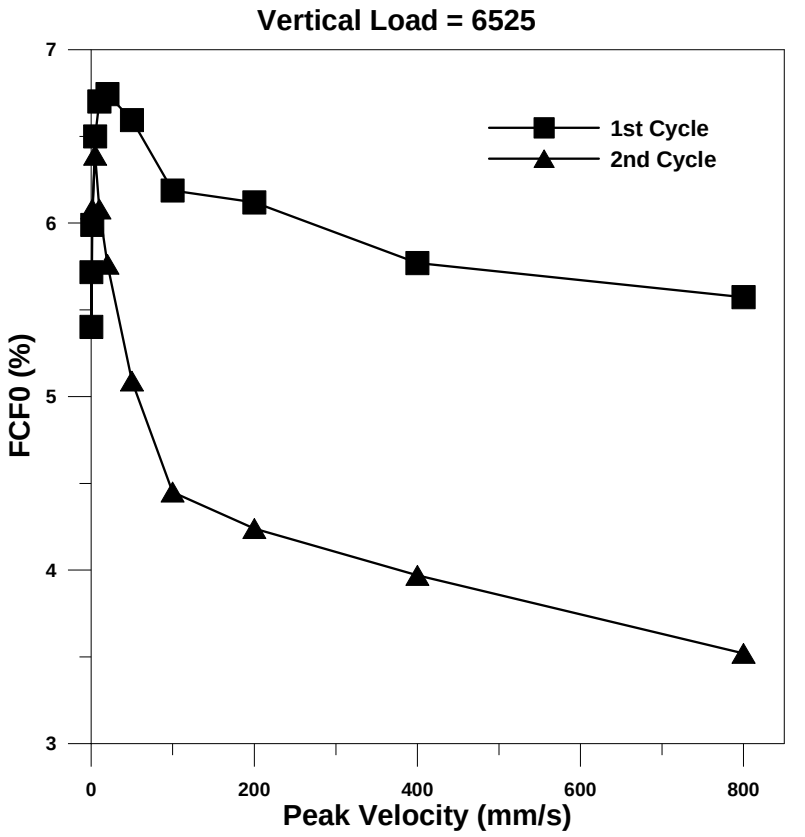

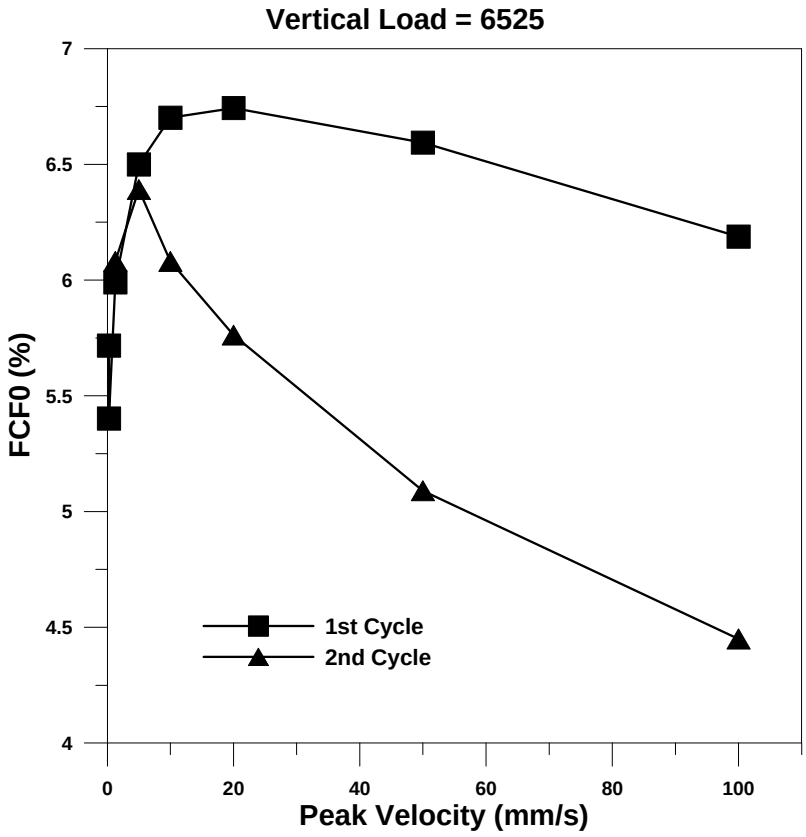

Figure 35 Friction coefficients for medium vertical load.

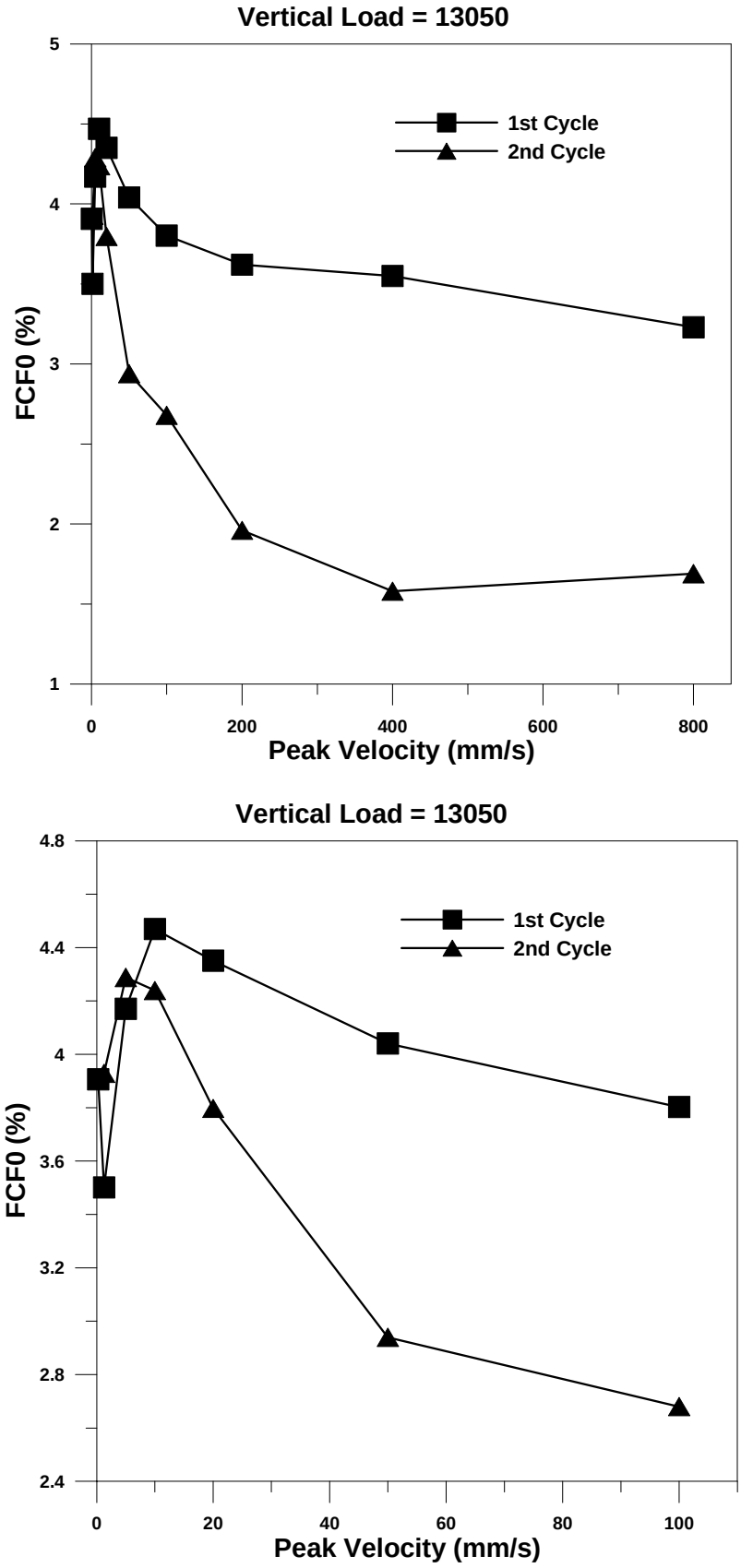

Figure 36 Friction coefficient for high vertical load.

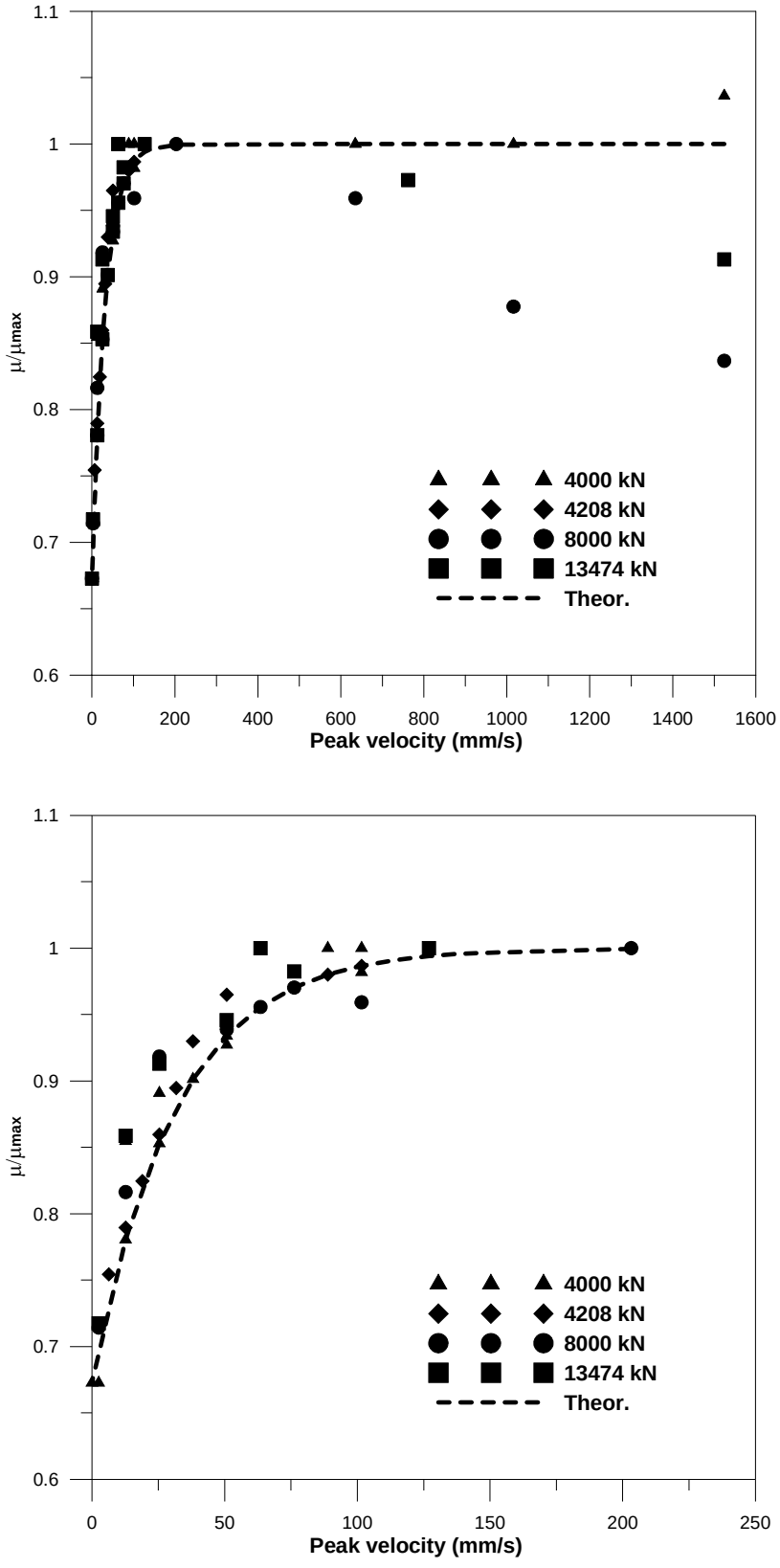

Figure 37 SRMD database- Effects of peak velocity on friction coefficients and numerical model (dashed line).

For these results an existing model, proposed by Mokka (Mokka et. al., 1988) and Constantinou (Constantinou et al., 1990) proved to be able to closely reproduce the variation of the coefficient of friction with sliding velocity. Specifically the model approximate the coefficient of sliding friction by the following equation:

$$\frac{\mu}{f_{max}} = 1 + \left(\frac{f_{min}}{f_{max}} - 1 \right) \exp(-av) \tag{27}$$

Where f_{max} and f_{min} are the maximum and minimum value of the friction coefficient, a is a constant for given bearing pressure and condition of interface and v the velocity. For the available set of data a value of a =0.8 s/in (0.0315 s/mm) provided the good agreement visible in Figure 37. The model cannot however be verified against high velocity effects due to the limited number of data available in this range of speed. For this reason the dashed line of Figure 37 reaches a constant value of 1 maintained for peak velocity higher than 200 mm/s.

The same equation was attempted for the tests object of this study with unsatisfactory results.
It can be noted, in fact, from Figure 34, Figure 35 and Figure 36 that the initial increase (with velocity) of the friction coefficients is steeper than what experienced in previous tests (different sliding material). A new equation and set of coefficients is proposed here in order to obtain an approximate variation of the friction coefficient with sliding velocity.

The proposed relationship between the friction coefficient μ and the peak velocity is:

$$\frac{\mu}{f_{max}} = f(v) = a_1 + a_2 \cdot v^{\alpha} \tag{28}$$

where α =0.3

and the parameters a_1 and a_2 are:

for velocity ≤ 20 mm/s

$a_1 = 0.7505;$
$a_2 = 0.1021;$

and for velocity > 20 mm/s

$$\begin{cases} \text{p} = 15\text{MPa} & \mu/\mu_{\max} = 1 \\ \text{p} = 30\text{MPa} & a_1 = 1.0814; a_2 = \text{-}0.0358 \\ \text{p} = 60\text{MPa} & a_1 = 1.1512; a_2 = \text{-}0.0618 \end{cases}$$

Figure 38 shows the experimental results and the theoretical curves (dashed) obtained with these parameters.

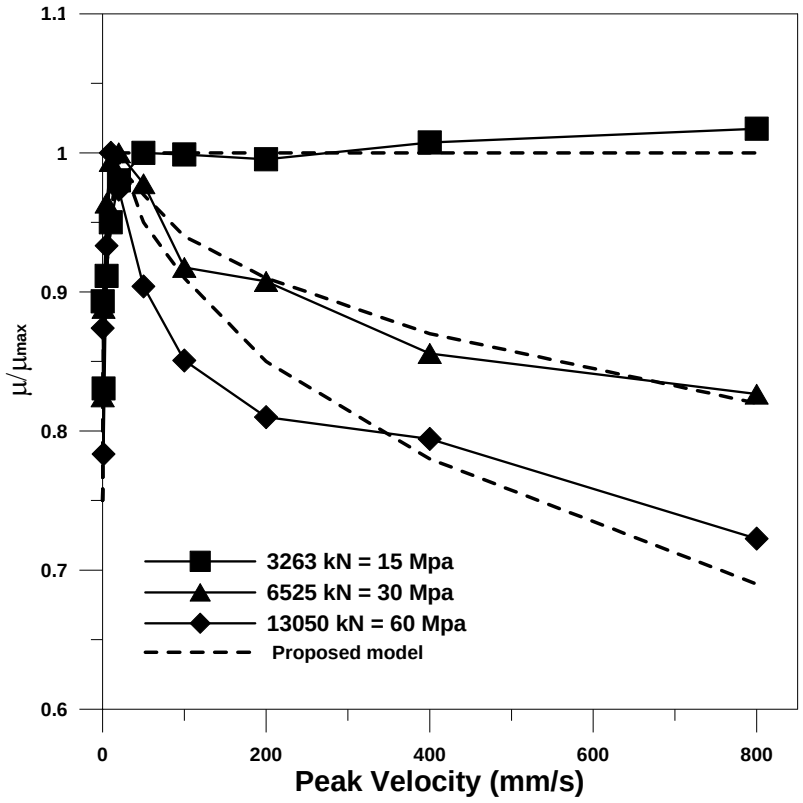

Figure 38 Normalized coefficient of friction function of peak test velocity (Experimental and Numerical)

Restoring Stiffness (K_{ra})

The restoring stiffness, reported in the results tables 7(a), 7(b) and 7(c) as Kra, is obtained as the average between an upper and lower value that represent the slope of the best-fit lines of the force-displacement loop, between ± 0.75 times the maximum displacement. Figure 39 shows the Kra values for different applied loads and peak test velocities. The graph indicates an initial increase of stiffness with velocity to about 20 mm/s. The case of lower vertical load appears to experience a reduction of restoring stiffness, after the initial increment, for peak velocity up to 200 mm/s. This phase of reduction is progressively smoothed for higher vertical loads. A continuous increment, in case of Vload=13050 kN, is, in fact, visible. The dashed lines represent the results for the second cycle, that indicates a significant reduction, with respect to the first cycle results, only for the high load case. The maximum Kra with respect to the reference tests, at velocity of 0.254 mm/s, is 30%, 10% and 12% for increasing vertical load cases.

The dash-dot lines shows the theoretical value, suggested in literature (Zayas et al. 1990), (Pranesh et al. 2000), for the restoring stiffness Kra. The authors propose Kra to be obtained as:

$$Kra = \frac{F_v}{R} \tag{29}$$

Were R is the radius of curvature of the concave portion of the bearing and F_v is the applied vertical load. For the present tests, it is particularly visible the disagreement between the proposed equation and the experimentally observed results. The difference is particularly significant for the high load case.

The proposed equation is based on the assumption that the restoring forces are calculated as indicated in Eq. 30, and visualized in Figure 40, where x is the relative displacement across the bearing and μ the friction coefficient.

$$F = \frac{F_v}{R} x + sign(\dot{x}) \mu F_v \tag{30}$$

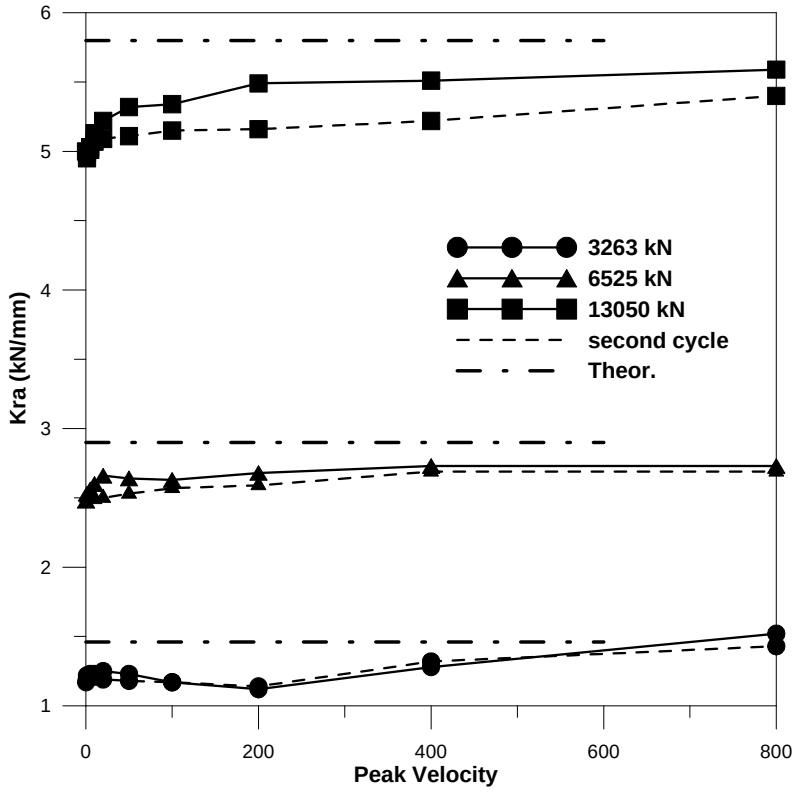

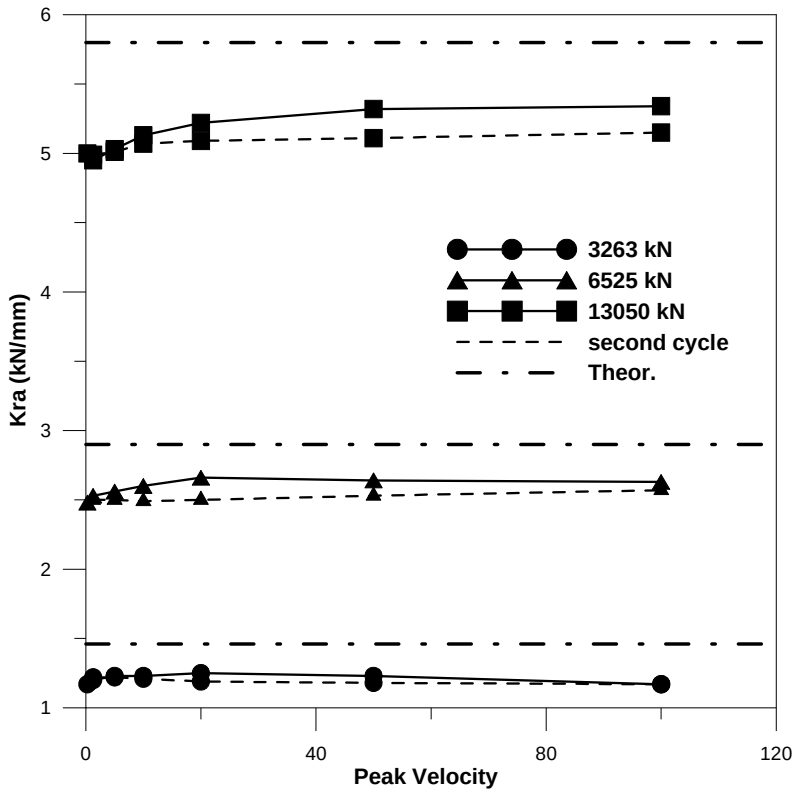

Figure 39 Restoring stiffness versus peak velocity

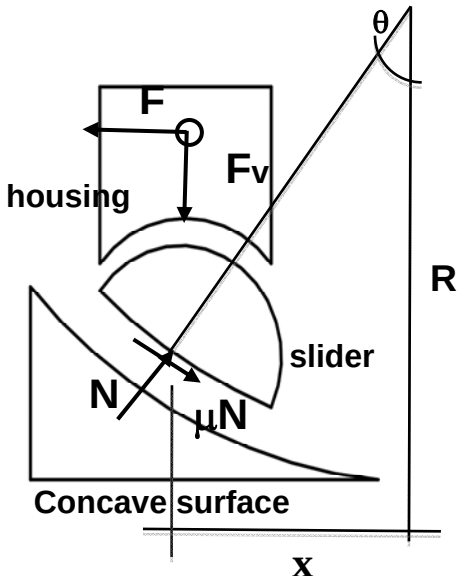

Figure 40a-*Tradition* Force Mechanism

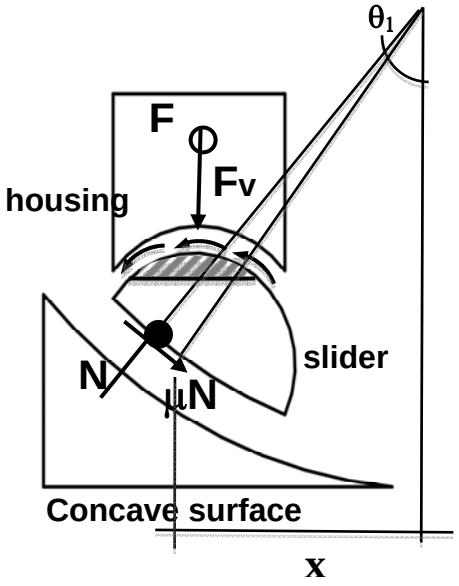

Figure 40b-*Modified* Force Mechanism

Equation 30 takes into account only the frictional forces developed at the interface between concave surface and articulated slider. However, in order to displace, the articulated slider needs to rotate inside the top housing of the device, where a composite material (with the same coefficient of friction of the composite at the bottom of the slider or of different friction characteristics) is applied. This interface develops frictional forces that result in an additional moment to be applied to the force balance mechanism.

During previous tests performed at the Caltrans SRMD Testing Facility, the results, in terms of Kra (Figure 22) indicated a general deviation from the indicated theoretical equation (Eq. 29), confirmed by the tests described in this report. A general trend however cannot be identified, based on the available results, in terms of influence of the vertical load in this phenomenon. A conclusive explanation of the variation of the parameter Kra is still subject of research, but preliminary considerations can be proposed.

With the assumption that the top and bottom sliding material are of identical characteristics, an analysis of the friction mechanism developed at both the moving interfaces of the slider indicated

that the previous equation needed to be modified as follows, in order to take into account the effect introduced by the moment developed at the top interface:

$$F_{\text{mod}} = F_v \tan\theta_1 + sign(\dot{x})\mu \frac{N_{\text{mod}}}{\cos\theta_1} \tag{31}$$

where :

$$\theta_1 = \arcsin\left(\frac{x}{R}\right) + \frac{F\,b}{N\,R} \tag{32}$$

and

$$N_{\text{mod}} = \frac{F_v}{\cos\theta_1 - sign(\dot{x})\mu} \tag{33}$$

where the variables are indicated in Figure 40.

The proposed formula, that contains a level of approximation, for instance in the definition of the level arm b needs further validation and development, but it is proposed here to raise attention to this specific phenomenon that deserve to be addressed.

This condition is, in fact, critically related to the vertical loads for several additional reasons. The pressure at the interface between slider and concave portion of the device is not uniform, as instead indicated in literature (Zayas, 1990). The resultant force, perpendicular to the bottom of the slider, is in fact not located at the center of the slider. This introduces concerns about possible edge gouging into the strainless steel overlay of the concave portion and about high frequency stick-slip type of motions. This uneven distribution of pressure should also be addressed in terms of effects on the friction coefficient, function of velocity and pressure (Constantinou et al. 1999).

RESPONSE TO BI-DIRECTIONAL MOTION.

A limited number of additional tests were completed for one bearing, in order to investigate the effects of bi-directional input. The test description is presented in Table 9.

TEST #	Test Description	Vload (kN)	Displ (mm)	Peak Vel. (mm/s)	# cycles	Motion direction
1	Cloverleaf low load	3260	200	88	3	Bi-direct.
2	Cloverleaf medium load	6525	200	88	3	Bi-direct.
3	Cloverleaf medium load -2	6525	200	88	3	Bi-direct.
4	Cloverleaf high load	13050	200	88	3	Bi-direct.
5	Medium load only in Long direction	6525	200	88	3	Longitudinal
6	Medium load Only in Lat direction	6525	100	45	3	Lateral

Table 9 Test matrix for bi-directional motion

The cloverleaf motion (Figure 41) was completed at the maximum displacement of 200 mm, in the longitudinal direction, consistently with the displacement used for the previous tests. The displacement amplitude in the lateral direction was 100 mm. Three levels of vertical load were applied: low (3260 kN), medium (6525 kN) and high (13050). The peak velocity was equal to 88 mm/s in the longitudinal direction and 45 mm/s in the lateral direction.

The small loops visible in Figure 41 indicate the entrance and exit loops applied to allow the table to achieve the desired peak velocity. The last two tests of Table 9 were performed with a mono-dimensional input identical to the two separate components of the clover-leaf tests.

Test 3 was a repetition of test 2, with identical input parameters.

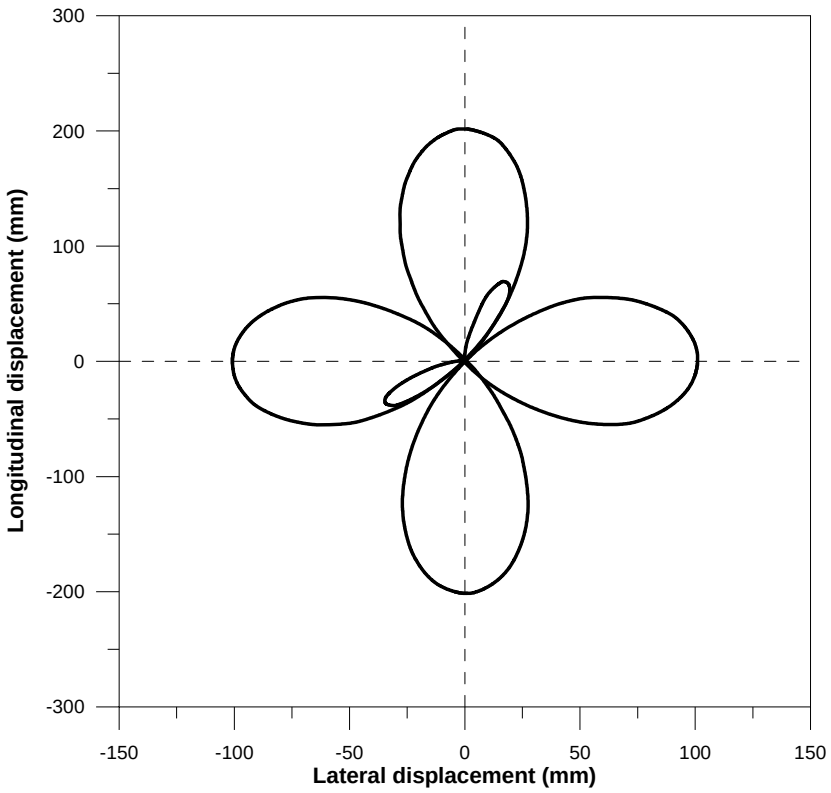

Figure 41 – Longitudinal and Lateral displacement of bi-directional motion.

The peak values of restoring force, developed by the bearing under different vertical loads are reported in Table 10.

The results, in terms of diagonal force, indicate an increase, for each vertical load level, of about 36% for the peak positive force. For the peak negative force (Fmin) the increment is 39% from low to medium vertical load and 81% from medium to high. It could be noted that, even though the amplitude of displacements in longitudinal direction is double the lateral component, peak force components are often higher in lateral direction.

After averaging the results for the medium load tests (tests 2 and 3) , the forces obtained in mono-directional tests (test 5 and 6) were compared with the related data from bi-directional motions.

Results from tests 5 indicate higher peak values of force compared to the cloverleaf motion under the same vertical load. Specifically the peak positive and negative forces are 7.5% and 14.3%

higher than the forces from the bi-directional tests, respectively. The lateral tests (Test 6) indicate an increase of force equal to 25.7% and 4.75% for positive and negative peaks, respectively.

#	Test	Diagonal		Longitudinal		Lateral	
		Fmax	**Fmin**	**Fmax**	**Fmin**	**Fmax**	**Fmin**
		(kN)	**(kN)**	**(kN)**	**(kN)**	**(kN)**	**(kN)**
1	Cloverleaf low load	626.92	-561.44	445.15	-480.13	573.35	-604.88
2	Cloverleaf medium load	861.76	-806.83	724.51	-739.48	849.98	-819.80
3	Cloverleaf medium load -2	836.99	-758.01	813.45	-707.49	802.77	-716.06
4	Cloverleaf high load	1168.21	-1419.22	1142.46	-1372.65	1116.38	-1055.90
5	Medium load only in Long direction	/	/	826.29	-827.04		
6	Medium load only in Lat direction	/	/	/	/	1038.71	-804.42

Table 10 Peak force results

Friction coefficients are reported in Table 11. The average friction values for the two cloverleaf tests at medium level of applied load (test 2 and 3) are 9.96%, 5.29% and 5.2% for first, second and third cycle, respectively. The reduction, due to increase in vertical load, in the bi-directional tests, is equal, for the first cycle, to 17.4% and 57.4% from low to medium and from medium to high load, respectively. Reductions are less significant for the second and third cycle.

Test		1st cycle	2nd cycle	3rd cycle
		%	(kN)	(kN)
1	Cloverleaf low load	12.06	6.93	6.58
2	Cloverleaf medium load	10.49	5.65	5.55
3	Cloverleaf medium load -2	9.43	4.94	4.86
4	Cloverleaf high load	4.22	3.05	2.78
5	Medium load only in Long direction	6.27	5.15	4.75
6	Medium load only in Lat direction	6.68	6.60	6.06

Table 11 Friction coefficients

The two tests in longitudinal and lateral direction (Test 5 and Test 6) indicate a significant smaller value for the friction coefficient of the first cycle, when compared to the results of the cloverleaf tests (6.27% and 6.68% versus 9.96%). Less variation is visible instead for the coefficients obtained for the second and third cycle. In general also the lateral-only test (Test 6) indicates a quite constant level of friction for all the three cycles.

The proposed study, far from representing a comprehensive analysis of the problem, indicate the need to consider the validity of bi-directional tests for a complete testing program of this type of bearings. In previous test programs, for specific bridge projects, tests were included in different direction of motions, but always as mono-directional displacements. The reduction in friction coefficients, when a 2D motion is applied, suggests the introduction in device qualification protocols of additional patterns of bi-direction motion, to identify possible variations of friction coefficients related to specific characteristics of the sliding materials as well as to thermal effects.

TORSIONAL EFFECTS INTRODUCED BY VERTICAL LOAD VARIATION ON SIDE BY SIDE DEVICES.

A typical single pier installation of two sliding devices is sketched in Figure 42 (Calvi et al., 2004). The horizontal inertial force, due to the horizontal earthquake components, is here applied at the center of mass of the deck G. The force *F* introduces an overturning moment M_R that need to be balanced by the axial force variation between the two isolators ΔN_R.

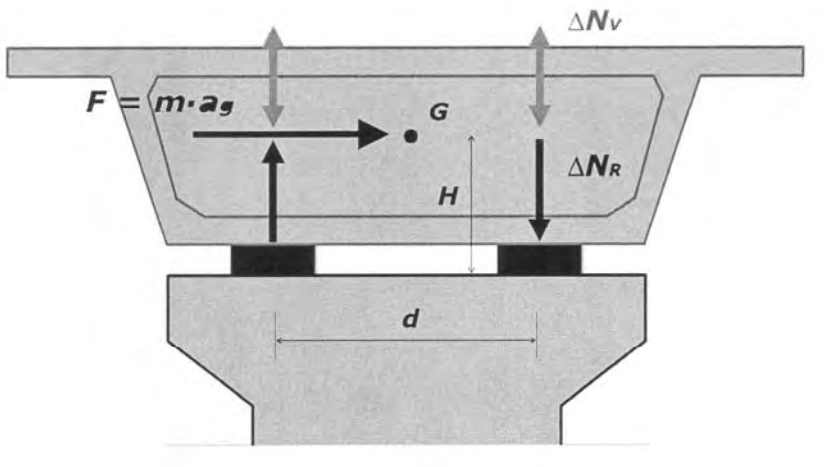

Figure 42 Typical two isolators installation

A unique characteristic of the Friction Pendulum bearings is the proportionality of the restoring forces to the vertical load applied. The term ΔN_R will, for this reason, generate a different response in the two installed bearings. The vertical load change is manly related to the ratio d / H (deck aspect ratio). In existing bridges, values of d / H between 1 and 3 are very common. This geometry can introduce a vertical force variation greater than 30% of the total deck weight, with consequent proportional change in the restoring forces of the isolators. The effective stiffness (or post-yielding stiffness) of the single bearing is obtained as ratio between the deck weight W and the radius of curvature *R* of the concave surface ($K_{eff} = W / R$). It is easy to demonstrate that, even in case of vertical load variation, the total effective stiffness of the two bearing installation of Figure 42 is double the stiffness of the single device $K_{eff_{total}} = 2W/R$. The two terms $+\Delta N_R$ and $-\Delta N_R$ in fact cancel. The same applies to the hysteretic force μW, where μ is the coefficient of friction. The overall system seems, in other words, to be unaffected by the axial force variation

that does not modify the global response of the system in terms of total shear demand for the pier. However, the uneven distribution of shear forces in the two devices causes an additional torsional demand, as visualized in Figure 43.

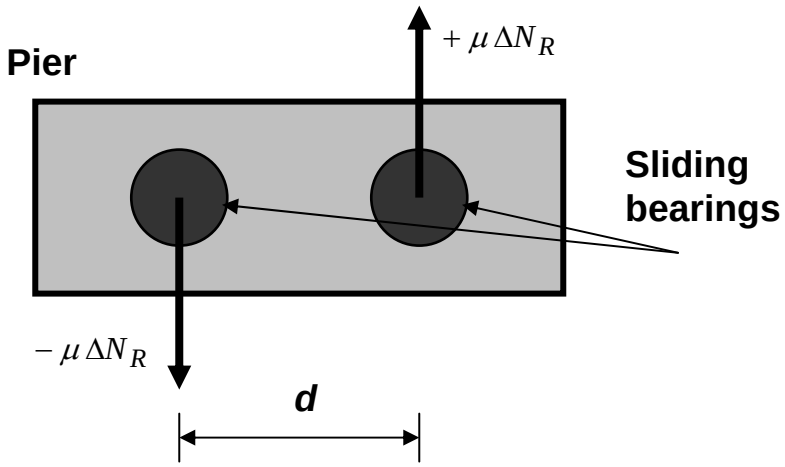

Fig. 43 Plan view: Additional torsional demand

This additional demand is not usually addressed, even in very recently completed numerical and experimental work. In Mosqueda et al. (2004) the experimental program confirms the described effect of cancellation of the effects of the overturning forces, in terms of displacement demand, but the torsional effect is not addressed and the author's conclusion that the effect of the vertical earthquake shaking are negligible is mainly motivated by an incomplete approach to the problem. Parametric analysis of Finite Element bridge models (Calvi et al, 2004), contributed by a visiting scholar at UCSD, indicate that, for straight bridges, the effect of axial load variation in terms of displacement demand is effectively marginal. The increase in total shear demand for the piers is instead significantly increased (up to 99%) in the presence of the vertical input component. For curved bridges the analyses indicate that due to the geometric effect of the structure, the axial force variation is distributed in non-uniform fashion between the isolators even without the vertical input component. Peak increments of pier shear demand were obtained as equal to 46% and 94% with or without vertical input component, respectively. Similar observations are confirmed by several authors (Priestley et al., 2002) (Anderson et al., 2001).

In order to verify the development of induced torsional effects, in case of varying axial loads, a limited experimental program was designed, taking advantage of the performance of the Caltrans SRMD testing rig. If two sliding bearings are installed side by side, as schematically shown in Figure 44, the table of the SRMD rig can be seen as the equivalent of the bridge pier top. The vertical reaction frame instead simulates the bridge deck and the variation of vertical load, between bearings, can be imposed simply rotating the table about the longitudinal axis (Roll) as indicated in Figure 44. This configuration allows, with imposed constant axial load (different between the two bearings) to obtain the system response under condition of artificially generated overturning moment. During motions of the table in the horizontal plane the moment that control the "in-plane" rotation of the table (Yaw moment) will provide a direct read-out of the introduced torsional demand on the pier.

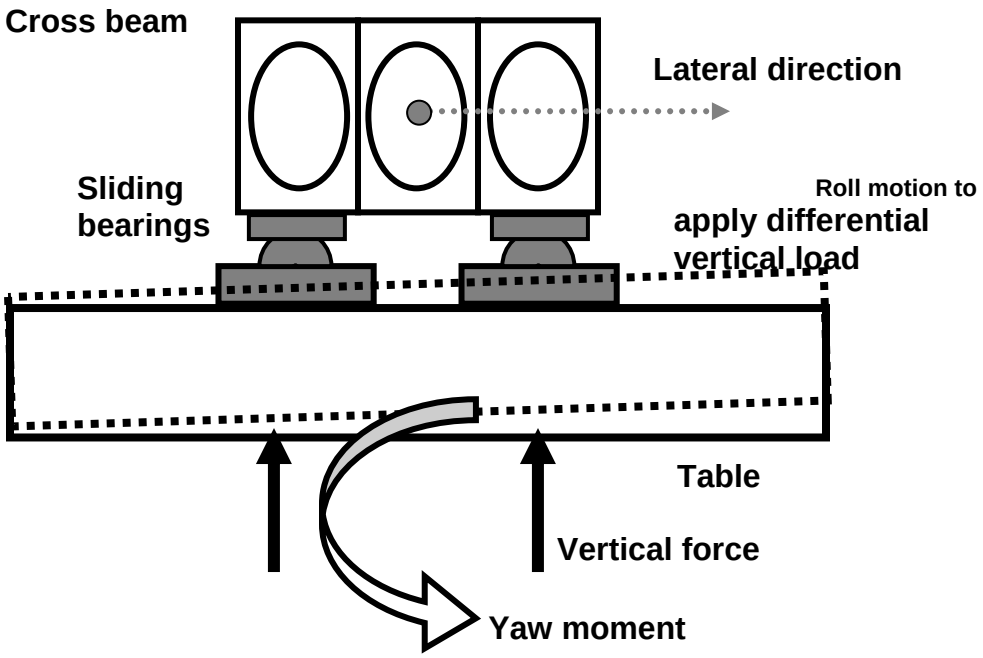

Fig. 44 Cross section of the test setup designed to simulate the installation of Fig. 42

Detailed drawings of the table installation of two identical bearings are presented in Figure 45, Figure 46 and Figure 47.

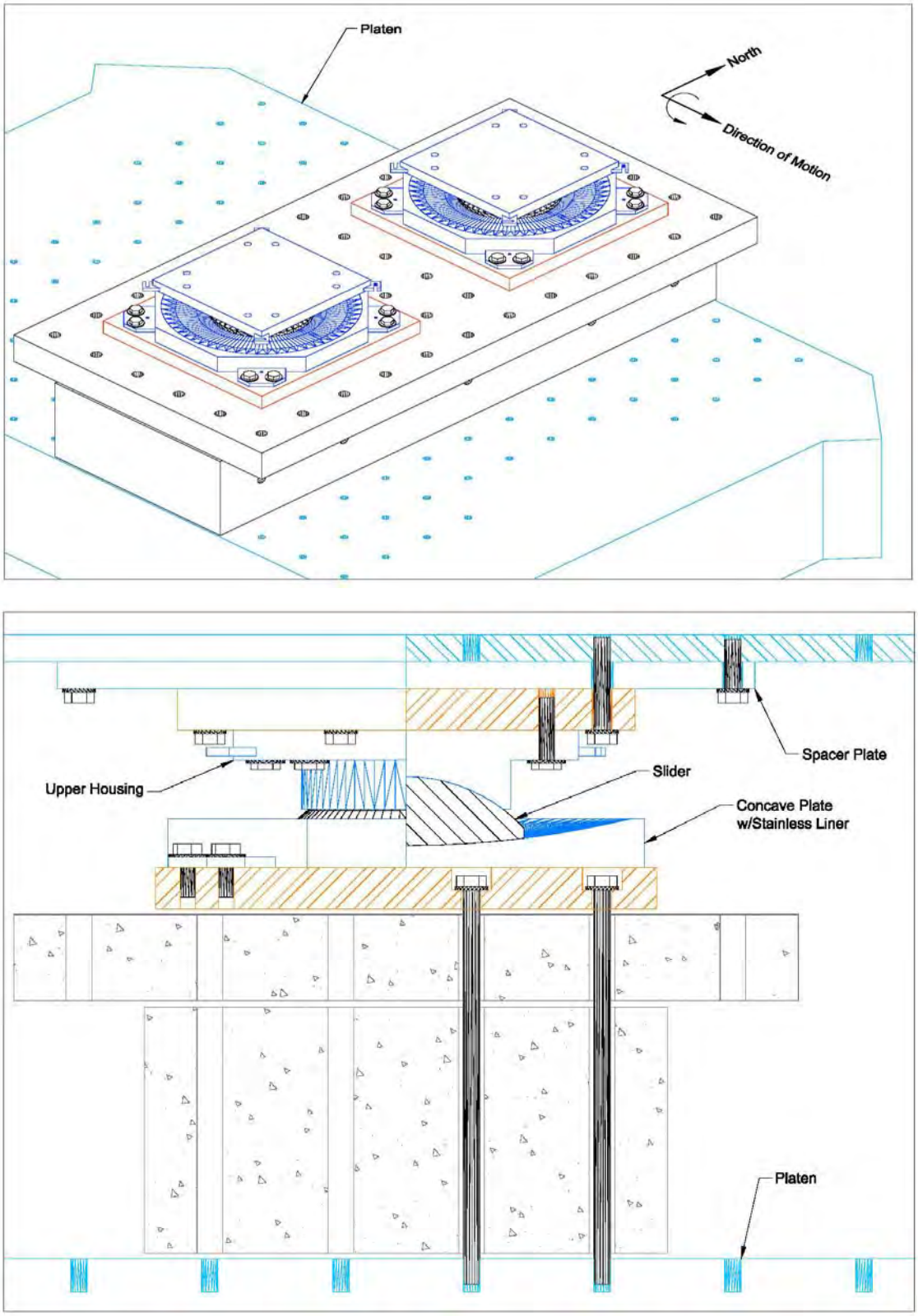

Figure 45 Overview of Test Setup

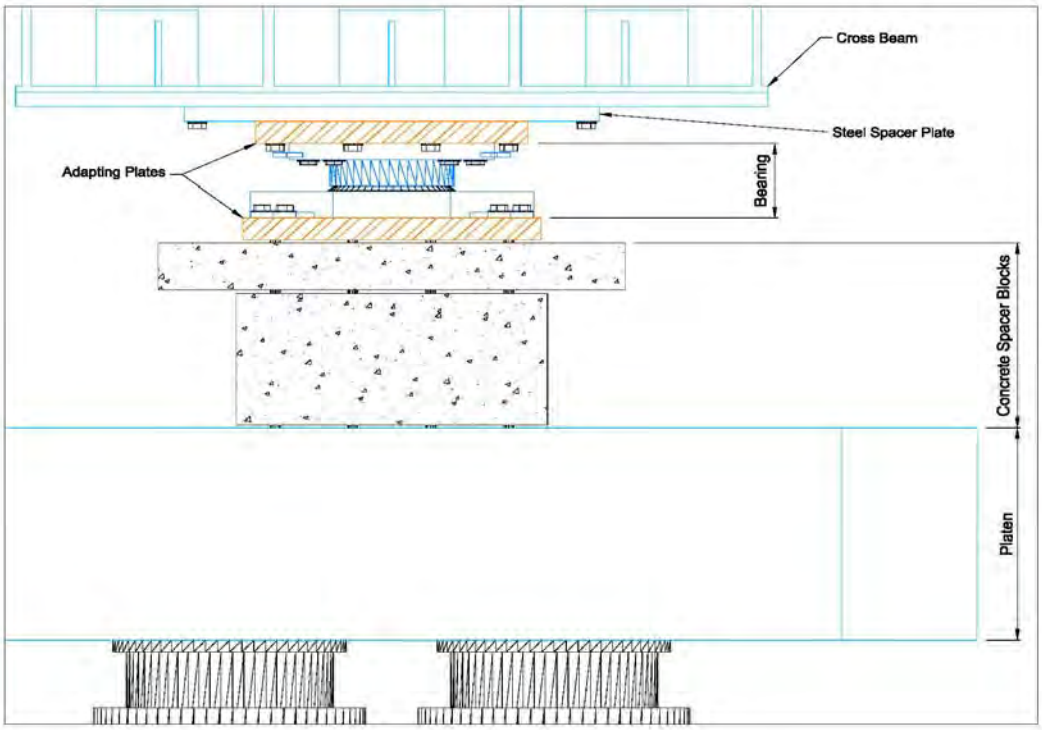

(a) Elevation Facing North

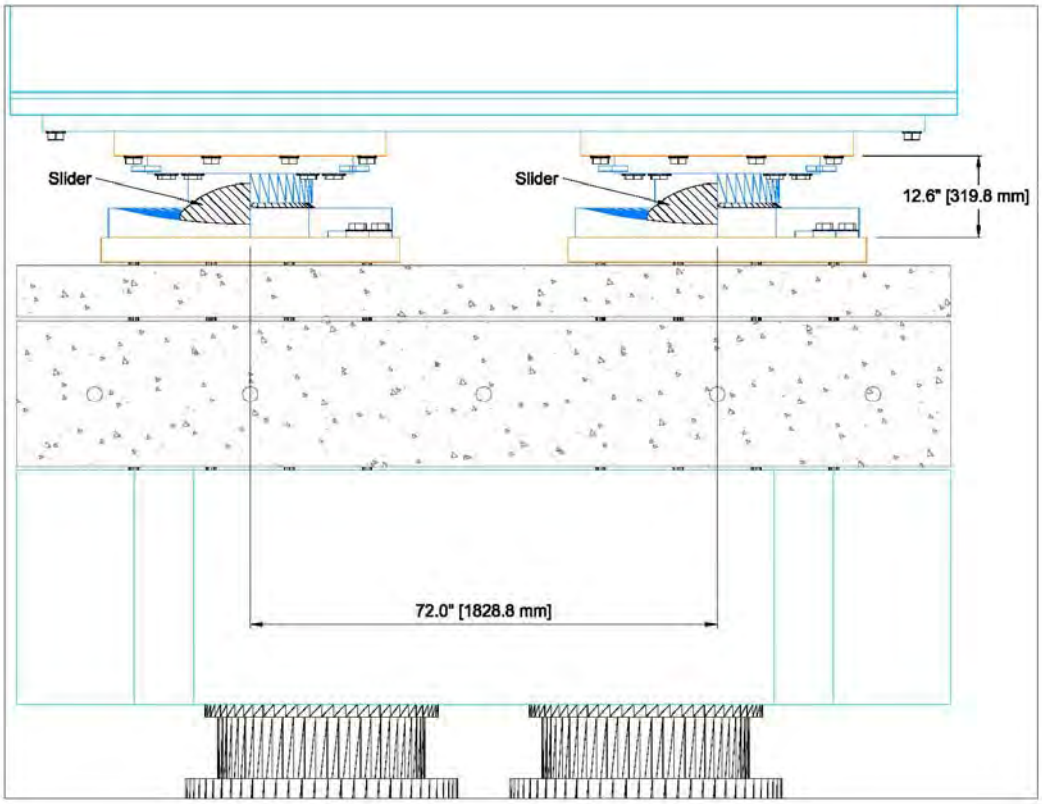

(b) Elevation Facing East

Figure 46 Test Setup Schematics

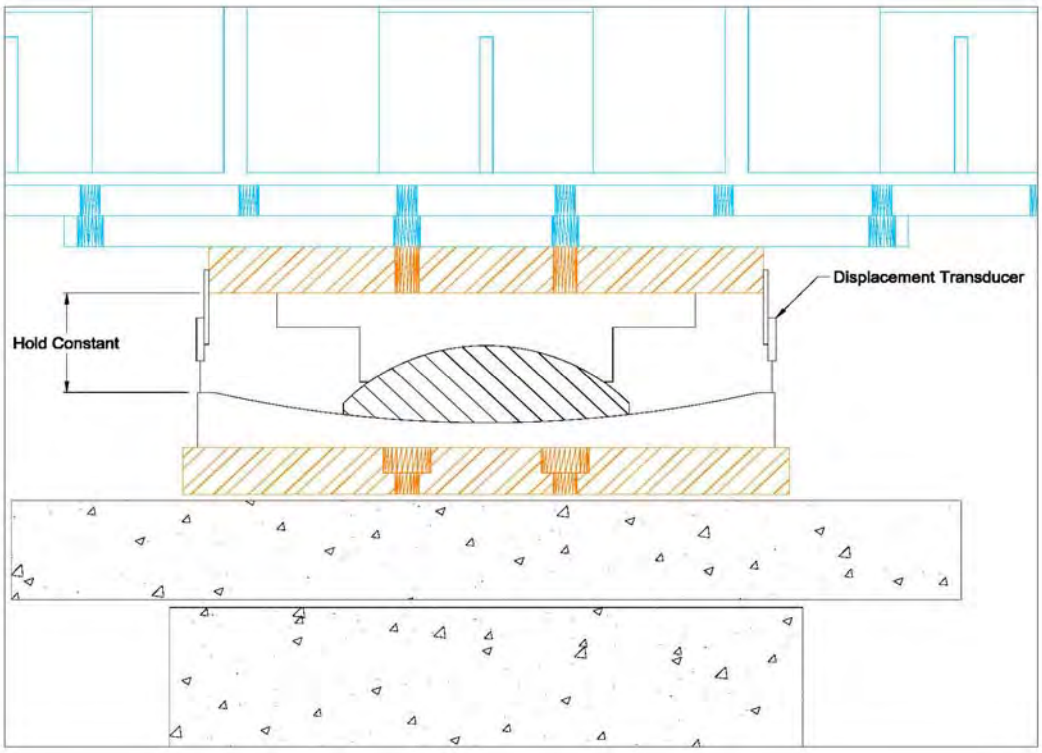

(a) Elevation Facing North

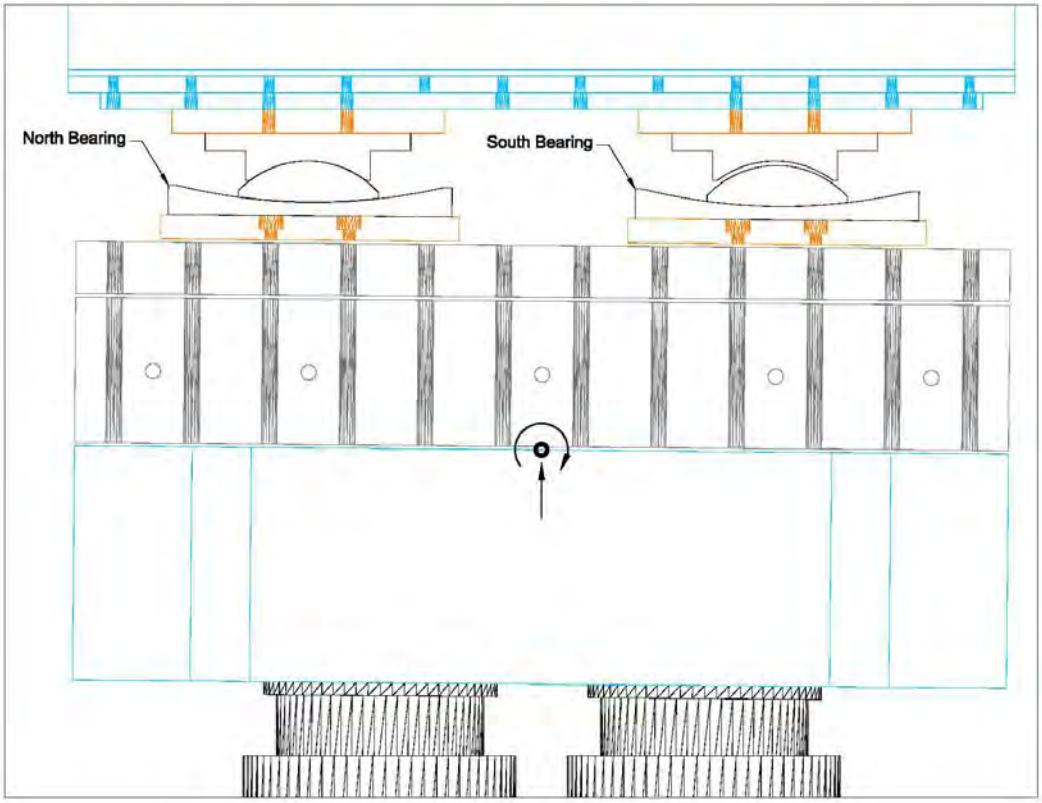

(b) Elevation Facing East

Figure 47 Rotated Configuration

The experimental program for this specific topic consisted of the series of tests listed in Table 12. The displacement and velocity figures are relative to motions in longitudinal direction.

Test #	Displ. (mm)	Velocity (mm/s)	North Bearing Vertical Load (kN)	South Bearing Vertical Load (kN)	# Cycles	Comments
1	200	100	6525	6525	3	Base Line Response @ 13050 kN
2	200	100	8050 (+ 23%)	5000 (-23%)	3	
3	200	100	10050 (+ 54%)	3000 (-54%)	3	
4	200	100	12050 (+85%)	1000 (-85%)	3	
5	200	100	8025	8025	3	Base Line Response @ 16050 kN
6	200	100	10025 (+25%)	6025 (-25%)	3	
7	200	100	12025 (+50%)	4025 (-50%)	3	
8	200	100	14025 (+75)	2025 (-75%)	3	

Table 12 Testing Protocol for differential axial load analysis

The amplitude of displacement and the peak velocity was maintained constant for all the tests at 200 mm and 100 mm/s, respectively. Two tests were completed for base line response at 13050 kN total (Test 1) and at 16050 kN total (Test 5). During these two tests the table was maintained parallel to the vertical reaction frame in order to guarantee the same applied vertical load in each bearing. The vertical load of Test 1 corresponds to the medium level of the previous tests. The load of Test 5 applies an increment of 23% to the previous load case.

After each base line test, the table was rotated about the east-west axis (Roll) in order to create a variation of vertical load between the north and south bearing. Each step of rotation corresponds to a variation of vertical load of about 2000 kN with respect to the previous test. The variation, with respect to the baseline test, is reported in percentage in Table 12 (in parenthesis).
In order to verify the applied load, the north bearing "target" vertical load was applied through the system while maintaining a separation between the south bearing slider and housing. Once the target vertical load was achieved, displacement transducers were installed along the east/west centerline of the north bearing and initial readings were recorded. The total vertical load (13050 kN or 16050 kN) was applied to the system while holding the displacement across the north bearing constant via the displacement transducers and modifying the vertical & roll displacement components. Once the total vertical load was achieved, the system was brought into vertical load force control and so maintained during the run. Figure 48 show the bearings at zero and maximum displacement. Basic results of the tests are reported in Table 13 where the response parameters are relative to the overall assembly of two bearings.

For comparison with previous tests on a single bearing, the values of FC_{FO} (friction coefficient) are averaged among the eight tests. For the first cycle the average is 5.92% and for the second cycle the average FC_{FO} is equal to 4.96%. These values can be compared with what indicated in Table 7(b) for the test (vel-m-7) performed at the same peak velocity (100 mm/s). The test on a single bearing indicate a friction coefficient of 6.19% and 4.45% for the first and second cycle, respectively. From Table 13 it could be noted that the reduction between friction coefficient of the second and third cycle is limited.

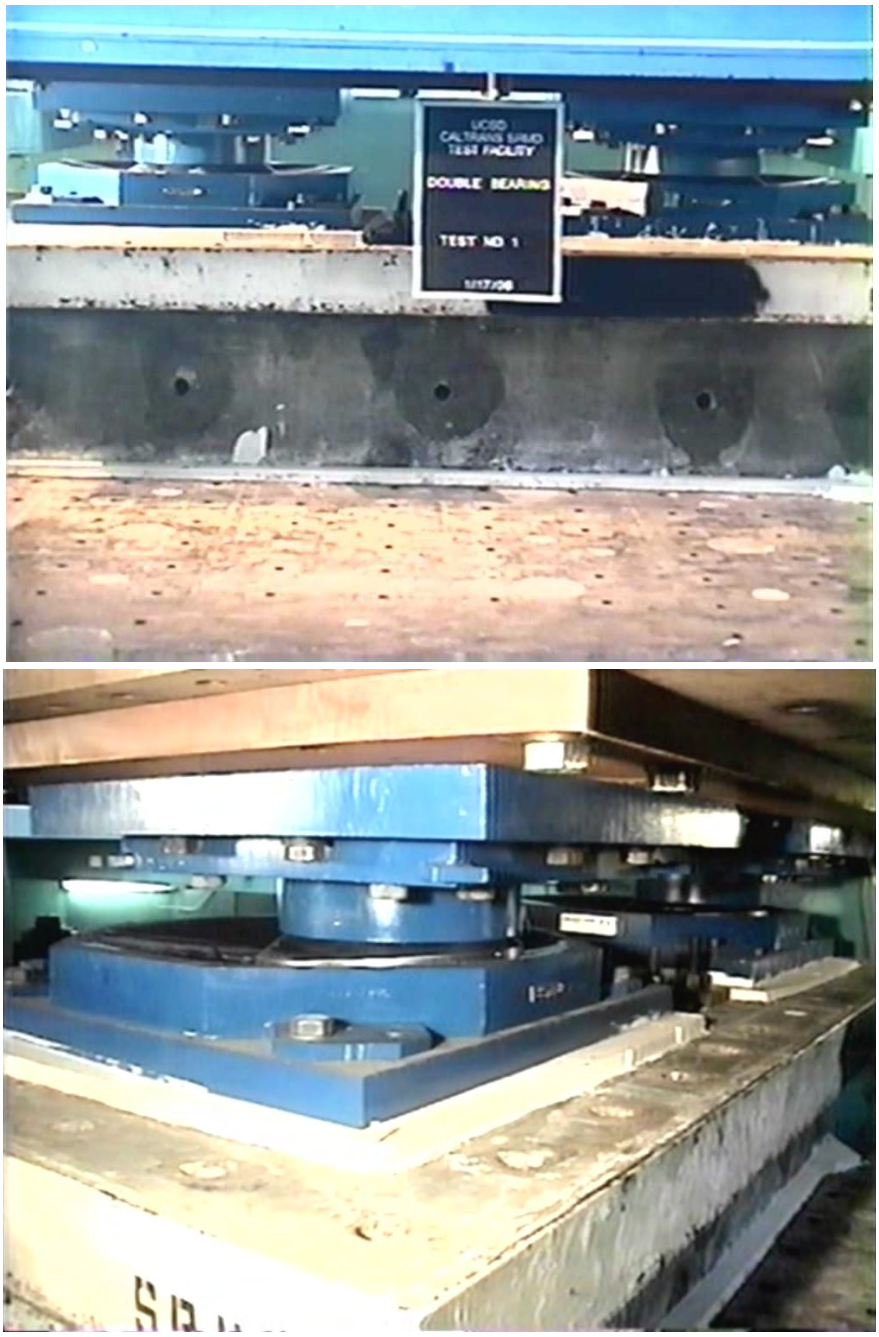

Figure 48 Overview of test setup at zero and maximum displacement.

Test	cycle	Fmax	Fmin	F0	Kra	Keff	EDC	FC_{F0}	FCedc	beq
		(kN)	(kN)	(kN)	(kN-mm)	(kN-mm)	(kN-mm)	(%)	(%)	(%)
Test #1	1	1692	-1641.9	783.01	5.17	8.30	633937.00	6.00	6.05	30.13
	2	1597.5	-1588.9	692.84	4.74	7.94	557679.00	5.31	5.32	27.75
	3	1589.7	-1586.1	536.86	4.86	7.91	546679.00	5.27	5.22	27.29
Test #2	1	1790	-1734.2	859.53	5.22	8.78	703096.00	6.59	6.71	31.63
	2	1683.9	-1645.9	731.15	4.84	8.30	590512.00	5.60	5.64	28.14
	3	1620.3	-1606.4	568.64	4.94	8.05	548337.00	5.25	5.24	26.99
Test #3	1	1809.9	-1726.7	854.10	5.25	8.81	692712.00	6.54	6.61	31.07
	2	1660.1	-1629.2	711.09	4.89	8.20	574806.00	5.45	5.49	27.73
	3	1603.9	-1585.3	537.50	4.97	7.96	528954.00	5.06	5.06	26.34
Test #4	1	1630.6	-1601	675.72	5.33	8.06	548009.00	5.18	5.23	26.91
	2	1490.4	-1511.2	538.29	4.99	7.48	434967.00	4.12	4.15	23.00
	3	1450.7	-1472.3	414.12	5.03	7.29	399973.00	3.88	3.82	21.73
Test #5	1	2166.1	-2056.1	989.12	6.42	10.51	798584.00	6.16	6.20	29.98
	2	1983.6	-1951.7	811.66	6.02	9.80	657219.00	5.06	5.10	26.48
	3	1921.7	-1909	577.60	6.13	9.54	604428.00	4.70	4.69	25.03
Test #6	1	2149.4	-2060.7	941.33	6.47	10.49	779828.00	5.87	6.05	29.37
	2	1944.7	-1933	774.75	6.01	9.67	626247.00	4.83	4.86	25.63
	3	1875.8	-1877.7	563.69	6.11	9.36	572728.00	4.48	4.45	24.22
Test #7	1	2088.1	-1999.1	900.28	6.38	10.19	736511.00	5.61	5.72	28.59
	2	1922.8	-1903.1	758.74	5.99	9.54	612891.00	4.73	4.76	25.43
	3	1874.9	-1880.9	592.90	6.09	9.37	574438.00	4.47	4.46	24.29
Test #8	1	2083.1	-2006.1	870.99	6.50	10.20	718787.00	5.43	5.59	27.91
	2	1928.6	-1898	738.62	6.05	9.55	596767.00	4.60	4.64	24.77
	3	1871.1	-1846.7	556.39	6.11	9.28	550053.00	4.24	4.28	23.50

Table 13 Results for double-bearing installation.

For the purpose of these tests, the yaw feedback moments are reported in Figure 49 and Figure 50 for a total vertical load of 13050 kN and 16050 kN, respectively. As indicated above they represent the total moment, detected at the center of the table, necessary to restrain the table from a rotation in plan, during the applied motion. These moments should be considered as the total torsional moment transmitted to the structure supporting the double-bearing configuration, given the same motion and vertical load level. In order to remove the effects of a small component of yaw that is always introduced in the table at the reversal of motion, the signals for tests 2, 3 and 4 were modified by subtracting the yaw moment obtained from Test 1. The same approach was applied to

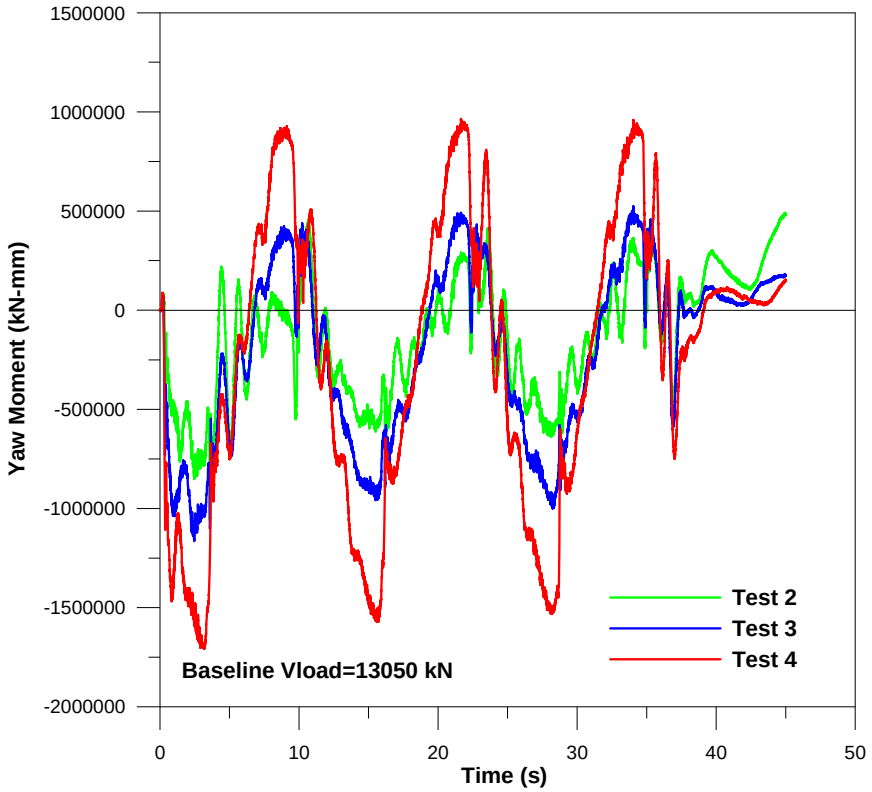

Figure 49 Yaw moment from Tests 2,3 and 4

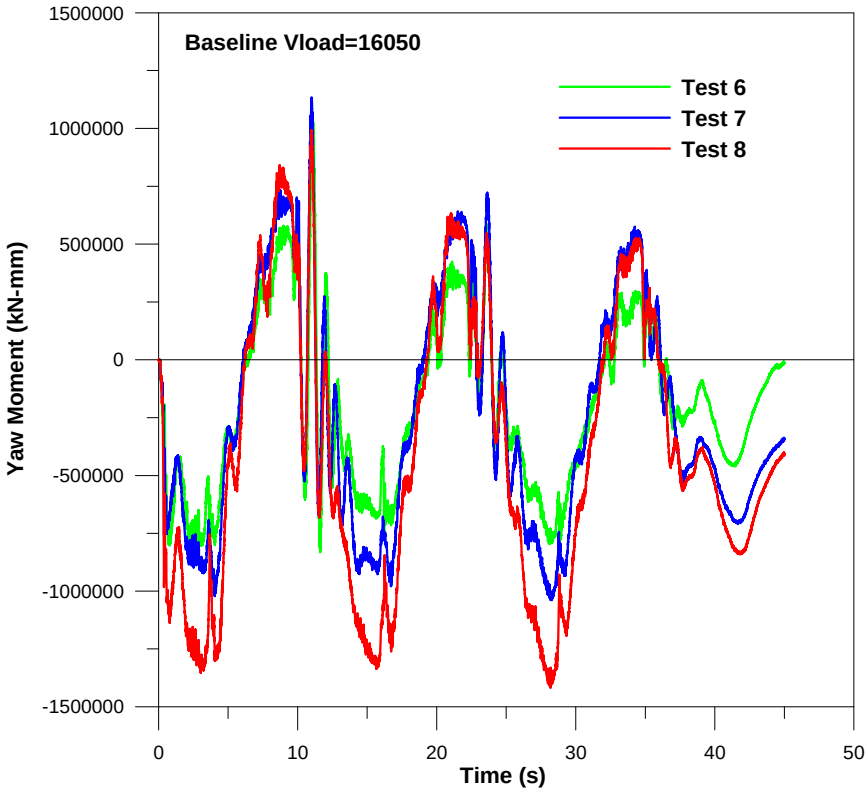

Figure 50 Yaw moment from Tests 6,7 and 8

tests 6,7 and 8 with respect to test 5. For this reason, the moments represent the component purely introduced by the differential vertical load in the two bearings.
The effects of the increase in vertical load variation are visible in both plots, with the cases at Vload=13050 kN (Figure 49) characterized by a regular variation on positive and negative peaks of the yaw moments. Figure 50 instead indicate a predominant variation of moments on the negative side. The increments in peak moment, from Test 2 to test 3 (10% on negative peaks and 6.8% on positive peaks) appear less significant than what observed from Test 3 to Test 4 (46.6% for negative peaks and 83% for positive peaks). More gradual appears instead the variation of yaw moment for the tests with baseline at 16050 kN. For negative peaks, in fact, the increment of moments is equal to 25% and 36% from Test 6 to Test 7 and from Test 7 to Test 8, respectively. The positive peaks of Figure 50 indicates a limited increment from Test 6 to Test 7 (8.7%) and a negligible variation for the next step in vertical load variation.

It must be noted that the simplified approach, of these tests, assumed a constant variation of vertical loads between the two bearings, generated instead, in real structures, by a dynamic lateral force applied to the bridge superstructure. For this reason a more realistic set of tests should include a ‘roll’ motion reproducing a time history of overturning moments applied to the bearings. This scenario should also include effects of vertical accelerations, considered a significant contributing factor by some Authors (Calvi et al., 2004). Further development of this issue is needed, for the above mentioned reasons, in order to achieve a comprehensive understanding on the realistic torsional effects. The presented limited number of tests however confirm the development of a torsional set of actions that should be taken into account for sliding bearings applications.

CONCLUSIONS

The effects of vertical load, strain rate and cycling on the response of large lead-rubber bearings were analyzed through a specifically designed experimental program. While a negligible variation in the performance parameters is associated to the change in vertical load, response characteristics like the characteristic strength and stiffness can be significantly affected by strain rate effects. The repetition of cycles introduces also a general reduction of shear force, particularly significant after the first cycle. The proposed numerical model, utilizes the structure of a previously presented analytical tool, introducing improvement in terms of continuity of the response and incorporating the above mentioned effects.

A sliding bearing, with concave bottom surface, was subjected to a range of tests to investigate the effects of vertical load and testing speed on the main performance characteristics. Three levels of vertical load were applied: low (3263 kN), medium (6525 kN) and high (13050 kN). Peak restoring forces as well as energy dissipated per cycle indicate a significant increase with velocity limited to an initial range. After reaching a peak value the general trend shows a significant reduction of these response parameters with further increase of velocity. Only the low axial load case reverse the general trend exhibited in the tests with very high speed.

For design purposes, the parameters that mostly indicate a dependency on the vertical load levels are related to the performance of the sliding devices. Specifically, the variation of the friction coefficient with the peak test velocity appears to be significantly dependent on the range of vertical loads. The vertical load variations also can contribute significantly to the development of torsional components for the bridge pier as described in the paragraph “Torsional Effects Introduced by Vertical Load Variation on Side by Side Devices”. Even though for lead-rubber bearings the completed tests did not indicate a significant change in performance with different levels of applied vertical load, for both type of devices it is suggested, for the bearing qualification phase, to repeat typical tests at different level of loads defined as lower limit, higher limit and design level.

In general terms the research program indicated, for every device, an higher importance of effects related to the speed of the motion applied. Every single response parameter analyzed was essentially modified by the peak velocity of the tests. If the approach introduced by AASHTO

Guide Specification was accepted, the λ factor associated with velocity effects should be established, as suggested in the Specifications, by tests. It is the Author's opinion that the testing protocol as well as the design process should include a detailed analysis of the velocity effects for a comprehensive characterization of the device performance.

REFERENCES

Aiken I.D., Kelly J.M., Clark P.W., Tamura K., Kikuchi M. and Itoh T., (1992) "Experimental Studies Of The Mechanical Characteristics Of Three Types Of Seismic Isolation Bearings", *Proceedings of the 10th World Conference on Earthquake Engineering, Madrid, Spain, July*

Anderson, E. L., Mahin S. A., Fenves, G., Whittaker, A., (2001) "Effect of Configuration on Seismically Isolated Bridges," *6th Caltrans Seismic Workshop, California Department of Transportation, Sacramento,* Ca, June 12-13

American Association of State and Highway and Transportation Officials (2000) *Guide Specifications for Seismic Isolation Design, AASHTO,* Washington D.C., USA

Benzoni G., Seible F. (1998) "Design Of The Caltrans Seismic Response Modification Device (SRMD) Test Facility," *Proceeding of the USA – ITALY Workshop on Protective Systems for Bridges, New York City, 26-28 April*

Benzoni, G., Seible F., (2000) " Benicia-Martinez Friction Pendulum Bearings – Prototype Test results," *Caltrans SRMD Testing Facility Report, SRMD 2000/4-17,* La Jolla, Ca

Benzoni, G., Seible, F., (2001). " Bearings BRG-K for Bolu Viaduct. Prototype Test Results," *Caltrans SRMD Testing Facility Report, SRMD 2001/26,* La Jolla, Ca

Benzoni, G., Innamorato, D., (2003) "Prototype tests of Sumitomo Co. Dampers Type RDT80 and RDT200" *Caltrans SRMD Testing Facility Report, SRMD 2003/01*, La Jolla, Ca, February.

California Department of Transportation, (1999) "Friction Pendulum Isolation Bearings, Dynamic Load Testing, Acceptance Criteria, Supplemental Data", *Benicia-Martinez Seismic Retrofit, Main Truss Spans, Construction Contract No. 04-0440U4.*

Calvi, G.M., Ceresa, P., Casarotti, C., Bolognini, D., Auricchio, F., (2004), " Effect of Axial Force Variation in the Seismic Response of Bridges Isolated with Friction Pendulum Systems", Journal of Earthquake Engineering, Vol. 8, Special issue 1.

Constantinou, M., Mokka, A., Reinhorn, A. (1990), "Teflon Bearings in Base Isolation. II: Modeling", Journal of Structural Engineering, Vol. 116, No. 2, February

Constantinou, M.C., Tsopelas, P., Kasalanati, A., Wolff, E., (1999) " Property Modification Factors for Seismic Isolation Bearings, *MCEER Technical Report, Multidisciplinary Center for Earthquake Engineering Research, Buffalo, N.Y.*

Kikuchi M., Aiken I.D. (1997), "An Analitical hysteresis model for elastomeric seismic isolation bearings", Earthquake Engineering and Structural Dynamics, *26:215-231.*

Mokha, A., Constantinou, M. C., Reinhorn, A. M., (1988) "Teflon Bearings in Aseismic Base Isolation: Experimental Studies and Mathematical Modeling", *Report NCEER-88-0038, National Center for Earthquake Engineering Research, Buffalo, N.Y.*

Mosqueda, G., Wittaker, A.S., Fenves, G. L., (2004), " Characterization and Modeling of Friction Pendulum Bearings Subjected to Multiple Components of Excitation", Journal of Structural Engineering, Vol. 130, No. 3, March.

Pranesh, M., Sinha, R., (2000), "VFPI: an Isolation Device for Aseismic Design", Earthquake Engineering and Structural Dynamics, Vol. 29.

Priestley, M.J.N., Calvi, G.M., (2002). "Strategies for Repair and Seismic Upgrading of Bolu Viaduct 1, Turkey," *Journal of Earthquake Engineering, Special Issue,* Vol. 6, 157-184

Skinner R.I., Robinson W.H., McVerry G.H. (1993), "An introduction to seismic isolation", Wiley

Thomson A.C., Whittaker A.S., Fenves G.L. and Mahin S.A., (2000) "Property Modification Factors For Elastomeric Seismic Isolation Bearings," *Proceedings of the 12th World Conference on Earthquake Engineering, Auckand, New Zealand, January.*

Zayas, V. A, Low, S. S., Mahin, S. A., (1990), "A Simple Pendulum Technique for Achieving Seismic Isolation", Earthquake Spectra, Vol. 6, No. 2.

Additional references (not cited in the text)

Aiken, I. D., Kelly, J.M., Clark, P. W., Tamura, K., Kikuchi, M., Itoh, T., (1992) " Experimental Studies of the Mechanical Characteristics of Three Types of Seismic Isolation Bearings", *Proceedings 10th World Conference on Earthquake Engineering, Madrid, Spain*

Benzoni, G., (2003, a), "Performance Of Seismic Response Modification Devices Under High SpeedTests," *American Concrete Institute, 2003 International Conference,* December 8-9, La Jolla, Ca.

Benzoni, G., (2003, b), "High Speed Tests Of Anti-Seismic Devices," G. Benzoni, *8th World Seminar on Isolation, Energy Dissipation and Active Vibration Control of Structures*, Yerevan, Armenia, Oct. 6-10

Buckle, I. G., Nagarajaiah, S., Ferrell, K., (2002) "Stability of Elastomeric Isolation Bearings: Experimental Study," J. of Structural Eng., Vol. 128 (1), pp/ 3-11, January.

Buckle, I. G., Kelly, J. M., (1986) "Properties of Slender Elastomeric Isolation Bearings During Shake Table Studies of a Large-Scale Model Bridge Deck,", *Joint Sealing and*

Bearing Systems for Concrete Structures (ACI), 1, pp. 247-269

CEN/TC 340, (2003). "Draft European Standard on Anti-Seismic Devices", Paris, March.

Ceresa, P., (2002). "Effects of Axial force Variation in the Seismic Response of Isolated Bridges" *University of Pavia, Ph.D. Thesis (in Italian).*

Hwang, J. S., Wu, J. D., Pan, T. C., Yang, G., (2002), "A mathematical Hysteretic Model for Elastomeric Isolation Bearings", Earthquake Engineering and Structural Dynamics, Vol. 31.

Koh, C. G., Kelly, J.M., (1986). " Effects of axial load on elastomeric bearings," Rep. UCB/EERC-86/12, *Earthquake Engineering Research Center, University of California Berkeley, California*.

Mellon, D., (1997). "Caltrans Proposed Testing of Seismic Response Modification Devices for the Toll Bridge Retrofit program," *National Seismic Conference on Bridges and Highways, Federal Highway Administration,* Sacramento, Ca, July 8-11.

Nagarajaiah, S., Ferrell, K., (1999). "Stability of Elastomeric Seismic Isolation Bearings," J. Struct. Eng., 125(9), pp. 946-954.

Ryan, K.L., Kelly, J. M., Chopra, A. K.,(2004), " Experimental Observation of Axial Load Effects in Isolation Bearings", *Proceedings 13th World Conference on Earthquake Engineering, Vancouver, Canada.*

Tsai, C.S., Huang, C.J., (1999). "Seismic Behavior of Isolated Curved Bridges with FPS Isolators," *Proc. 2nd World Conference on Structural Control, John & Wiley, Chichester, England; Vol. 1, 103-112*

APPENDIX A

LEAD-RUBBER BEARINGS

The results previously presented for the lead-rubber bearing are presented in this section in a different format in order to enphasize the effects of the applied vertical loads. It must be noted that the labels of vertical loads are also completed with the levels of pressure. The calculated pressure is based on the bonded diameter of the device.

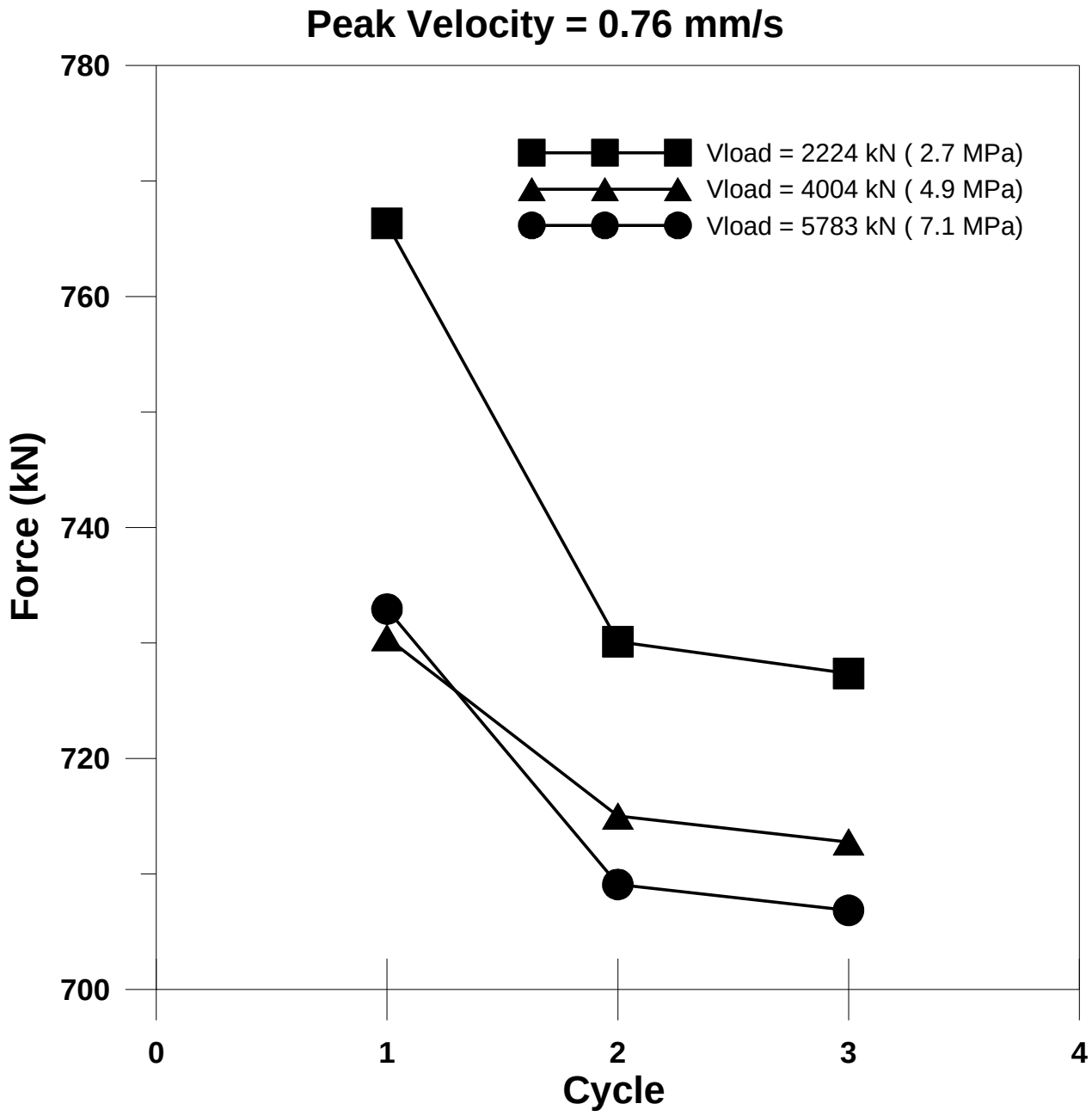

Figure A-1 Maximum Force for tests at 0.76 mm/s

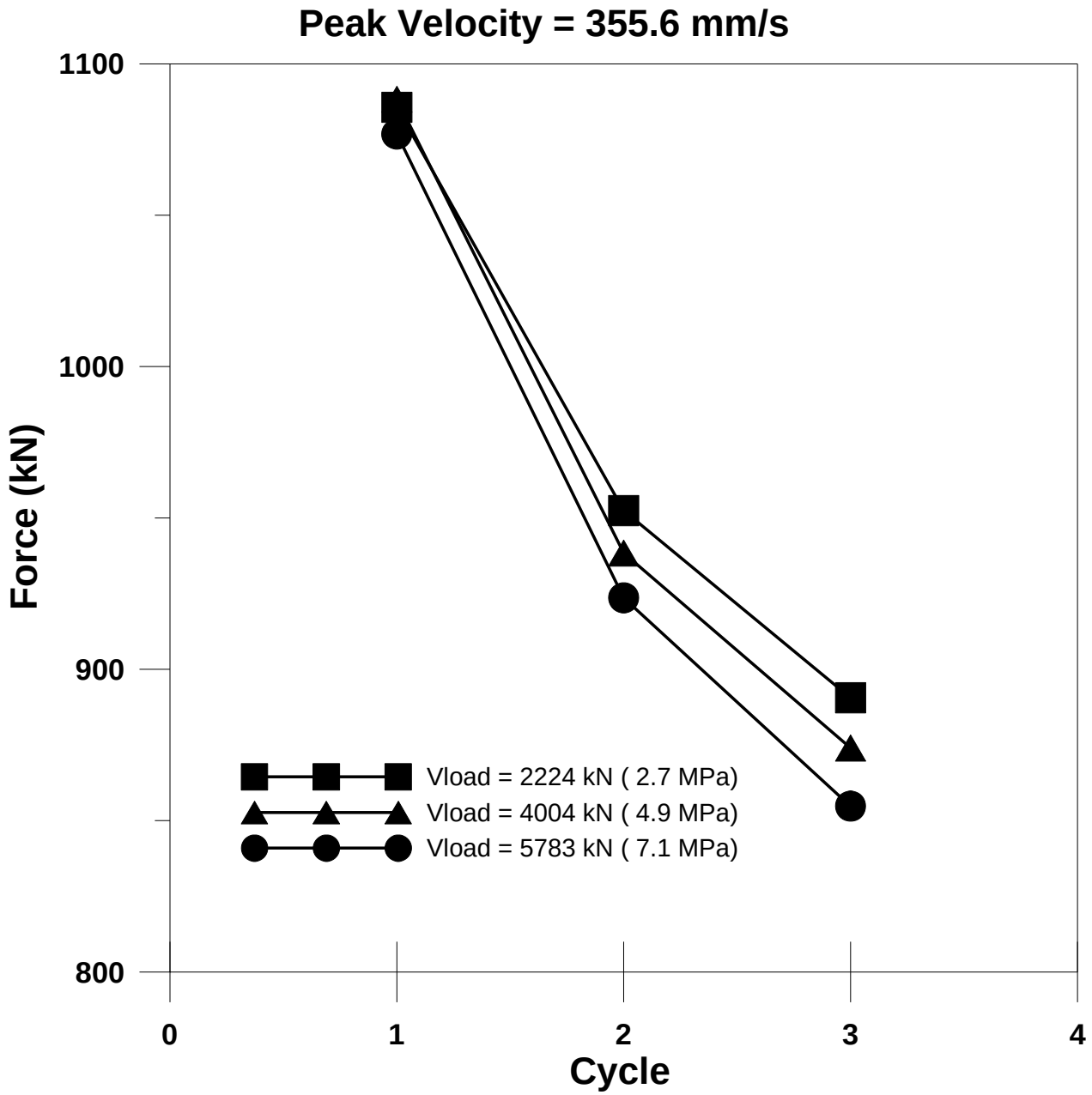

Figure A-2 Maximum Force for tests at 355.6 mm/s

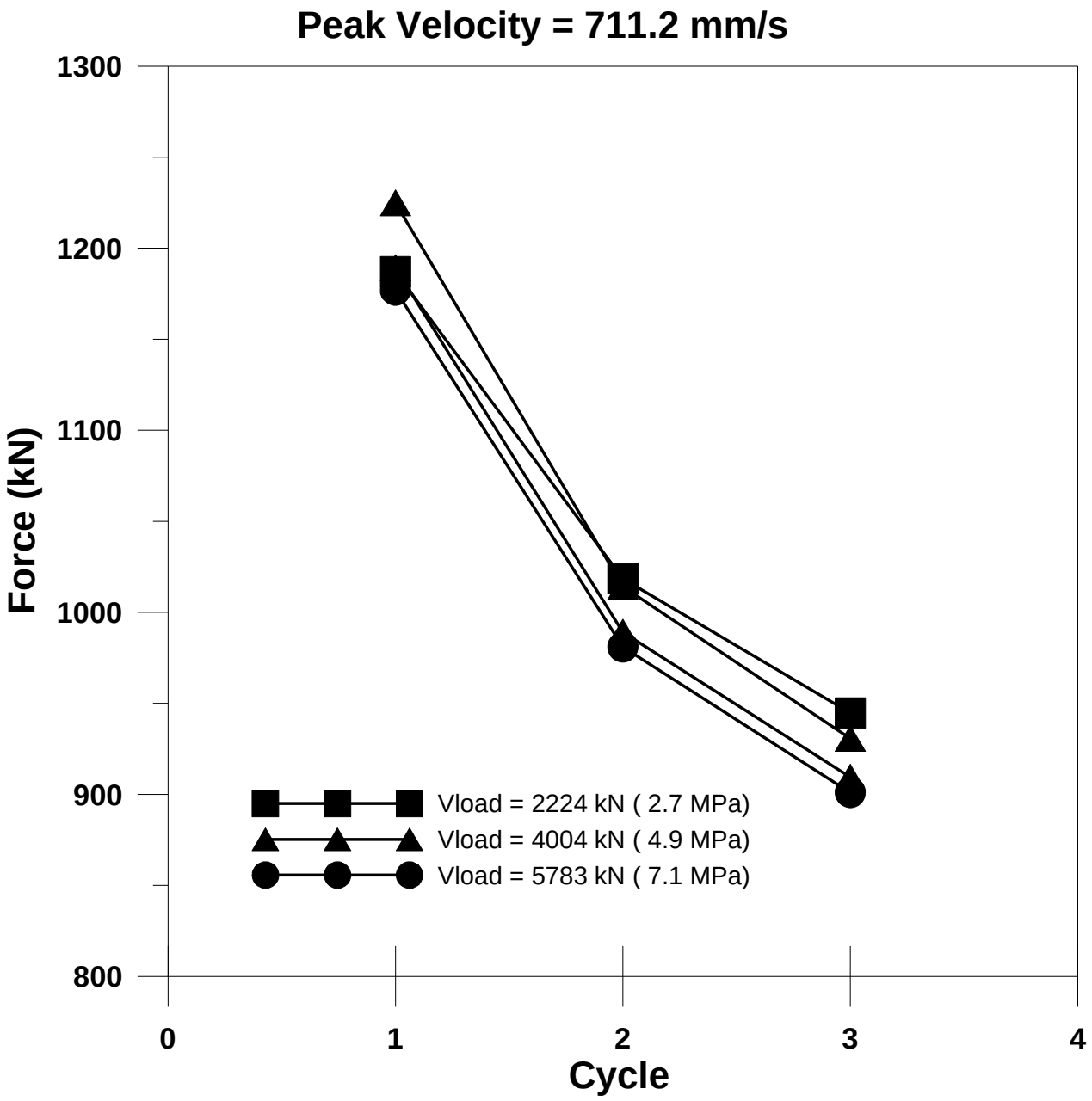

Figure A-3 Maximum Force for tests at 711.2 mm/s

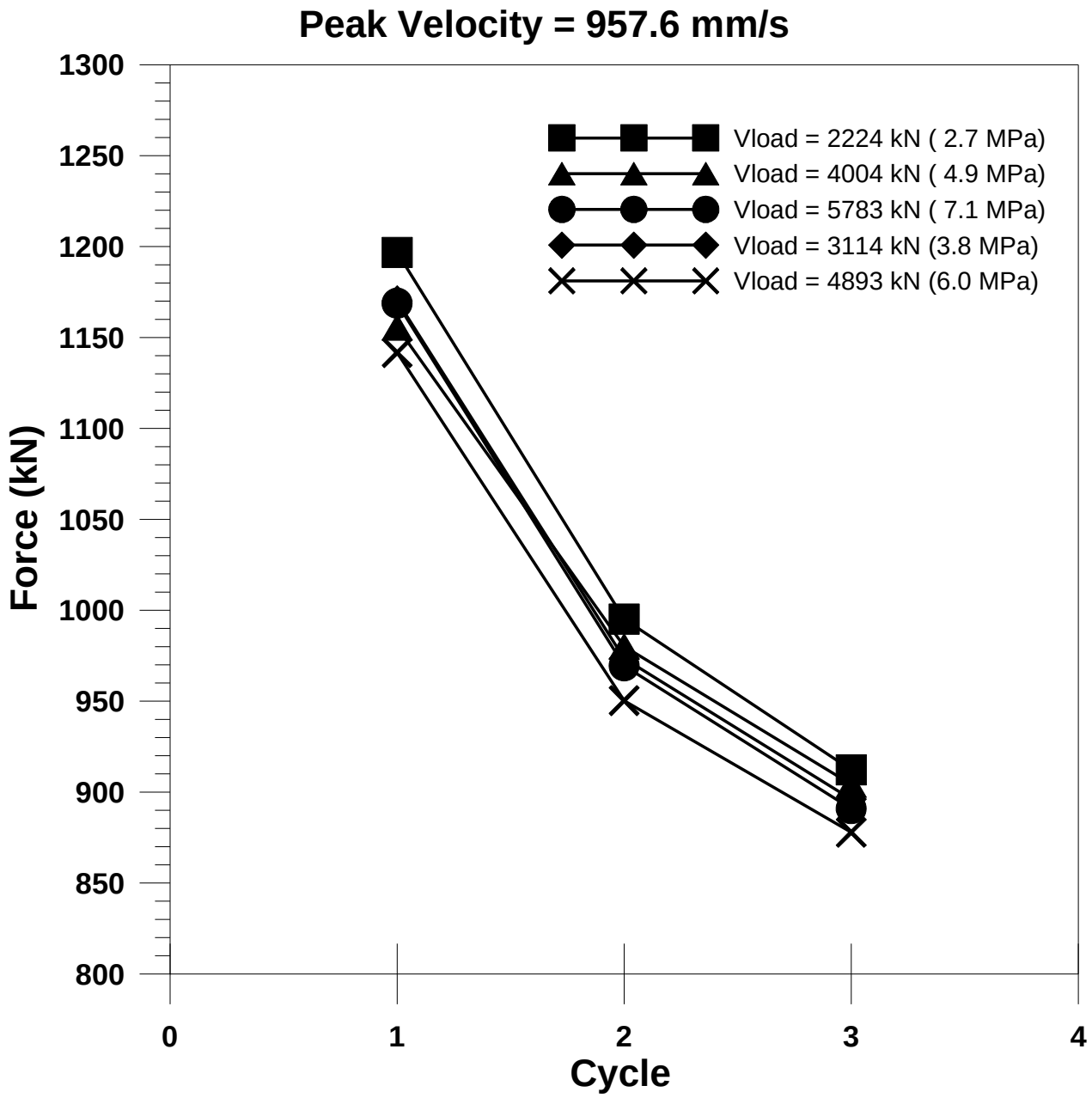

Figure A-4 Maximum Force for tests at 957.6 mm/s

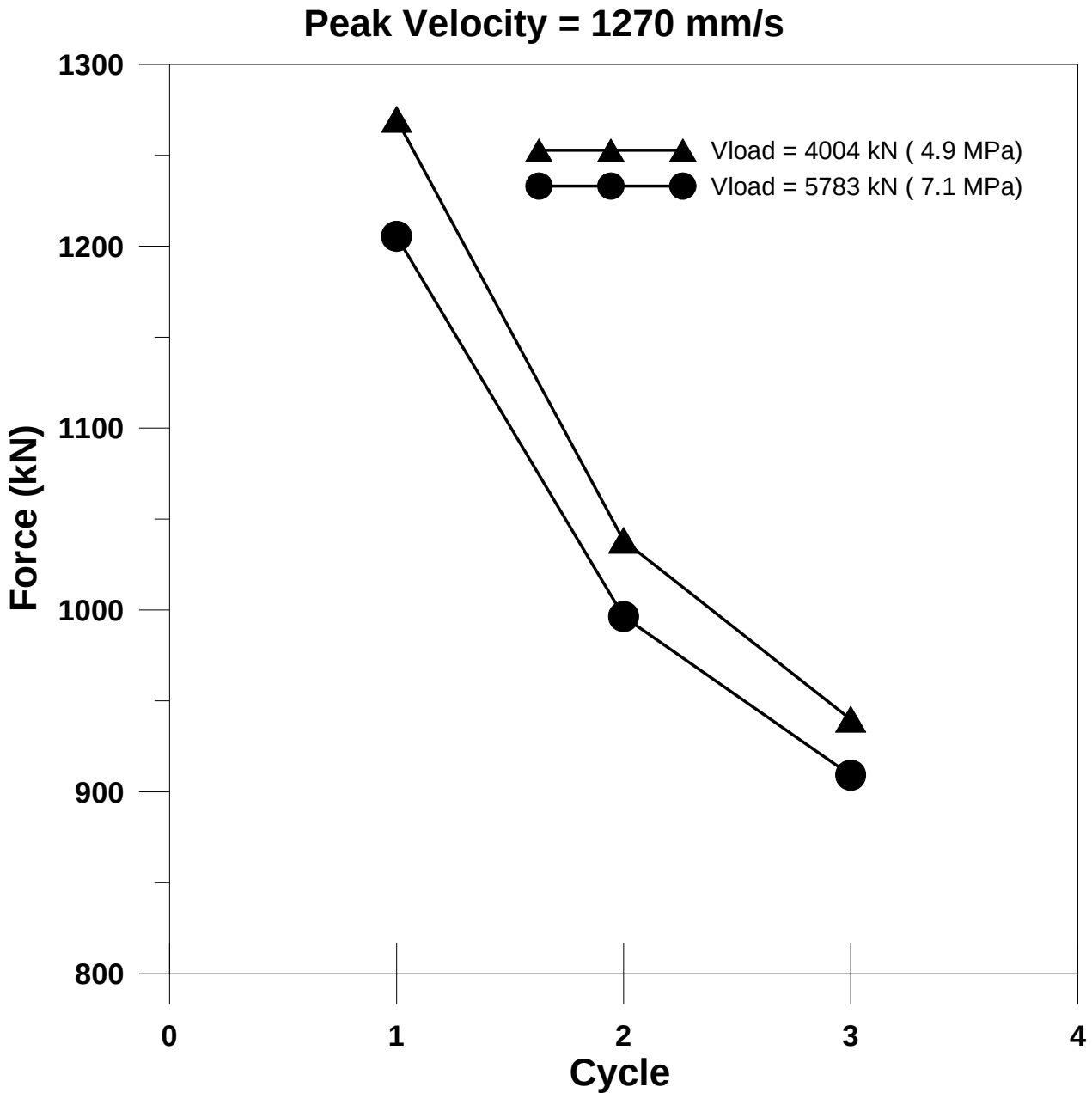

Figure A-5 Maximum Force for tests at 1270 mm/s

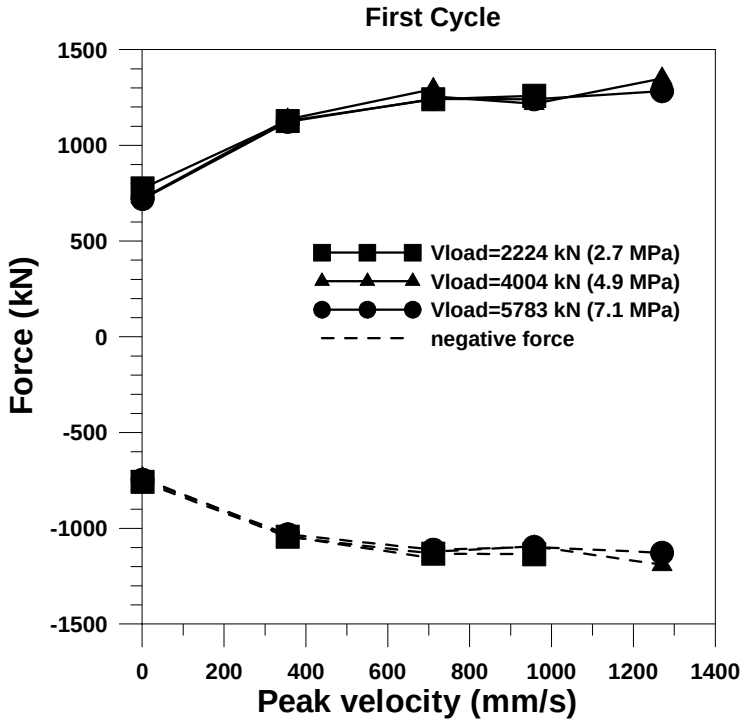

Figure A-6a Maximum Force for first cycle of tests at different vertical load and velocity

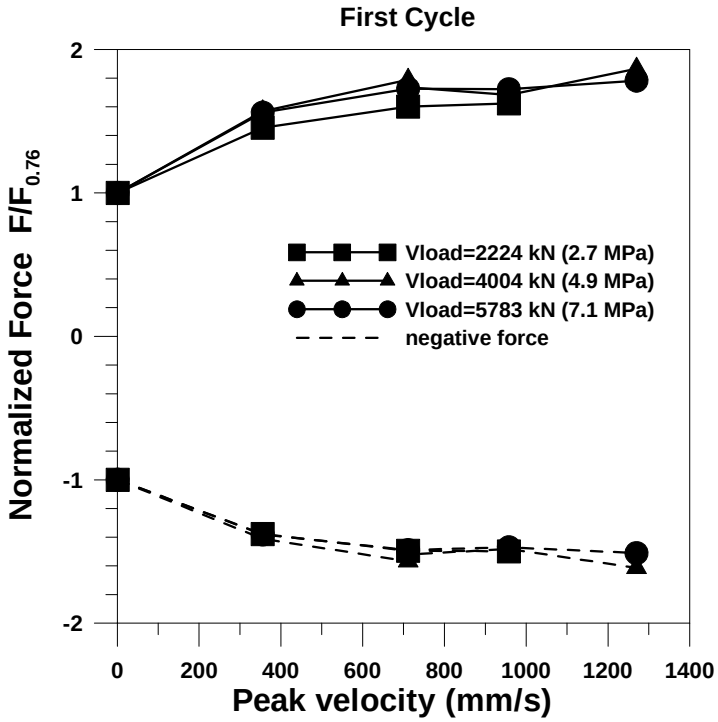

Figure A-6b Ratio of peak force to the peak force for tests at 0.76 mm/s

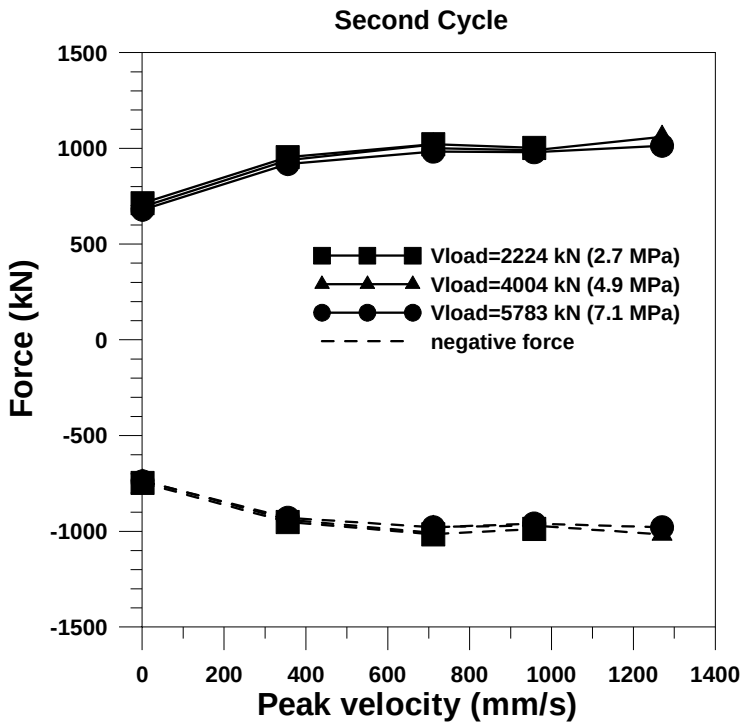

Figure A-7a Maximum Force for second cycle of tests at different vertical load and velocity

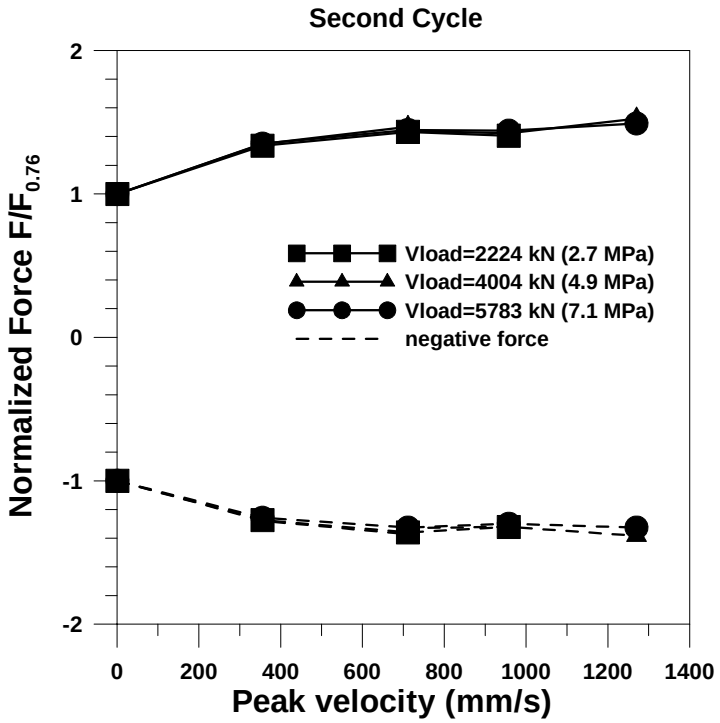

Figure A-7b Ratio of peak force to the peak force for tests at 0.76 mm/s

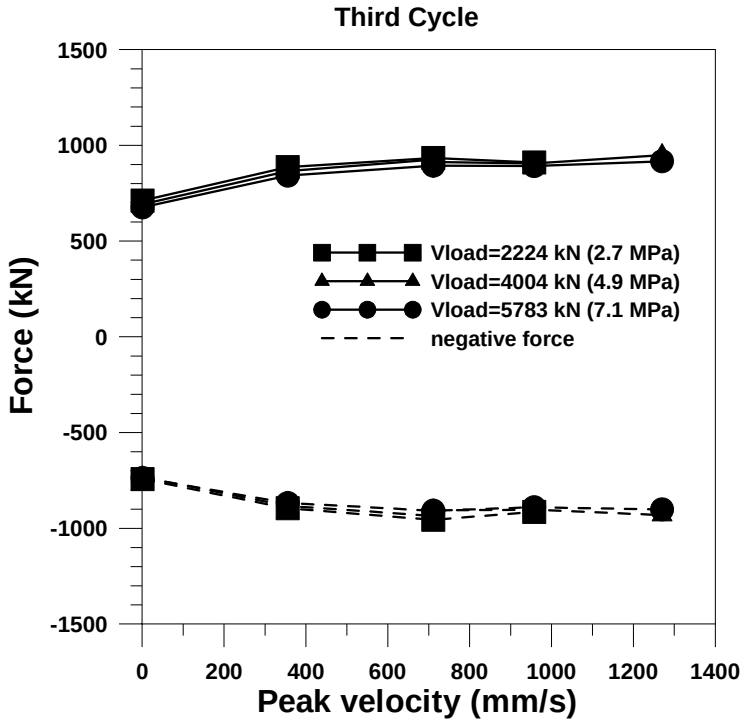

Figure A-8a Maximum Force for third cycle of tests at different vertical load and velocity

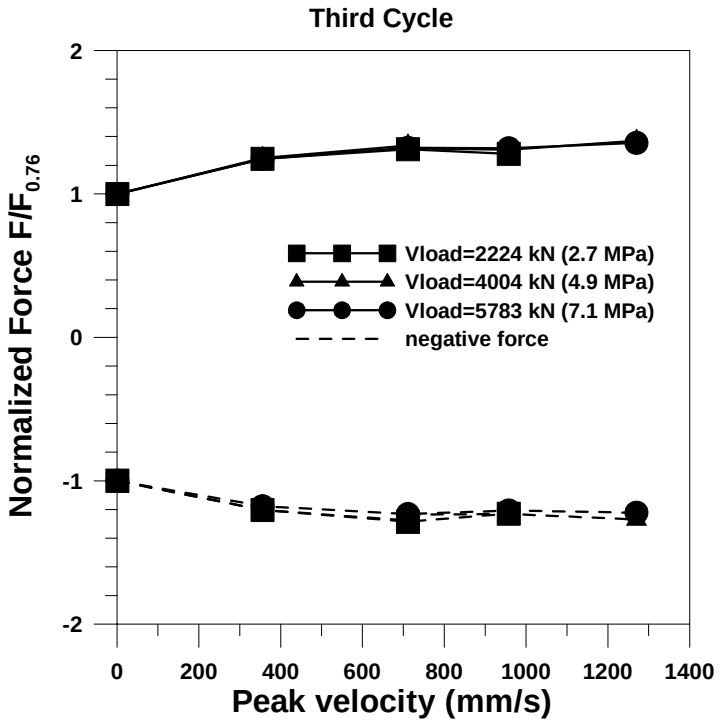

Figure A-8b Ratio of peak force to the peak force for tests at 0.76 mm/s

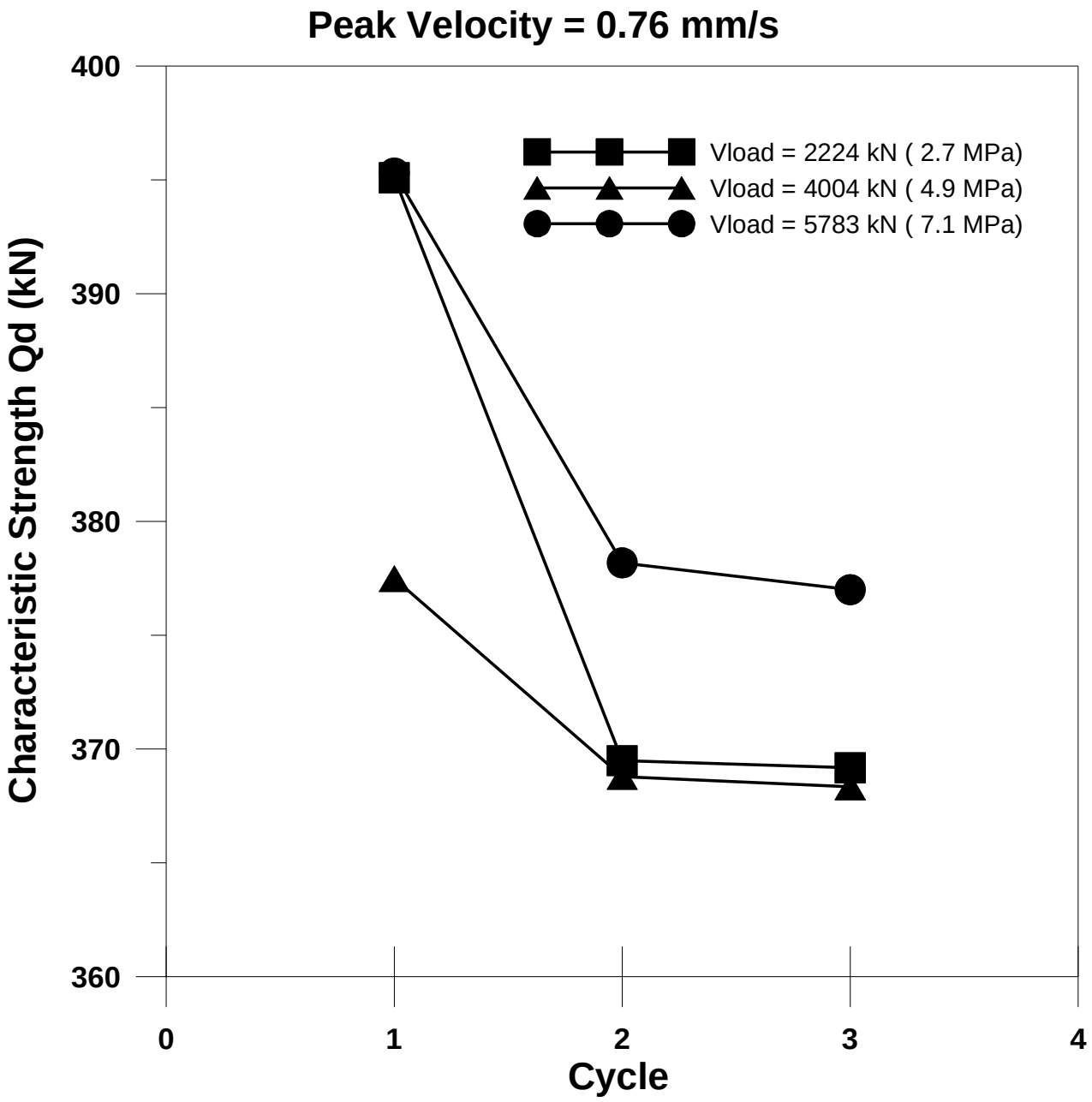

Figure A-9 Characteristic strength (Qd) for tests at 0.76 mm/s

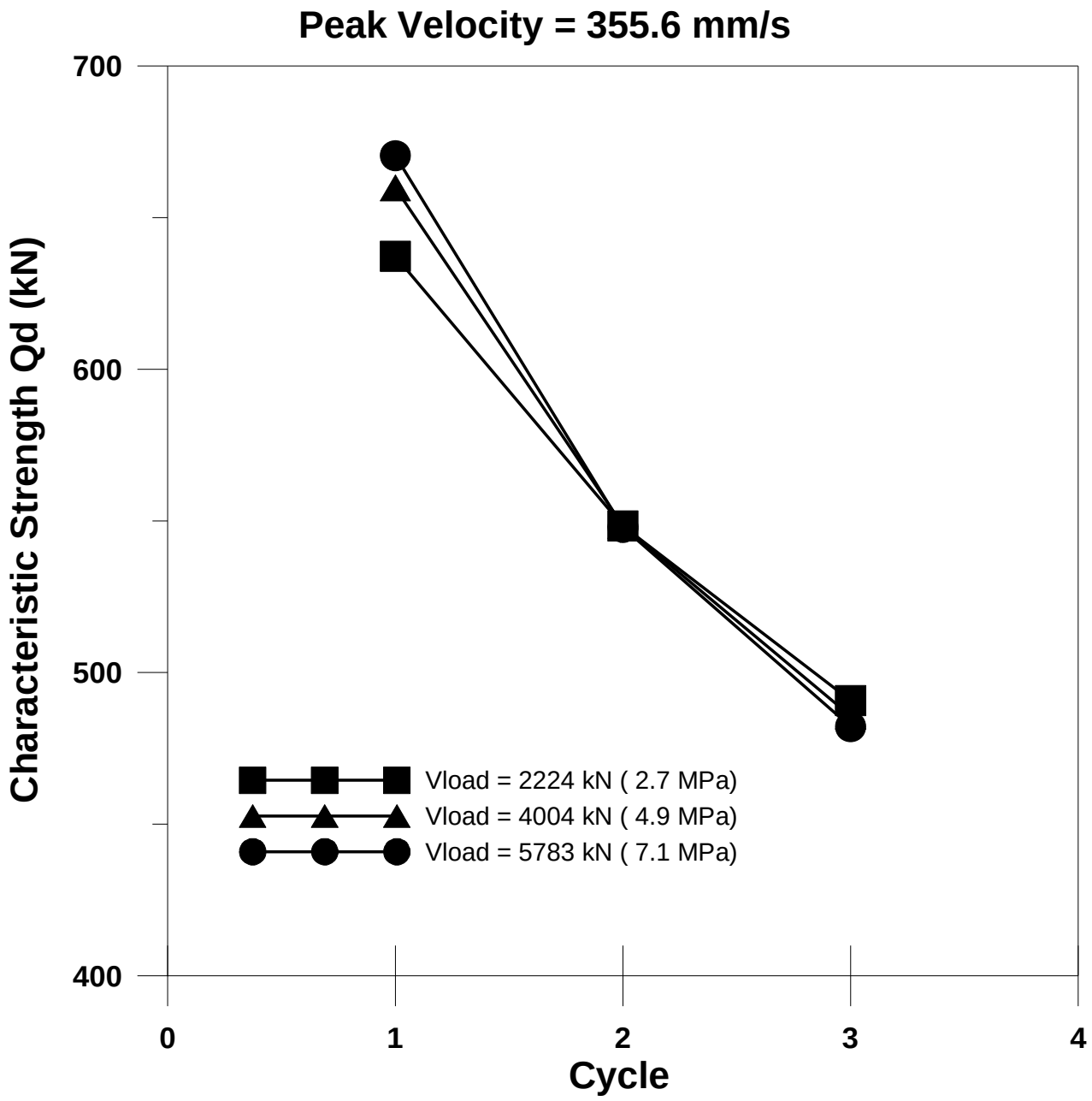

Figure A-10 Characteristic strength (Qd) for tests at 355.6 mm/s

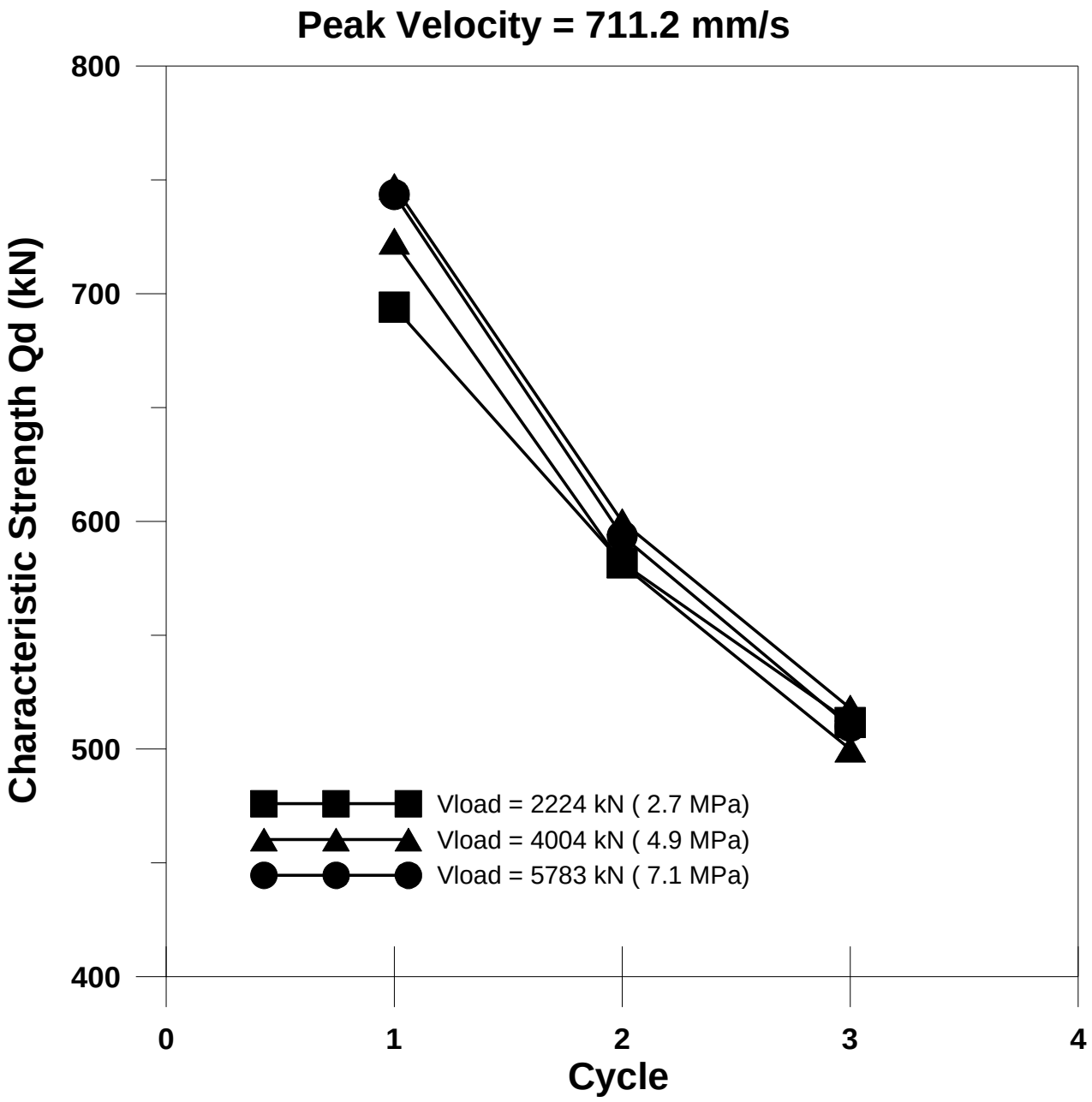

Figure A-11 Characteristic strength (Qd) for tests at 711.2 mm/s

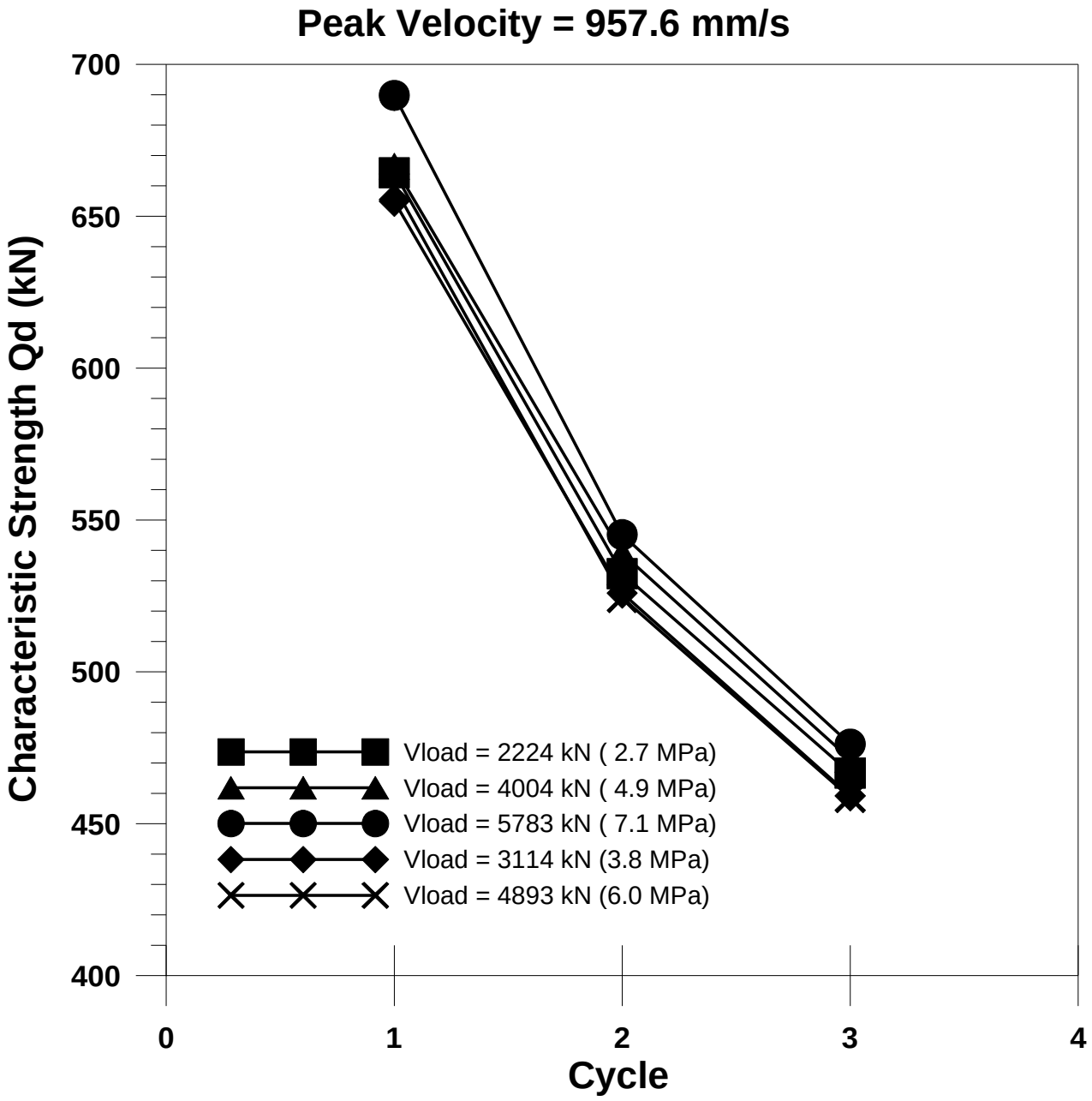

Figure A-12 Characteristic strength (Qd) for tests at 957.6 mm/s

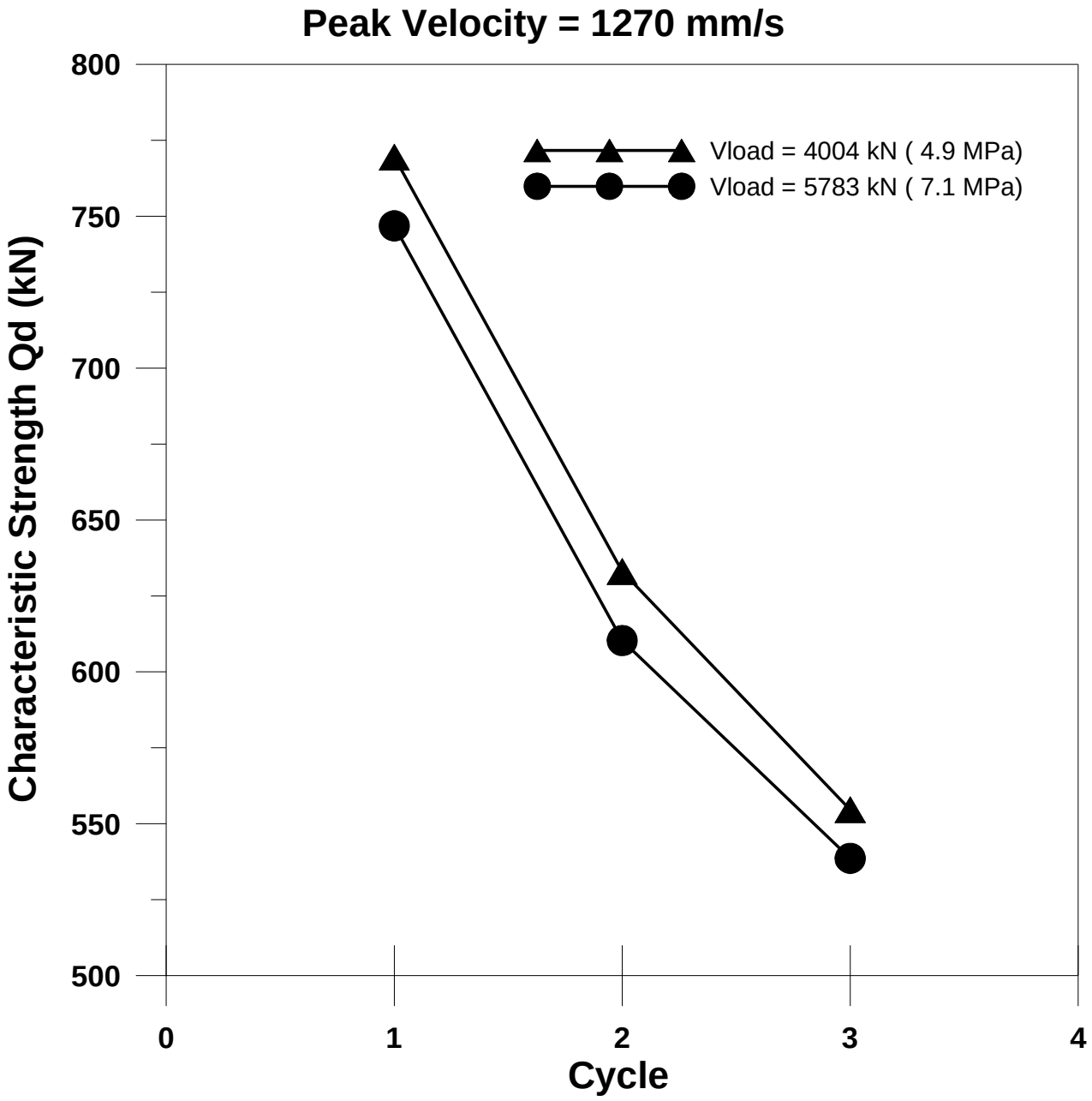

Figure A-13 Characteristic strength (Qd) for tests at 1270 mm/s

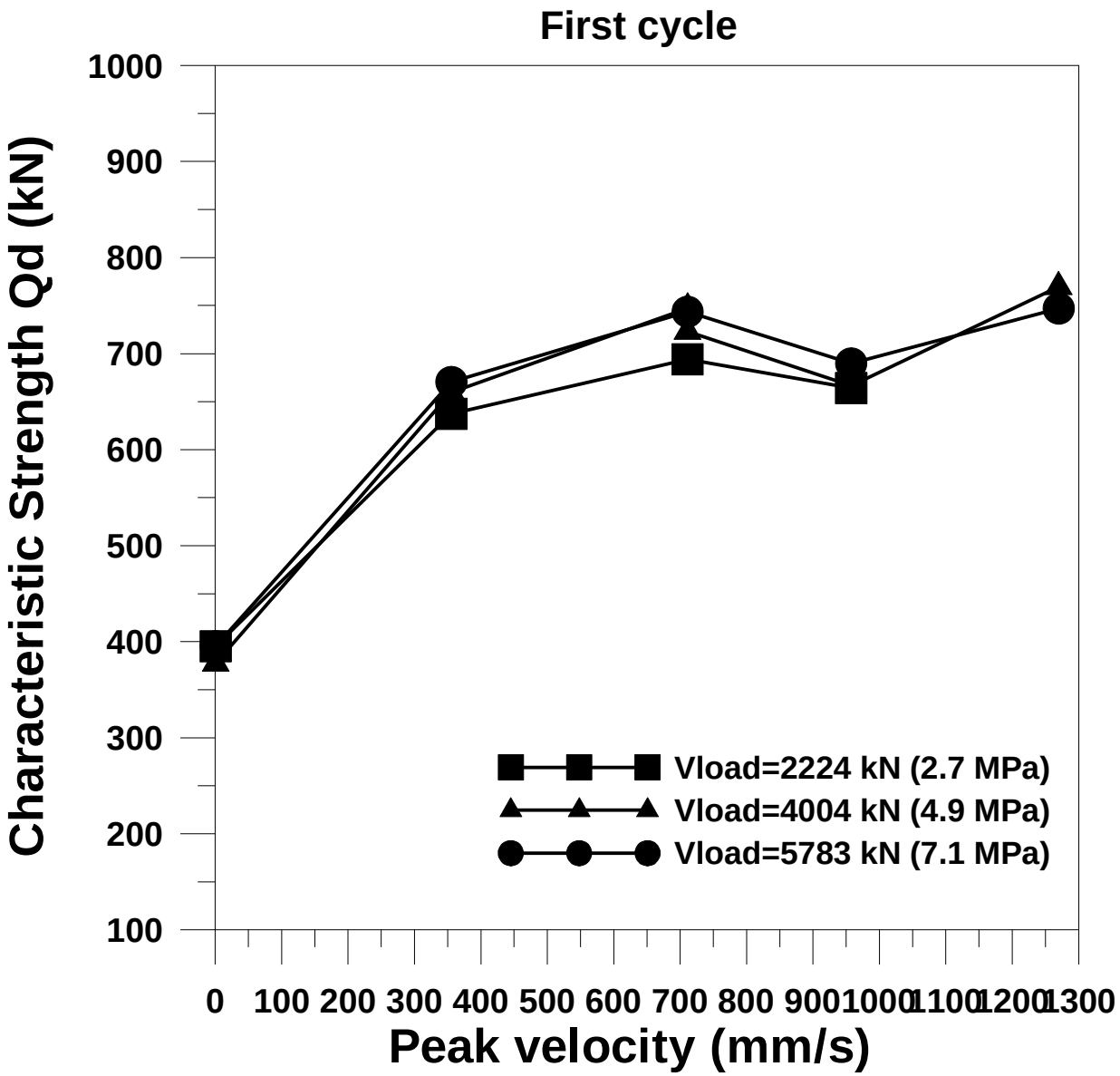

Figure A-14 Characteristic strength for first cycle of tests at different vertical load and velocity

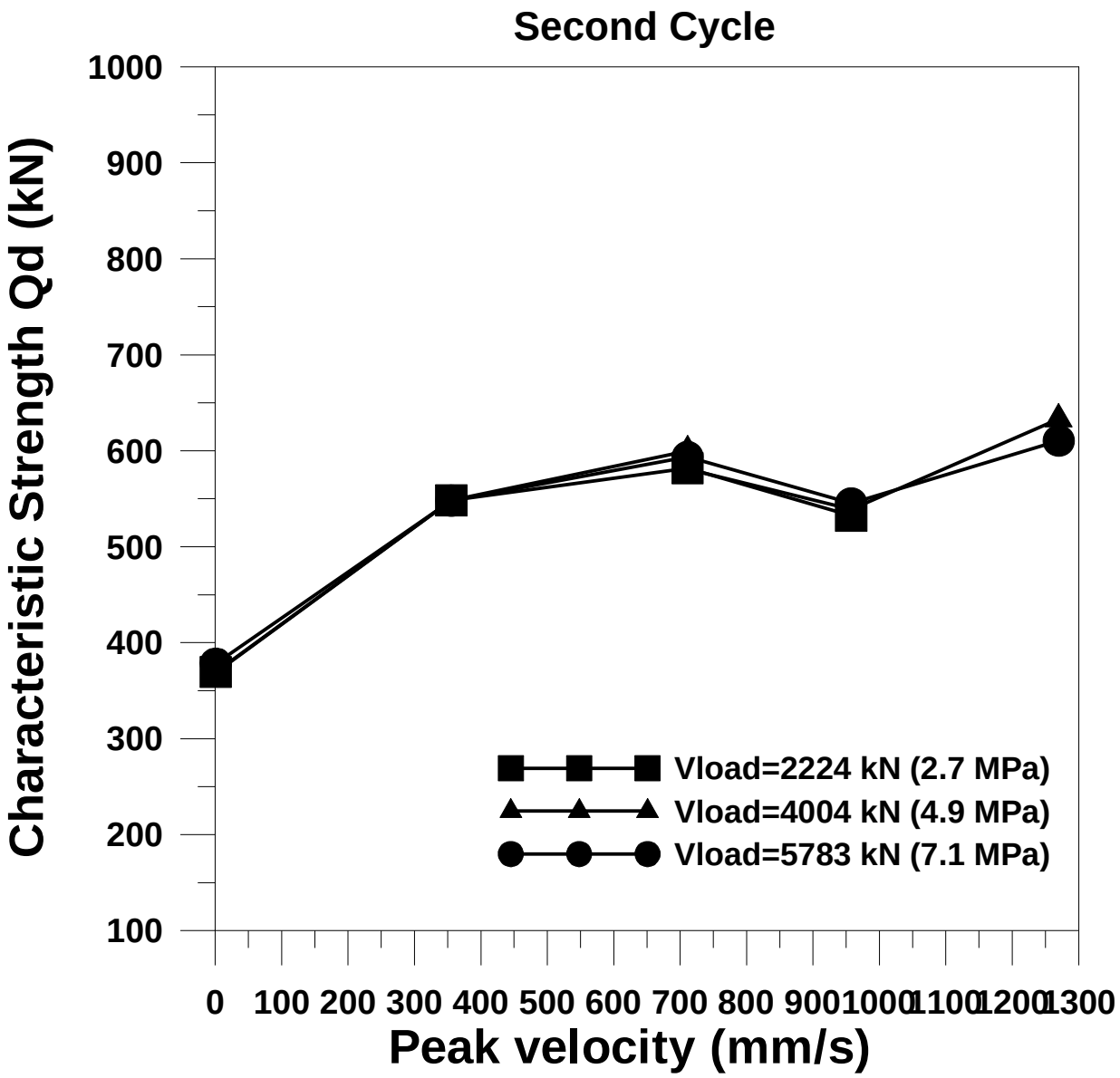

Figure A-15 Characteristic strength for second cycle of tests at different vertical load and velocity

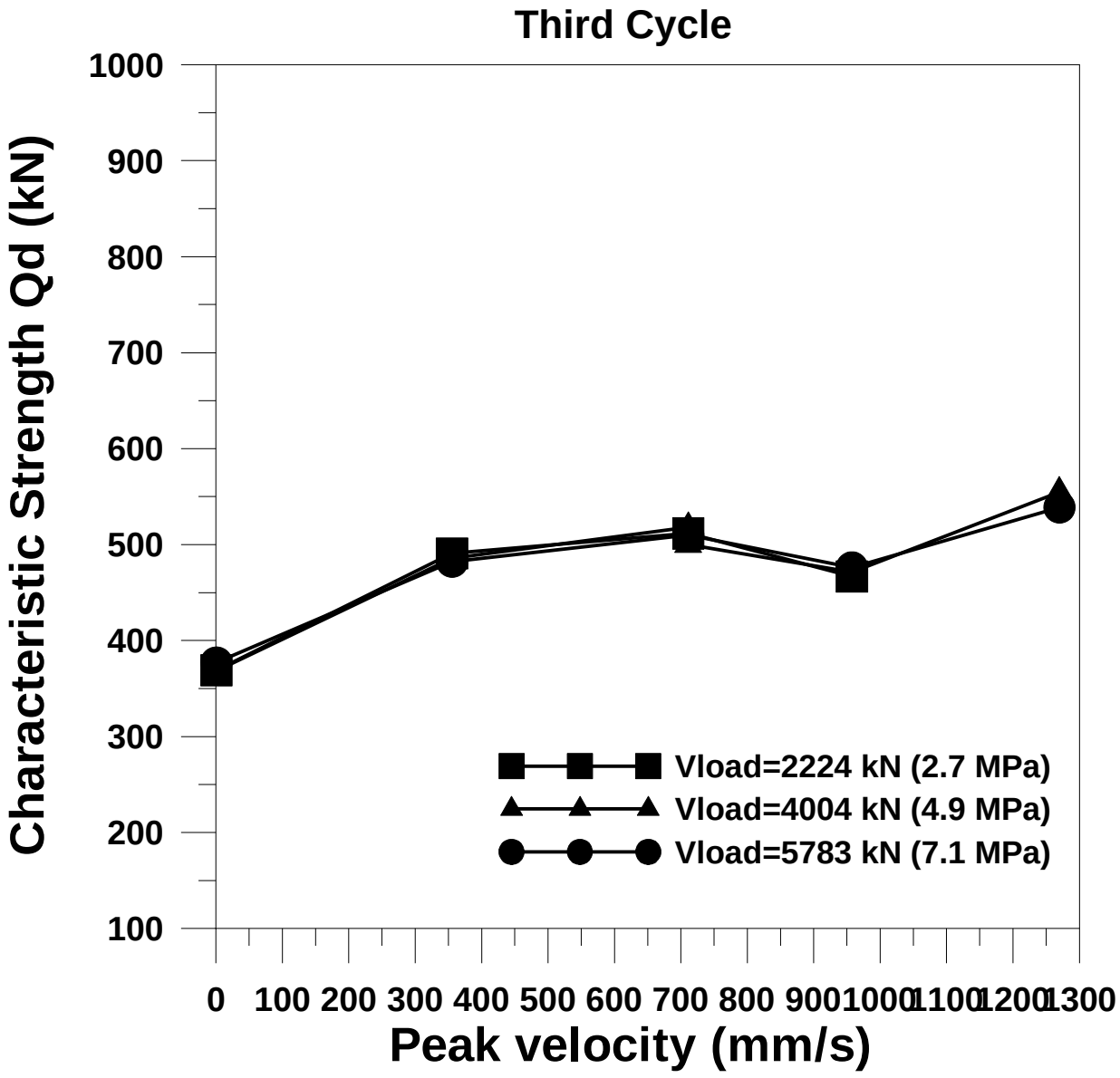

Figure A-16 Characteristic strength for third cycle of tests at different vertical load and velocity

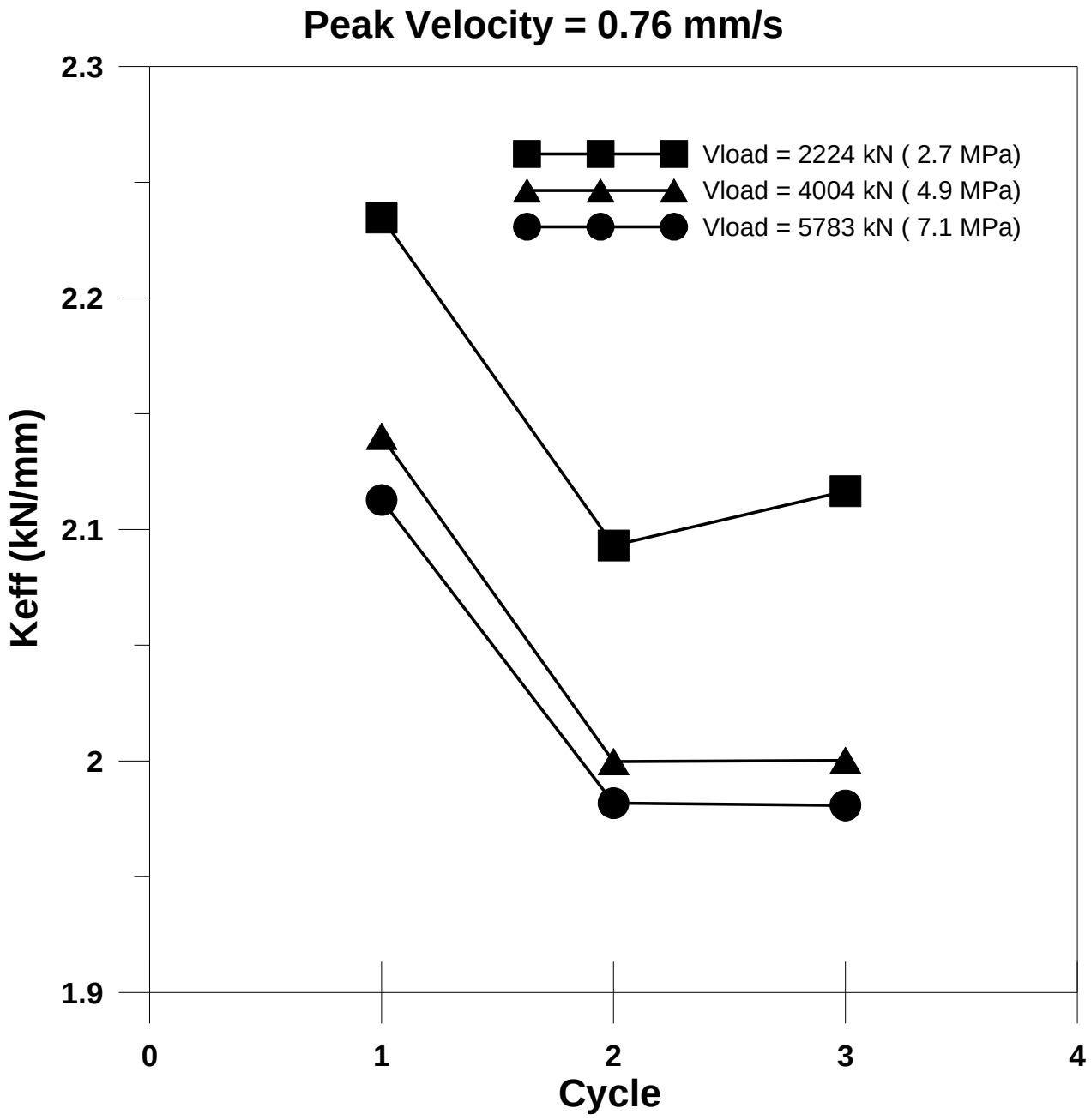

Figure A-17 Effective Stiffness (Keff) for tests at 0.76 mm/s

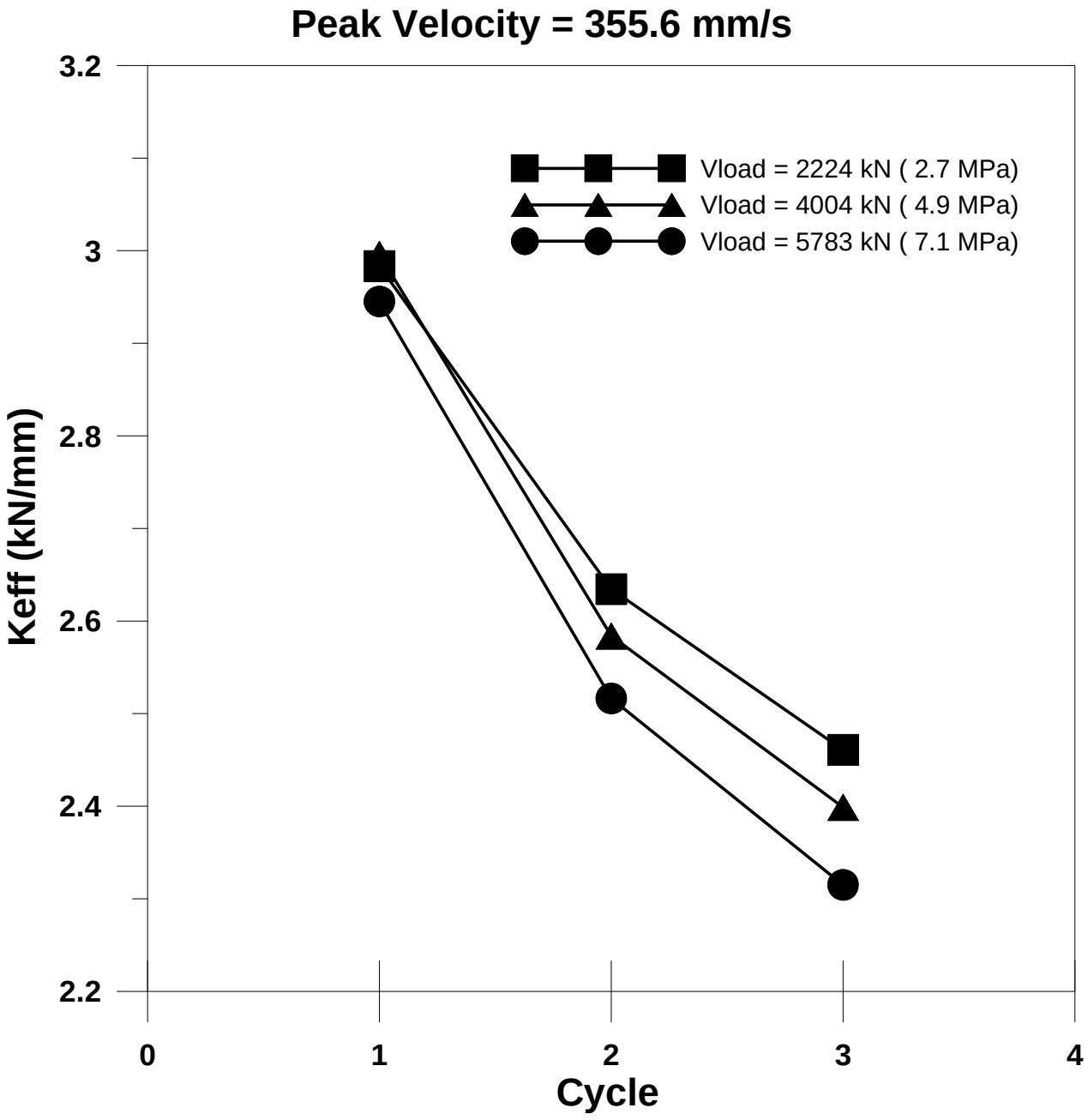

Figure A-18 Effective Stiffness (Keff) for tests at 355.6 mm/s

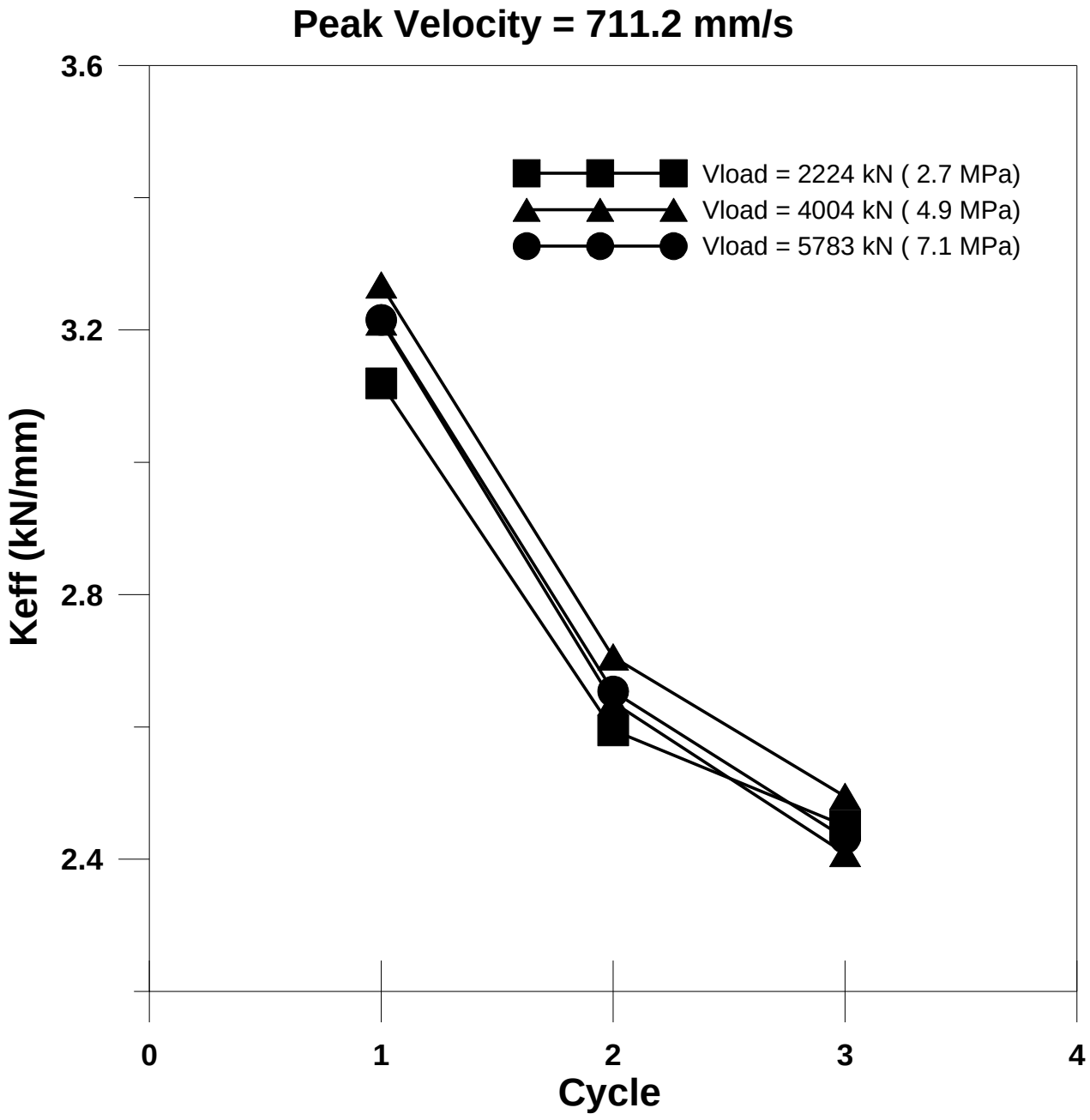

Figure A-19 Effective Stiffness (Keff) for tests at 711.2 mm/s

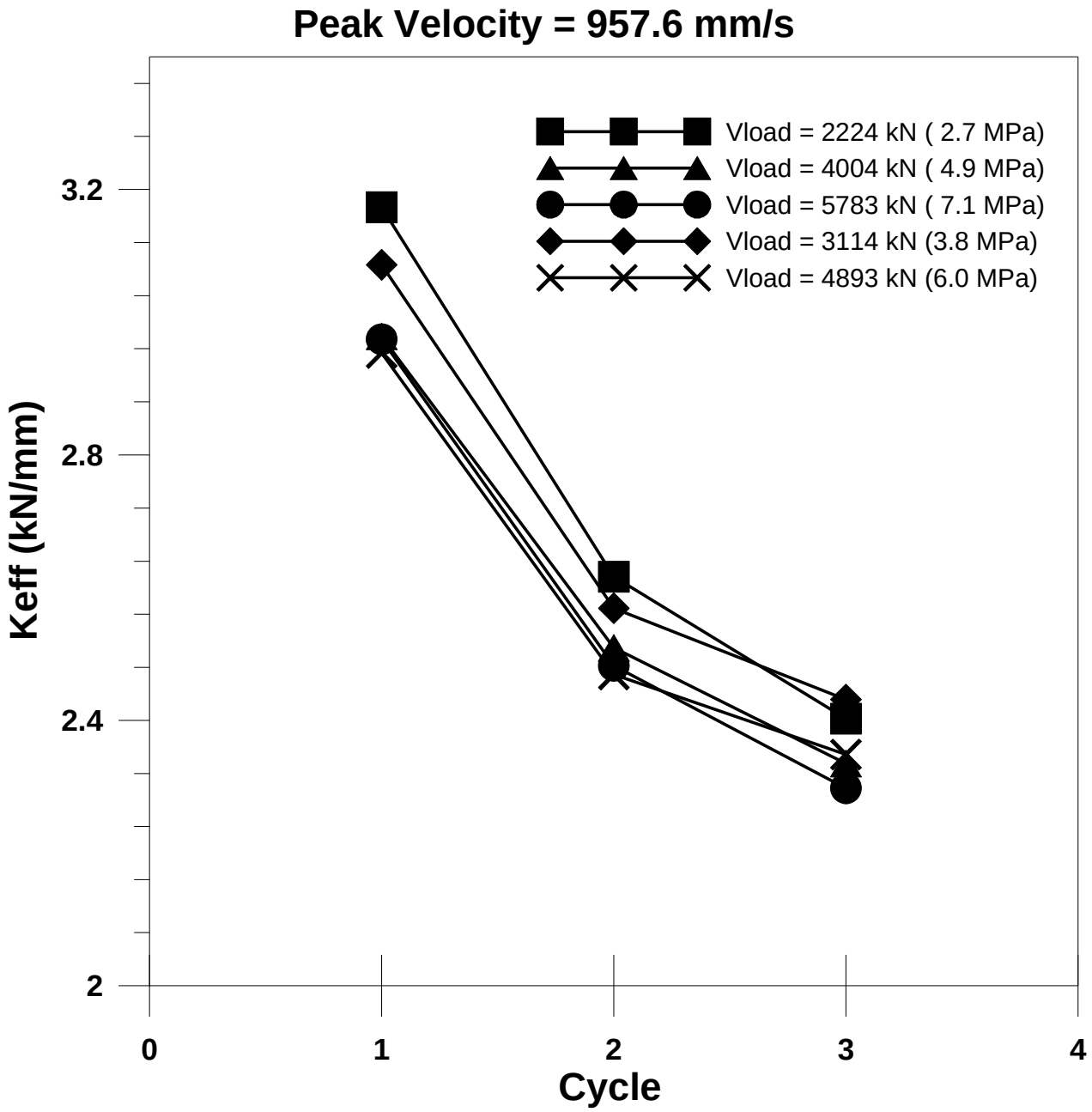

Figure A-20 Effective Stiffness (Keff) for tests at 957.6 mm/s

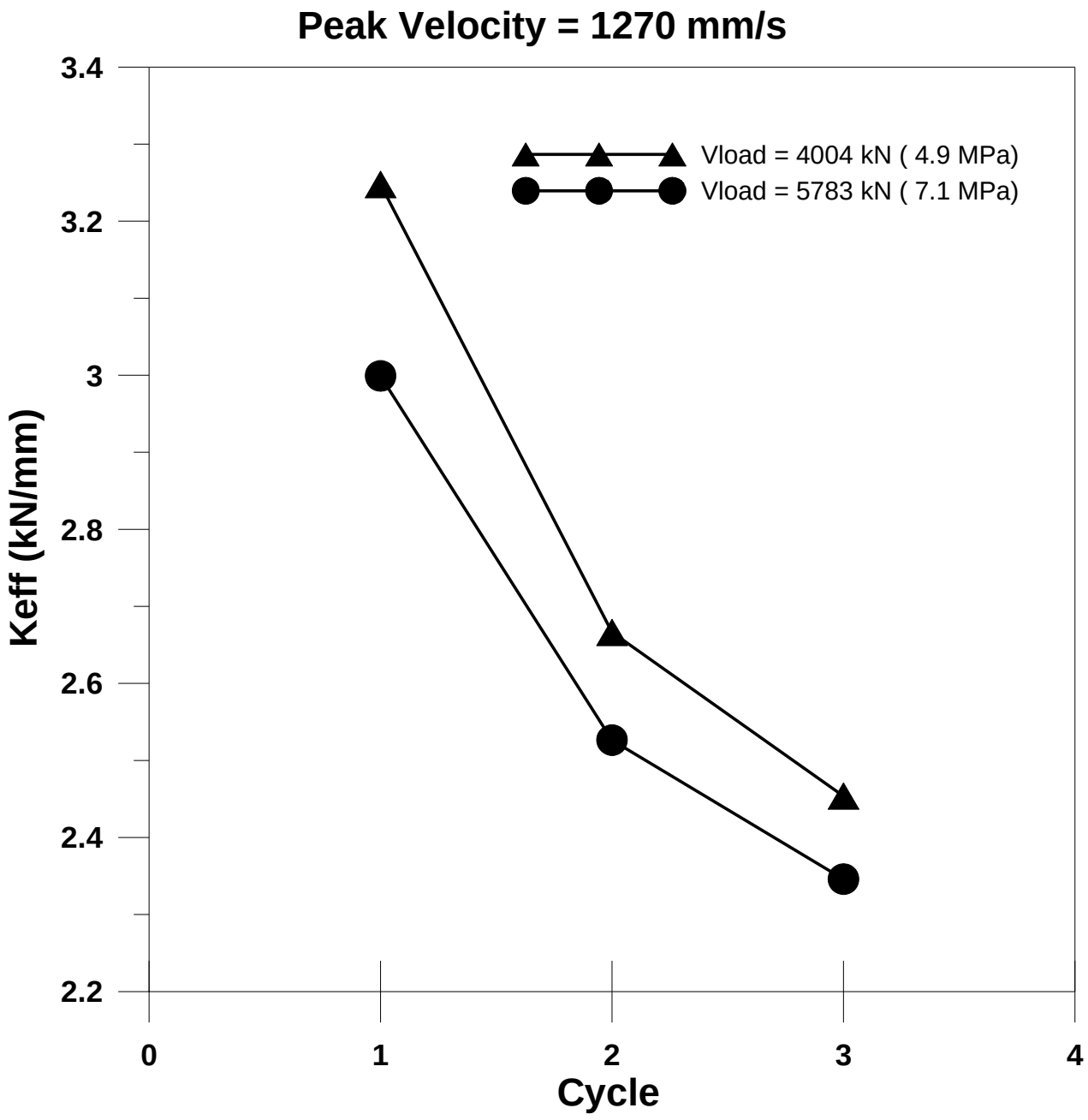

Figure A-21 Effective Stiffness (Keff) for tests at 1270 mm/s

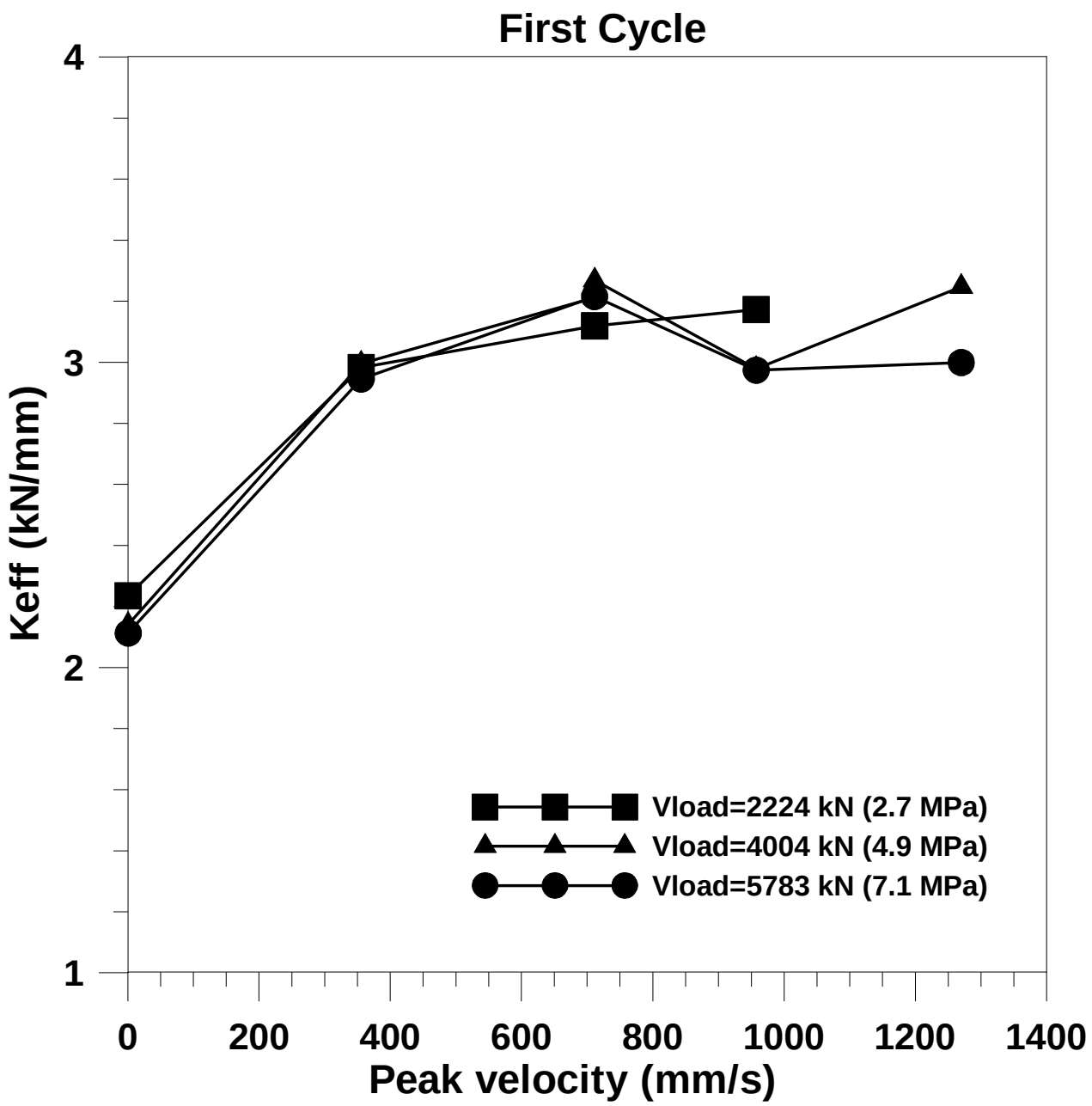

Figure A-22 Effective Stiffness for first cycle of tests at different vertical load and velocity

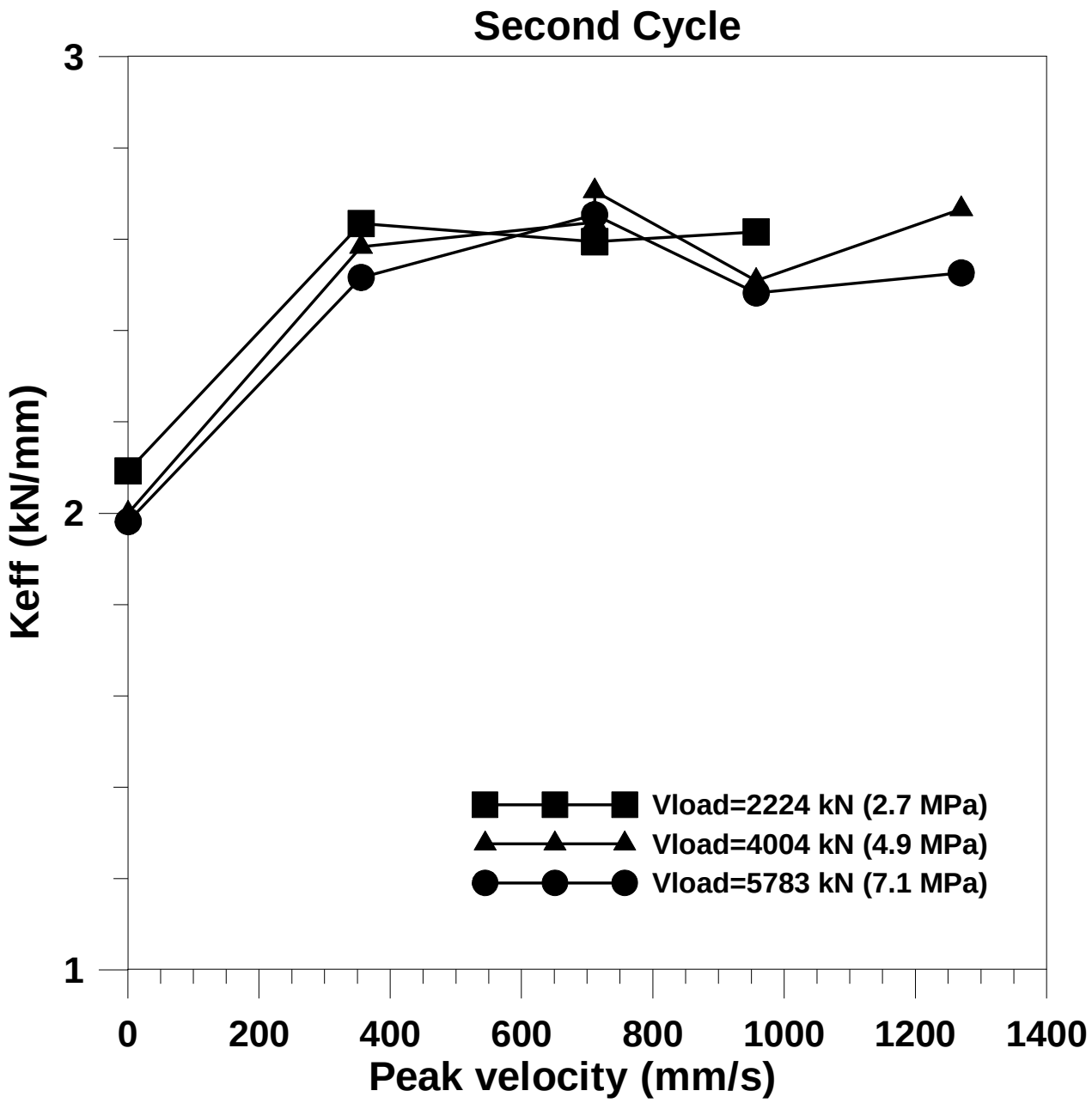

Figure A-23 Effective Stiffness for second cycle of tests at different vertical load and velocity

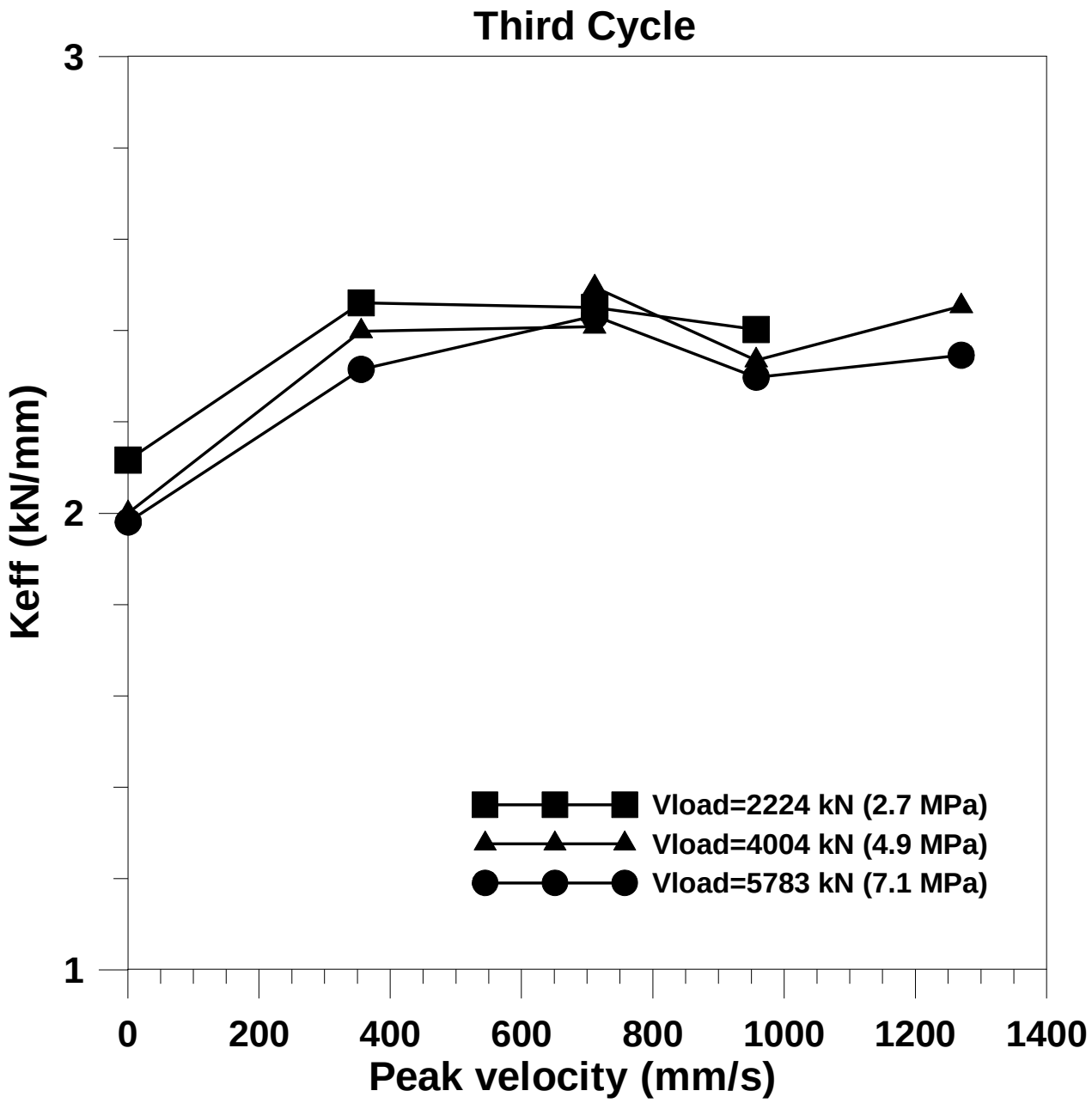

Figure A-24 Effective Stiffness for third cycle of tests at different vertical load and velocity

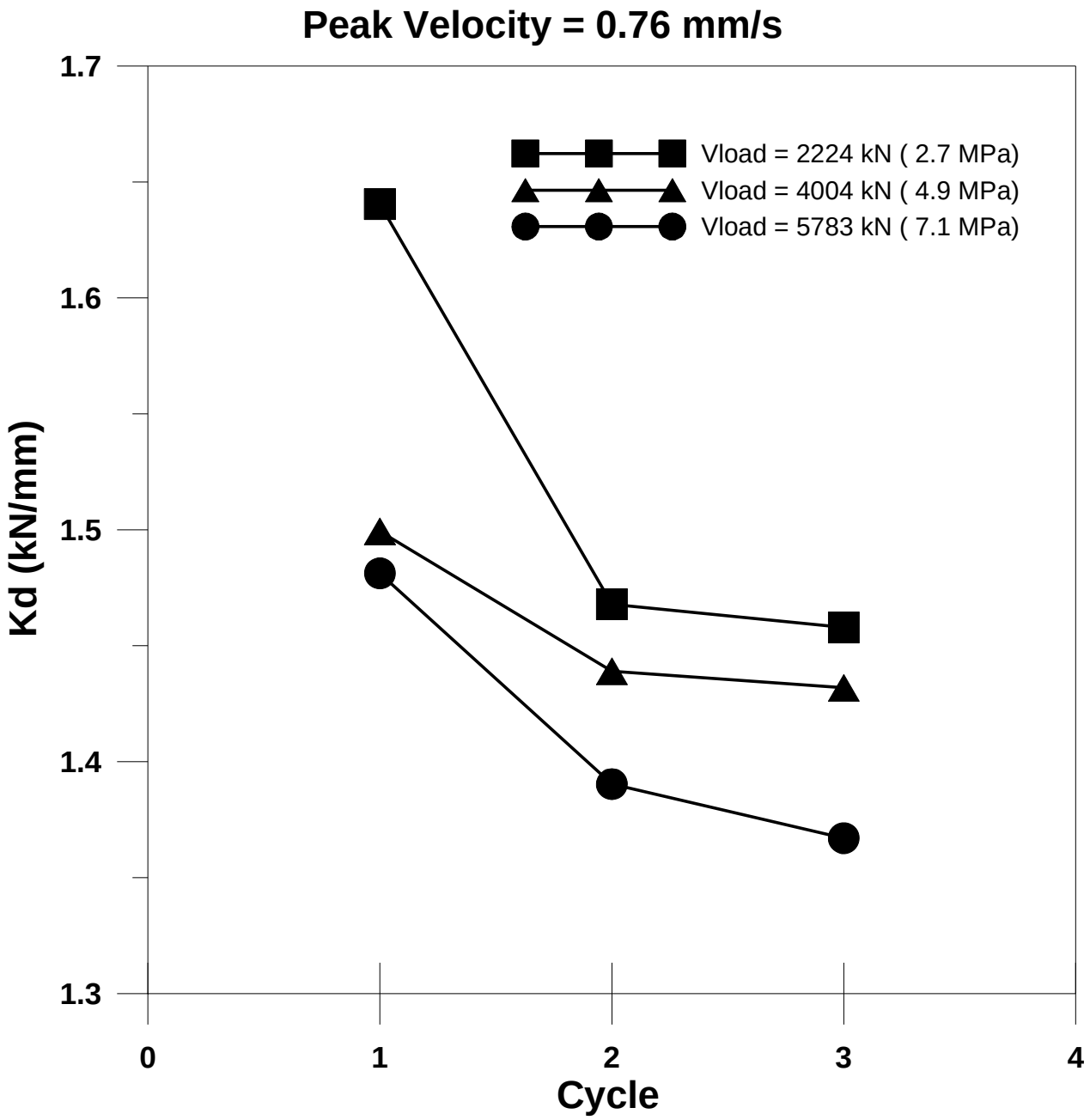

Figure A-25 Post-Yield Stiffness (Kd) for tests at 0.76 mm/s

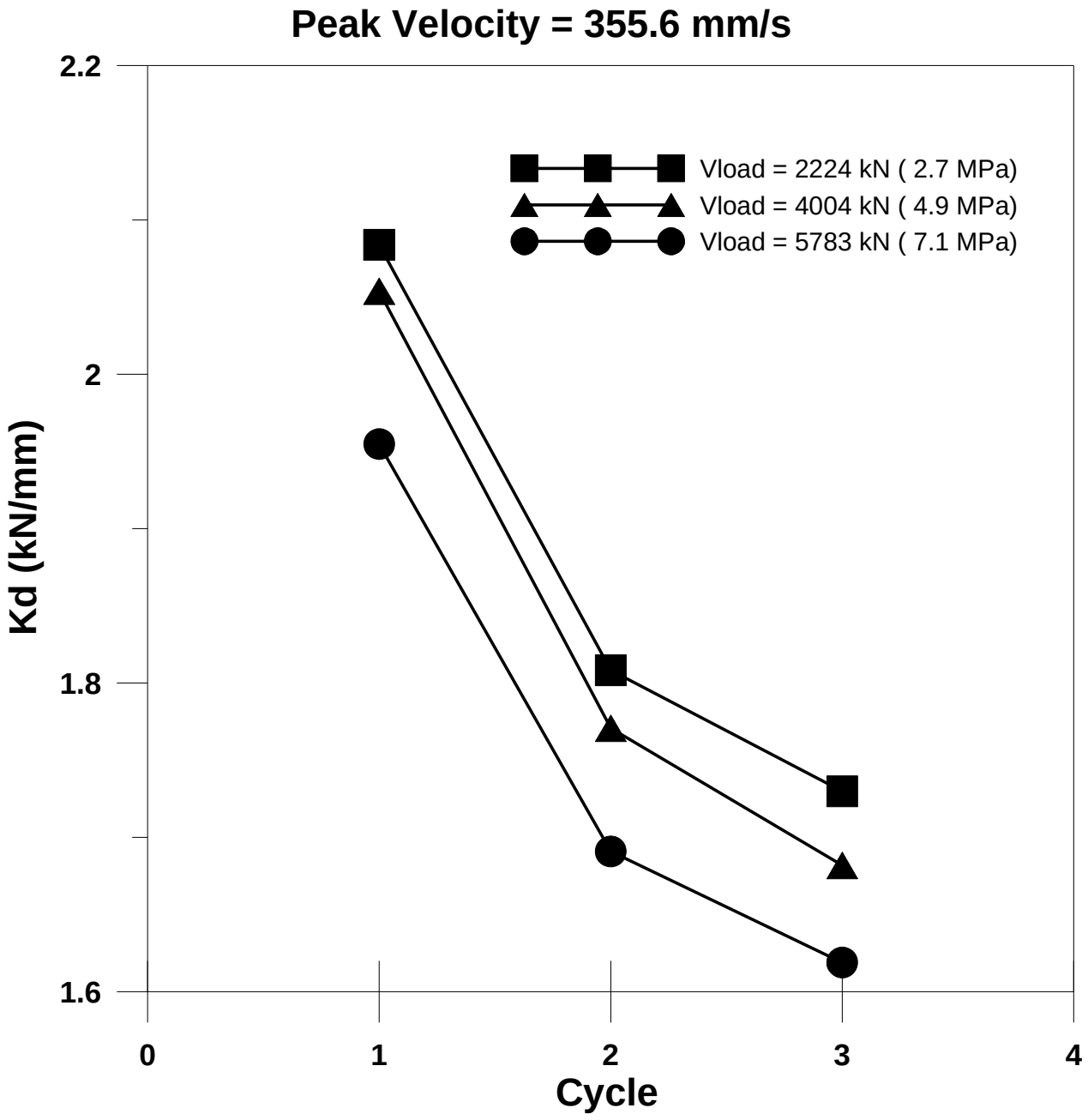

Figure A-26 Post-Yield Stiffness (Kd) for tests at 355.6 mm/s

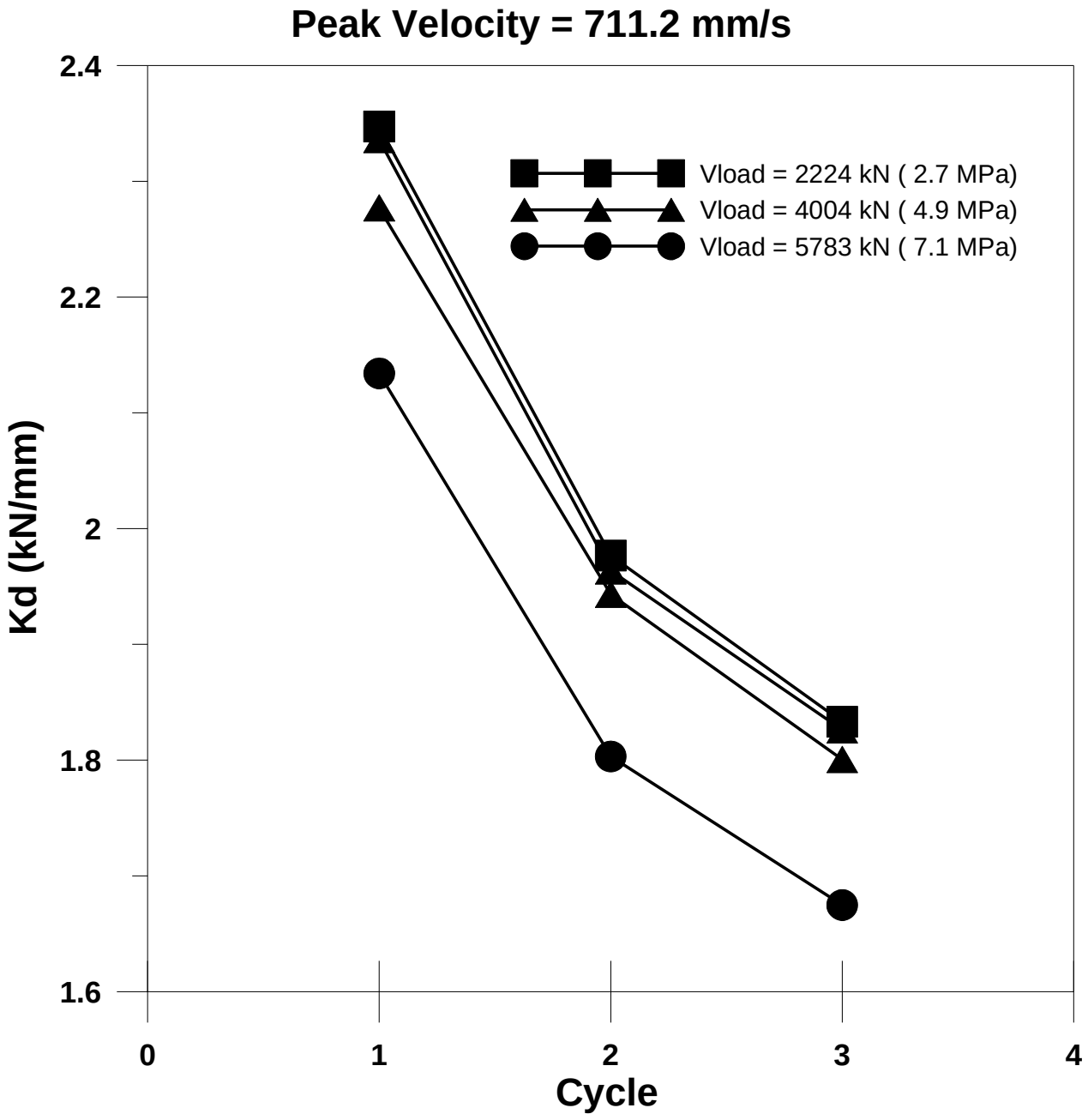

Figure A-27 Post-Yield Stiffness (Kd) for tests at 711.2 mm/s

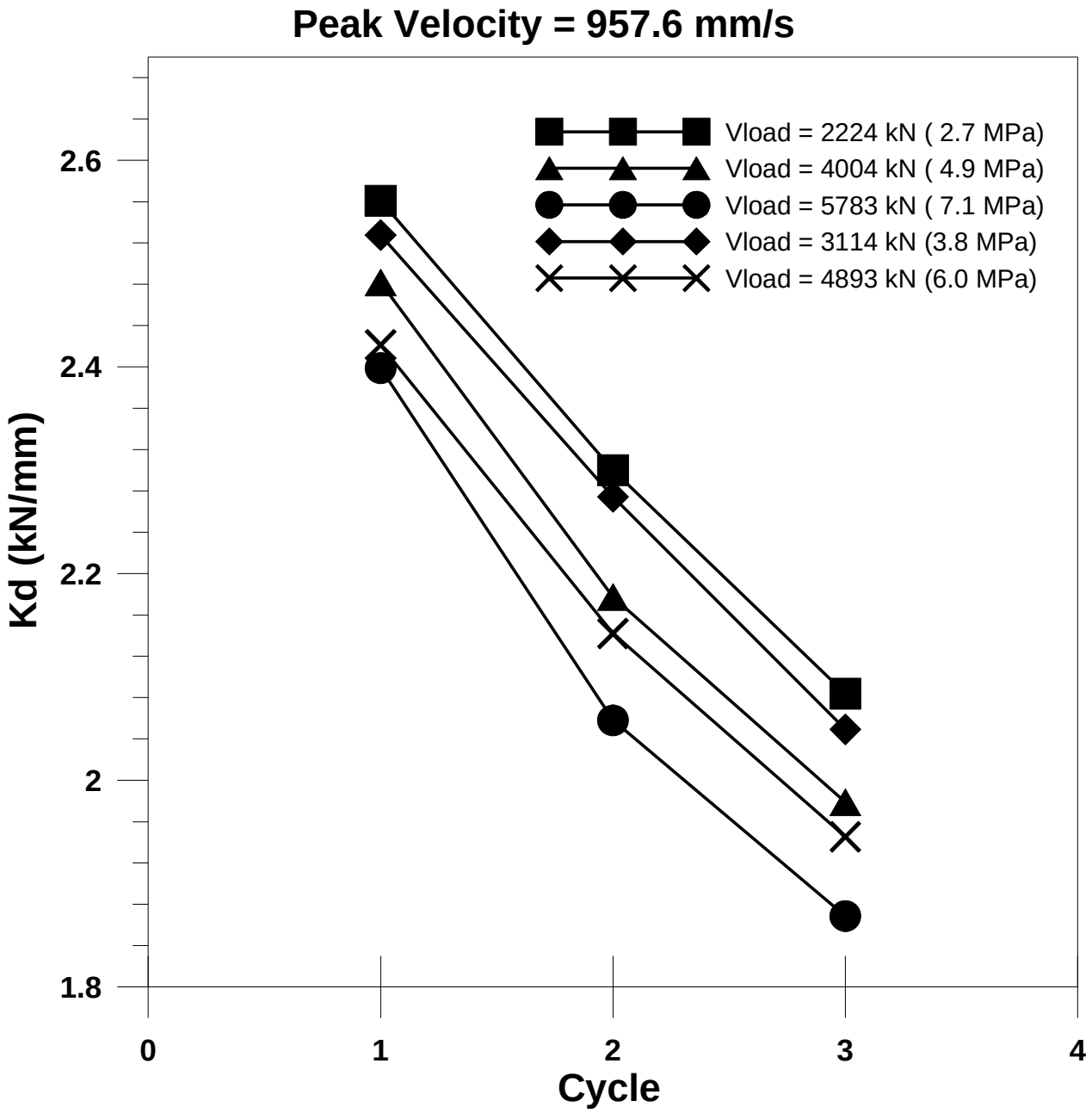

Figure A-28 Post-Yield Stiffness (Kd) for tests at 957.6 mm/s

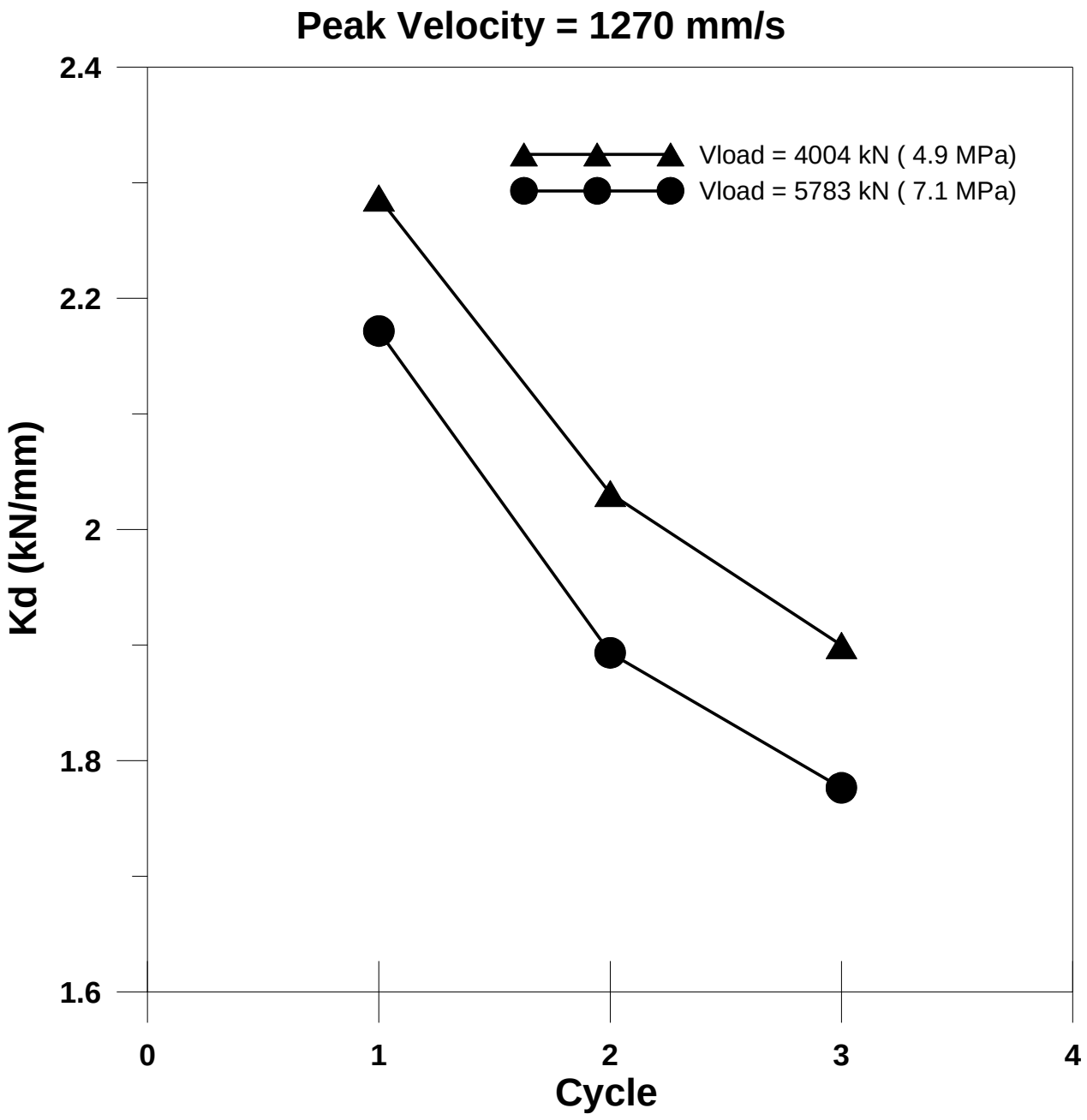

Figure A-29 Post-Yield Stiffness (Kd) for tests at 1270 mm/s

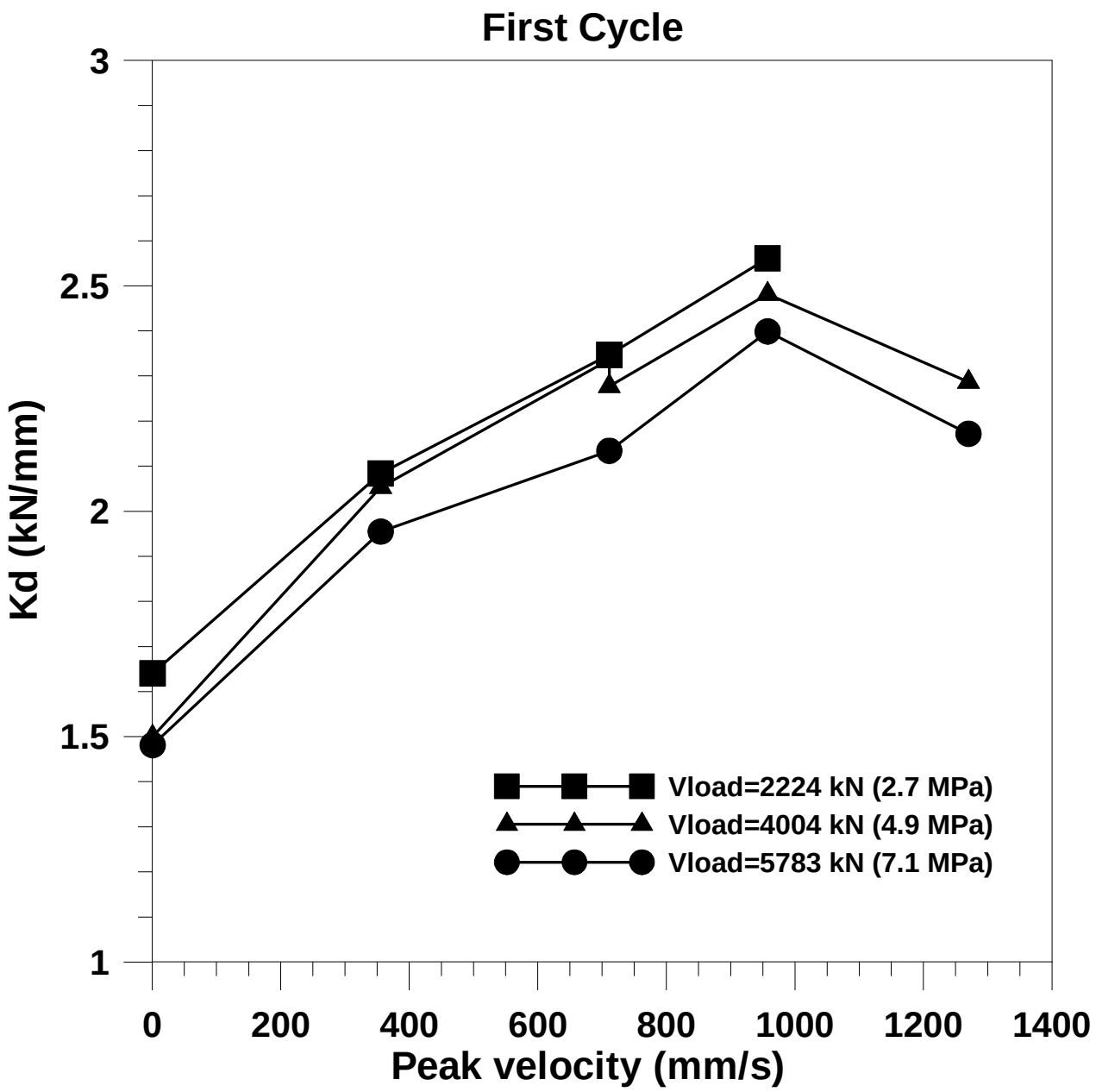

Figure A-30 Post-Yield Stiffness for first cycle of tests at different vertical load and velocity

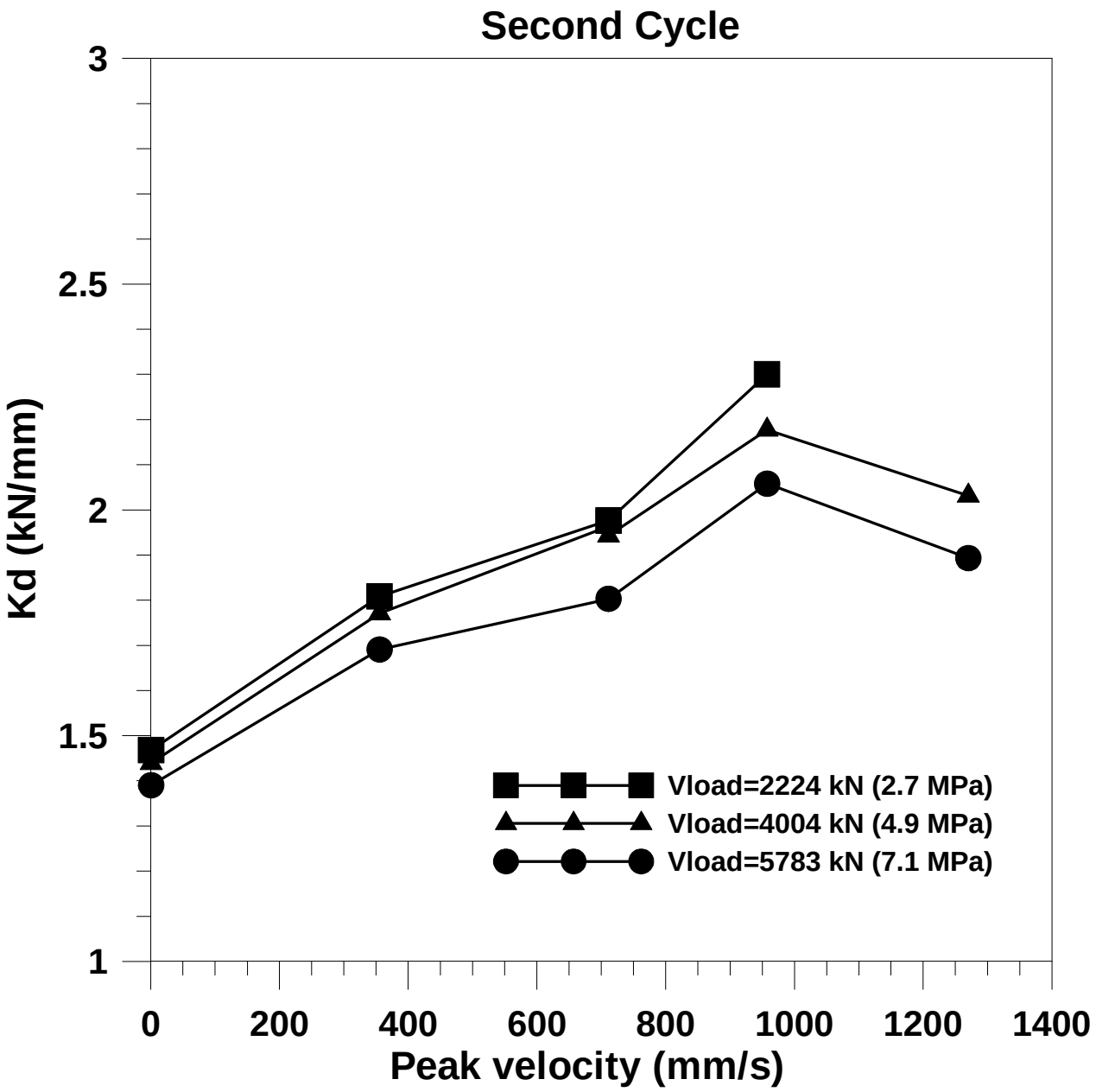

Figure A-31 Post-Yield Stiffness for second cycle of tests at different vertical load and velocity

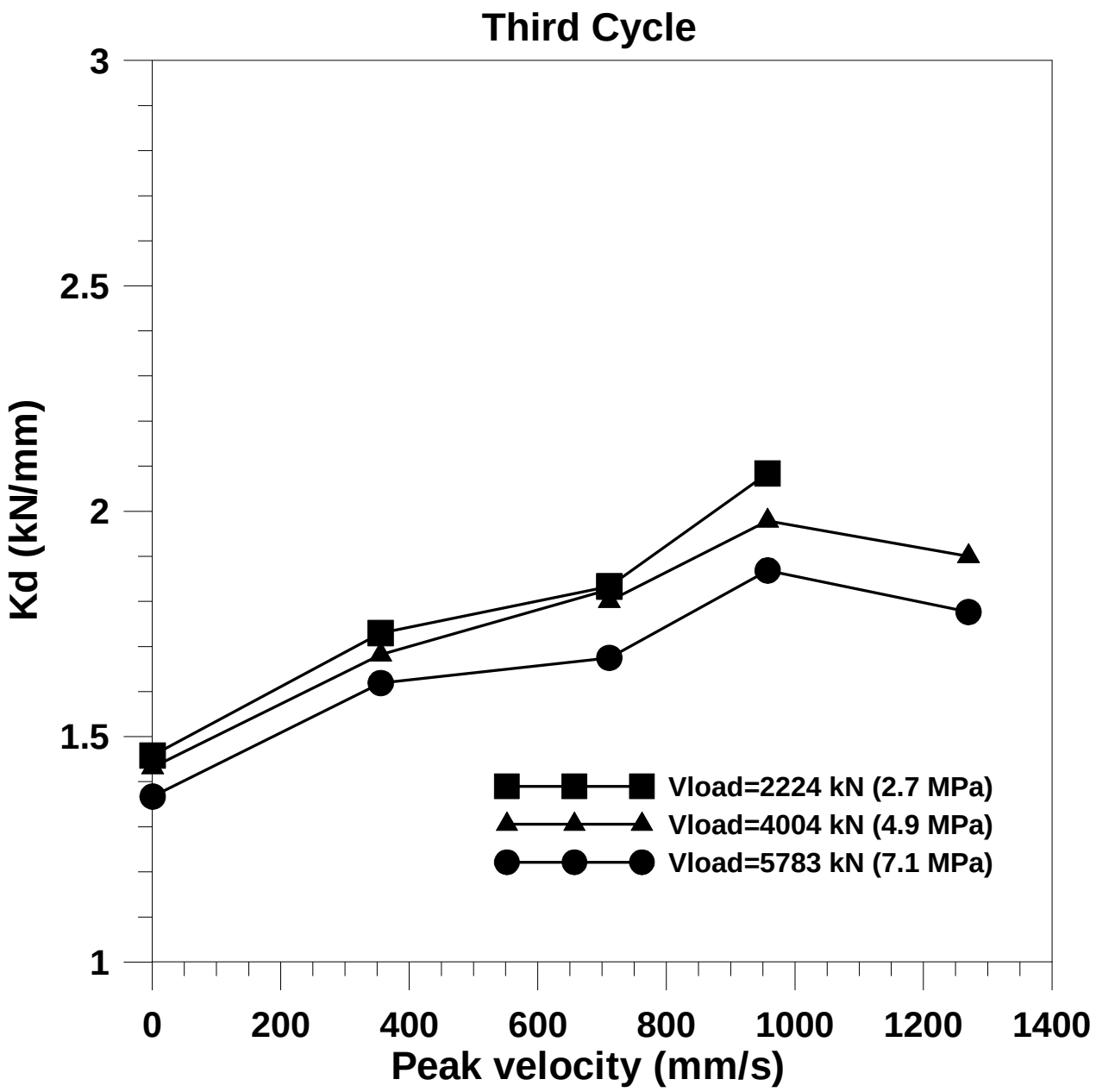

Figure A-32 Post-Yield Stiffness for third cycle of tests at different vertical load and velocity

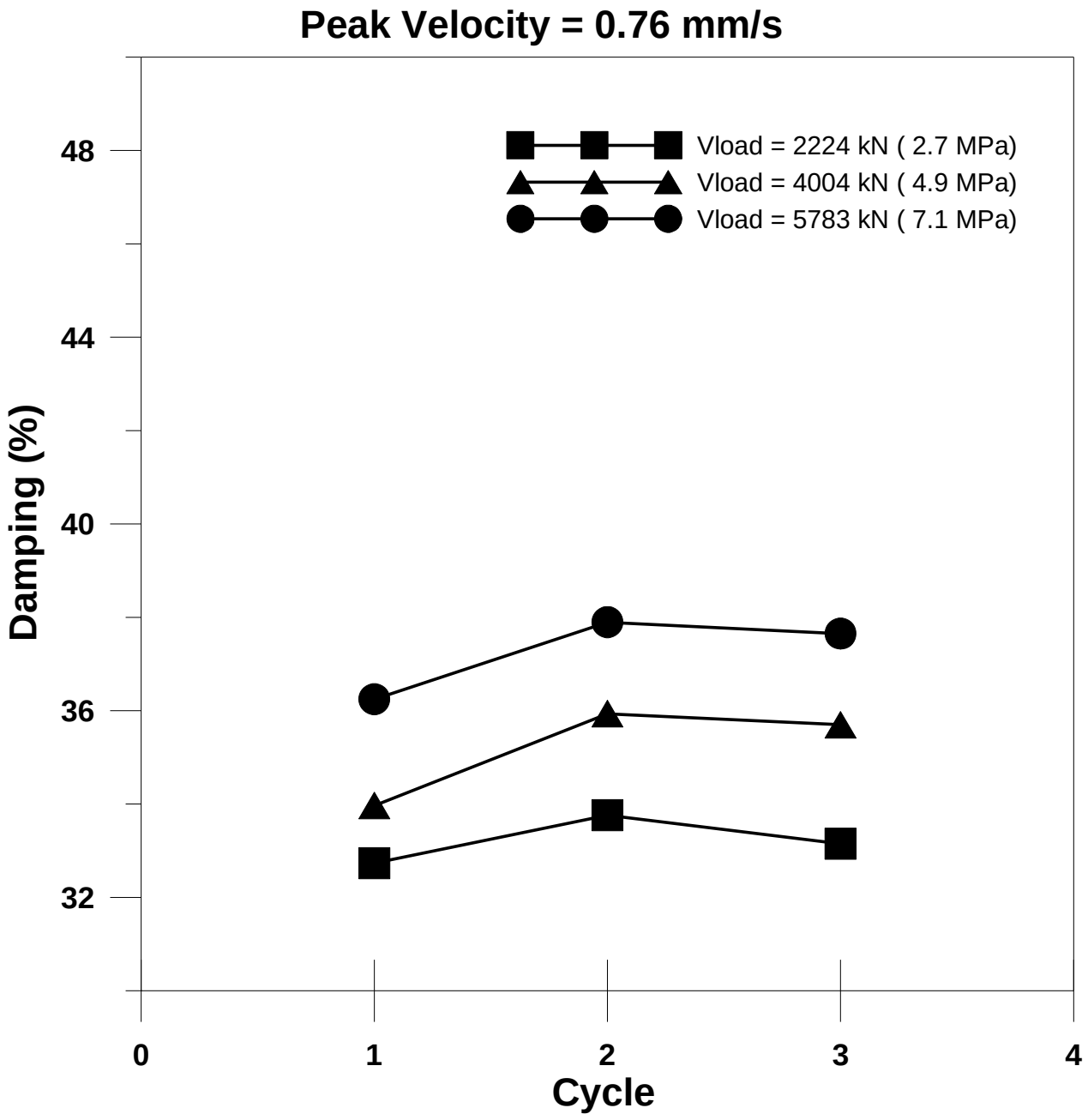

Figure A-33 Damping (%) for tests at 0.76 mm/s

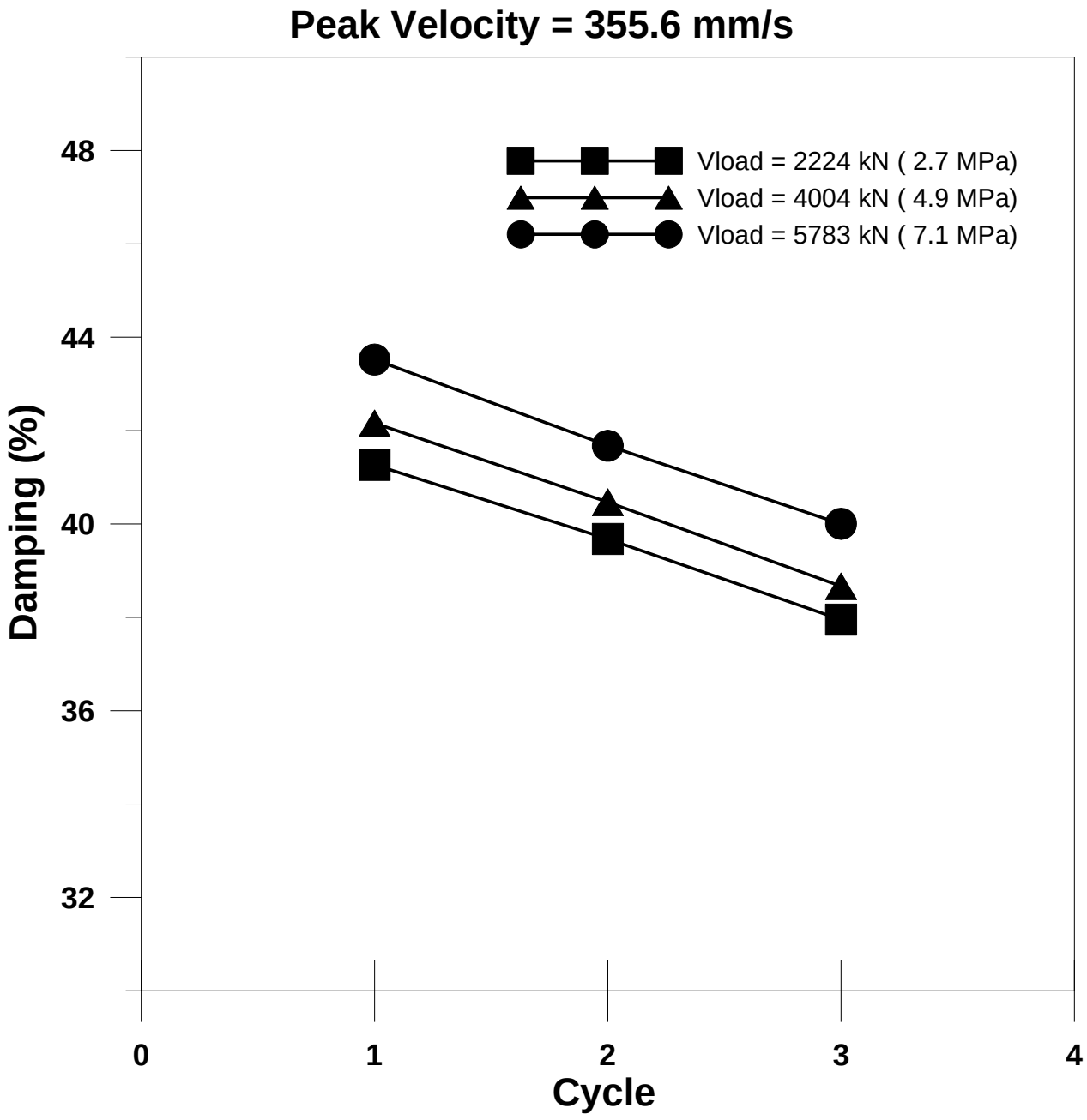

Figure A-34 Damping (%) for tests at 355.6 mm/s

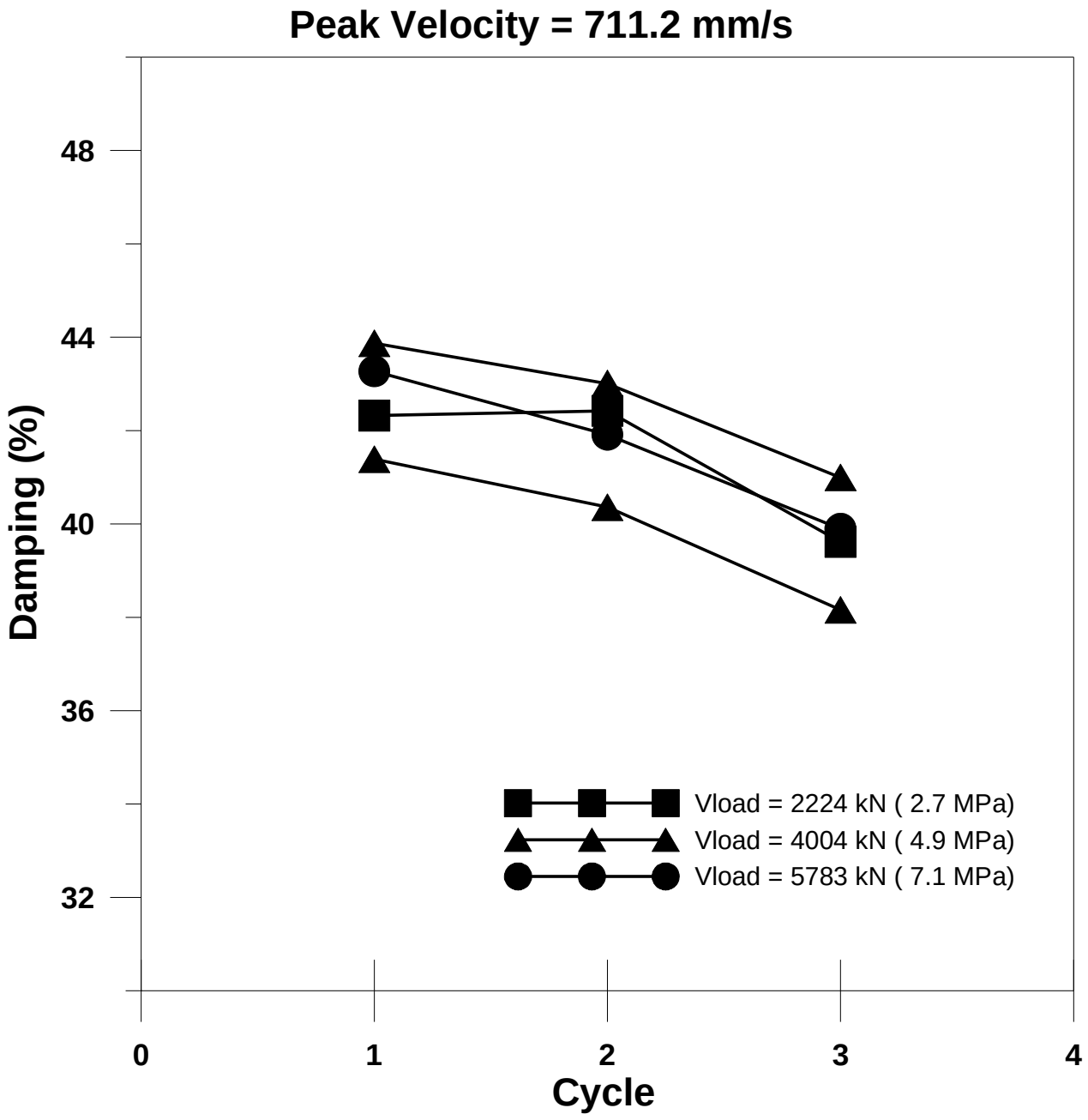

Figure A-35 Damping (%) for tests at 711.2 mm/s

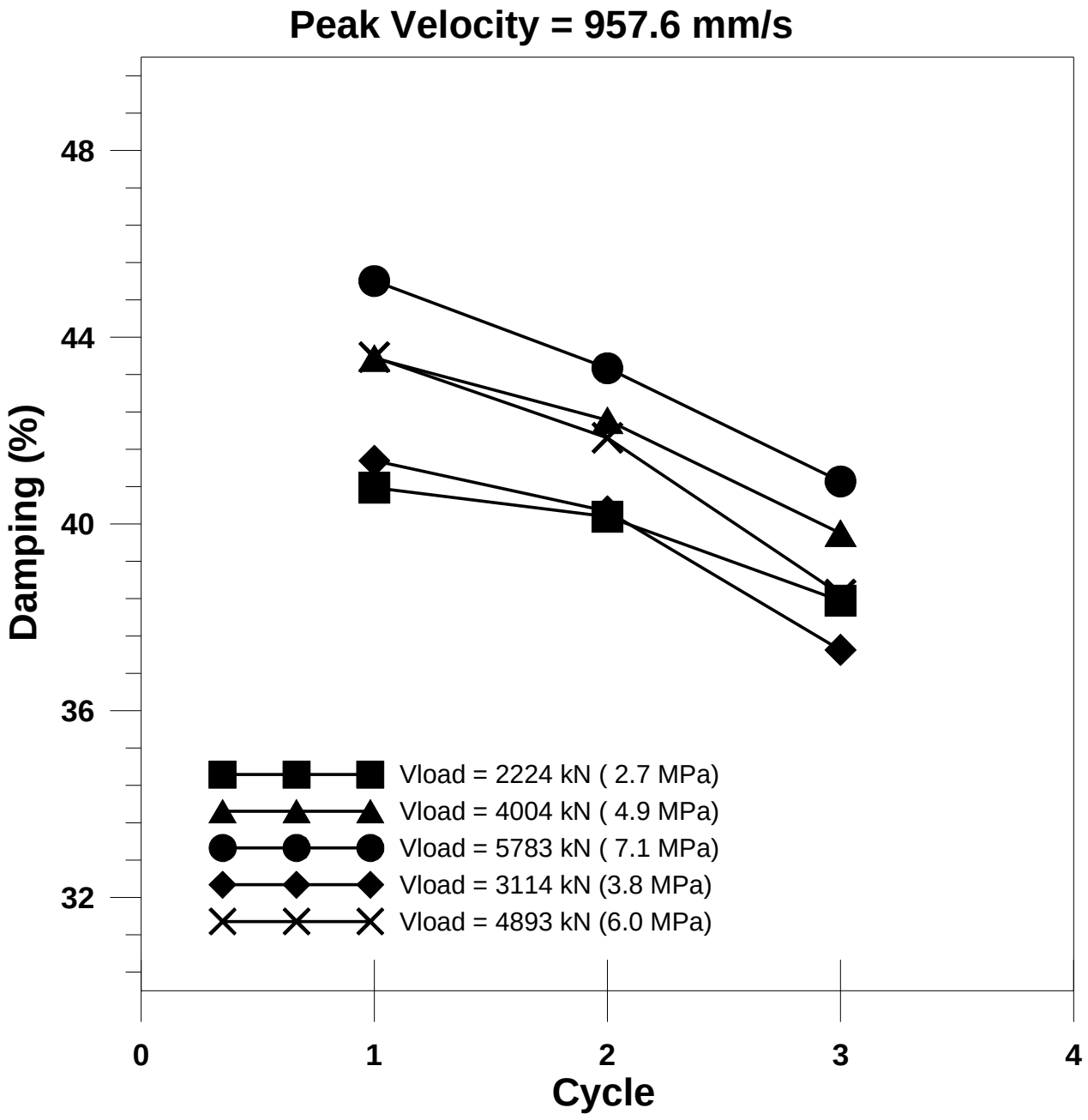

Figure A-36 Damping (%) for tests at 957.6 mm/s

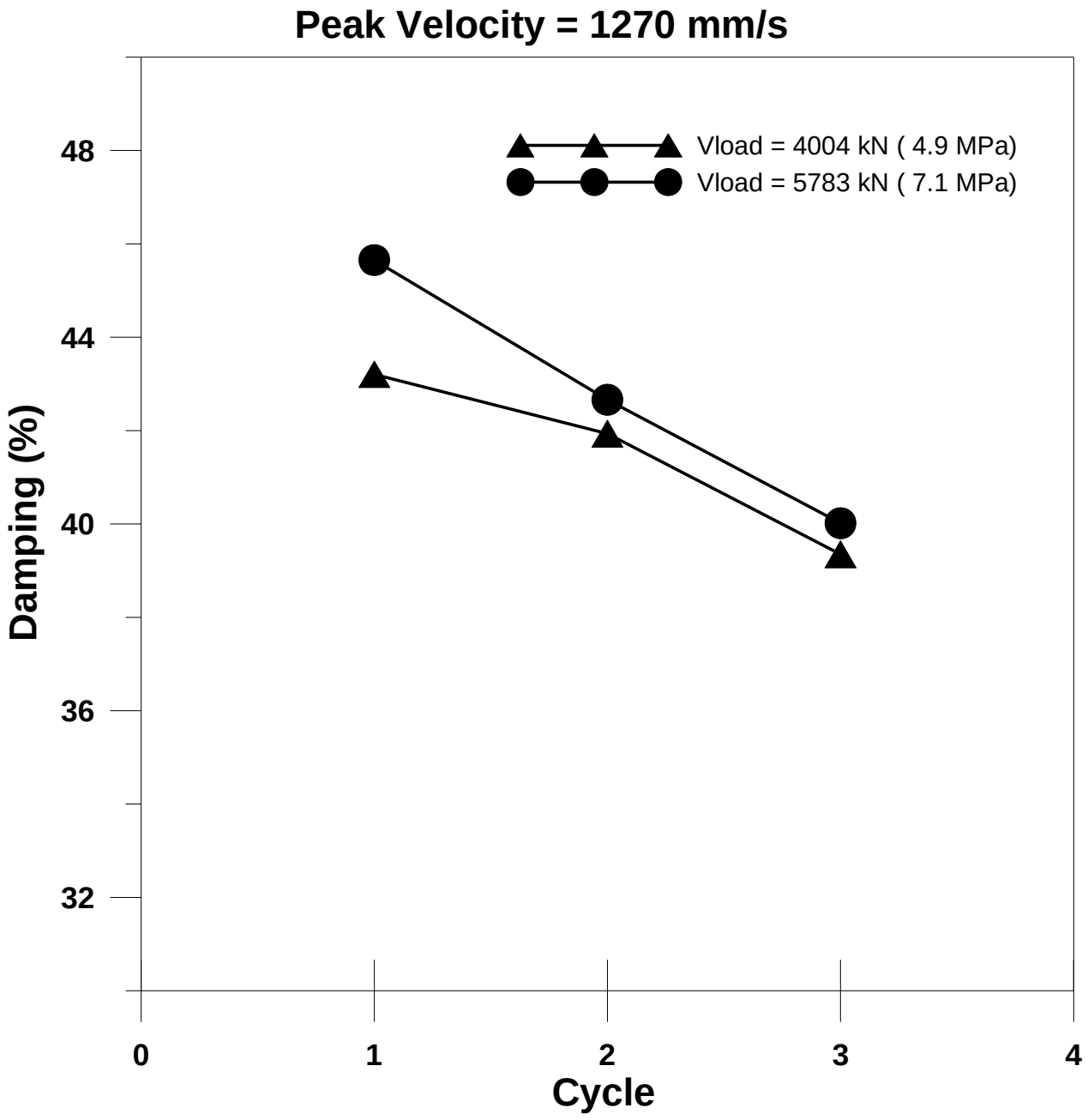

Figure A-37 Damping (%) for tests at 1270 mm/s

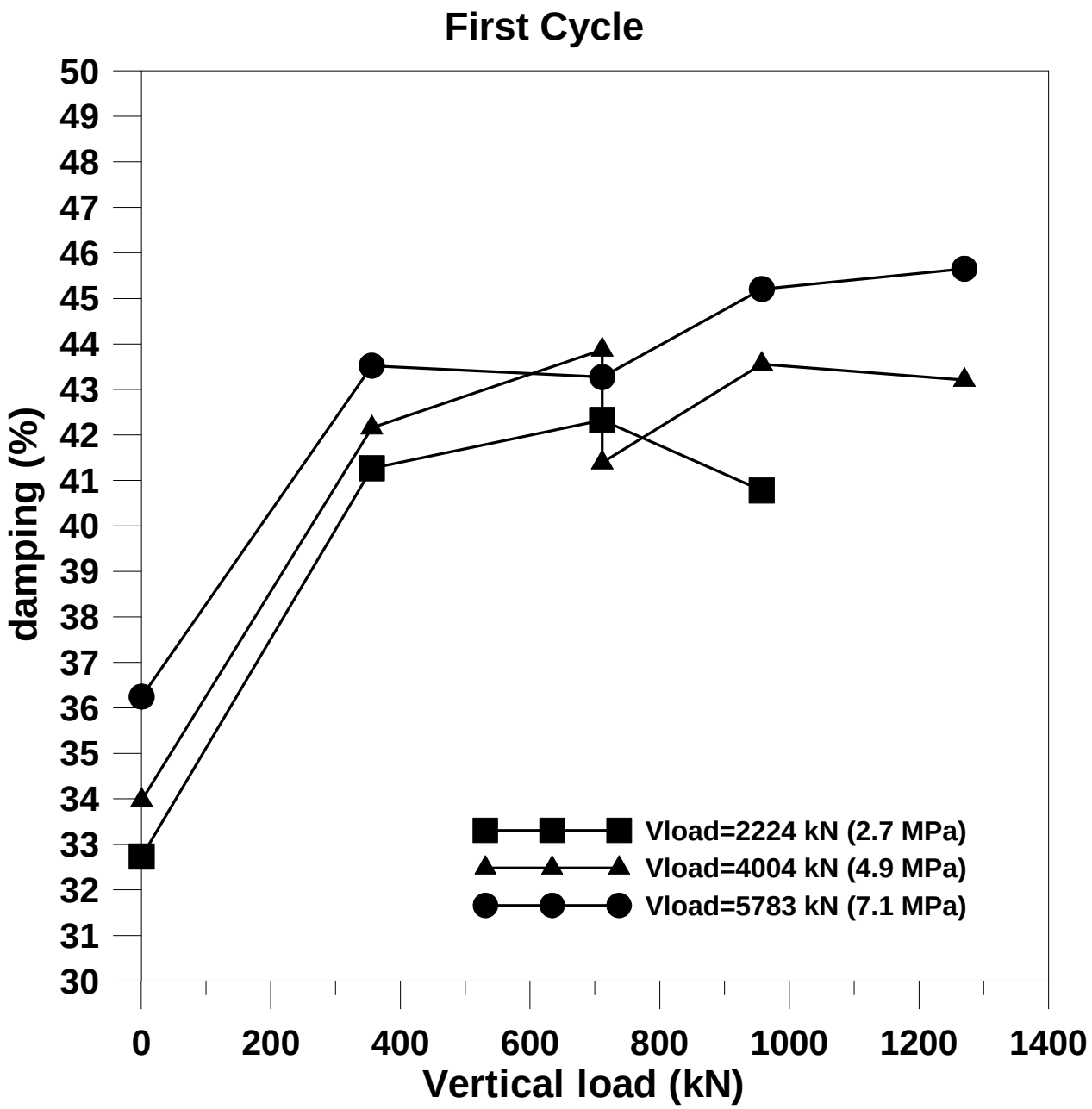

Figure A-38 Damping (%) for first cycle of tests at different vertical load and velocity

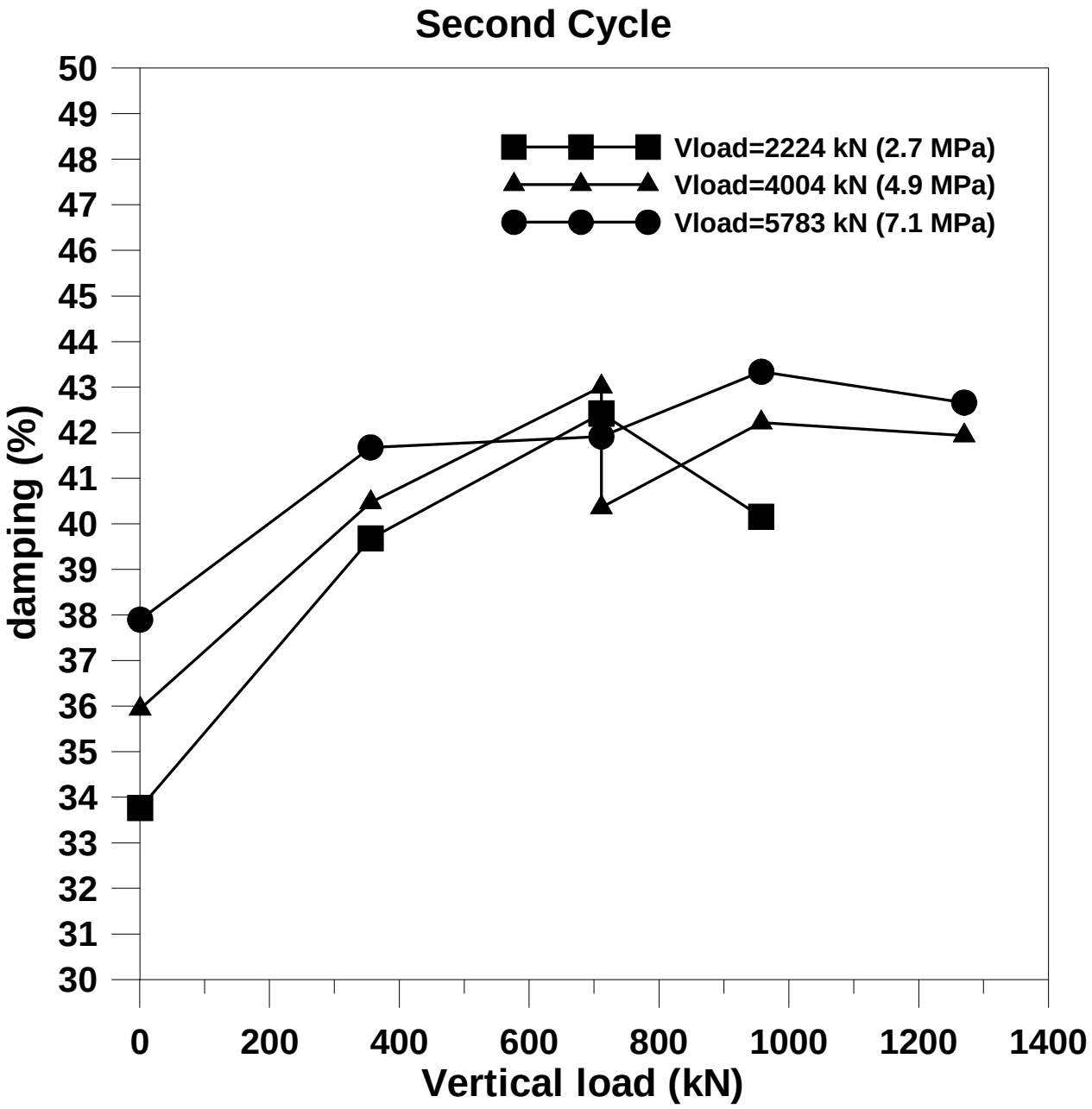

Figure A-39 Damping (%) for second cycle of tests at different vertical load and velocity

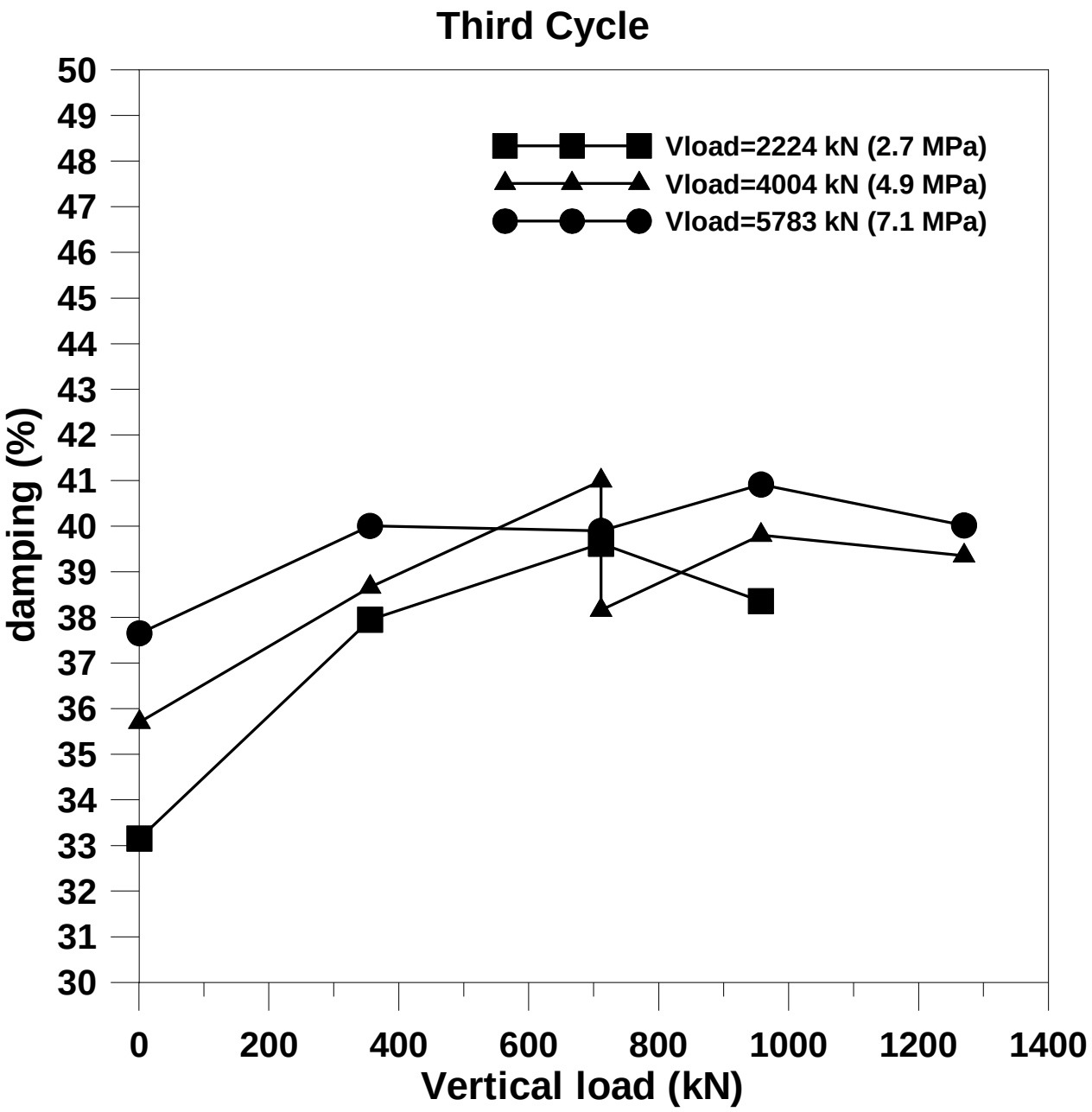

Figure A-40 Damping (%) for third cycle of tests at different vertical load and velocity

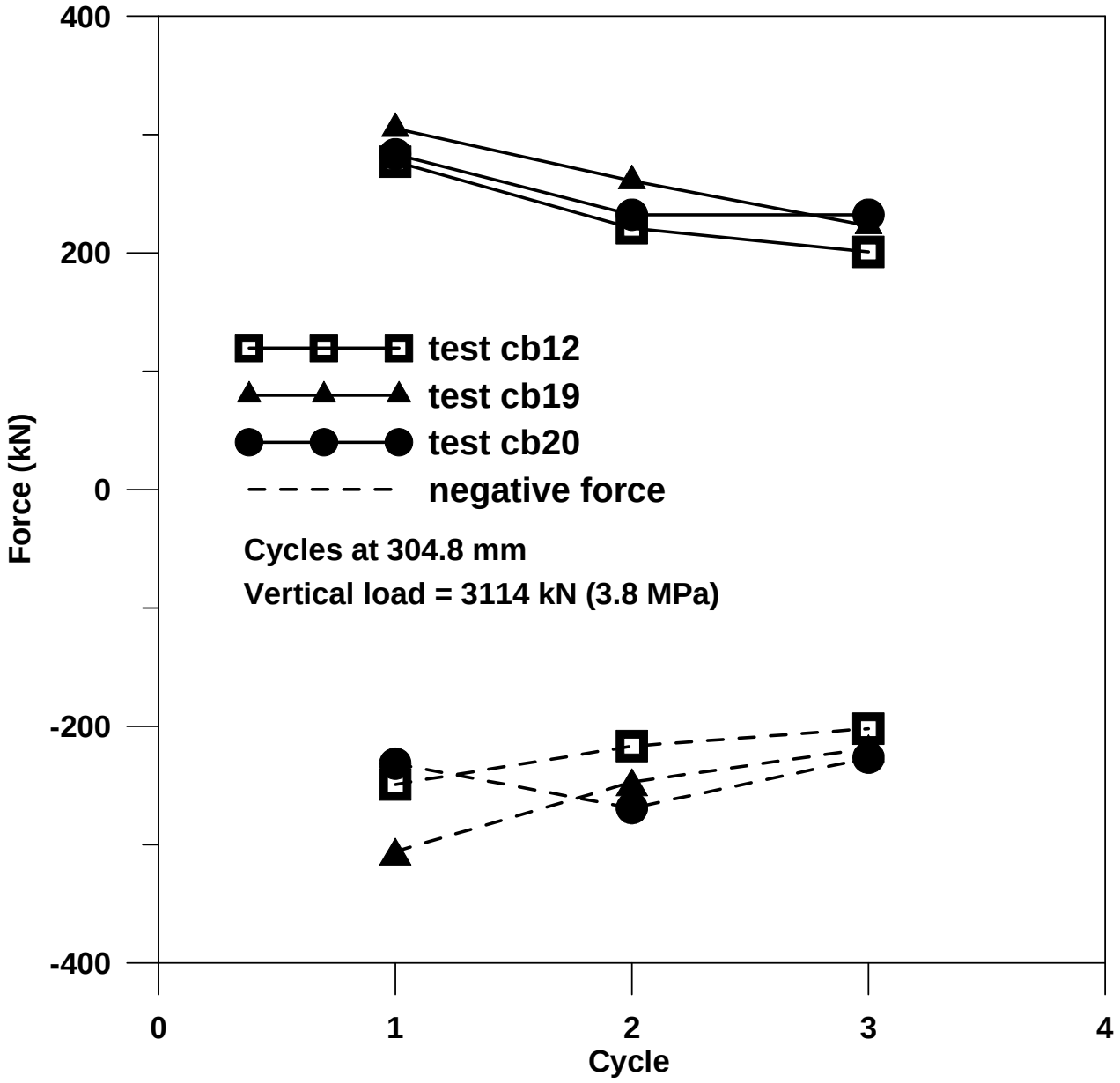

Figure A-41 Peak forces for tests cb12, cb19, cb20.

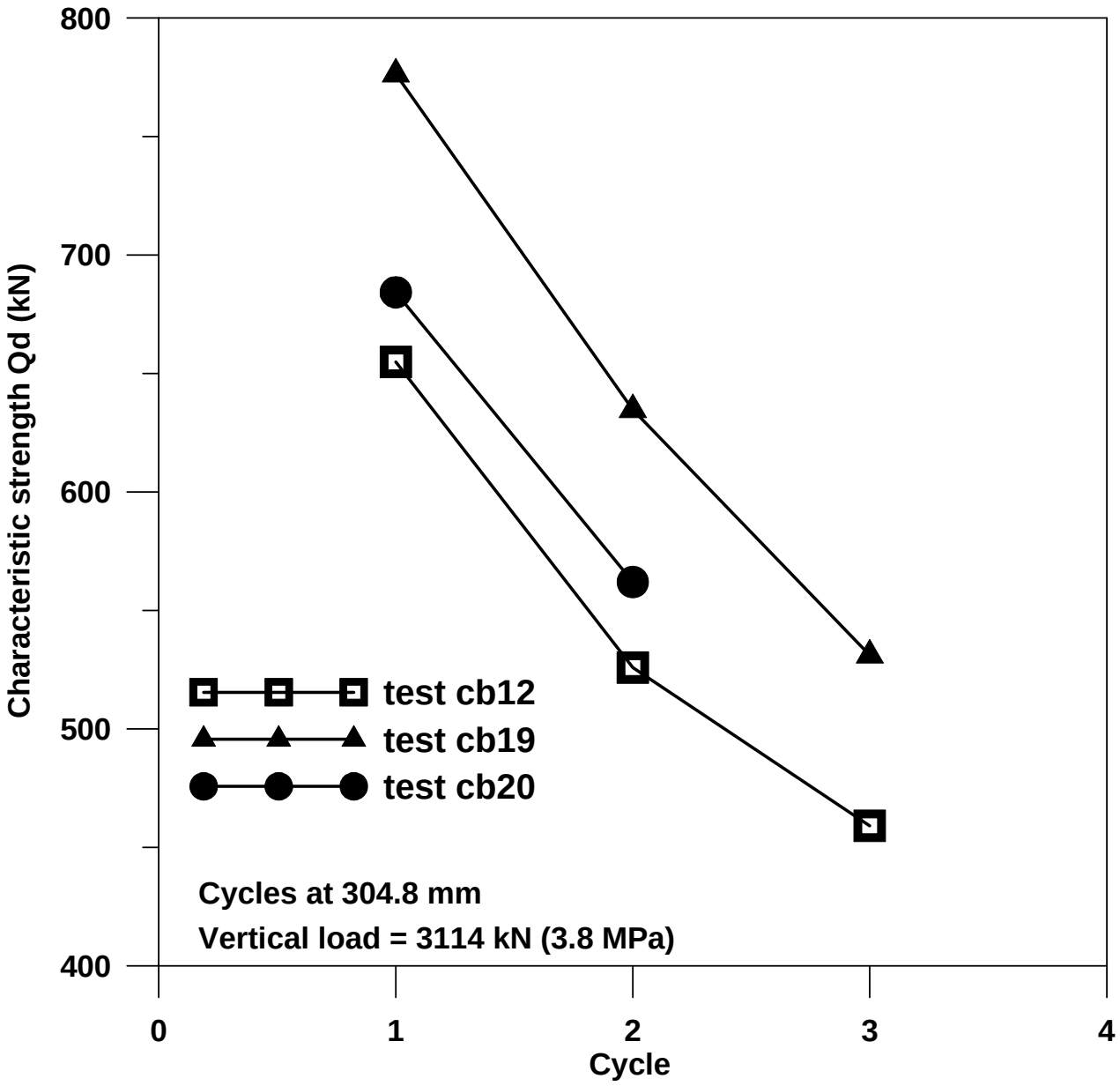

Figure A-42 Characteristic strength for tests cb12, cb19, cb20.

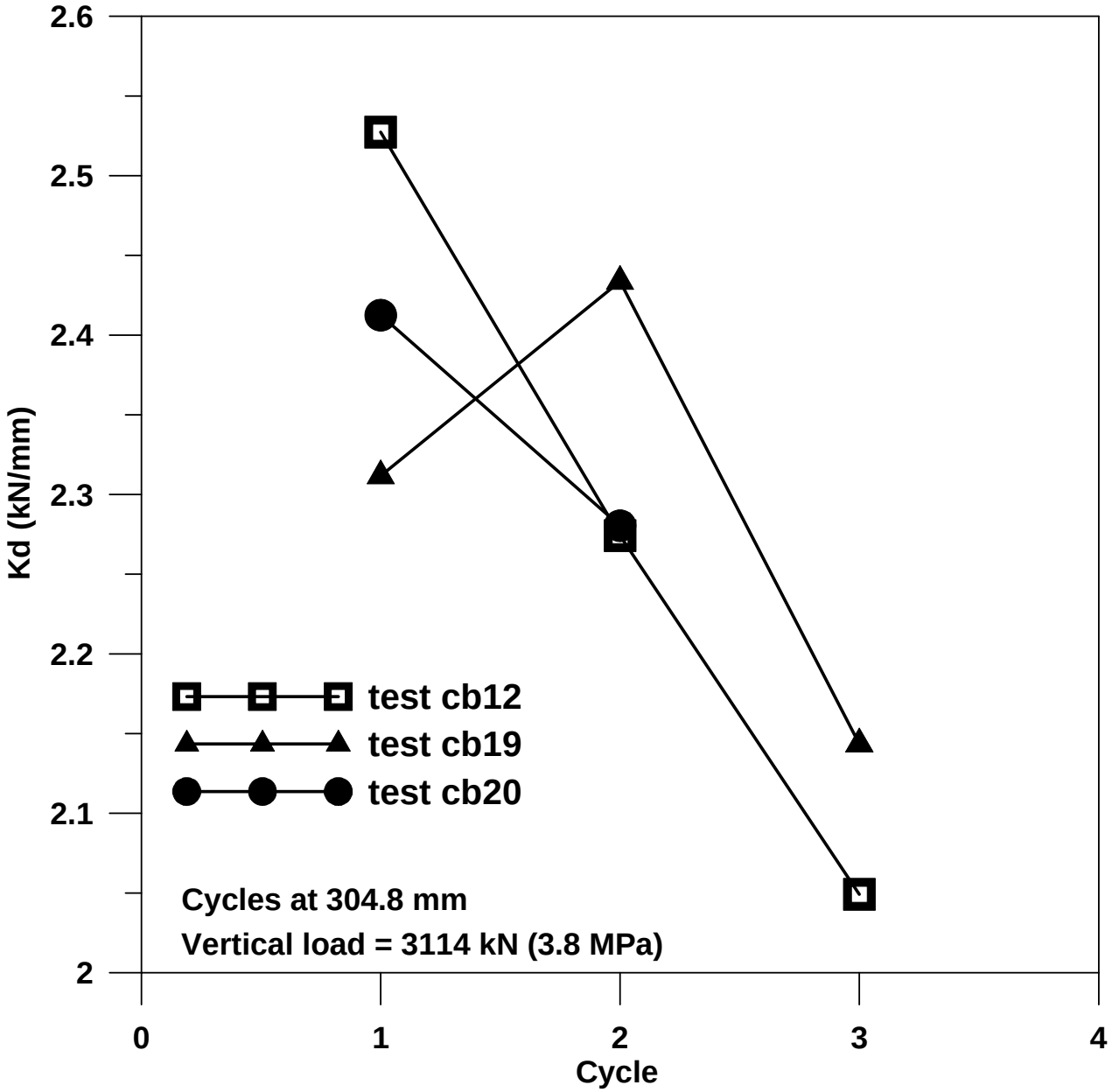

Figure A-43 Post-yield stiffness for tests cb12, cb19, cb20

APPENDIX B

SLIDING BEARINGS

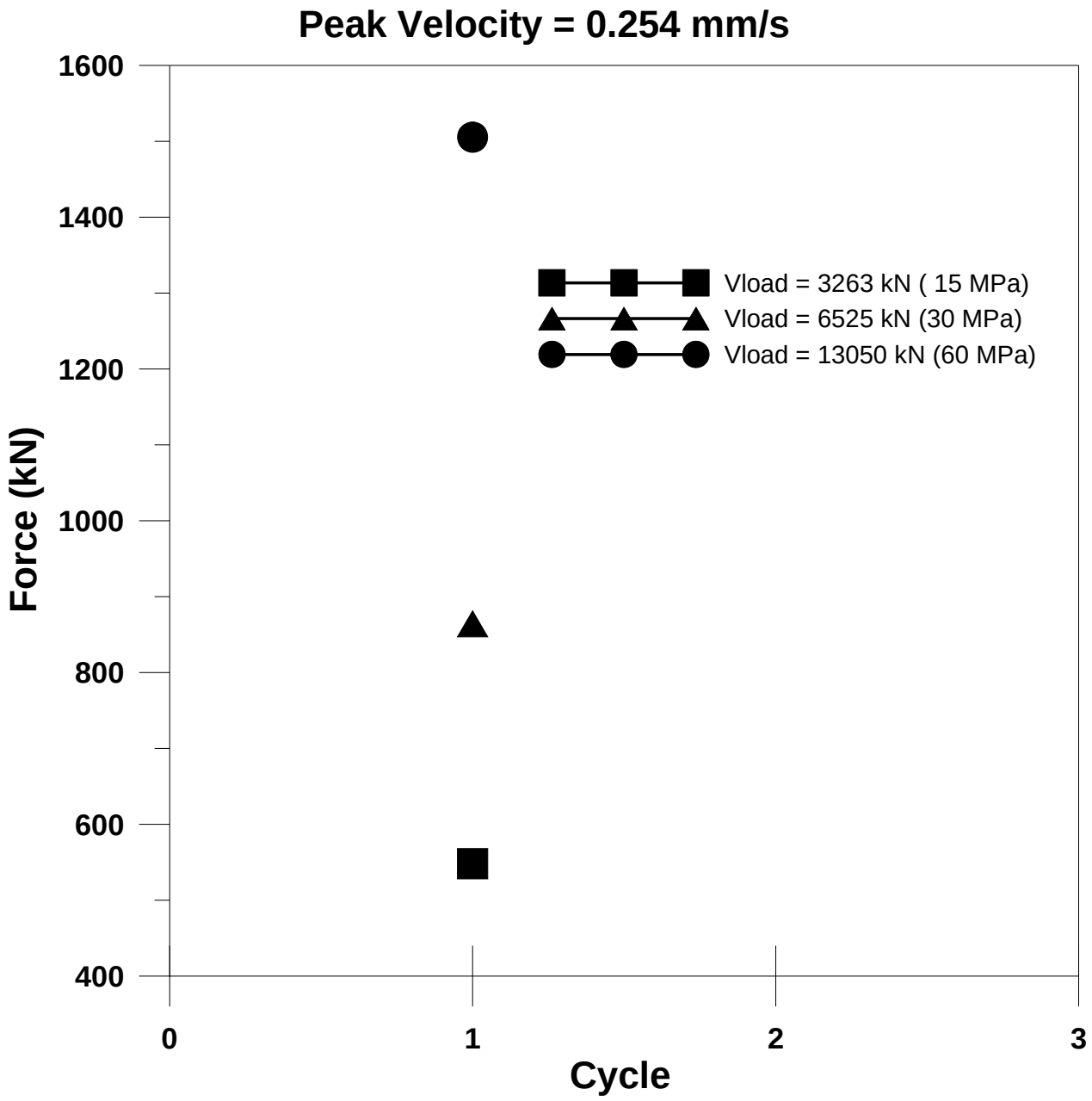

Figure B-1 Maximum Force for tests at 0.254 mm/s

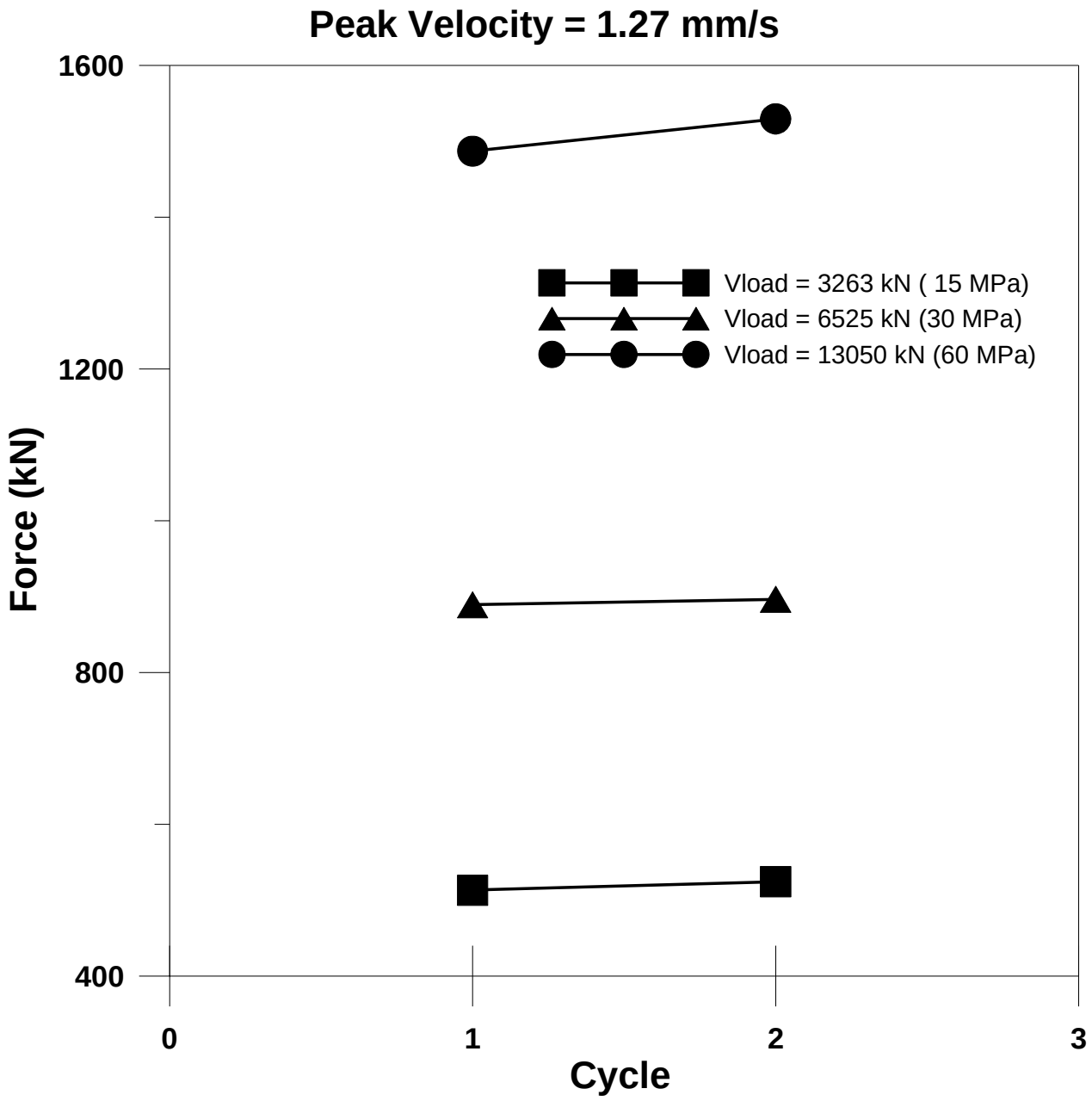

Figure B-2 Maximum Force for tests at 1.27 mm/s

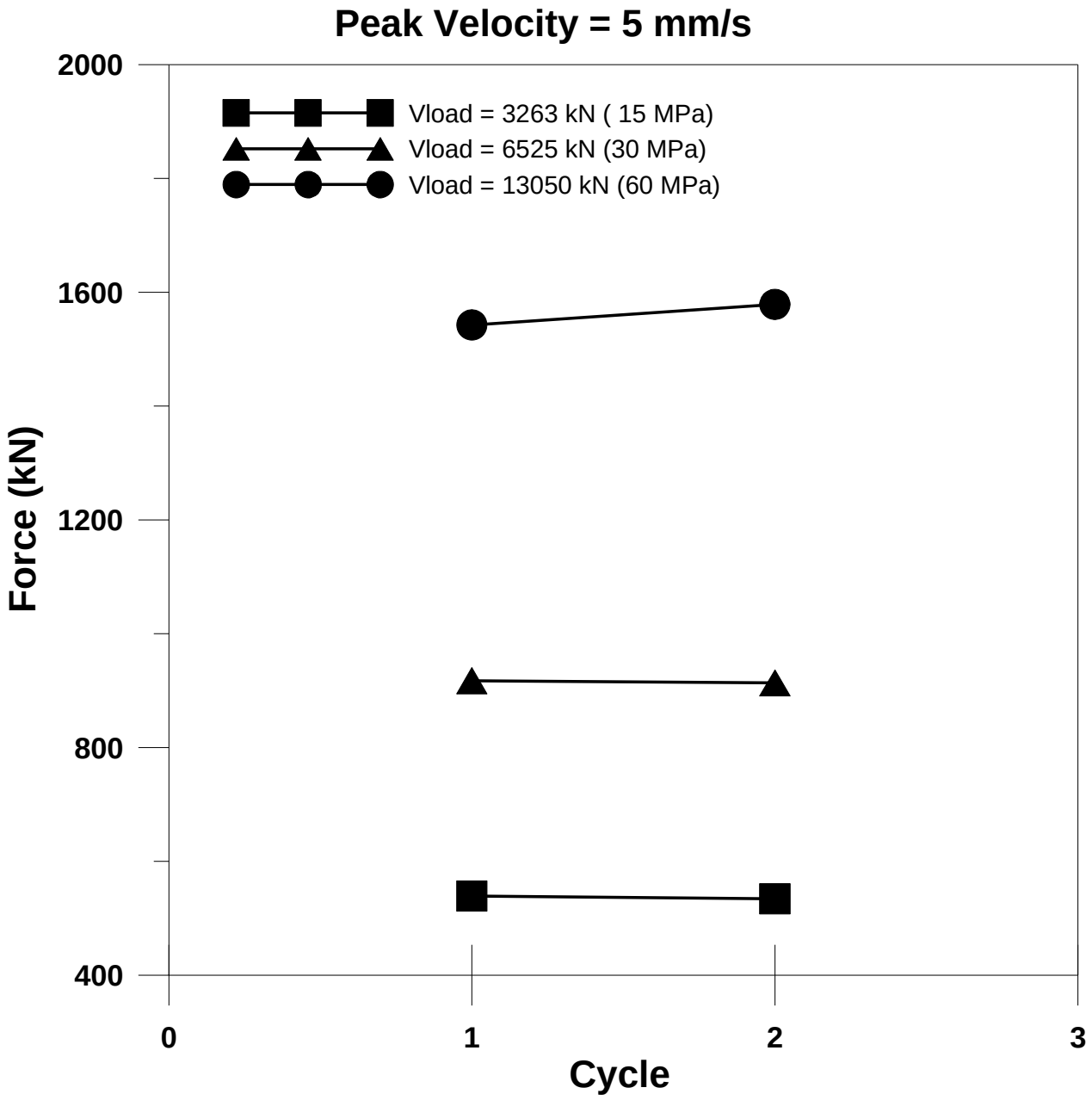

Figure B-3 Maximum Force for tests at 5.0 mm/s

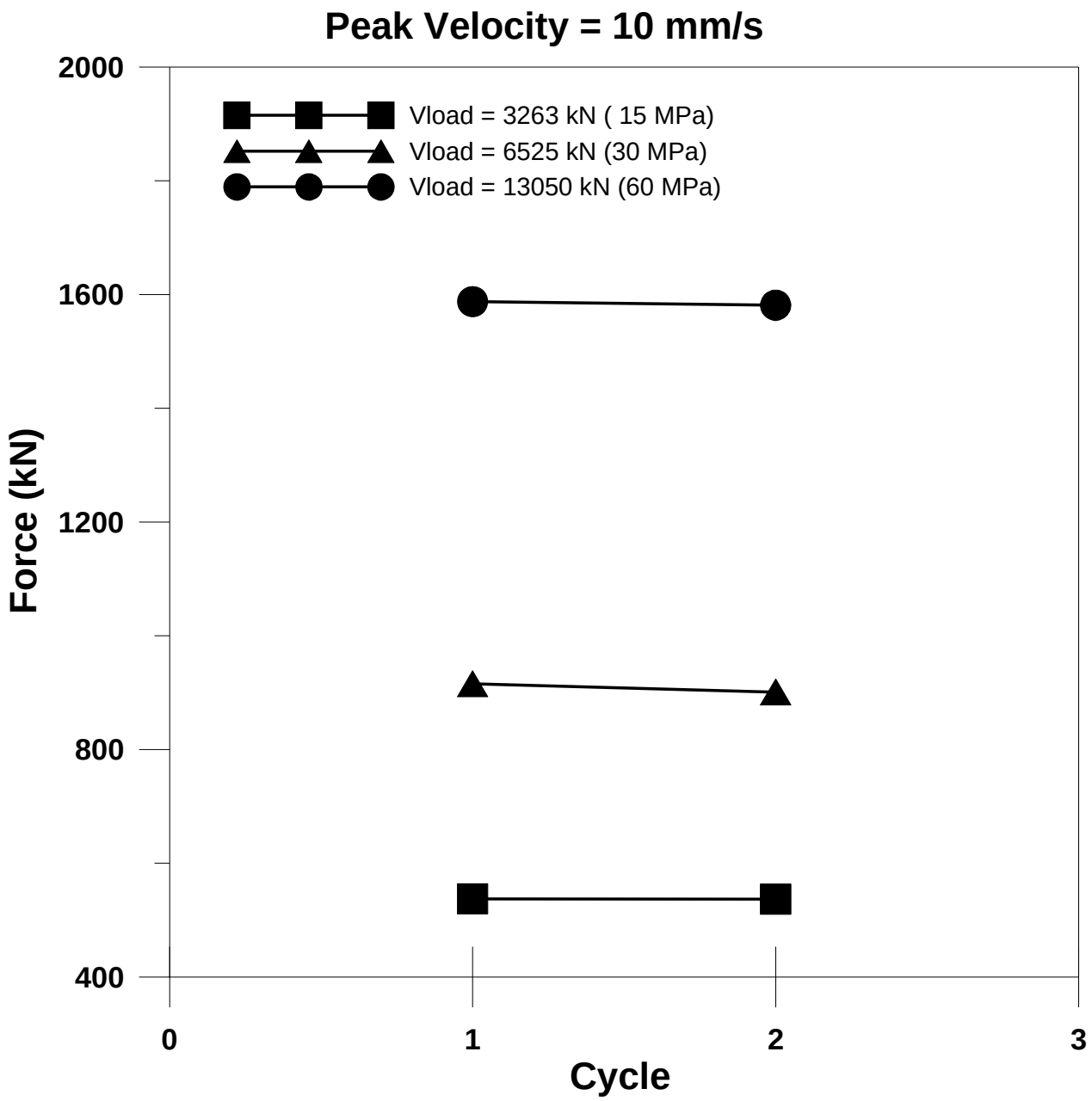

Figure B-4 Maximum Force for tests at 10.0 mm/s

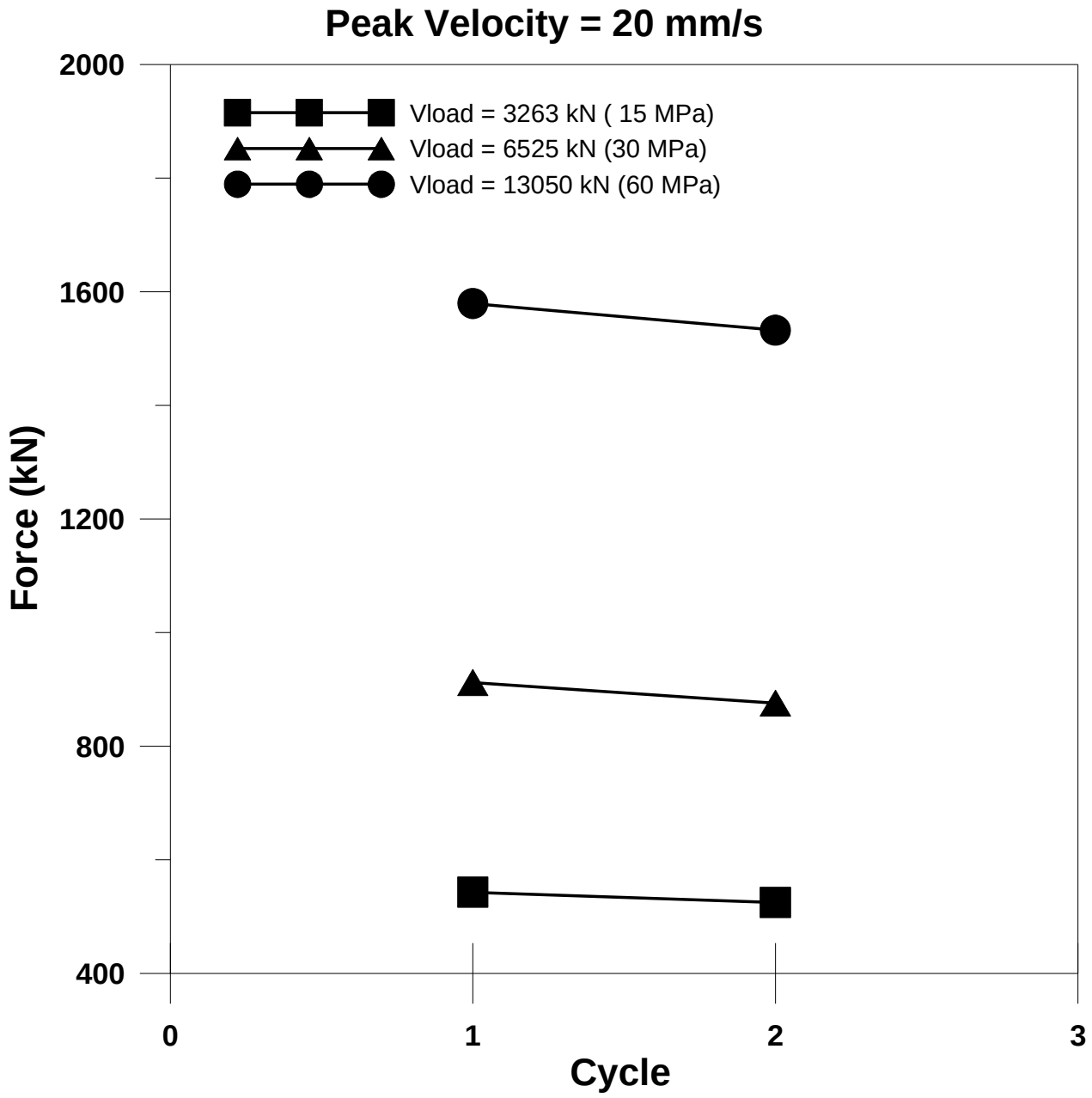

Figure B-5 Maximum Force for tests at 20.0 mm/s

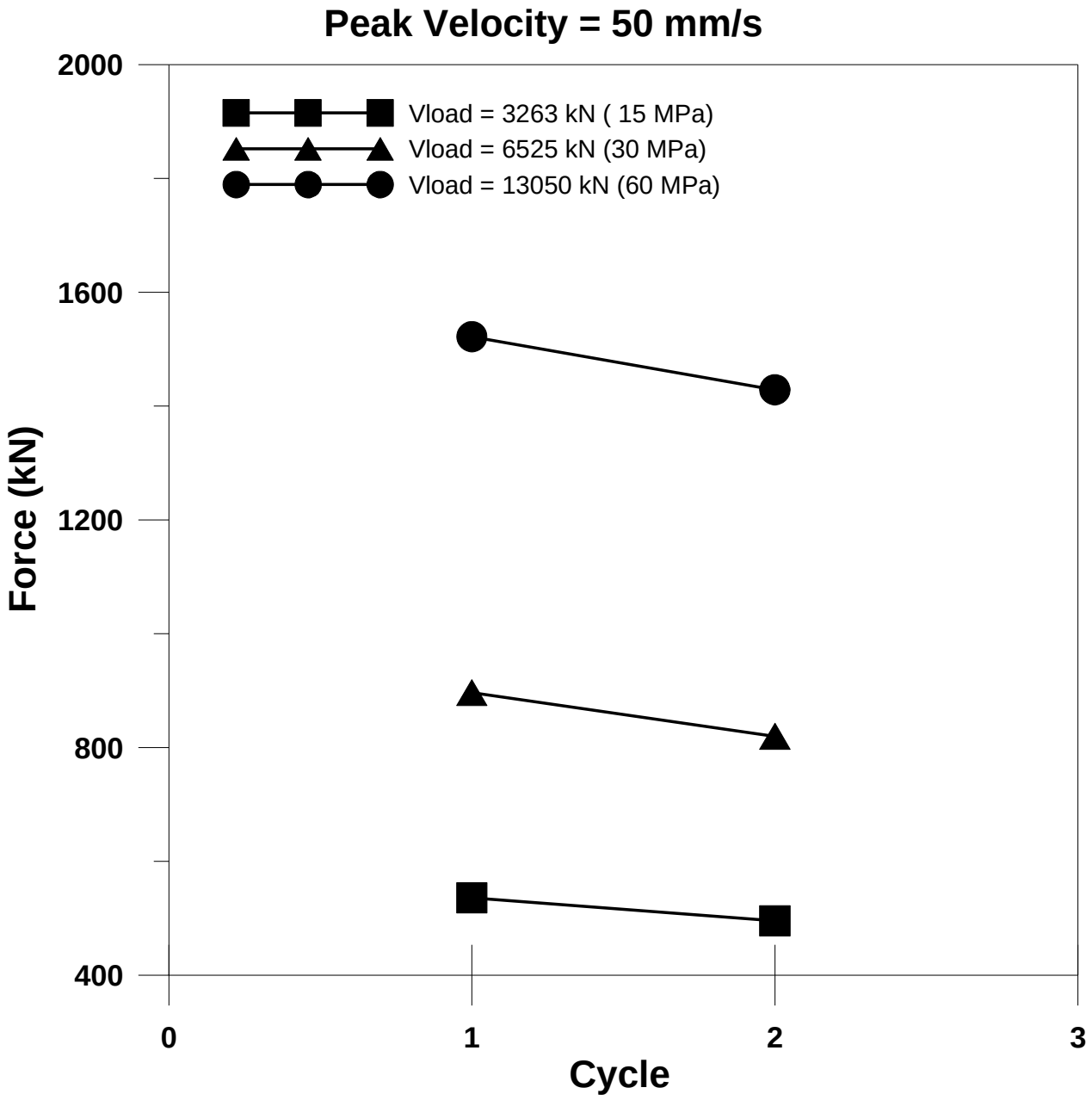

Figure B-6 Maximum Force for tests at 50.0 mm/s

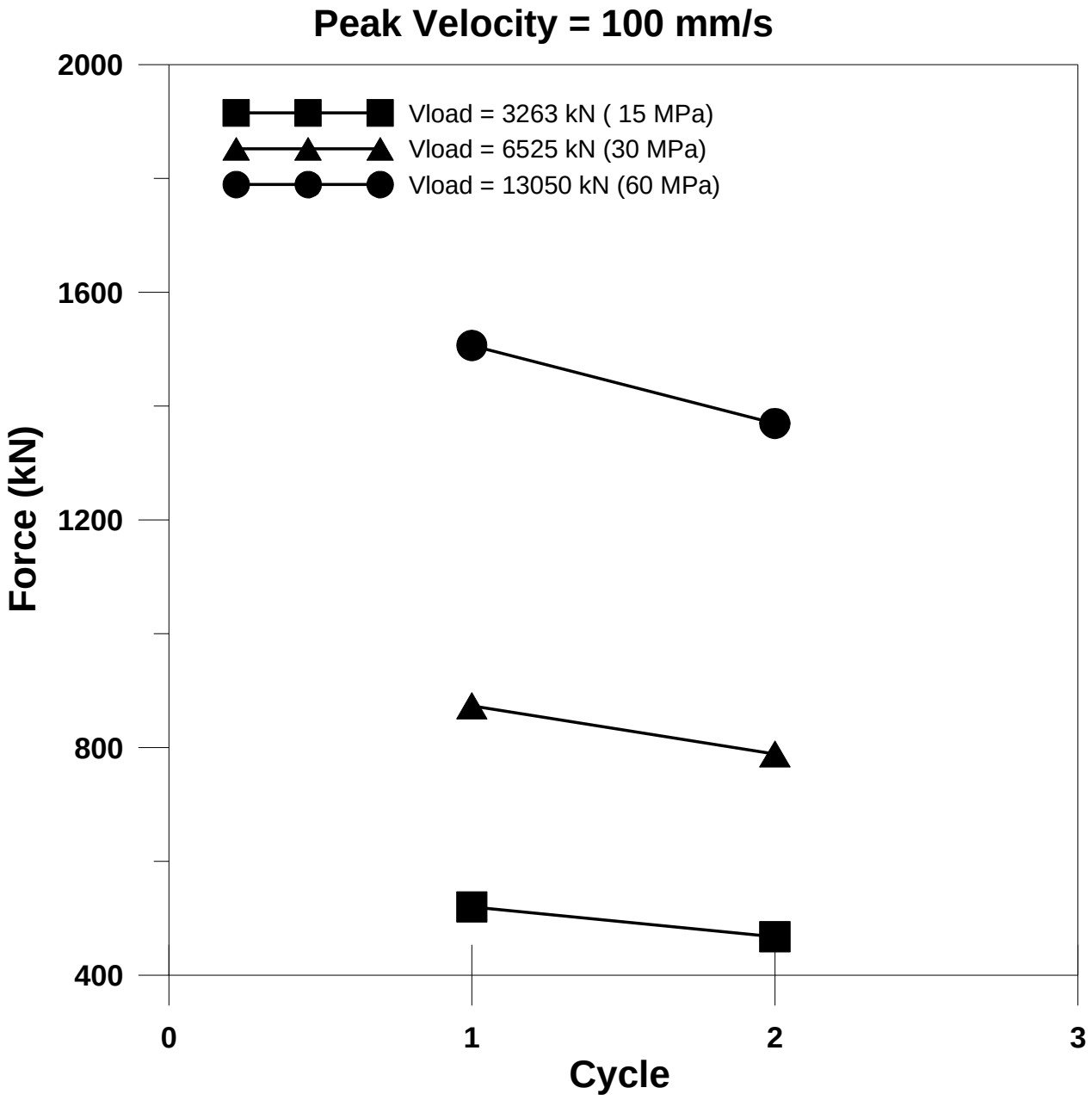

Figure B-7 Maximum Force for tests at 100.0 mm/s

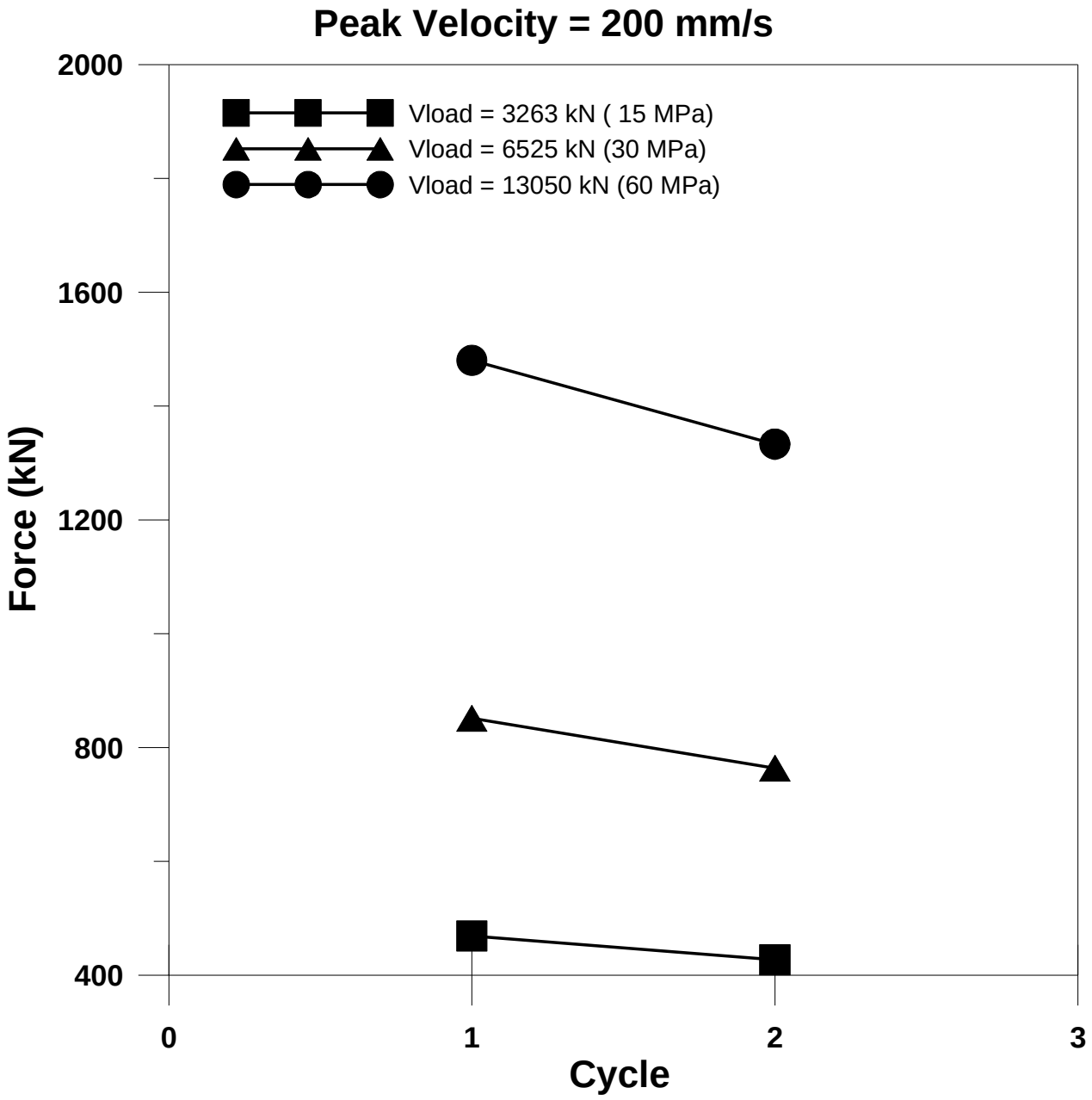

Figure B-8 Maximum Force for tests at 200.0 mm/s

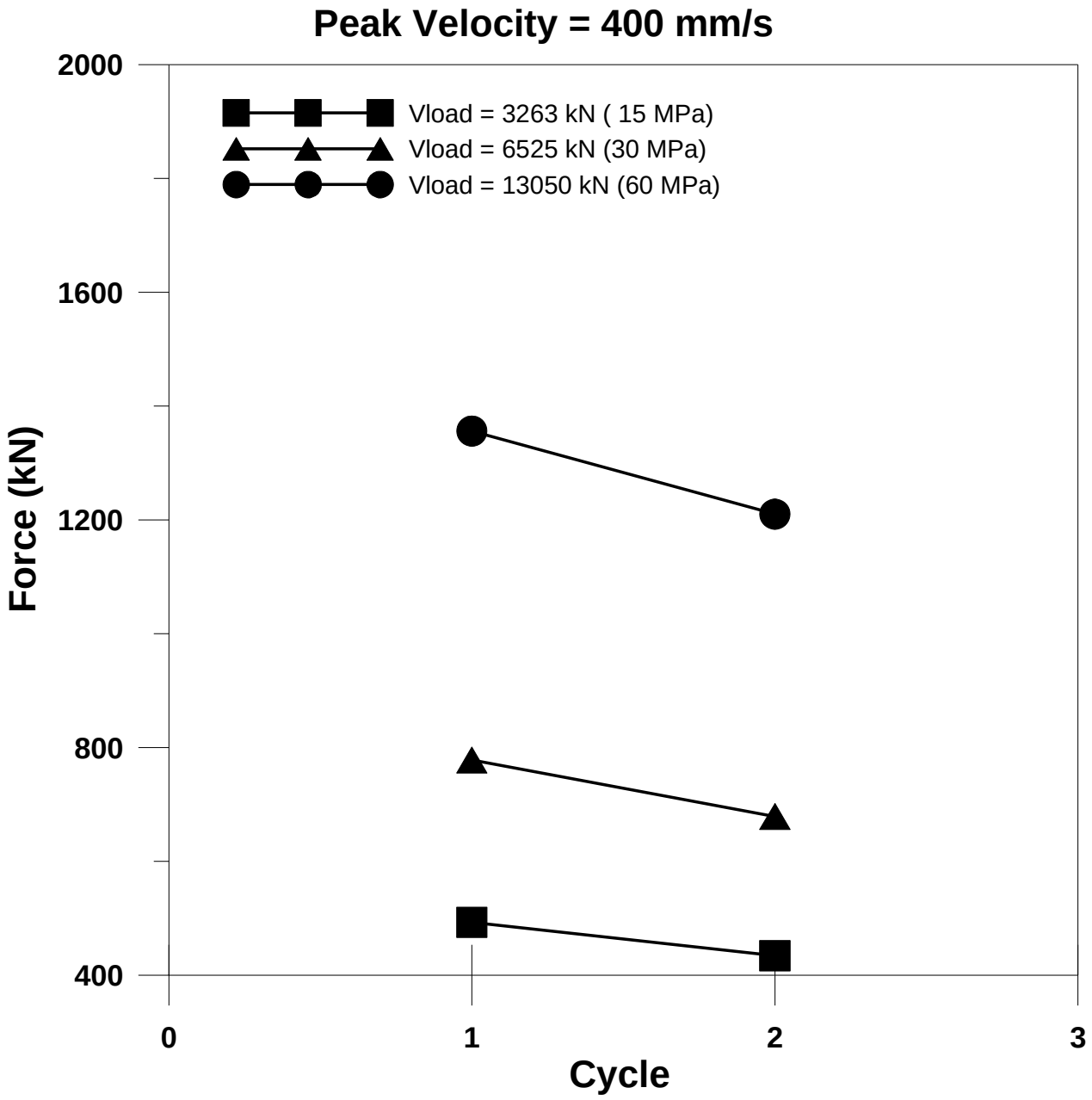

Figure B-9 Maximum Force for tests at 400.0 mm/s

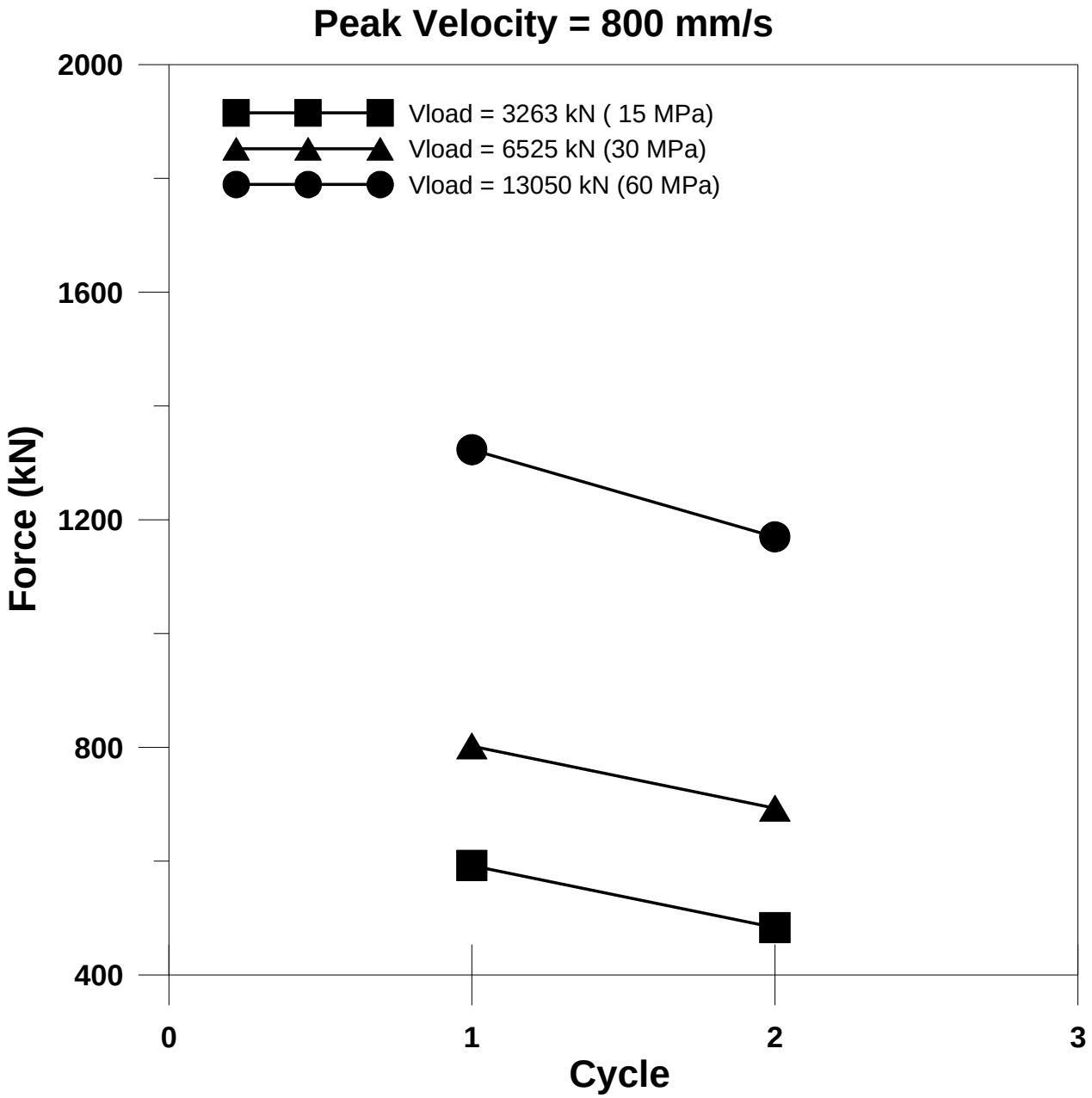

Figure B-10 Maximum Force for tests at 800.0 mm/s

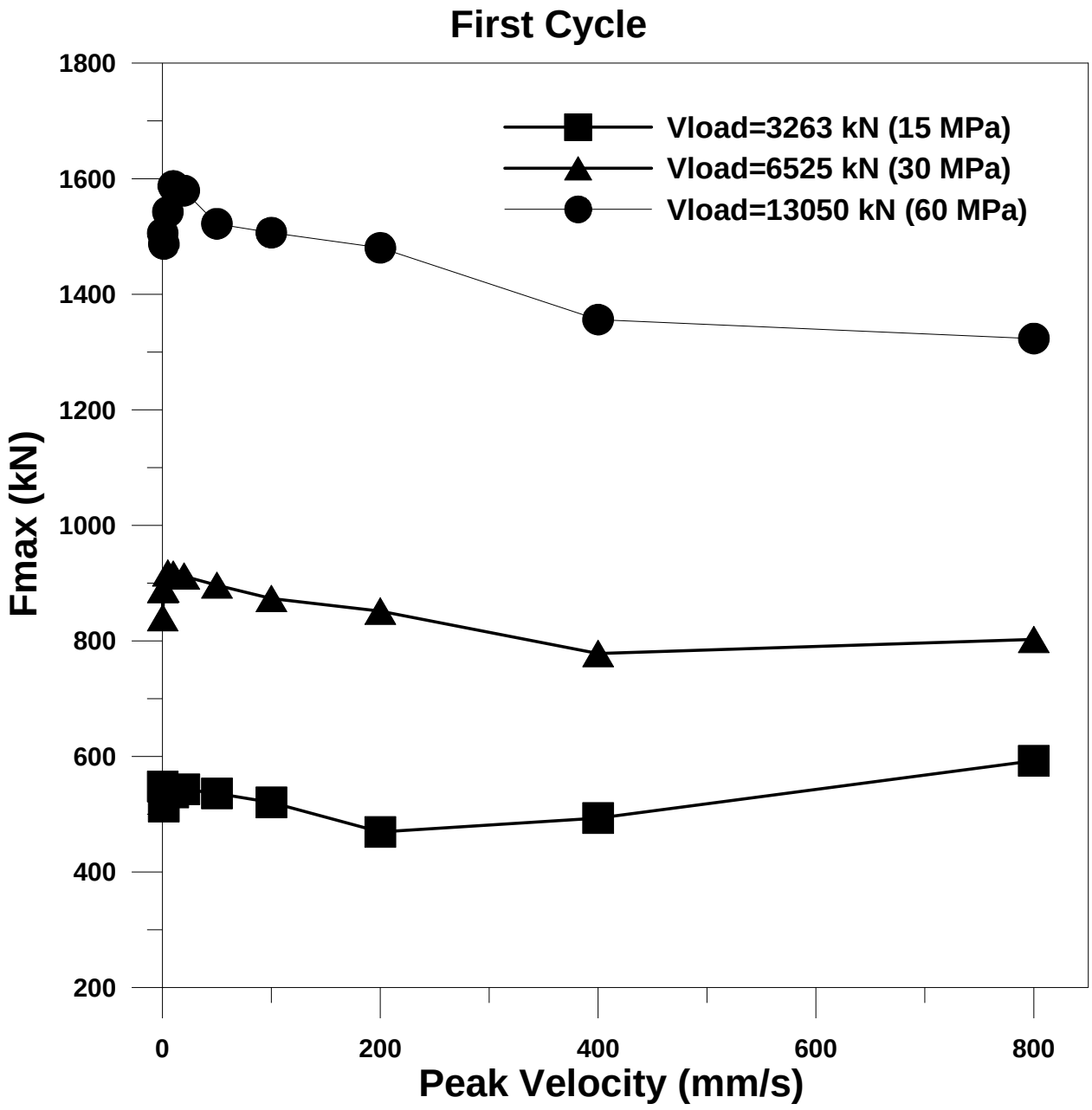

Figure B-11 Maximum Force for first cycle of tests at different vertical load and velocity

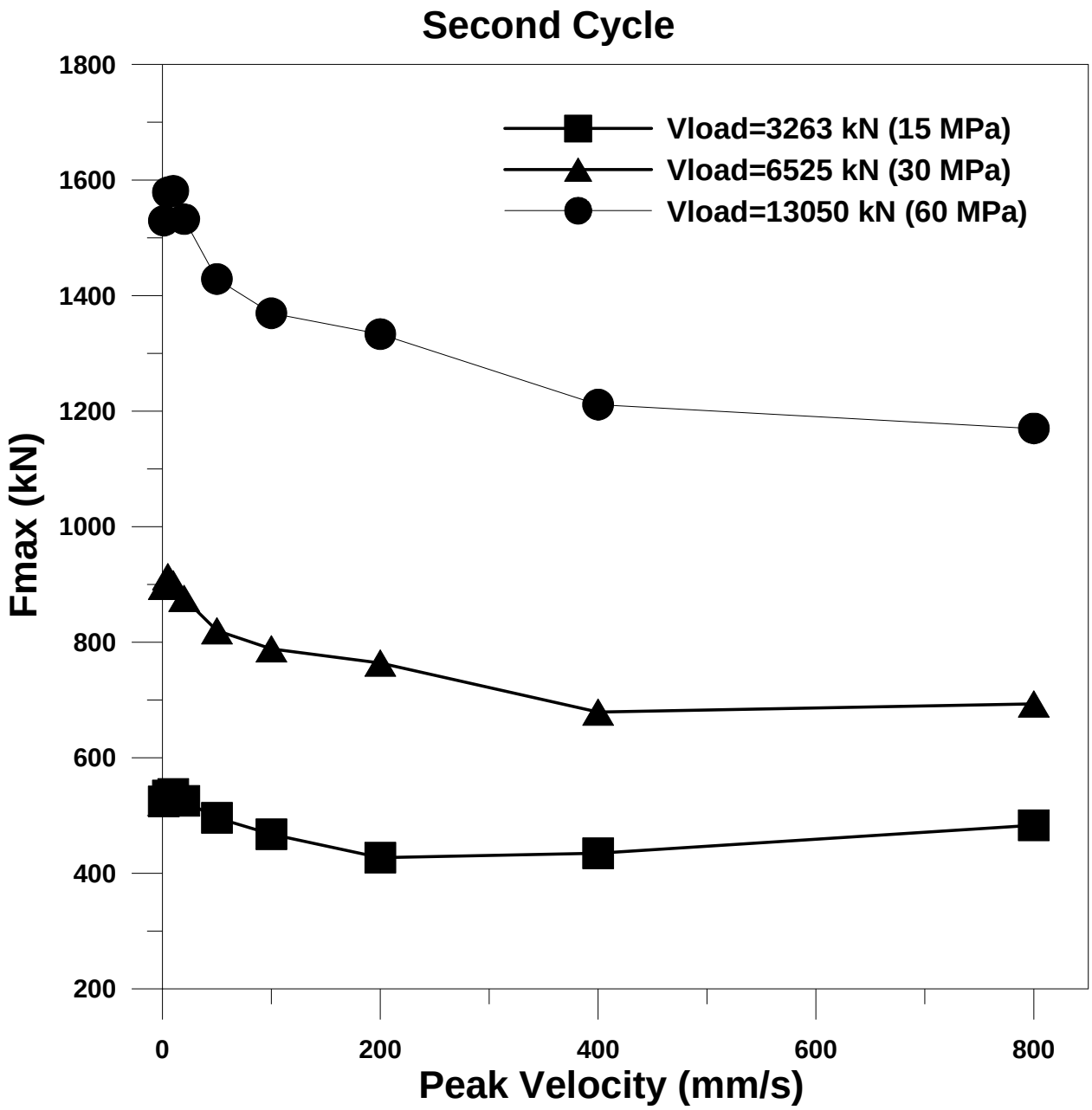

Figure B-12 Maximum Force for second cycle of tests at different vertical load and velocity

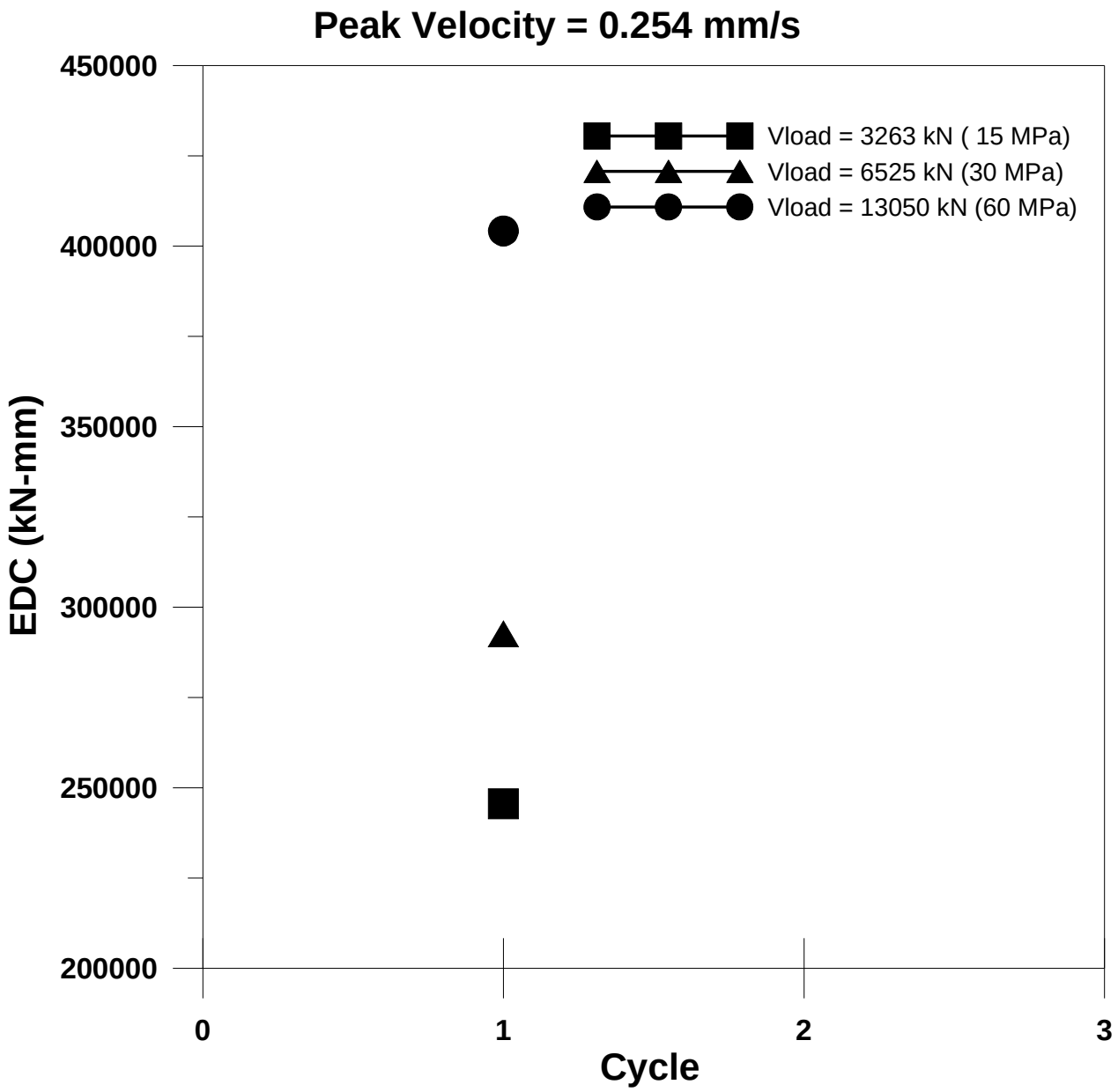

Figure B-13 EDC for tests at 0.254 mm/s

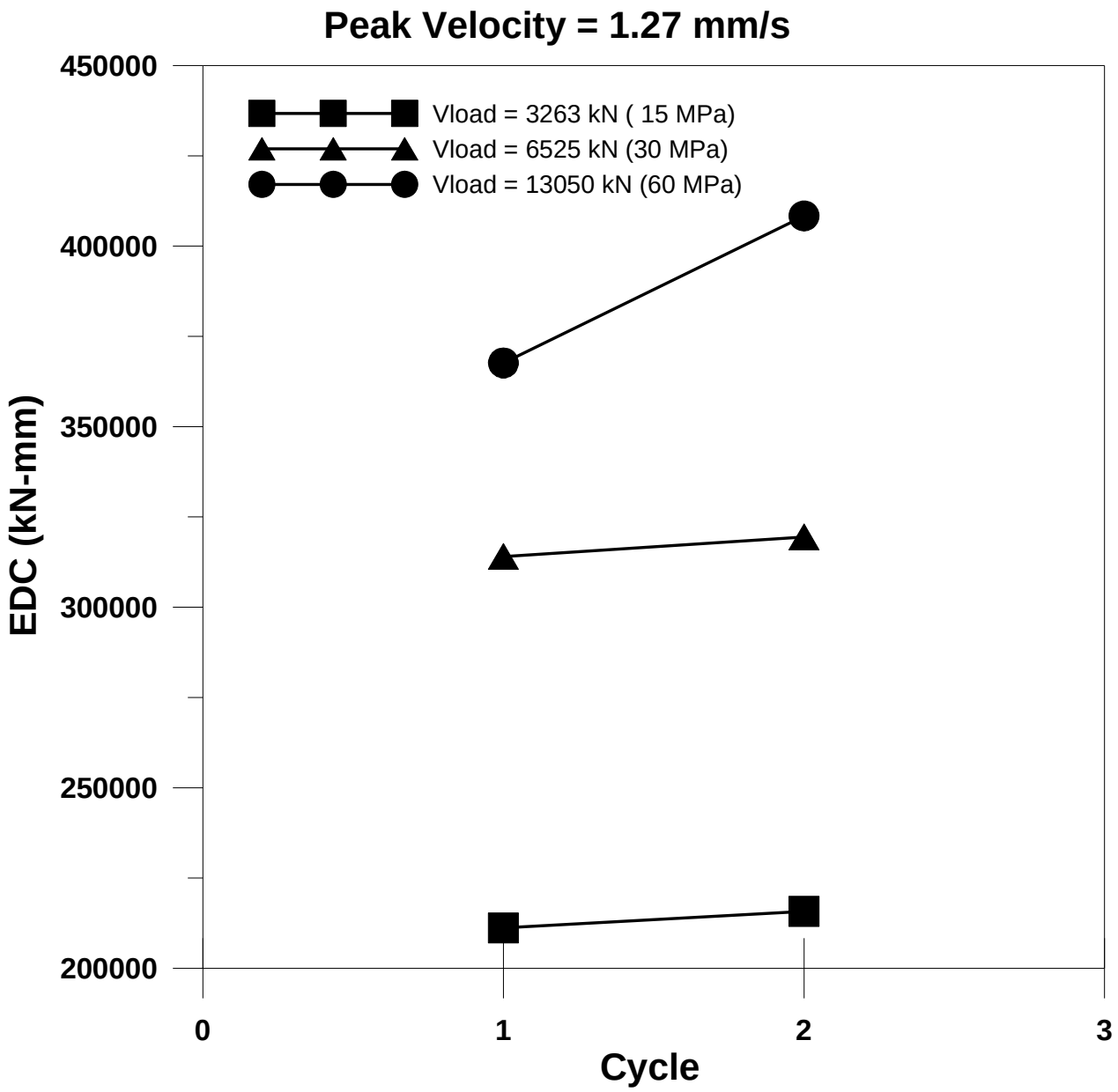

Figure B-14 EDC for tests at 1.27 mm/s

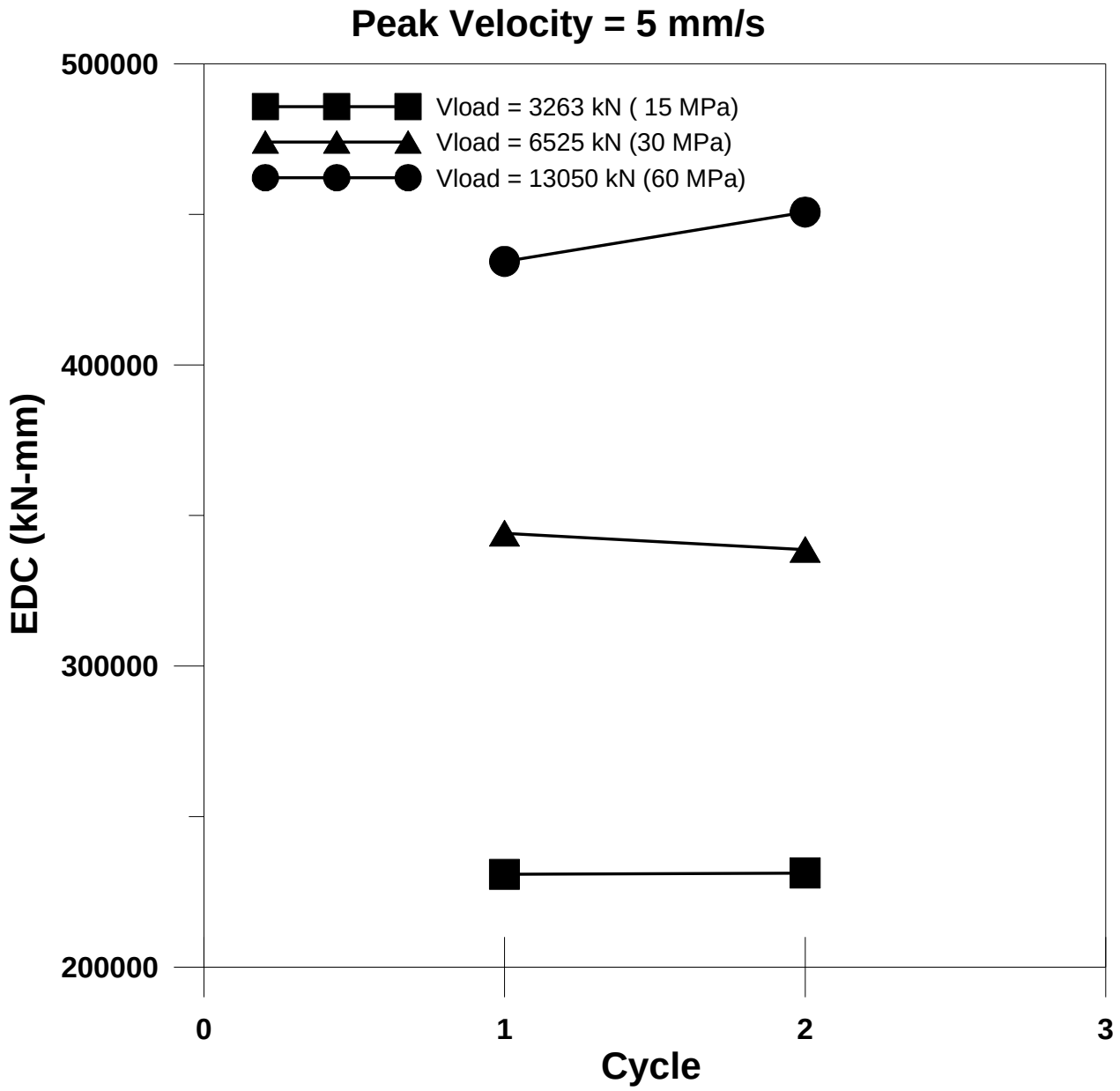

Figure B-15 EDC for tests at 5.0 mm/s

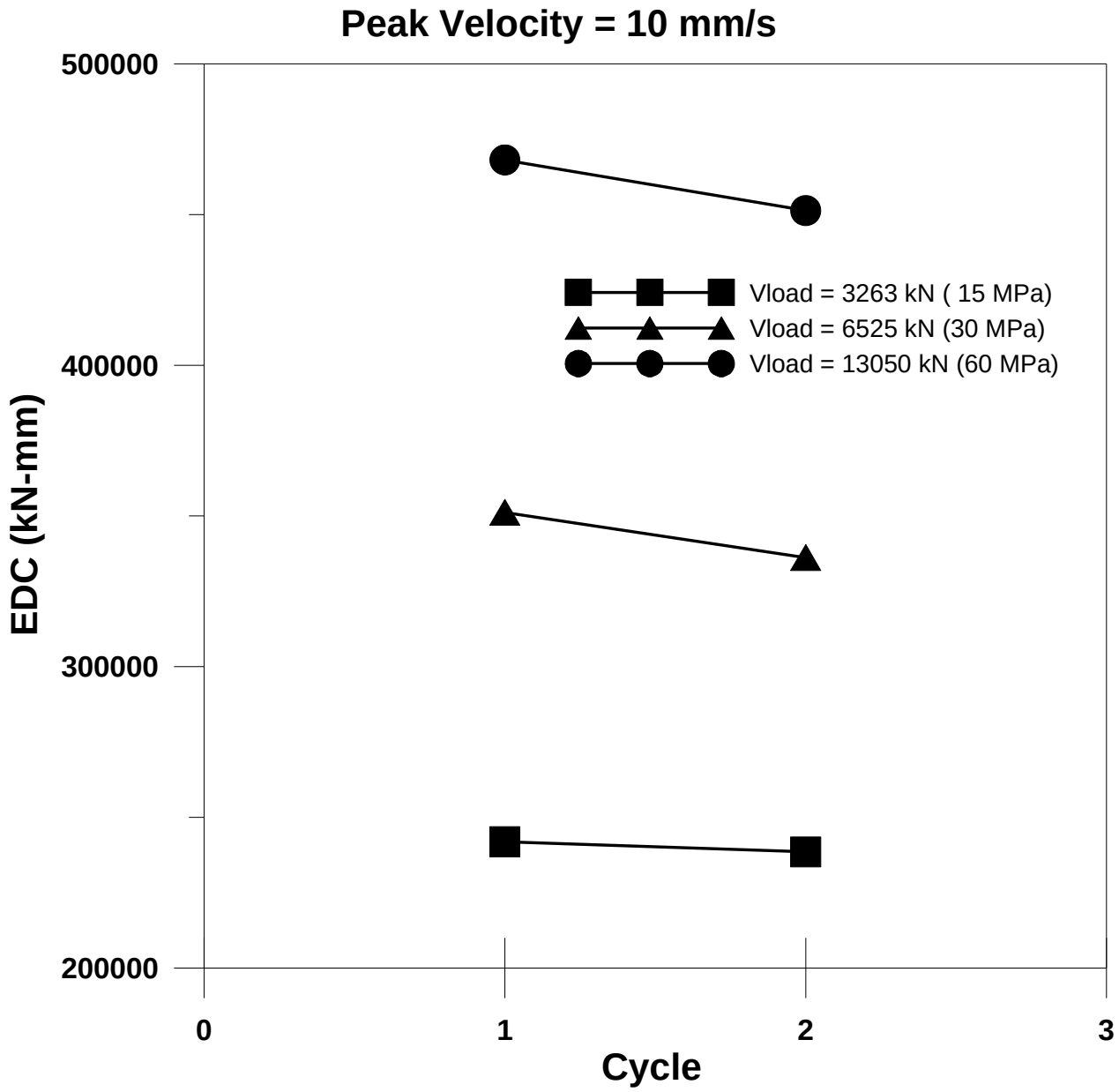

Figure B-16 EDC for tests at 10 mm/s

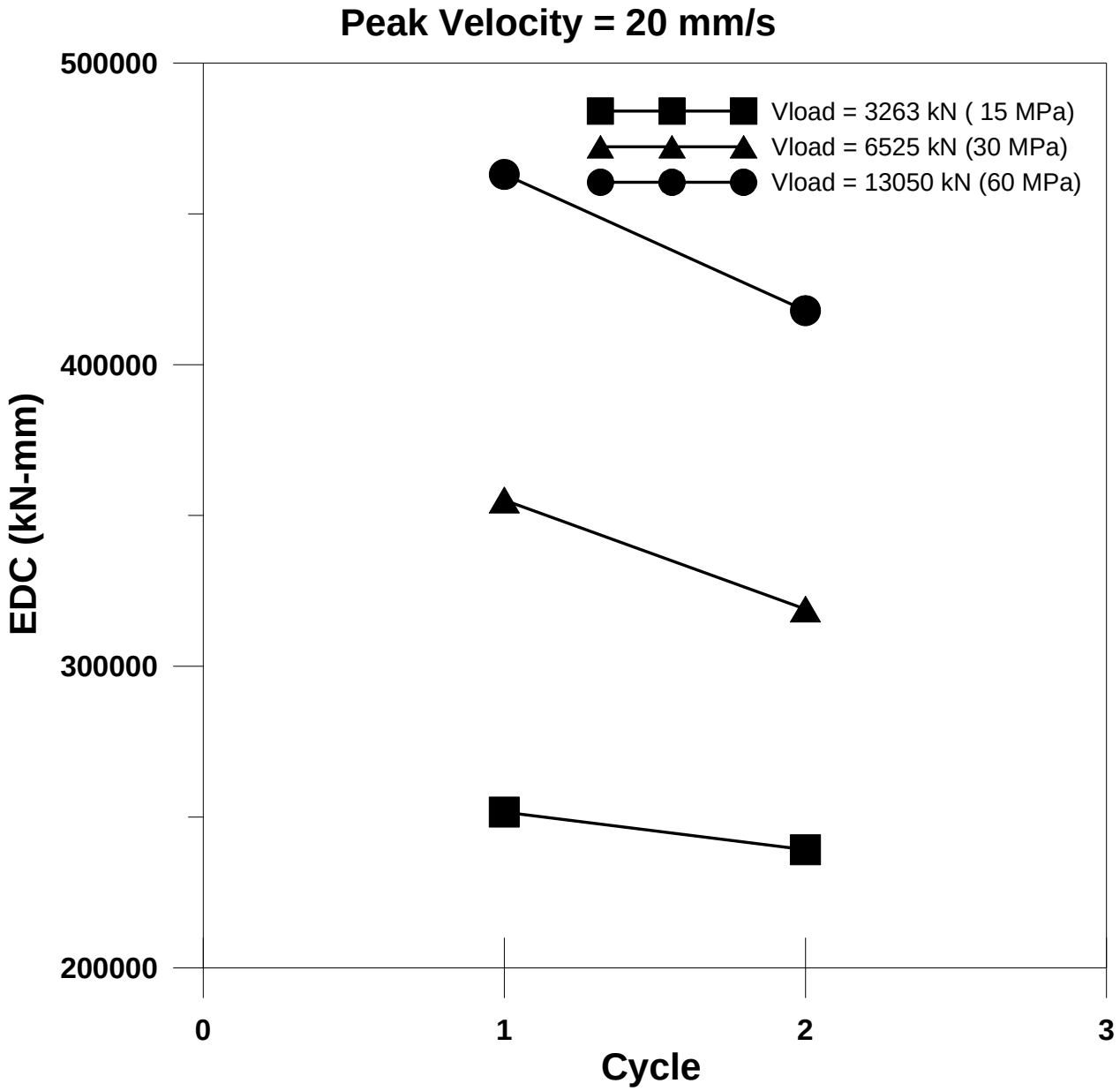

Figure B-17 EDC for tests at 20 mm/s

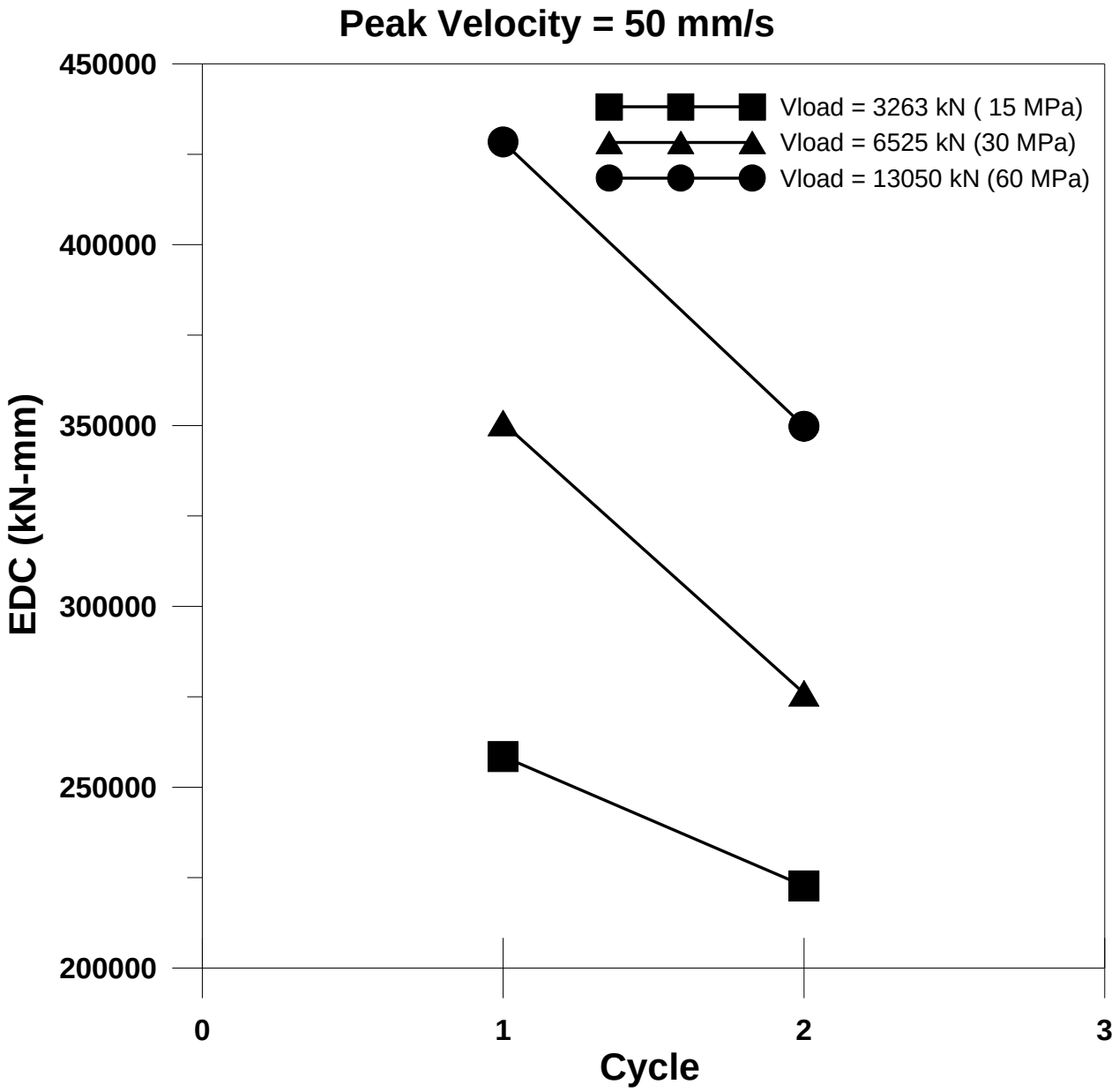

Figure B-18 EDC for tests at 50 mm/s

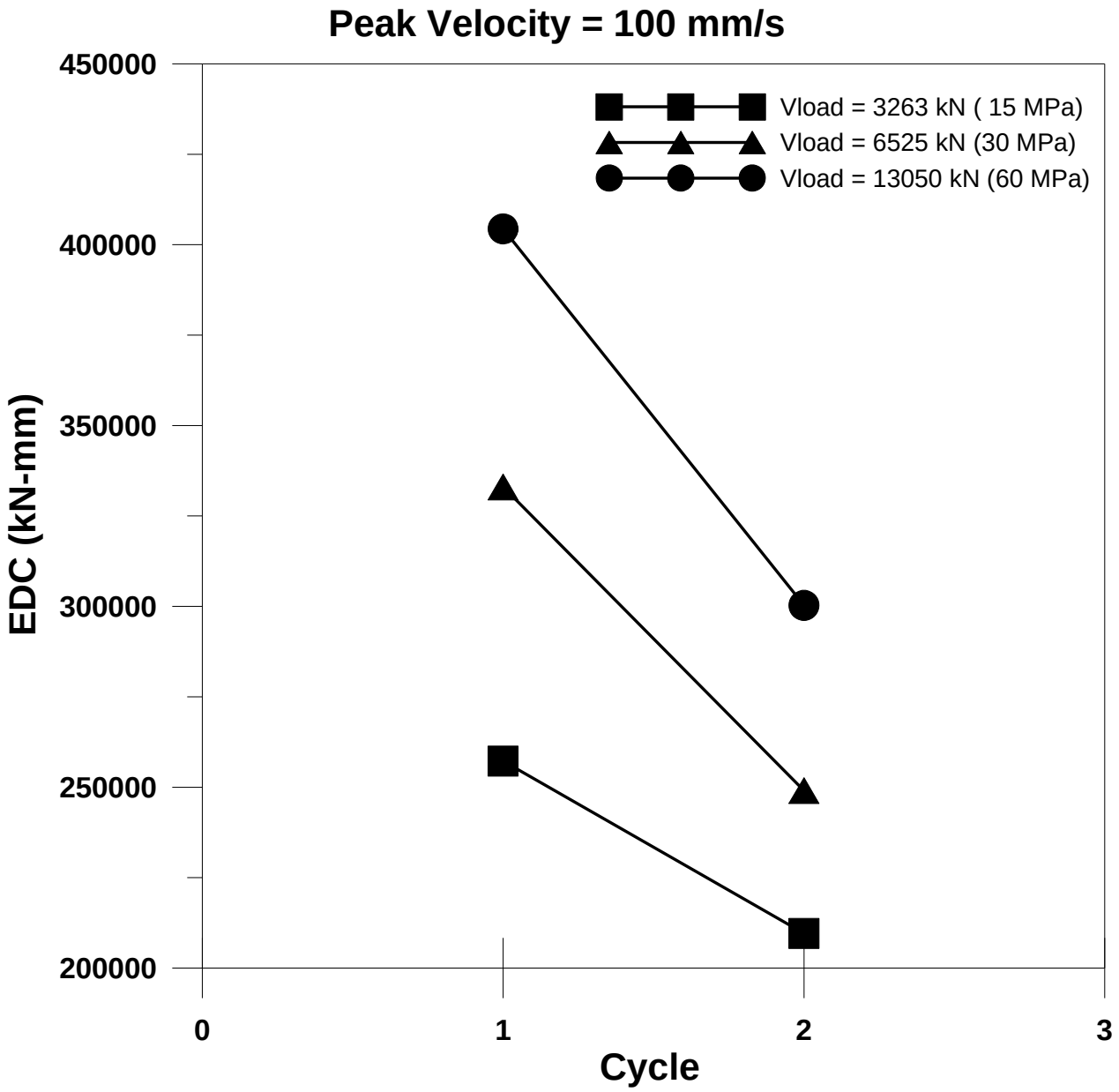

Figure B-19 EDC for tests at 100 mm/s

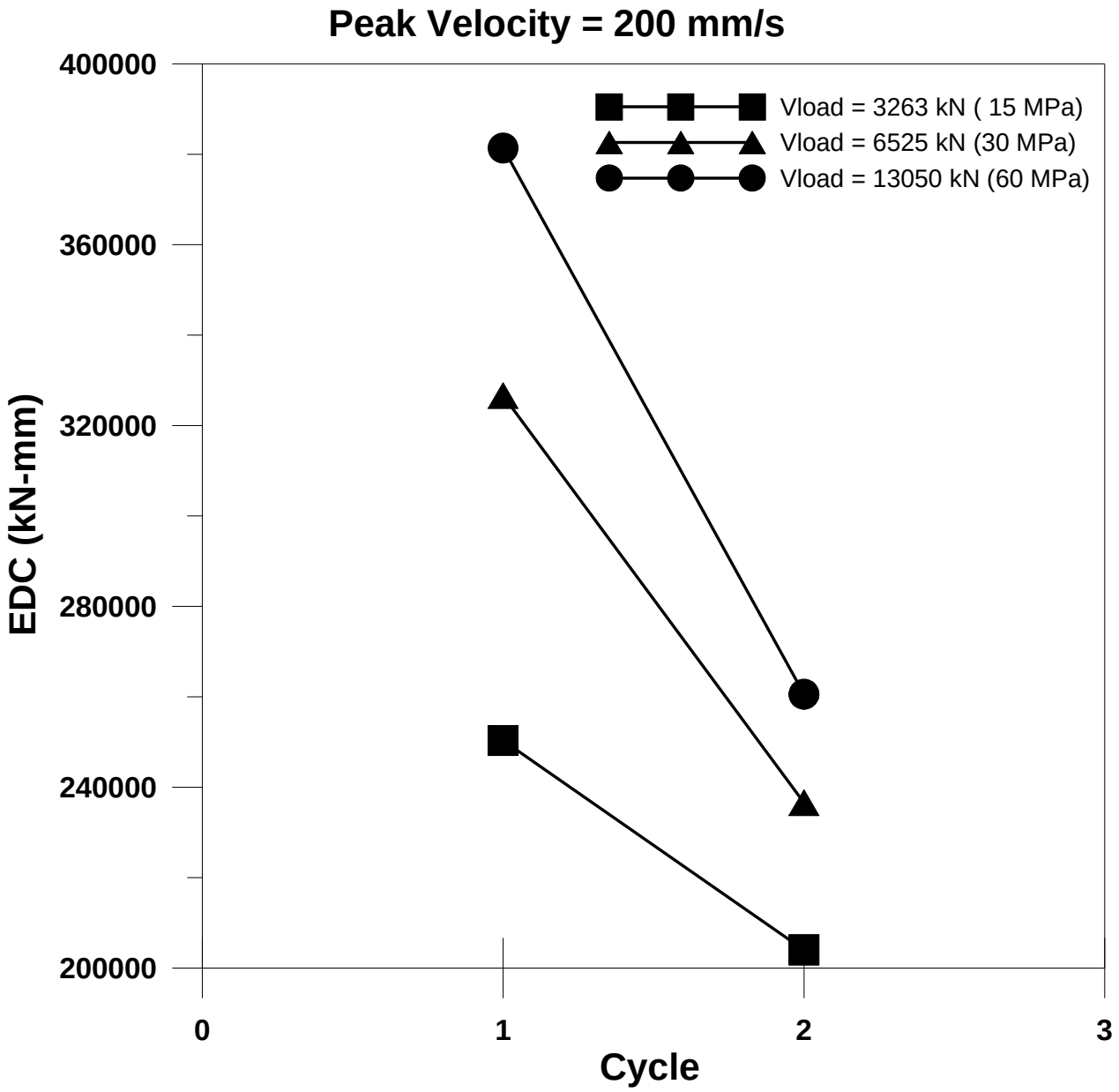

Figure B-20 EDC for tests at 200 mm/s

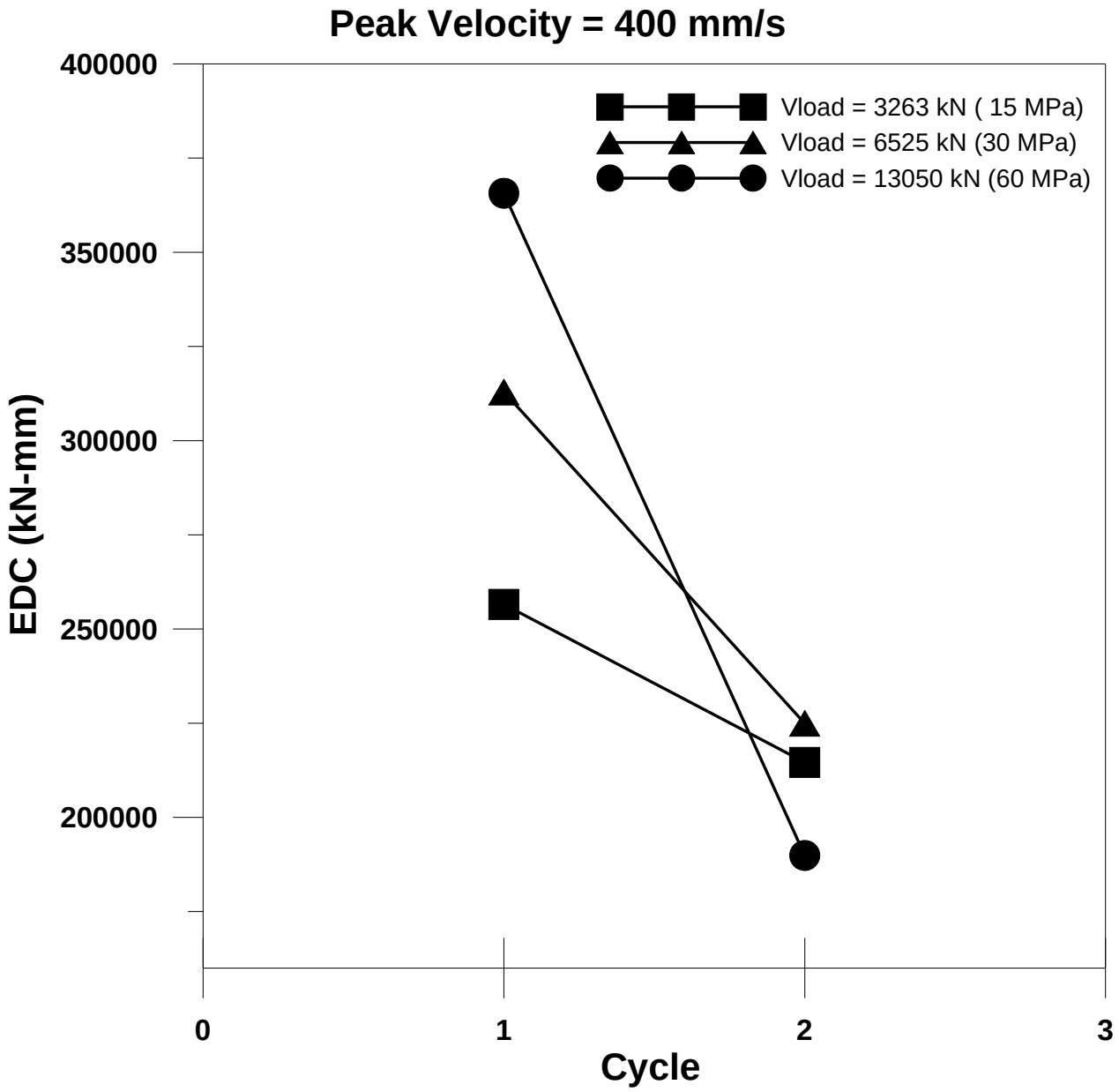

Figure B-21 EDC for tests at 400 mm/s

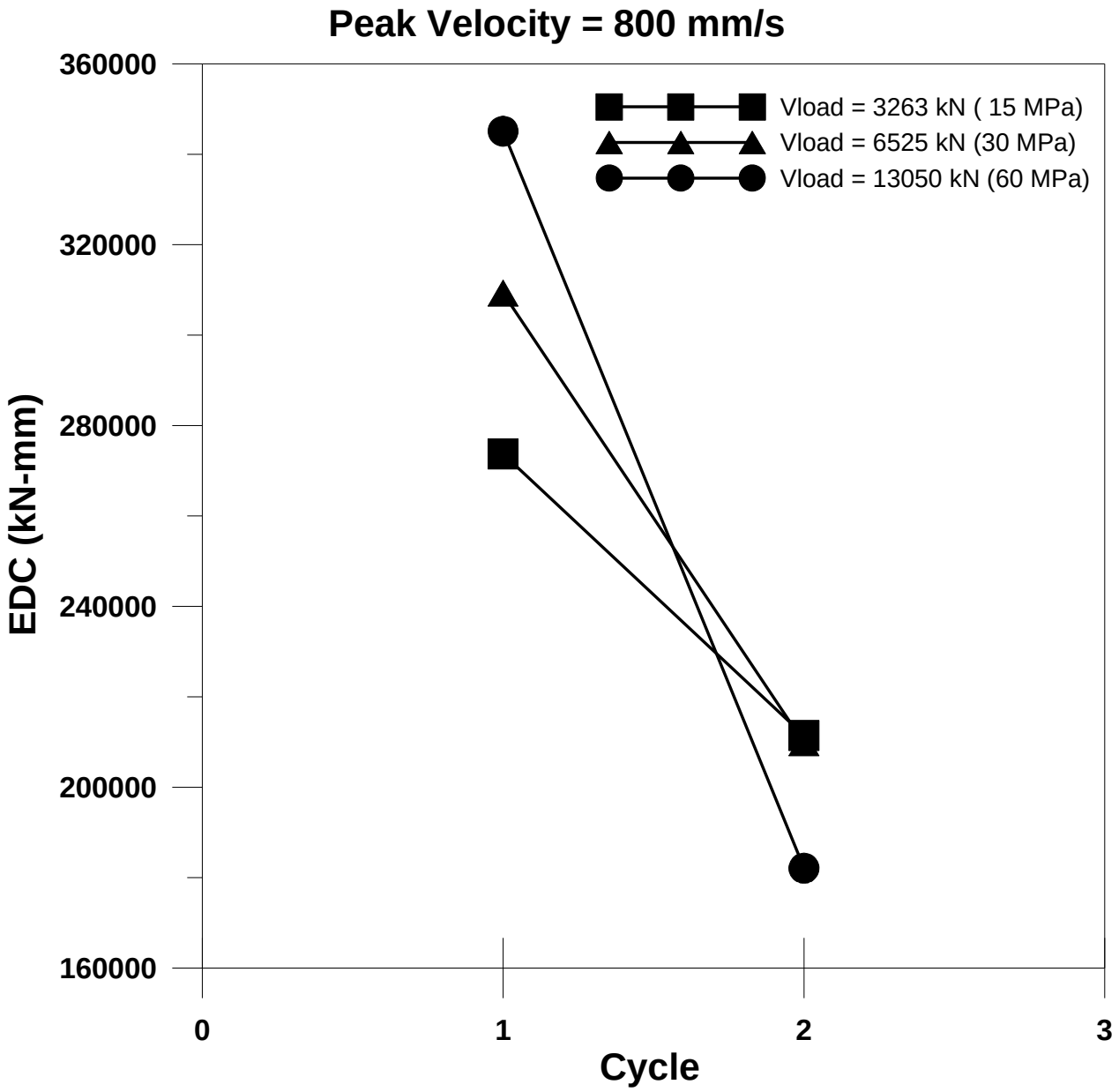

Figure B-22 EDC for tests at 800 mm/s

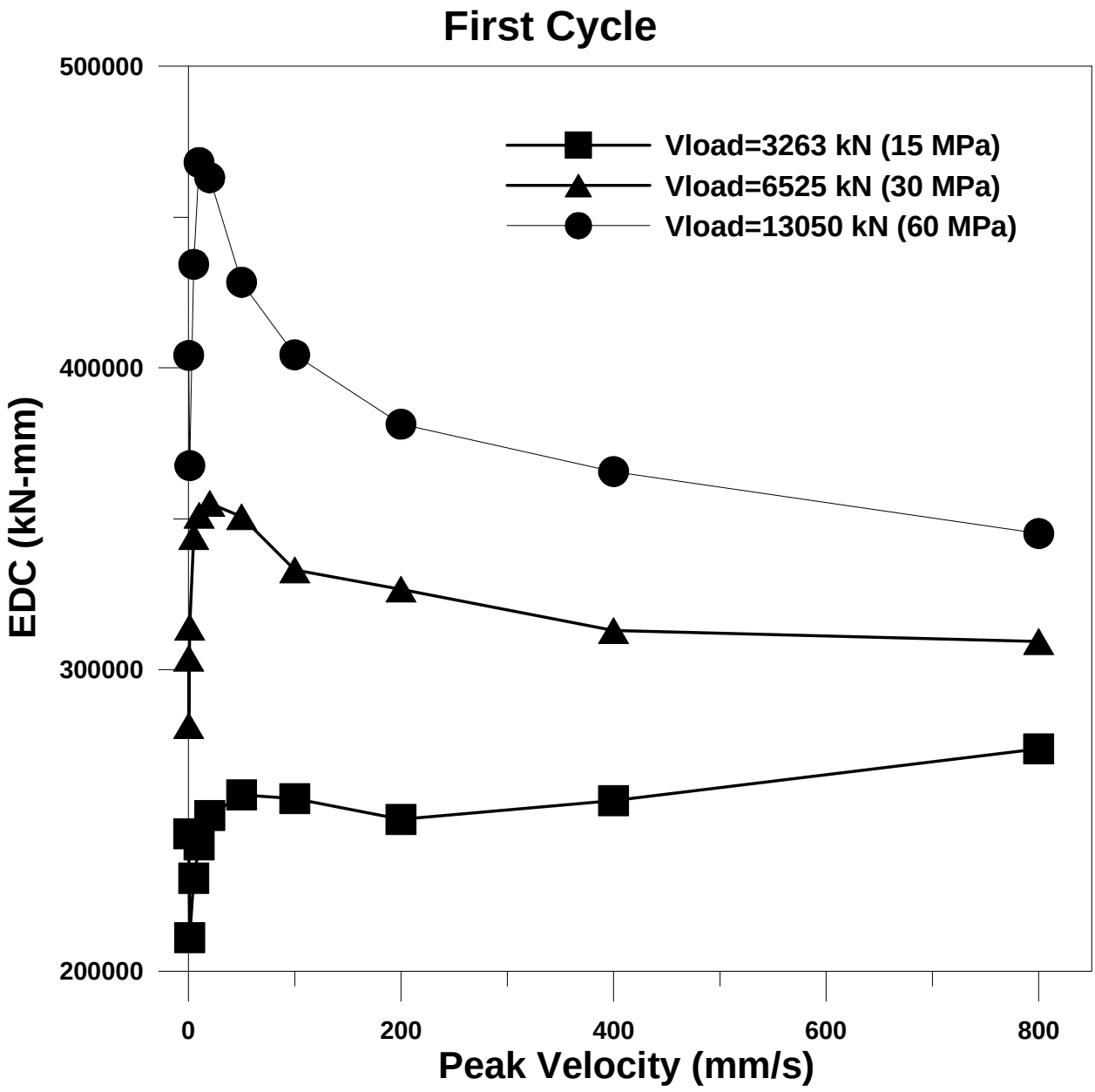

Figure B-23 EDC for first cycle of tests at different vertical load and velocity

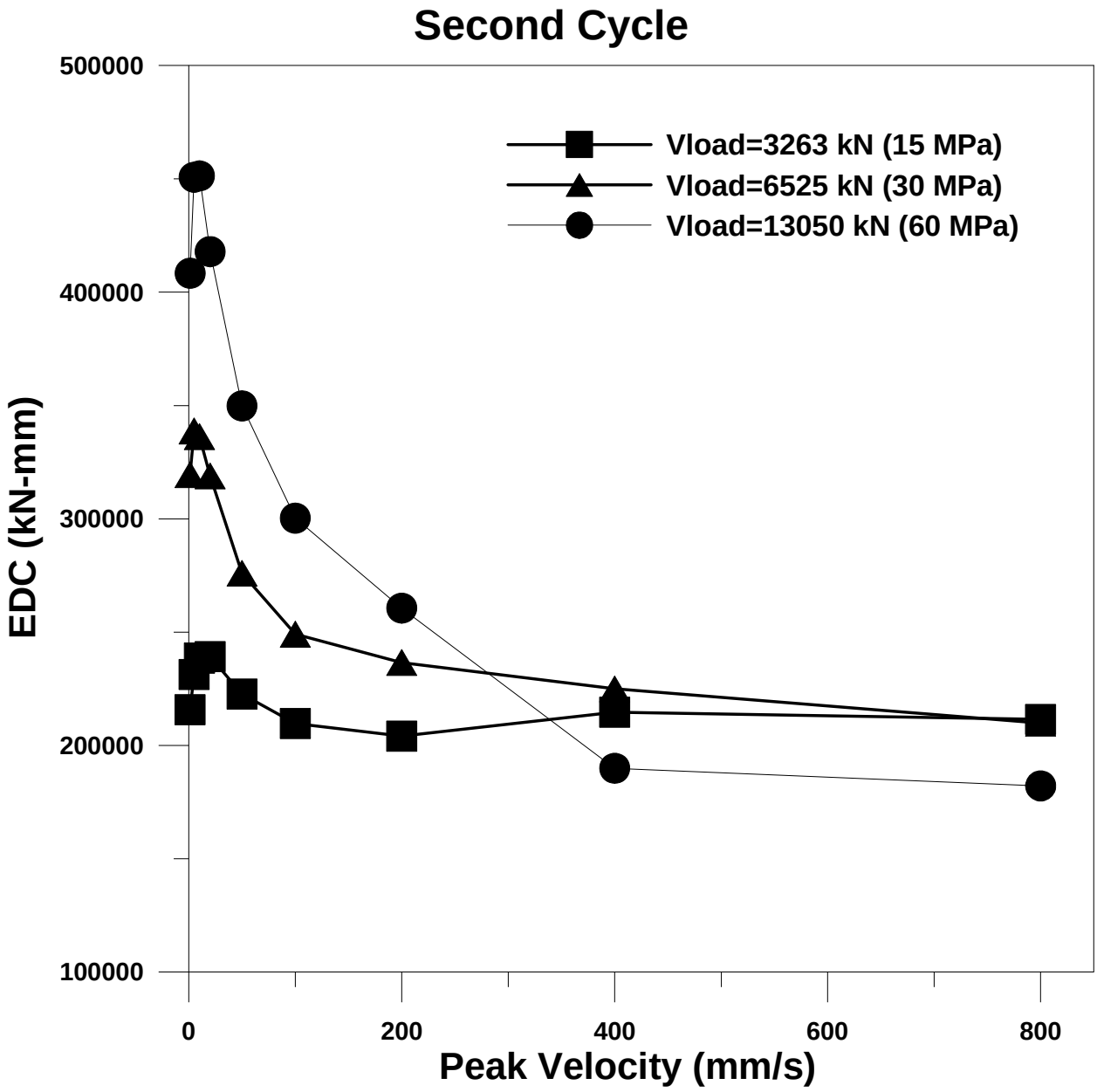

Figure B-24 EDC for second cycle of tests at different vertical load and velocity

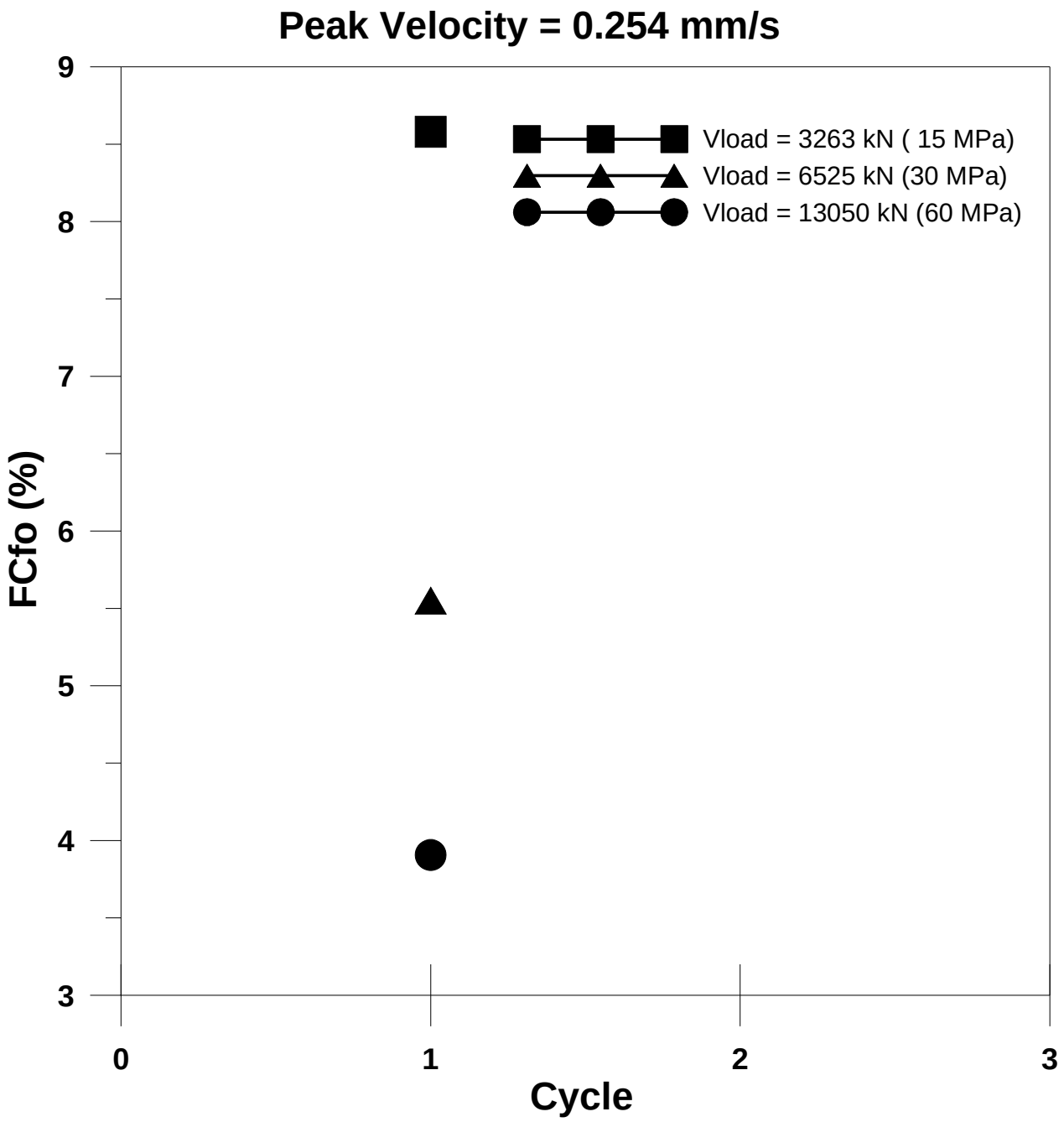

Figure B-25 Friction Coefficient (FCF0) for tests at 0.254 mm/s

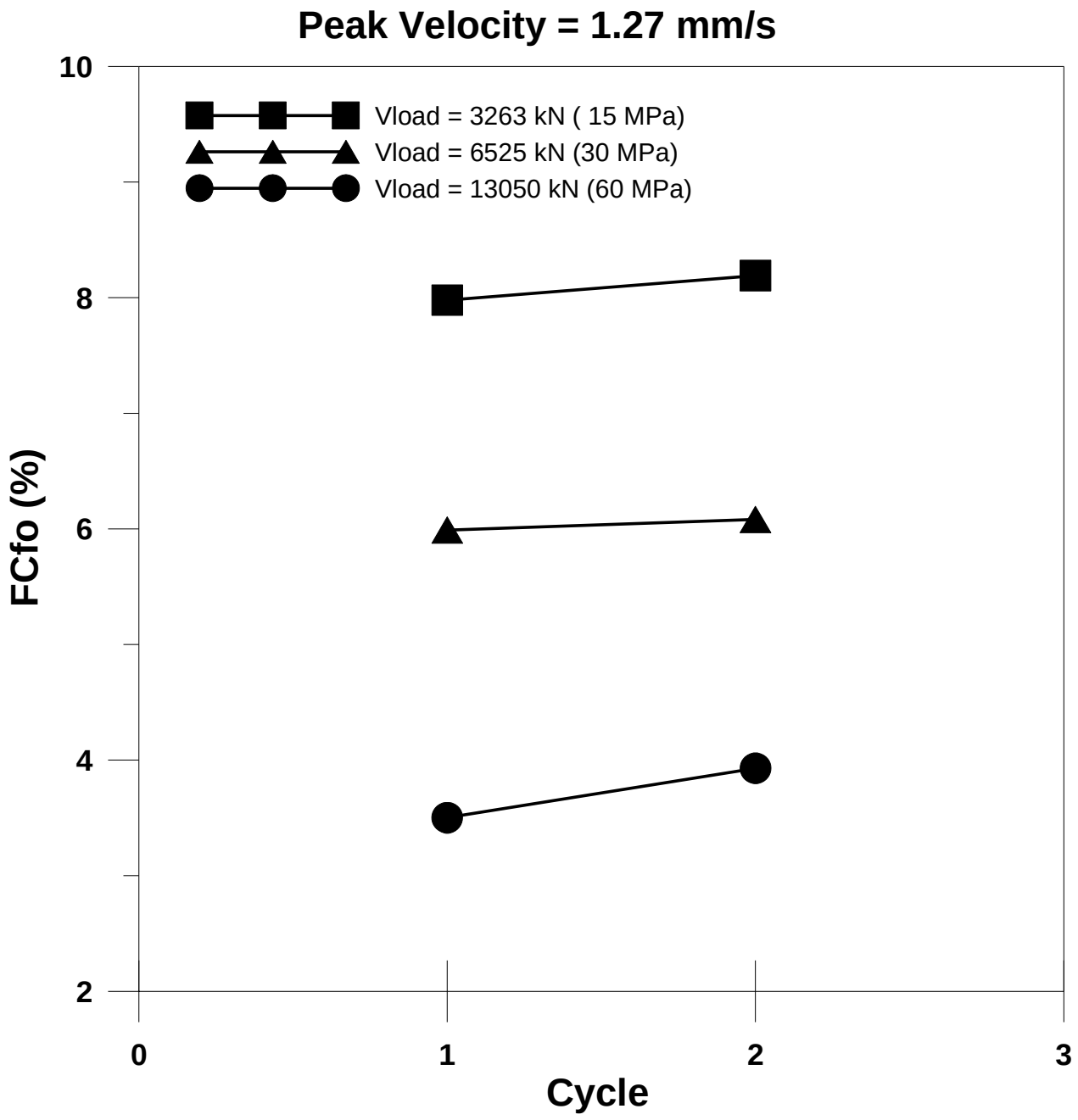

Figure B-26 Friction Coefficient (FCF0) for tests at 1.27 mm/s

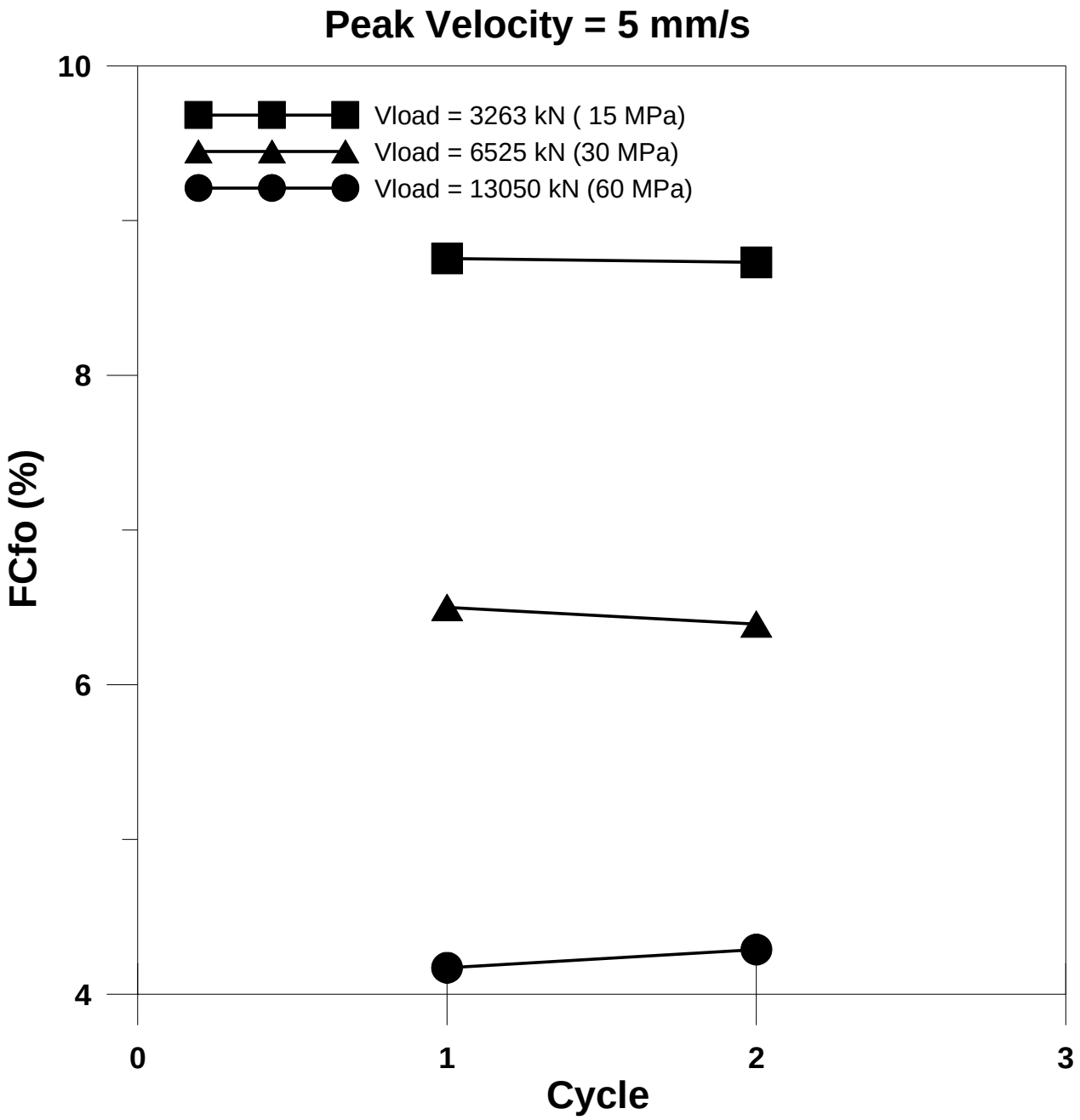

Figure B-27 Friction Coefficient (FCF0) for tests at 5.0 mm/s

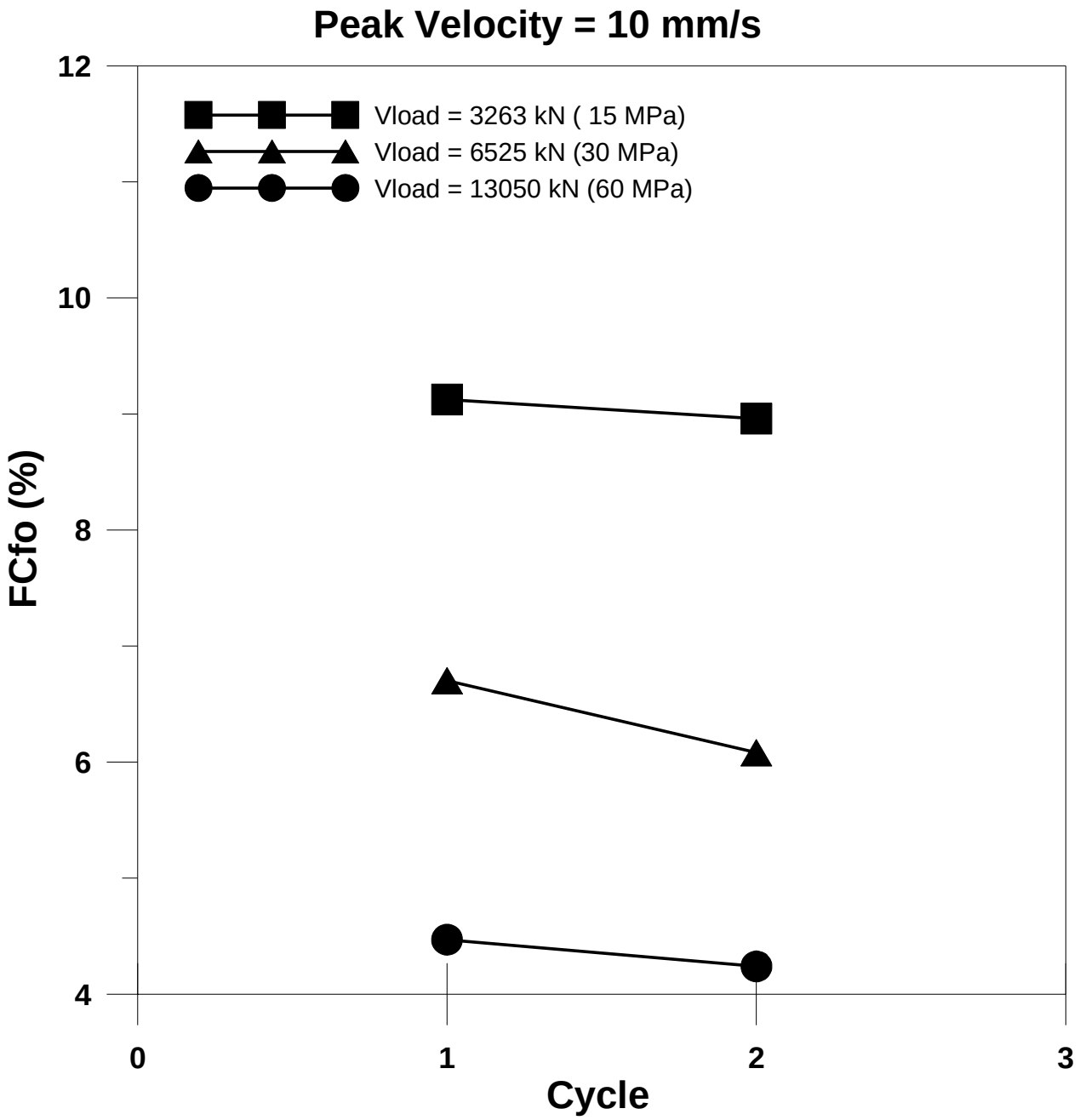

Figure B-28 Friction Coefficient (FCF0) for tests at 10.0 mm/s

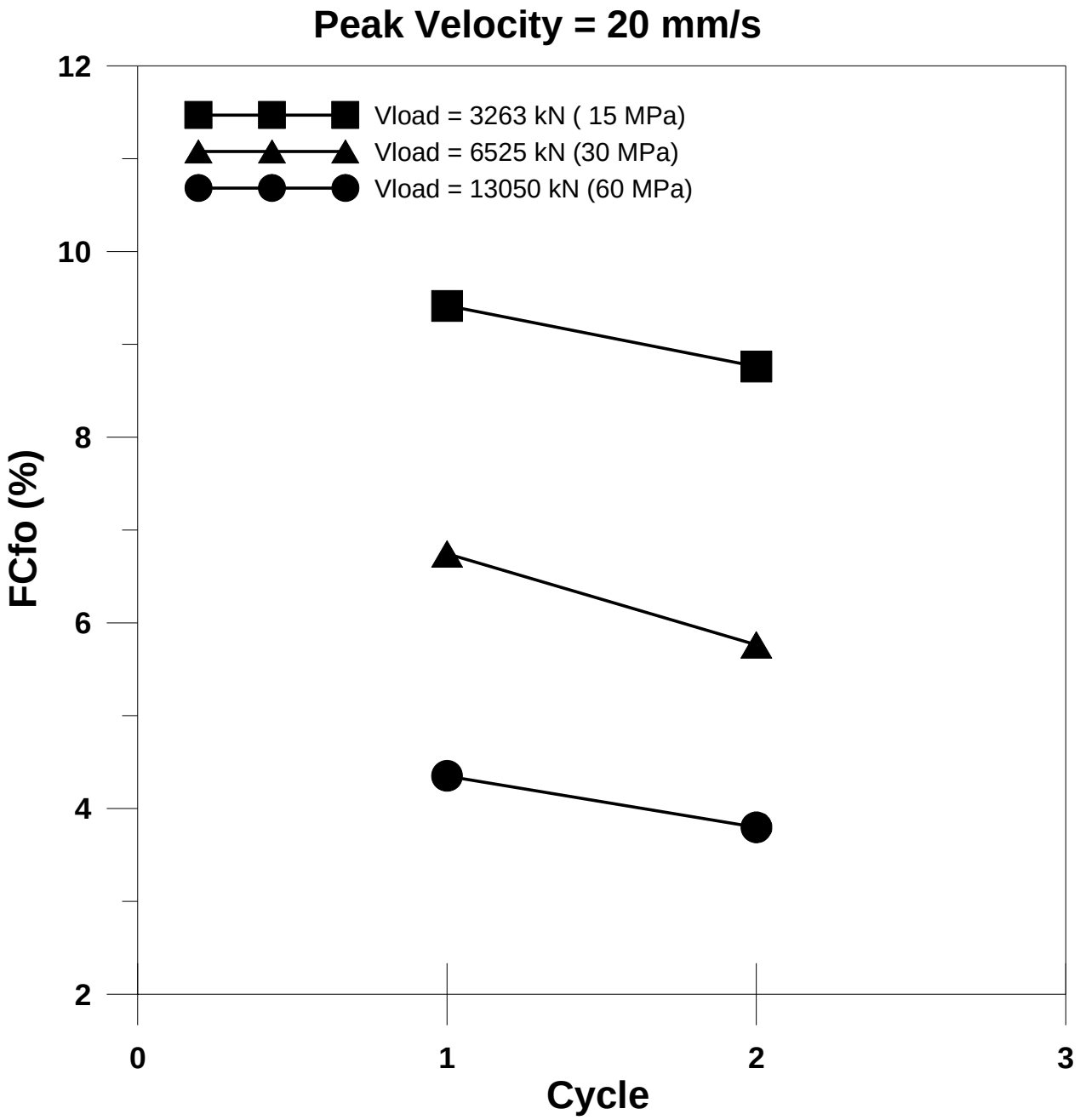

Figure B-29 Friction Coefficient (FCF0) for tests at 20 mm/s

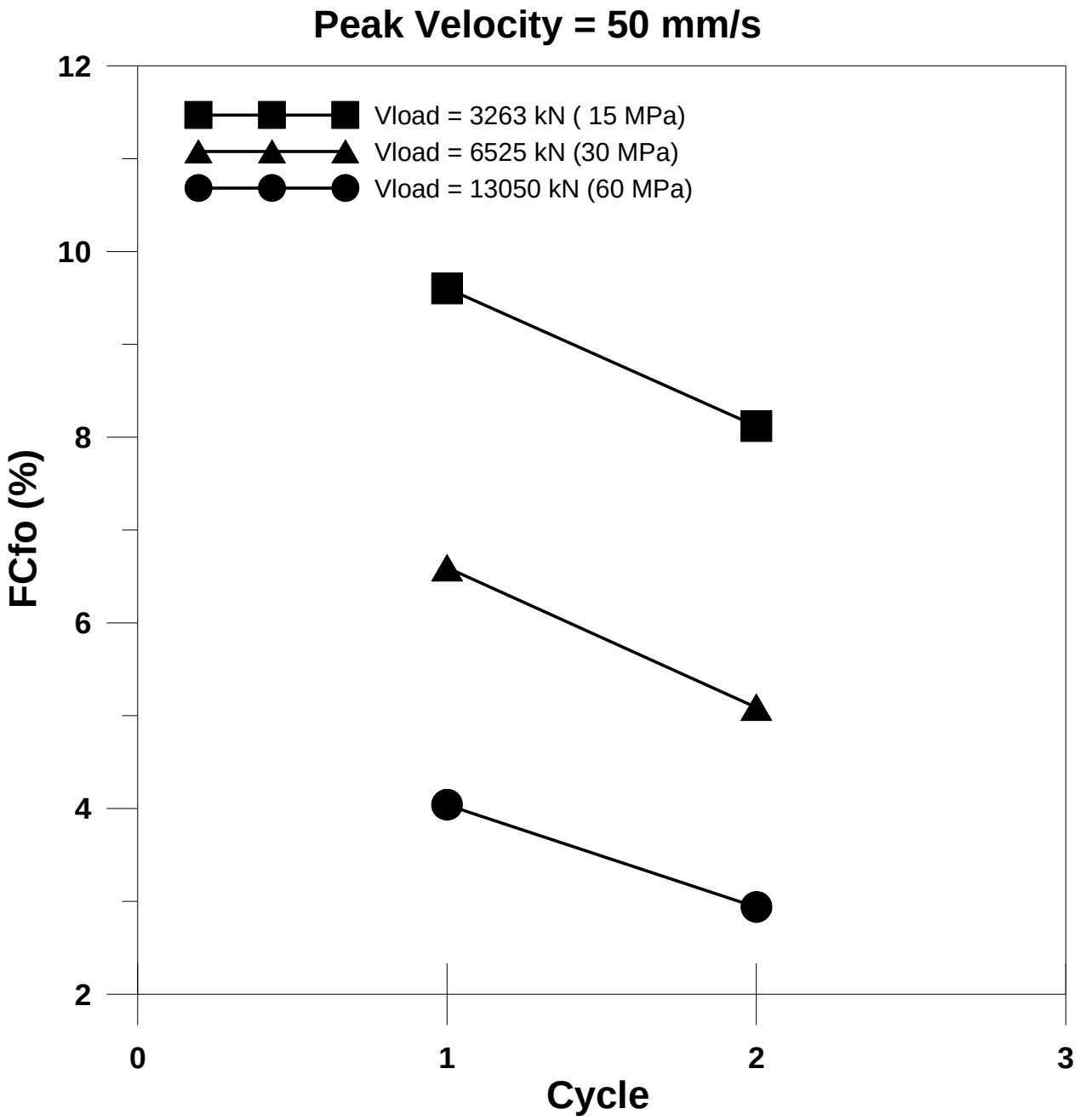

Figure B-30 Friction Coefficient (FCF0) for tests at 50 mm/s

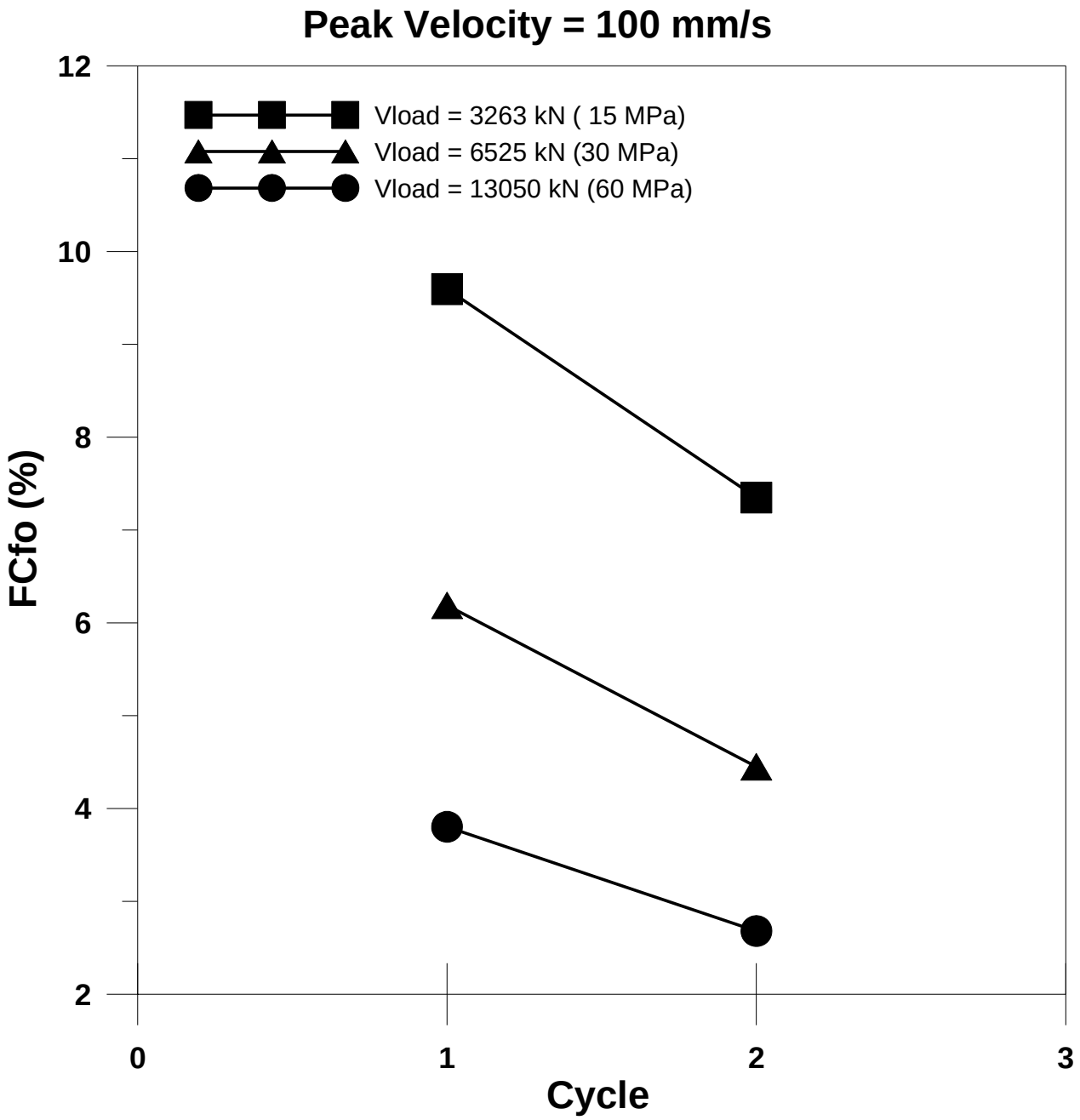

Figure B-31 Friction Coefficient (FCF0) for tests at 100 mm/s

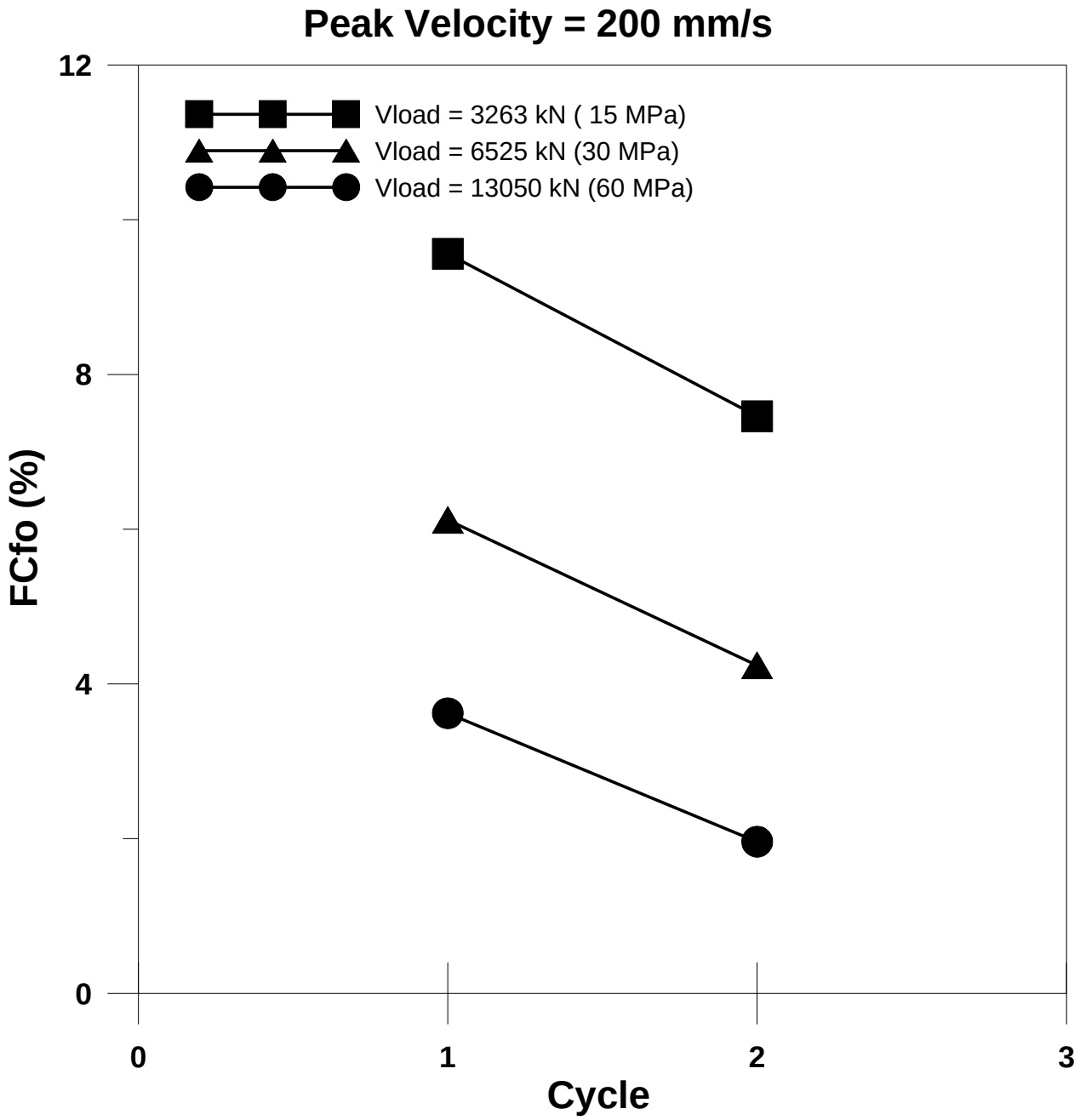

Figure B-32 Friction Coefficient (FCF0) for tests at 200 mm/s

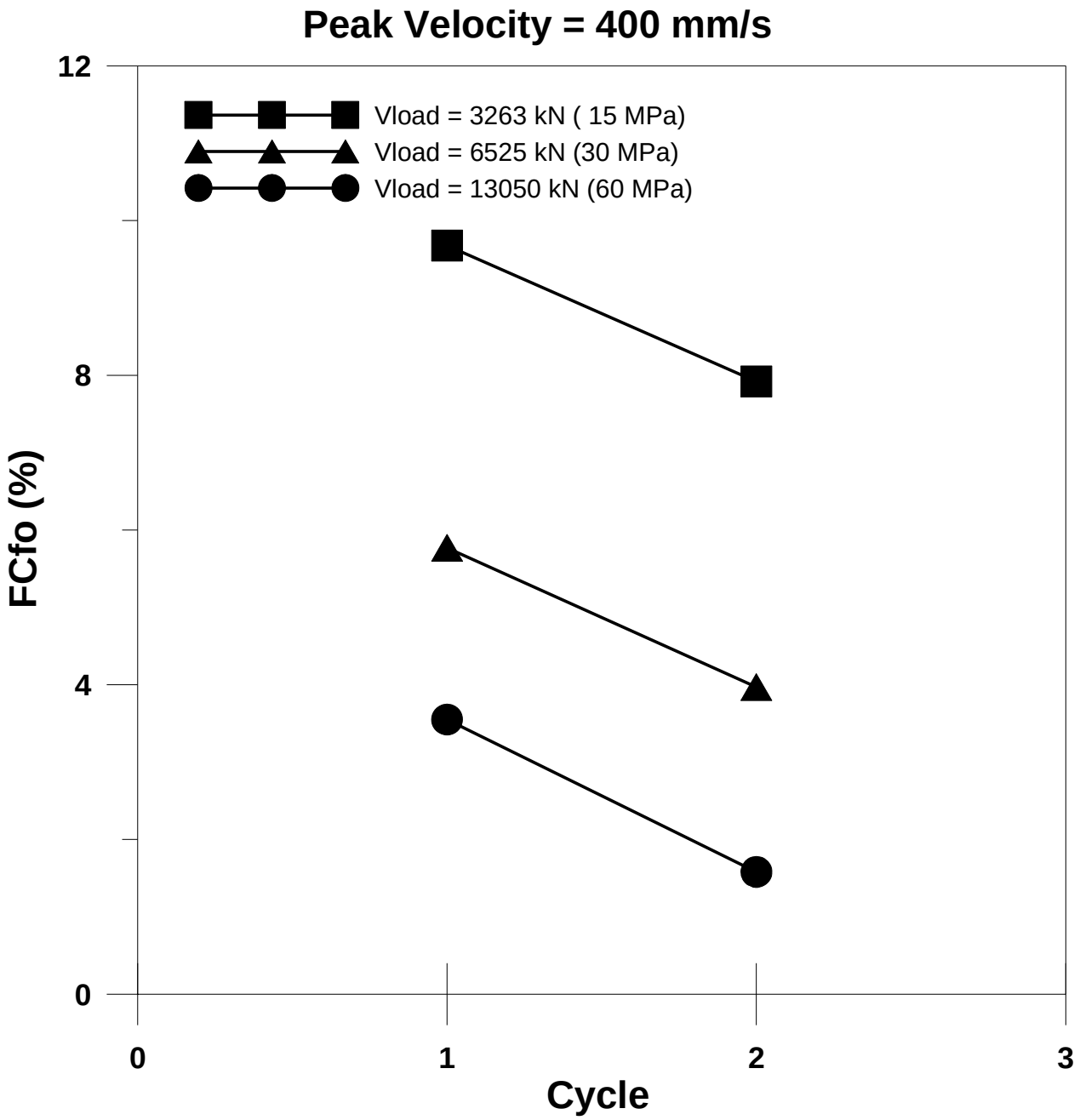

Figure B-33 Friction Coefficient (FCF0) for tests at 400 mm/s

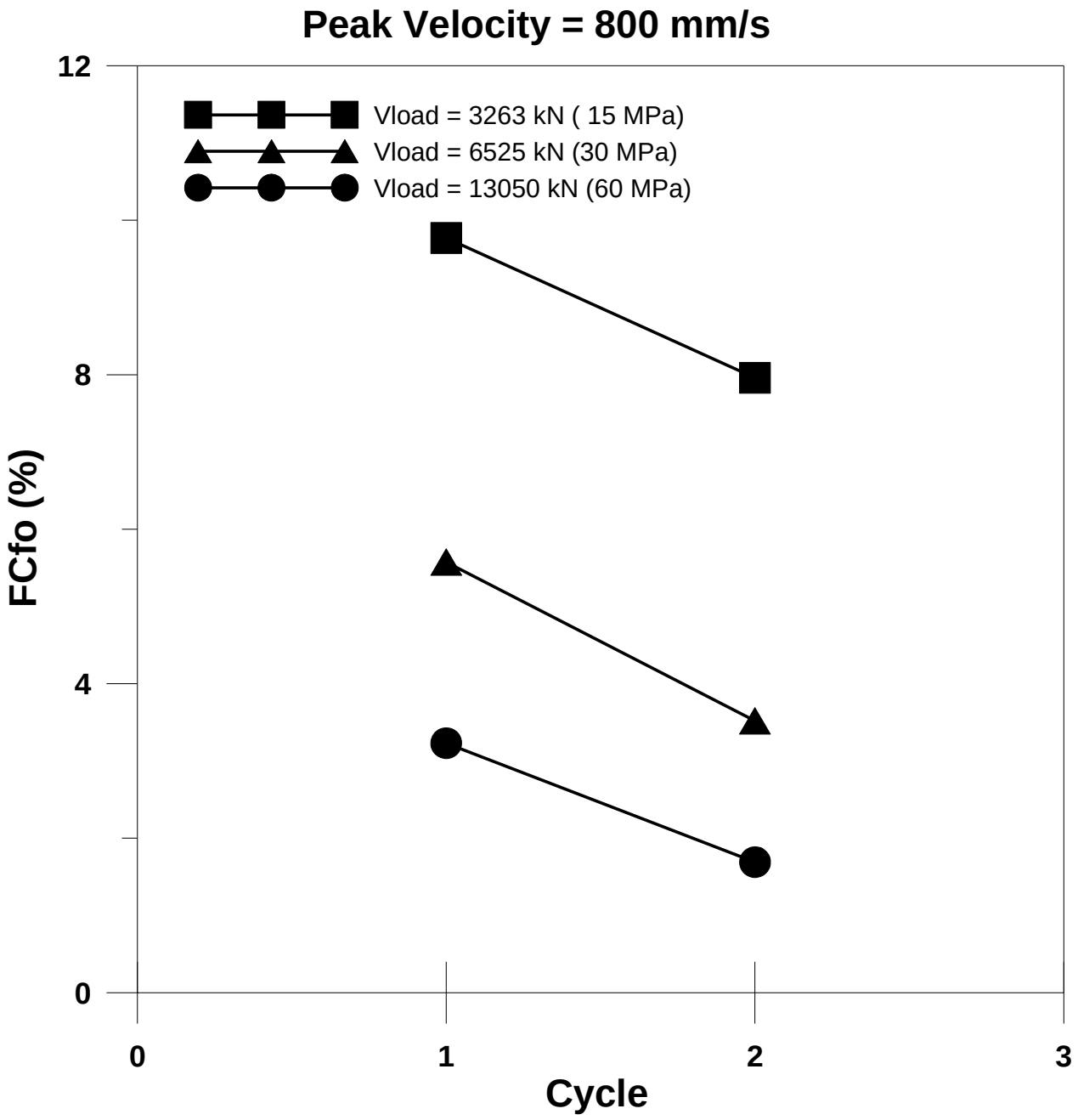

Figure B-34 Friction Coefficient (FCF0) for tests at 800 mm/s

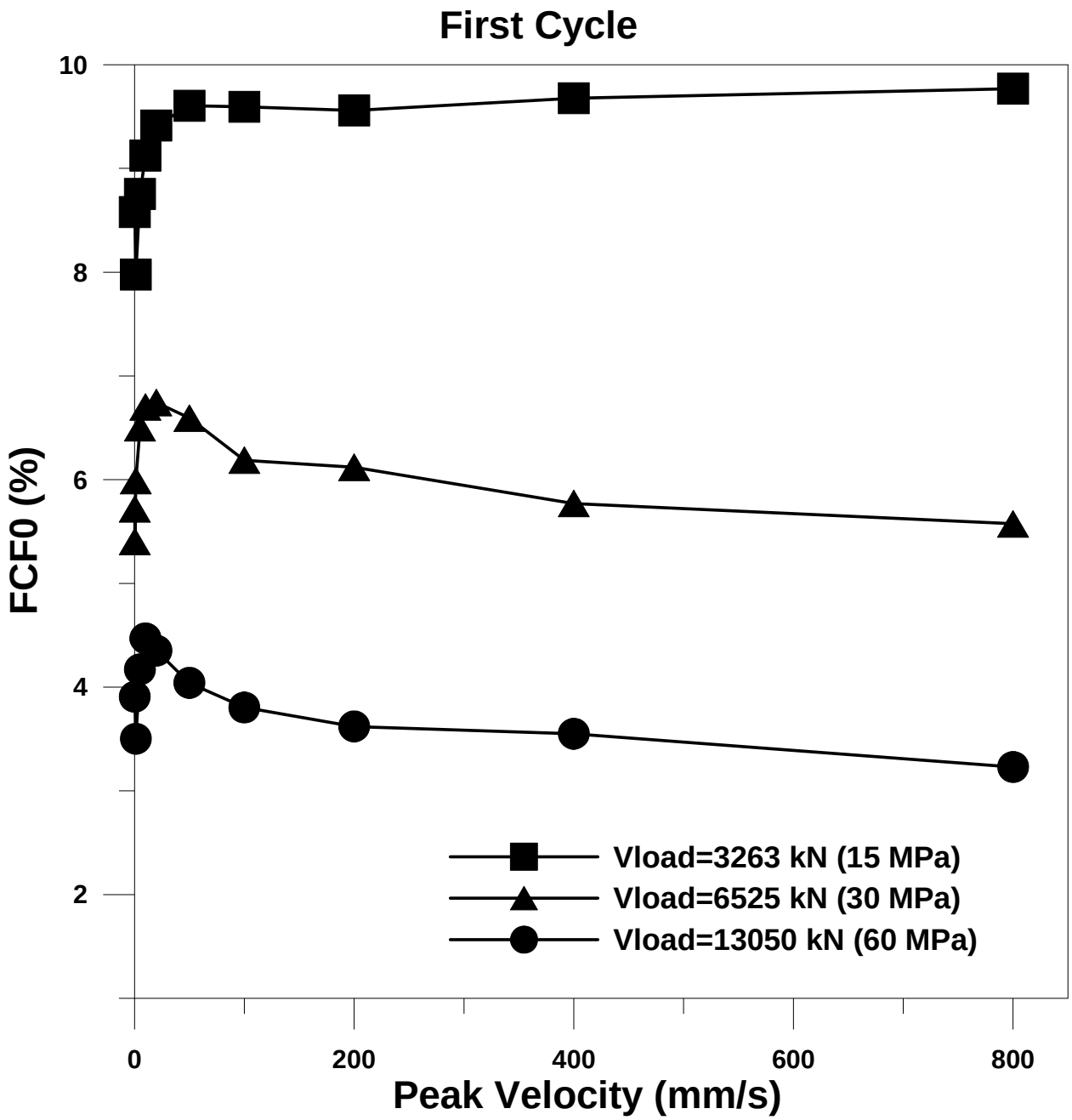

Figure B-35 FCF0 for first cycle of tests at different vertical load and velocity

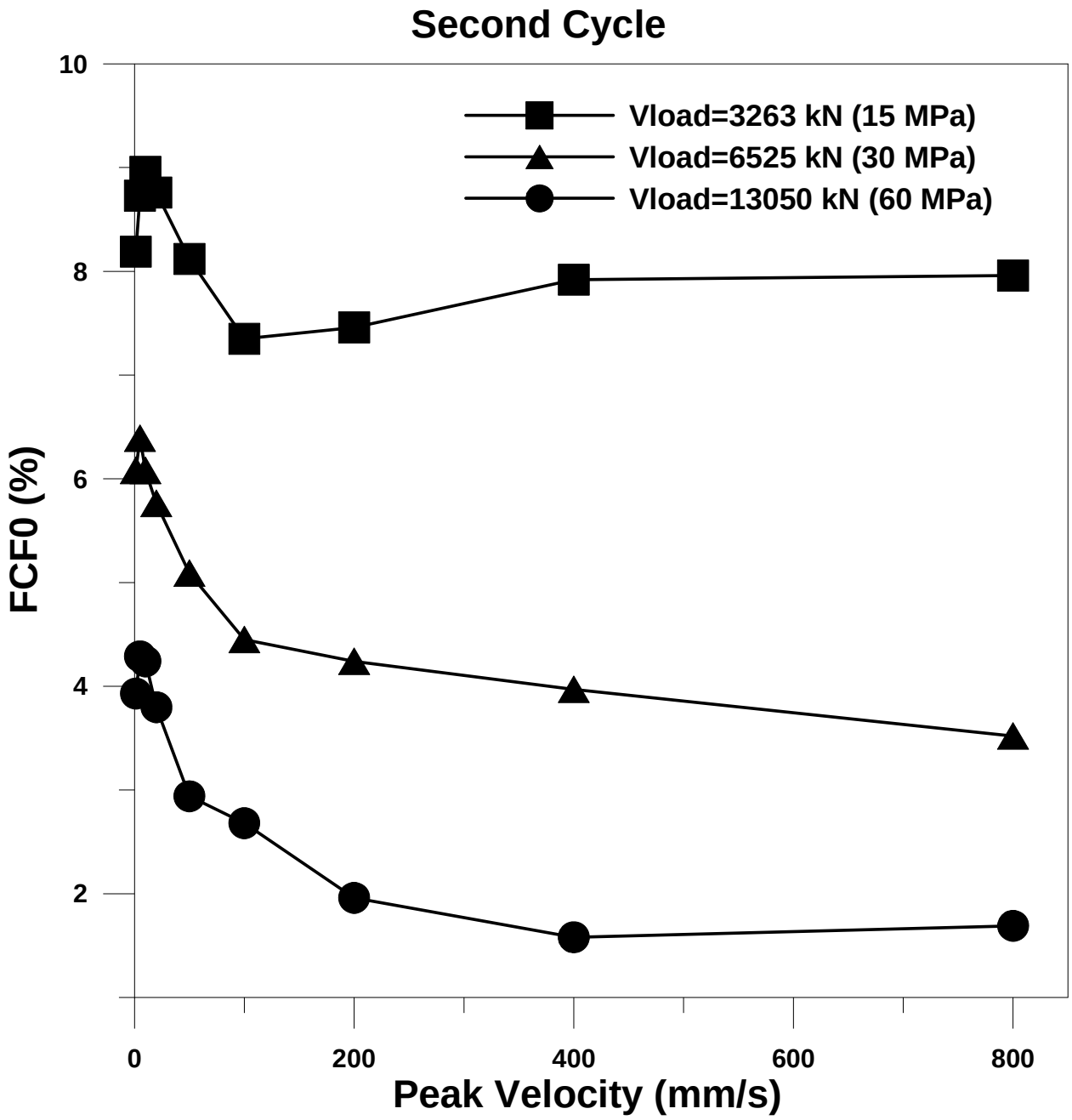

Figure B-36 FCF0 for second cycle of tests at different vertical load and velocity

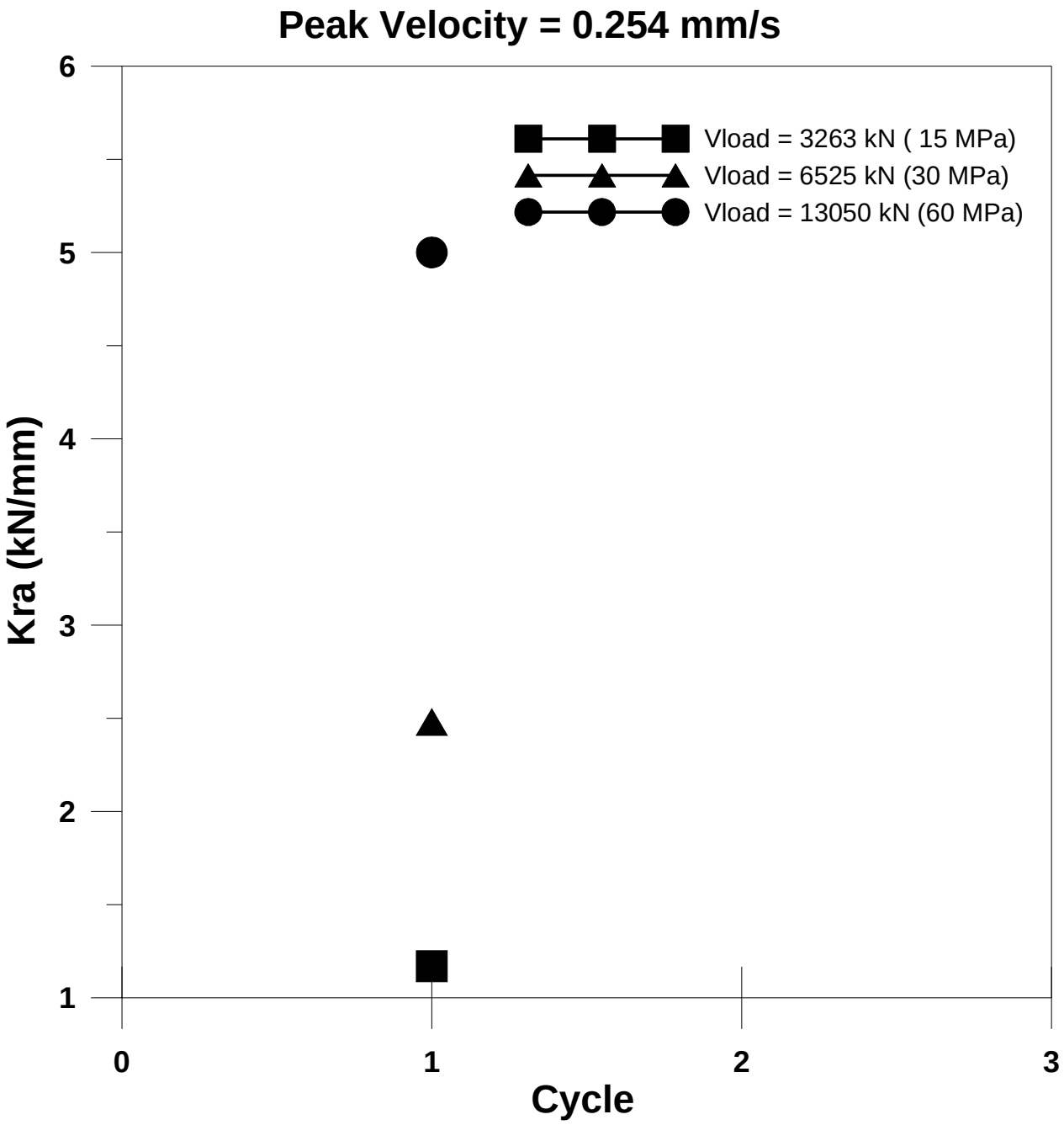

Figure B-37 Restoring Stiffness (Kra) for tests at 0.254 mm/s

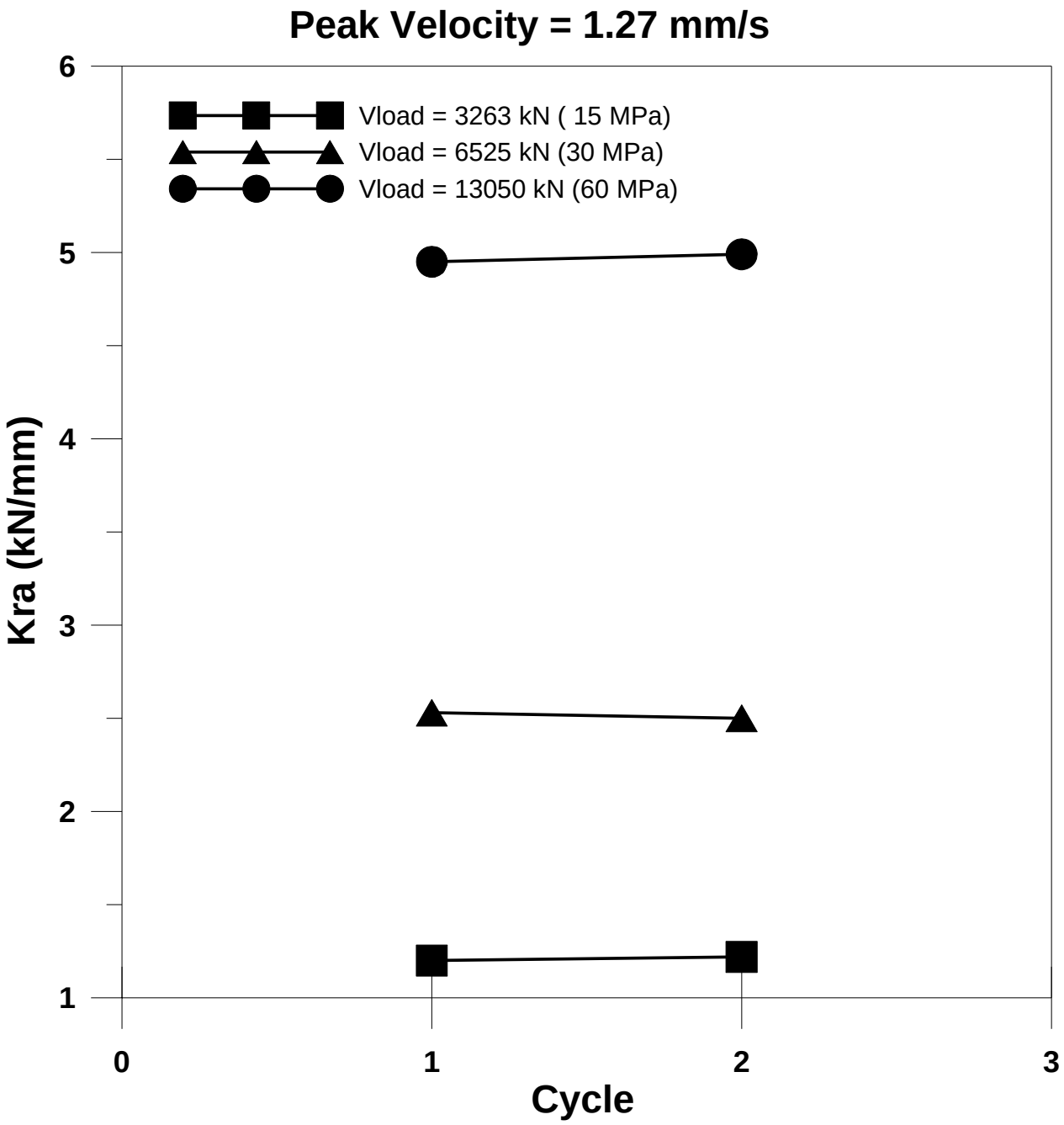

Figure B-38 Restoring Stiffness (Kra) for tests at 1.27 mm/s

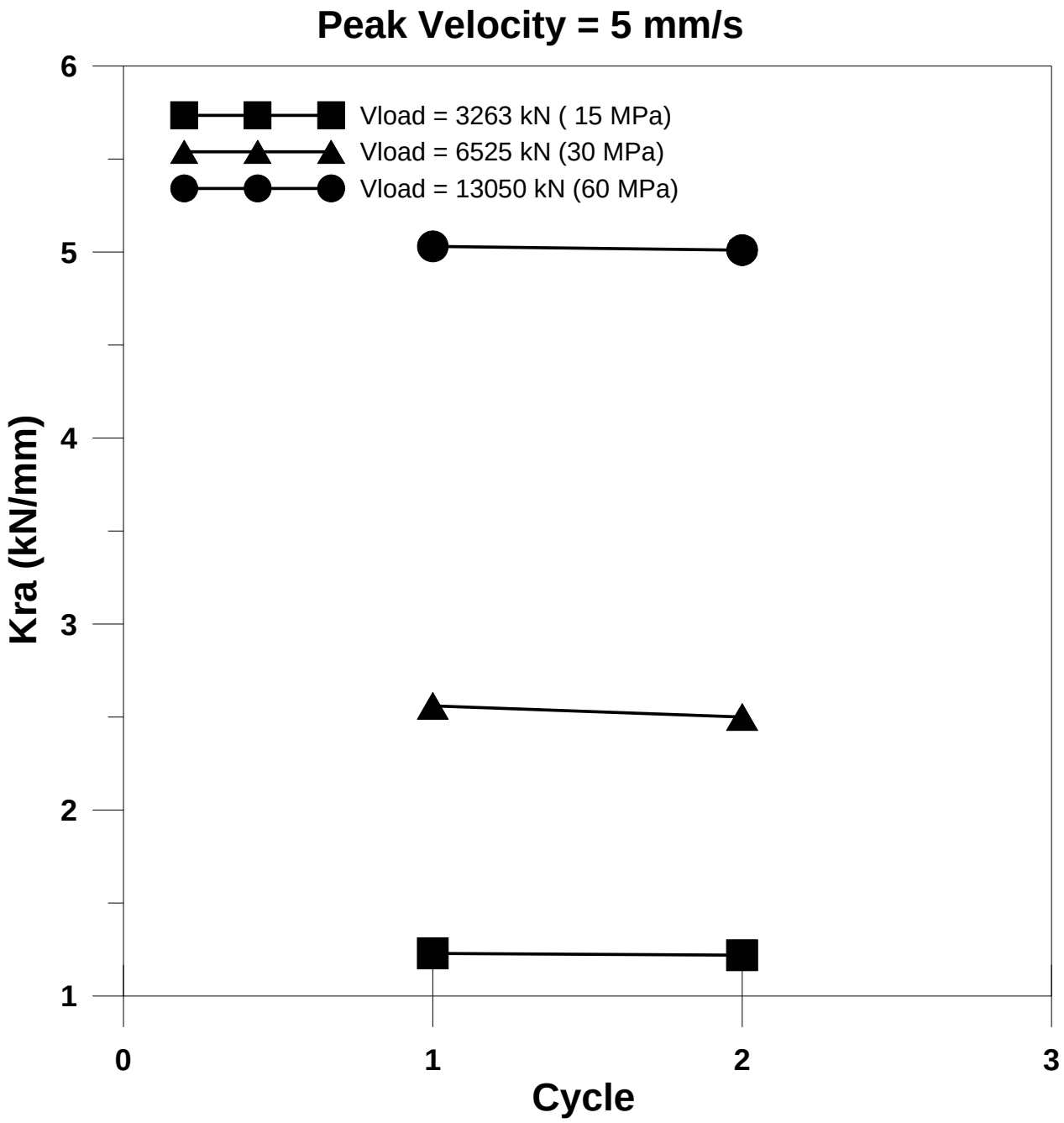

Figure B-39 Restoring Stiffness (Kra) for tests at 5.0 mm/s

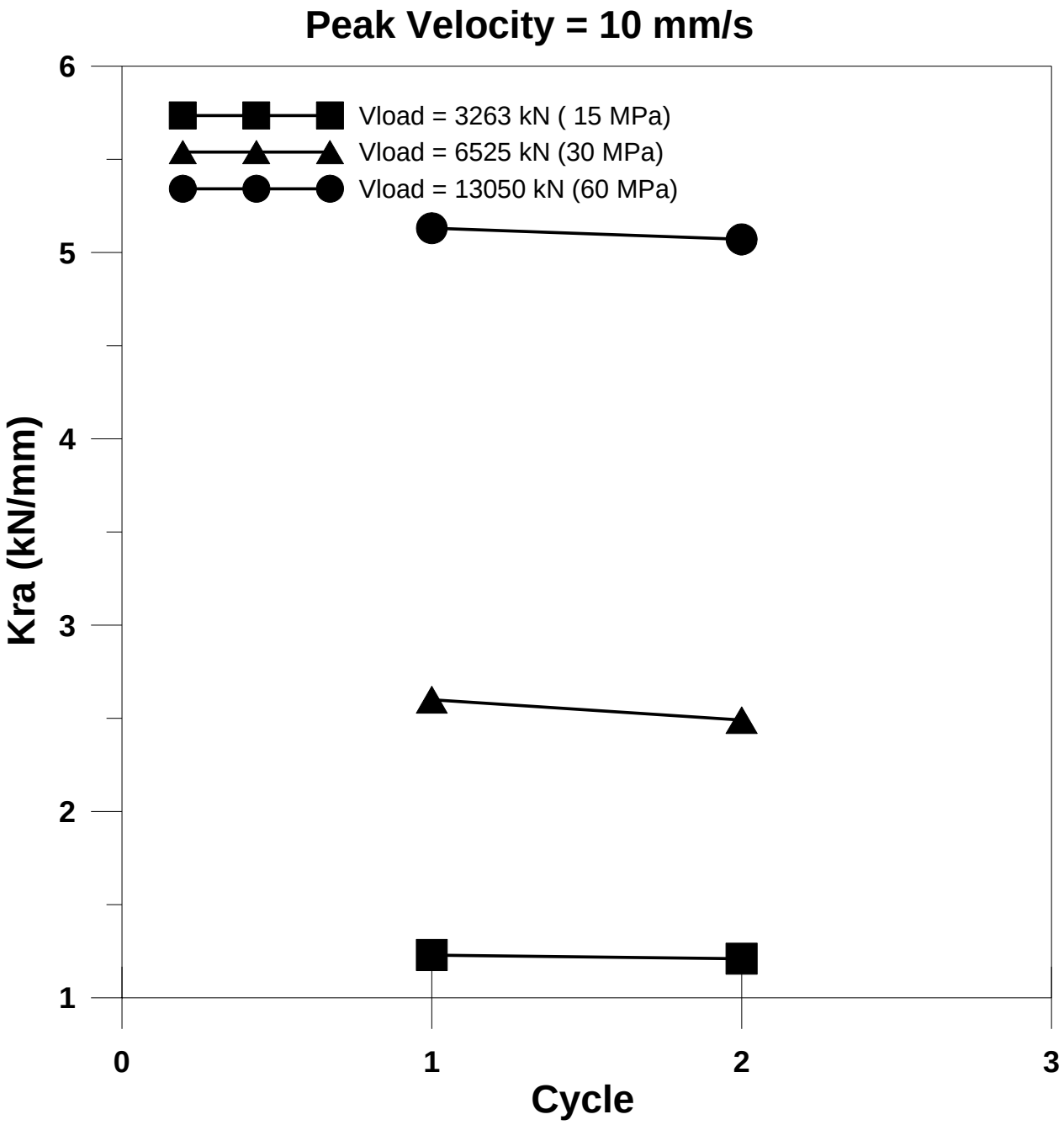

Figure B-40 Restoring Stiffness (Kra) for tests at 10 mm/s

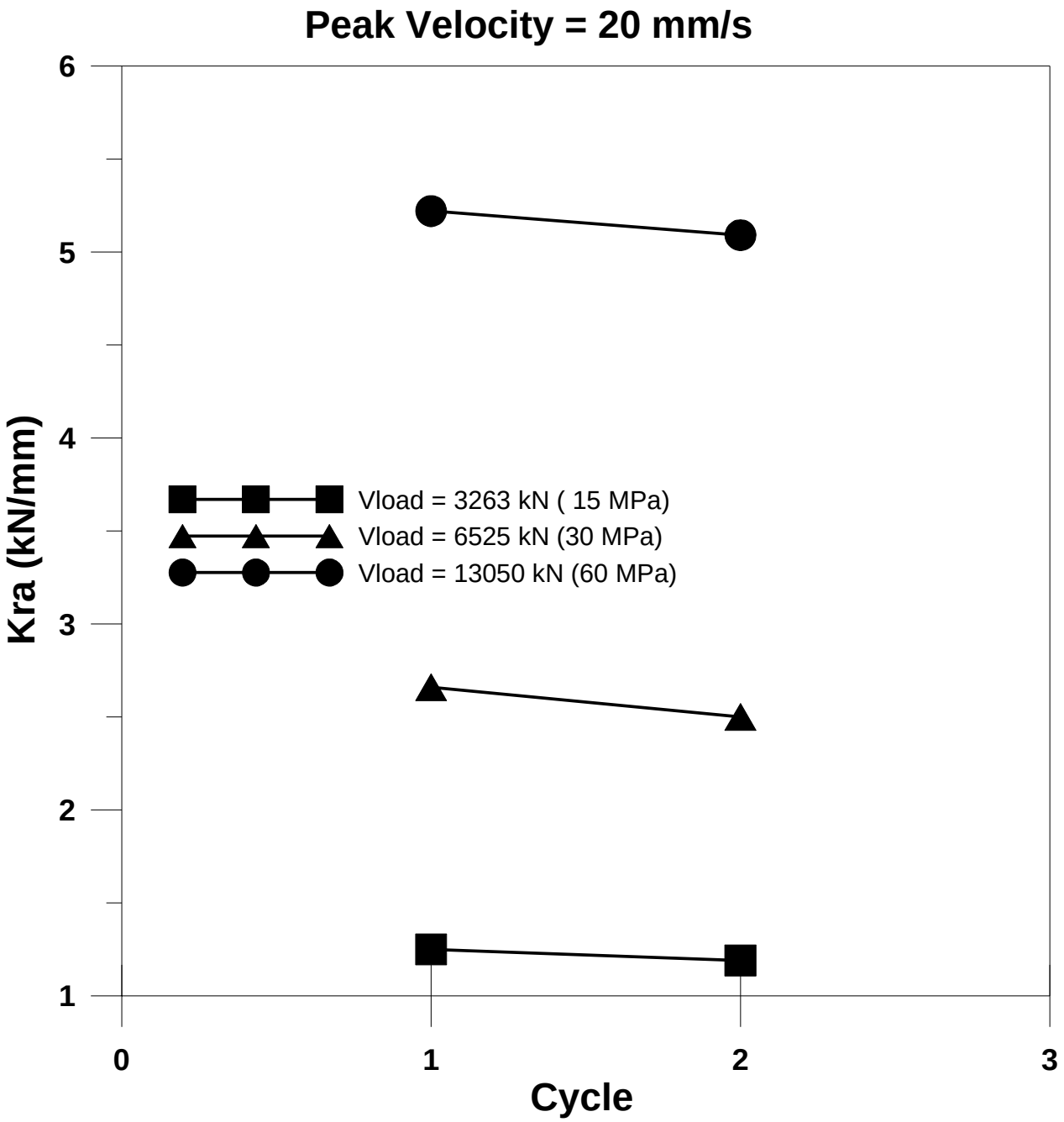

Figure B-41 Restoring Stiffness (Kra) for tests at 20 mm/s

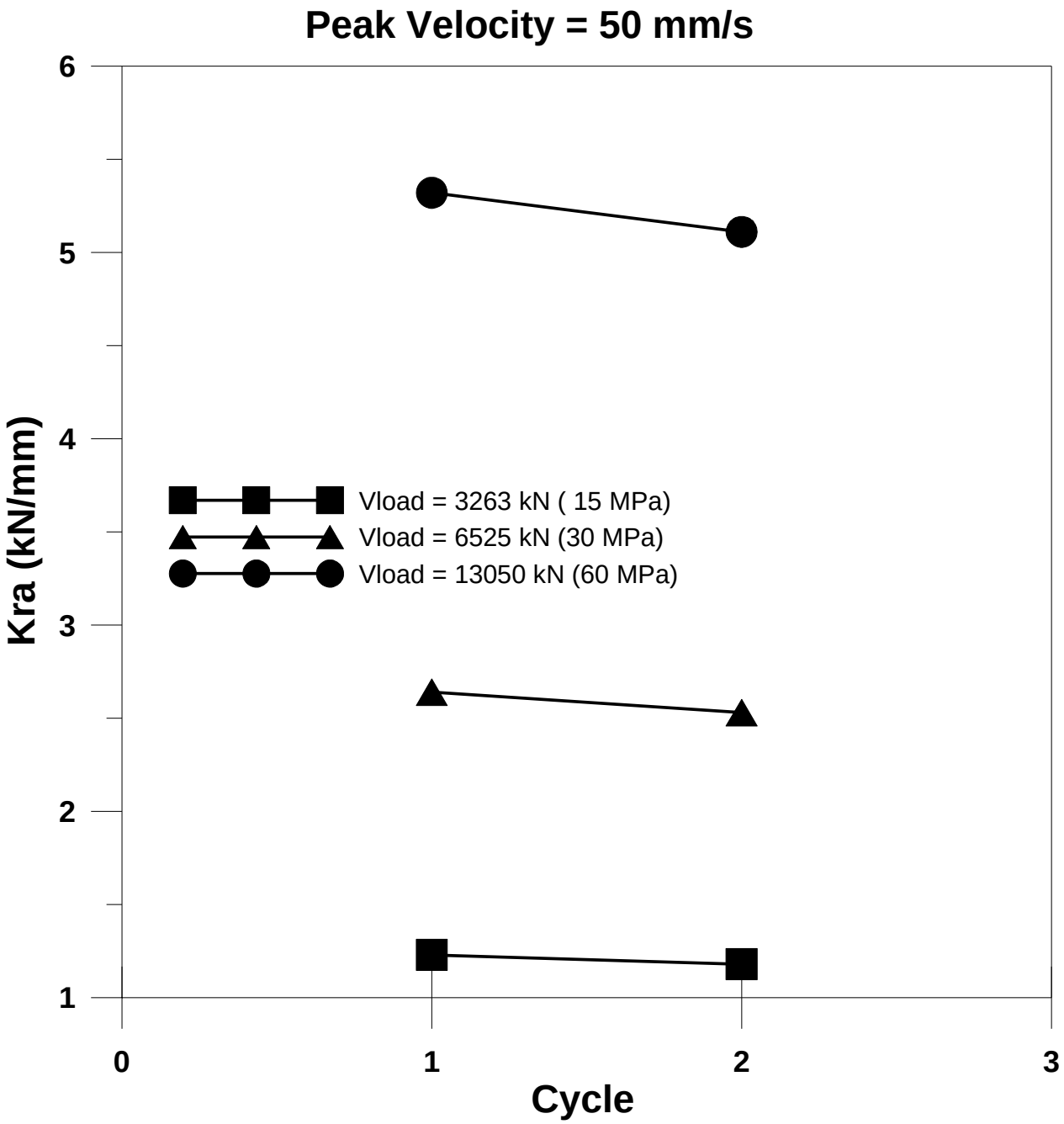

Figure B-42 Restoring Stiffness (Kra) for tests at 50 mm/s

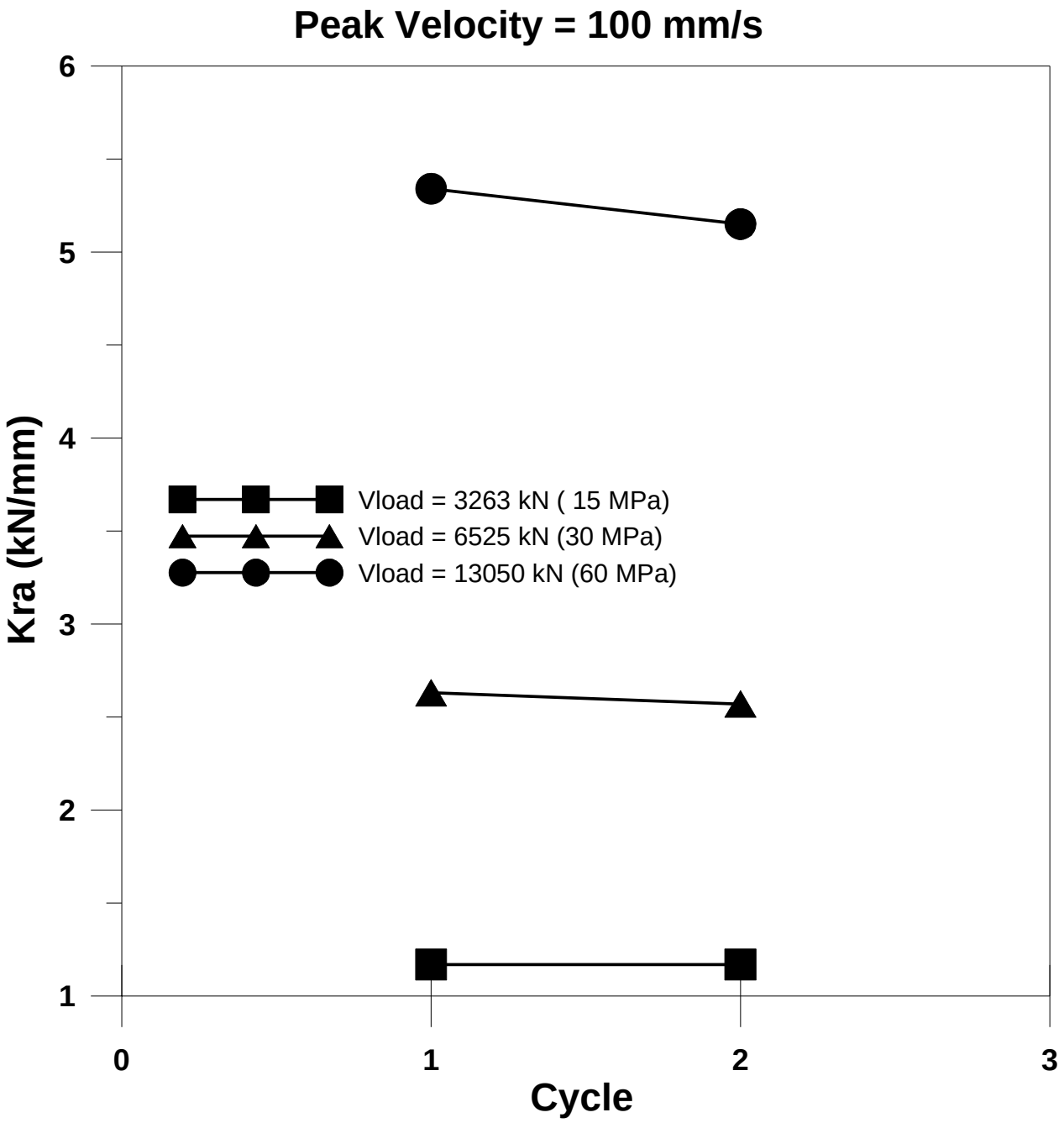

Figure B-43 Restoring Stiffness (Kra) for tests at 100 mm/s

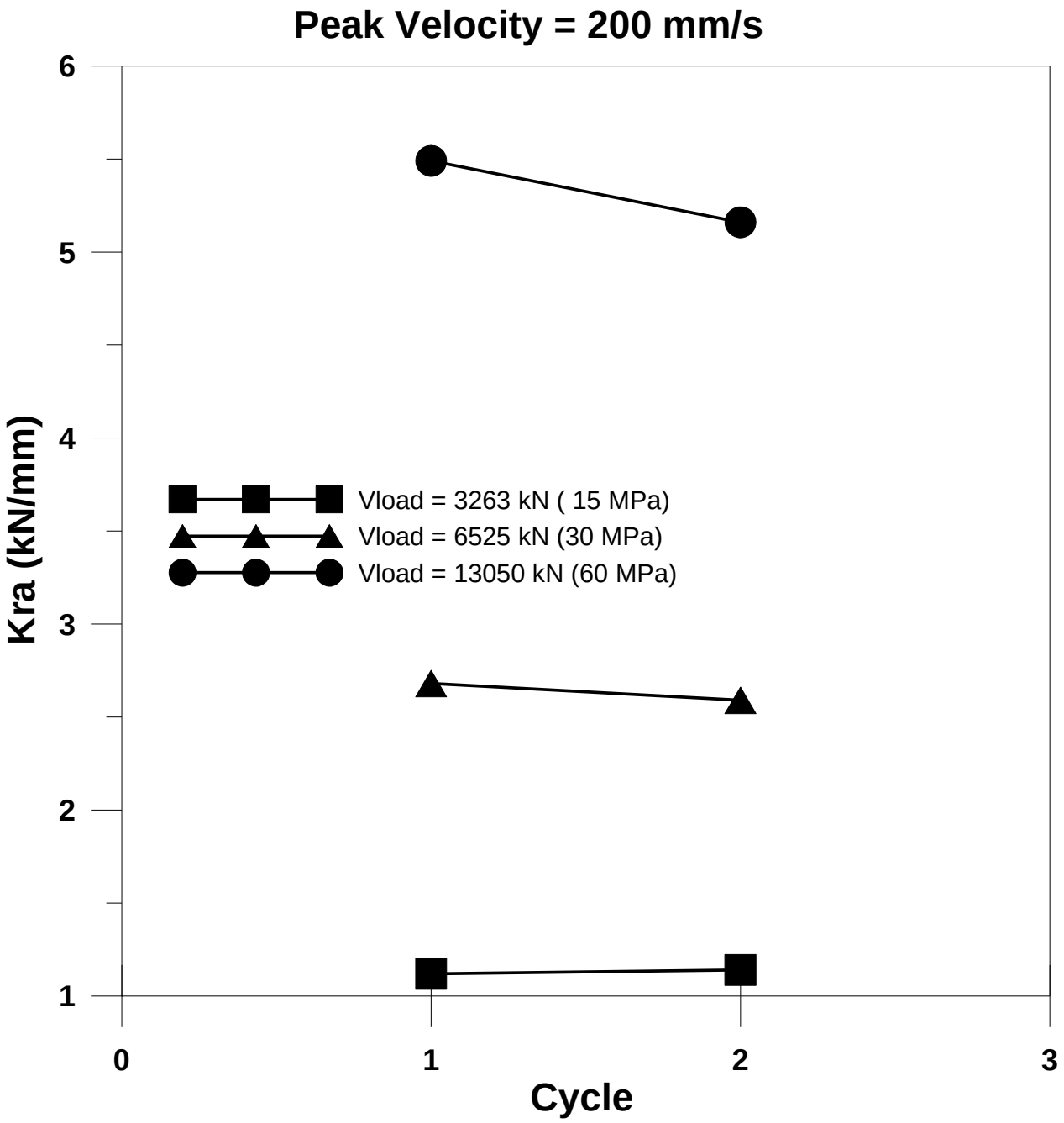

Figure B-44 Restoring Stiffness (Kra) for tests at 200 mm/s

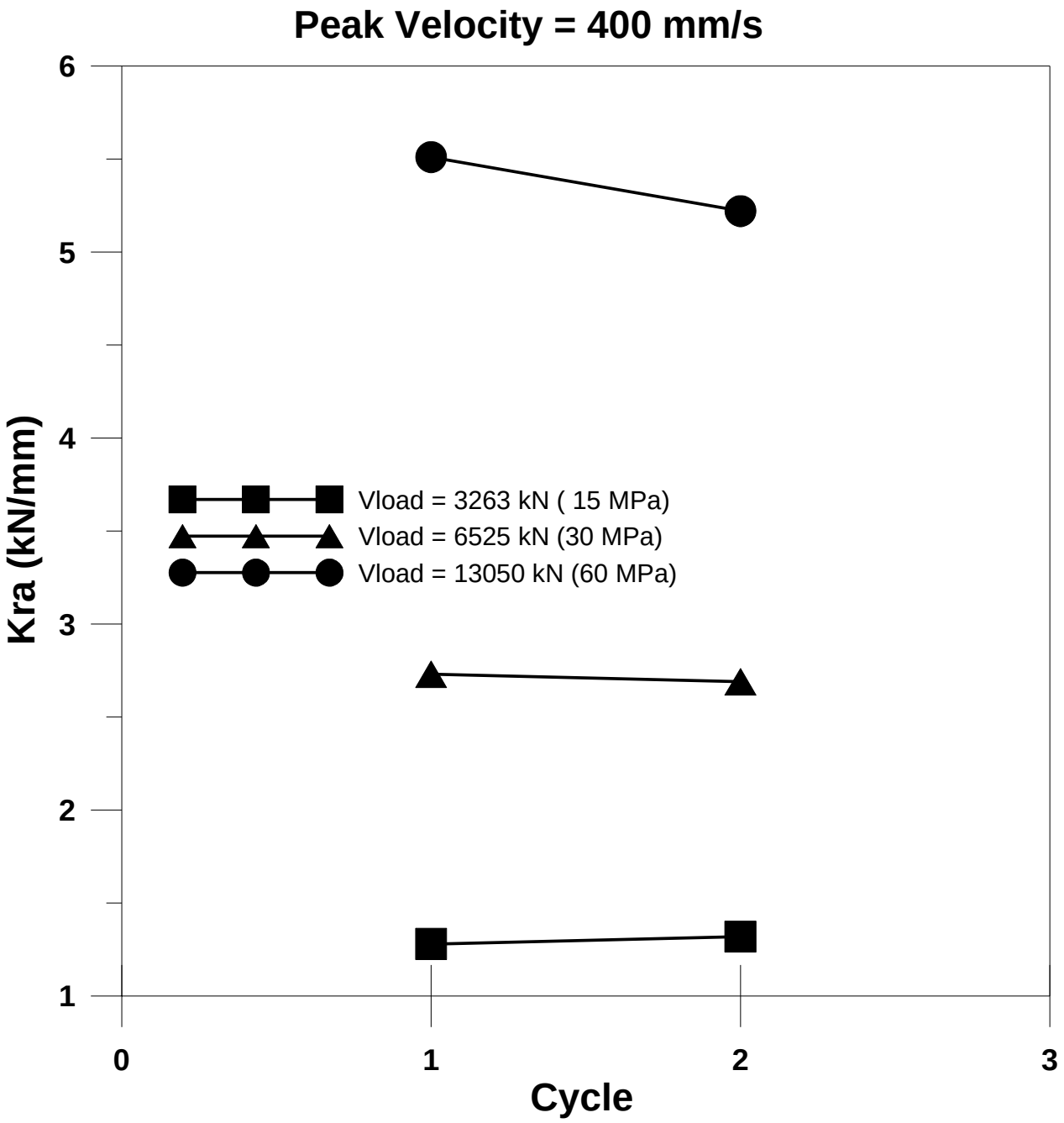

Figure B-45 Restoring Stiffness (Kra) for tests at 400 mm/s

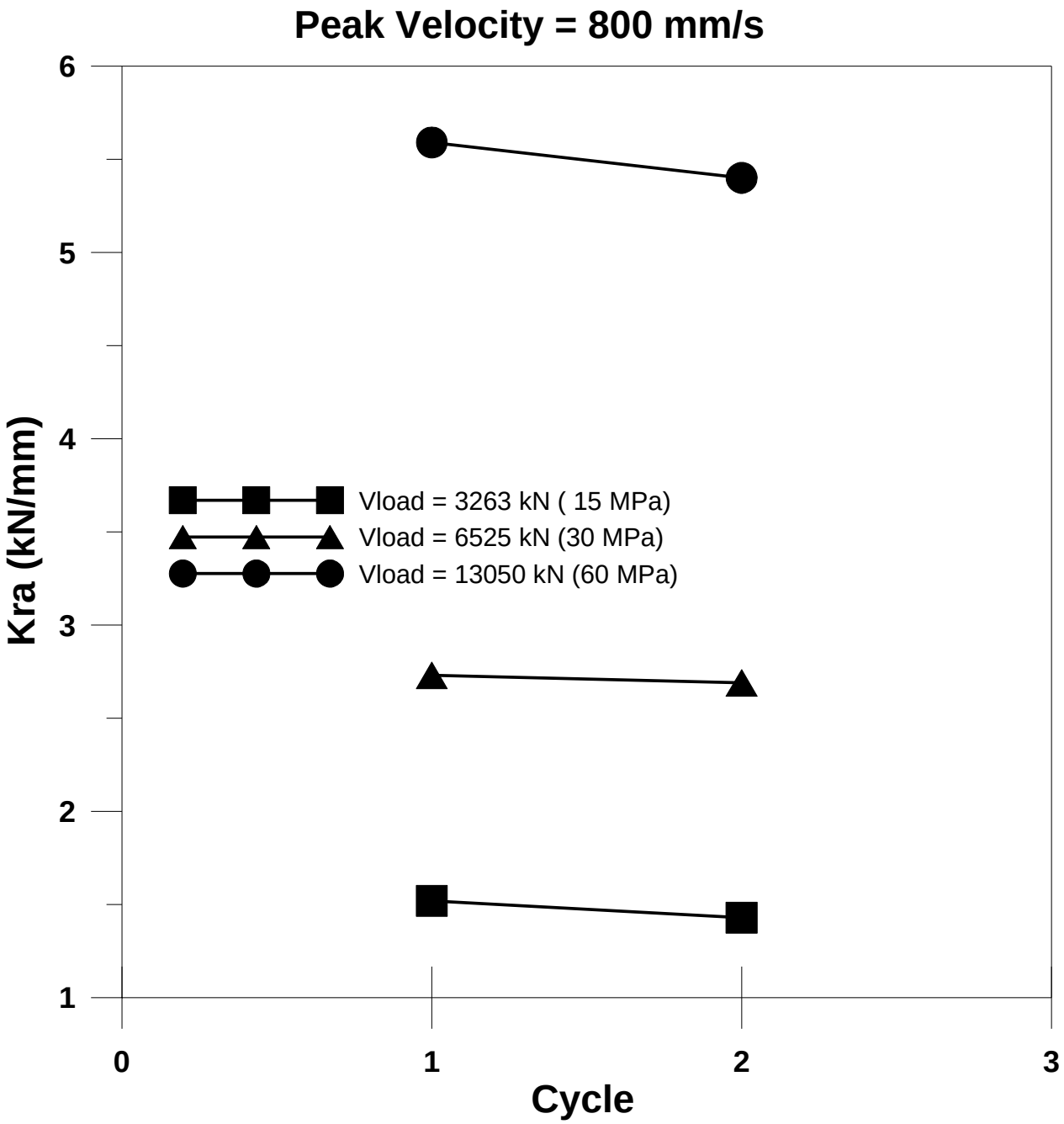

Figure B-46 Restoring Stiffness (Kra) for tests at 800 mm/s

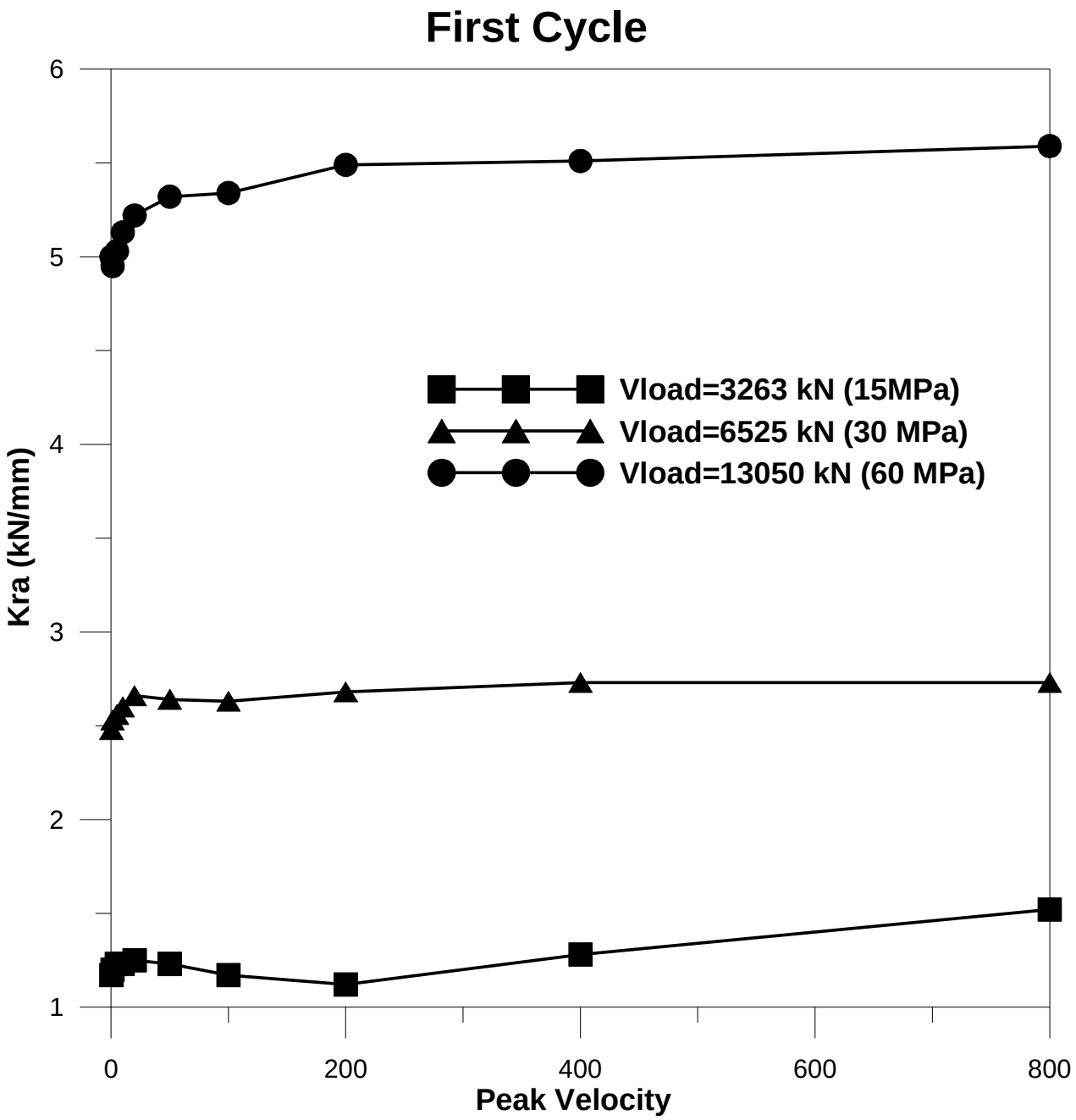

Figure B-47 Restoring Stiffness for first cycle of tests at different vertical load and velocity

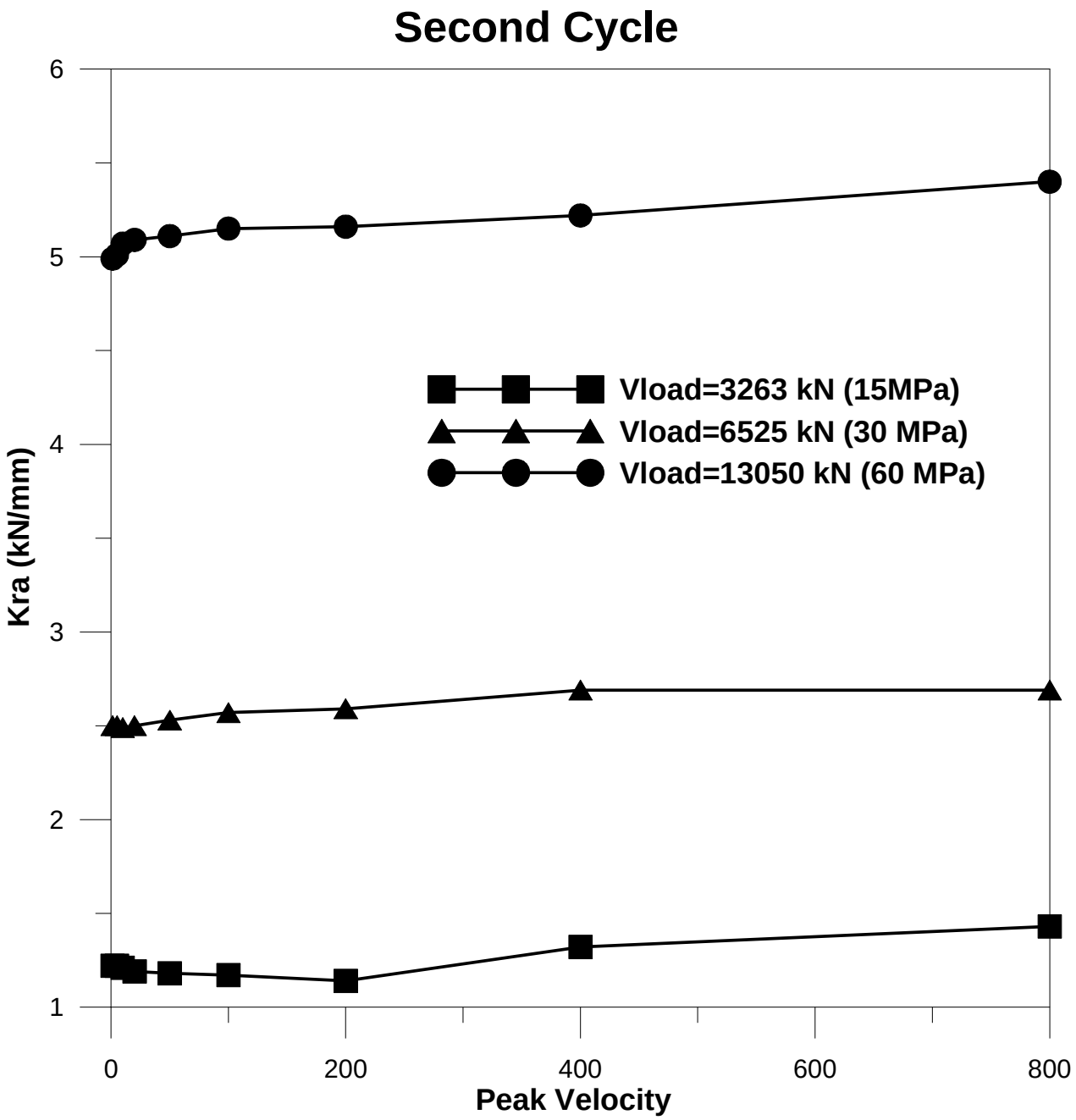

Figure B-48 Restoring Stiffness for second cycle of tests at different vertical load and velocity